Developing a non-viral gene therapy for *CHM* and *USH2A* retinopathy using Scaffold Matrix Attachment Region DNA plasmids

Lyes Toualbi

UCL Institute of Ophthalmology
and
The Francis Crick Institute
PhD Supervisor: Prof Mariya Moosajee

A thesis submitted for the degree of
Doctor of Philosophy
University College of London
May 2023

Declaration

I Lyes Toualbi confirm that the work presented in this thesis is my own. Where information has been derived from other sources, I confirm that this has been indicated in the thesis.

Abstract

Gene therapy for inherited retinal diseases (IRDs) has had to overcome many pitfalls to reach the clinic, and still has many challenges to address, such as expanding the carrying capacity of vectors, ensuring long-term transgene expression, and limiting inflammatory reactions. The development of alternative non-viral vectors is therefore crucial to broaden the gene therapy possibilities. In this thesis, non-viral scaffold matrix attachement region (S/MAR) plasmid DNA vectors were investigated in two examples of IRDs, that would benefit from gene augmentation therapy: Choroideremia and Usher syndrome type IIA. S/MAR vectors containing the human *CHM* (1.9kb) or *USH2A* (15.6kb) coding sequences, which produce the proteins REP-1 and usherin, respectively, were successfully generated. These vectors were assessed in different patient-cell disease models. CHM-S/MAR vectors restored REP-1 expression with a 75% rescue of prenylation function in CHM patient fibroblasts. CHM human induced pluripotent stem cells (hiPSC) were generated and differentiated into RPE, for further experiments. USH2A-S/MAR vectors drove transgene expression in patient fibroblasts, with Usherin presence confirmed by qPCR, western blots, and immunostainings. This work also gave new insights on USH2A patient-derived cell cilia defects and usherin function in focal adhesion and cell migration. S/MAR vectors have shown promise as a novel non-viral retinal gene therapy, warranting further development for both choroideremia and USH2A-related diseases.

Impact statement

There are currently no treatments available for choroideremia (CHM) and USH2A-related retinopathy. Both would be good candidates for gene augmentation therapy. However, the *USH2A* coding sequence (15.6kb) is too large to be amenable by AAV viral vectors, and although the *CHM* coding sequence (1.9kb), producing the protein REP1, fits into AAV capsids, the latest clinical trials did not meet primary endpoints with reported sight-threatening intraretinal inflammation. Therefore, efforts must be taken to develop alternative non-viral strategies. In this thesis, I have cloned and validated a REP1-S/MAR DNA vector toolbox that showed proof-of-concept in both patient-derived CHM fibroblasts and a *chm* zebrafish model. In addition, I have cloned and validated a S/MAR DNA plasmids containing a full human *USH2A* coding sequence. These USH2A-S/MAR plasmids are the first reported and are valuable as a gene therapy tool for *USH2A* retinopathies, and to explore usherin function in different cell and animal models. I also generated *USH2A* and *CHM* hiPSC lines, allowing the production of retinal organoids and RPE respectively. These cell lines are valuable models to better understand *USH2A* and *CHM* pathomechanisms and to test innovative treatments. Moreover, this work has contributed to new insights into the role of usherin in ciliogenesis, focal adhesion and neurite outgrowth. Going forwards, these vectors will be assessed with innovative vehicles (nanoparticles and liposomes) and in larger animals models.

Acknowledgements

First of all, I would like to thank Professor Mariya Moosajee, for giving me the opportunity to do my PhD in her team, and for her support during all my PhD. Thank you for your mentorship, for believing in me, especially in the moment I needed it the most! I feel very privileged to have had the opportunity to work with you on such exciting research projects.

I would like to thank Professor Richard Harbottle, his team especially Dr. Patrick Vingadas Almeida for helping me with my project, it has been a pleasure to start my PhD with a placement in his lab to make the S/MAR plasmids.

A big thank you as well, to all the Moosajee lab members! I will start with Dr. Maria Toms, for her support and the fantastic work she has done that helped my PhD going forward. Thank you to my fellow PhD students, it made everything easier with them around: Phillipa Harding, Jonathan Eintracht, Hajrah Sarkar, Katy Linkens and Daniel Jackson!

I would like to thank the post-docs for their support an scientific input: thank you to Dr. Nick Owens for your scientific advice and the journal clubs, thank you to Dr. Cécile Méjécase for the science talks, the coffee at the Crick and taking care of my cells when not around.

Thank you also, to all the others, that I do not forget, Dr Sara Vazquez, Dr. Dulce Lima Cunha, Constance Maurer, Dhani Tracy-White and Naheed Kanuga for her efficiency as lab manager,

Thank you to Santen and UCL for funding my PhD, the Institute of Ophthalmology and Crick institute and the people running the facilities.

Finally, I would like to thank my partner for her support and the scientific discussions we have (you are next!). And I am very grateful to my parents and my sisters, for their love and flawless support, thank you!

Awards and publications

Papers

L Toualbi, M Toms, M Moosajee. USH2A-retinopathy: From genetics to therapeutics (2020). Experimental Eye Research 201, 108330

C Méjécase, P Harding, H Sarkar, J Eintracht, D Lima Cunha, **L Toualbi**, M Moosajee. Generation of two human control iPS cell lines (UCLi016-A and UCLi017-A) from healthy donors with no known ocular conditions. (2020) Stem Cell Research, 49, 102113.

H Sarkar, C Méjécase, P Harding, J Eintracht, **L Toualbi**, D Lima Cunha, M Moosajee. Generation of two human iPSC lines from patients with autosomal dominant retinitis pigmentosa (UCLi014-A) and autosomal recessive Leber congenital amaurosis (UCLi015-A), associated with RDH12 variants (2021). Stem Cell Research, 54, 102449.

L Toualbi, M Toms, M Moosajee (2021). The landscape of non-viral gene augmentation strategies for inherited retinal diseases. International Journal of Molecular Sciences 22 (5), 2318

N Owen, M Toms, Y Tian, **L Toualbi**, R Richardson, R Young, D Tracey-White, P Dhami, S Beck, M Moosajee. Loss of the crumbs cell polarity complex disrupts epigenetic transcriptional control and cell cycle progression in the developing retina (2023)

M Toms*, **L Toualbi***, P V Almeida, R Harbottle, M Moosajee. Successful large gene augmentation of USH2A with non-viral episomal vectors. Submitted to Molecular Therapy (Under review)

L Toualbi, Maria Toms, P V Almeida, M Bozza, Richard Harbottle3, Mariya Moosajee1,2,4,** Chm paper Gene augmentation of CHM using non-viral episomal vectors in models of choroideremia

C Méjécase, **L Toualbi**, M Moosajee. Photoreceptor glycan-binding proteins pattern in human retina and in mature retinal organoids derived from induced pluripotent stem cells (In writing)

Awards

2nd Best Research Image “Retinal Flower Bouquet” - ECR symposium meeting 2022 -

Best poster prize. SenSyT Symposium 2019, Sensory Systems, Technologies and Therapies

Presentations

Toualbi L, Toms M, Vingadas-Almeida P, Harbottle R, Moosajee M. Developing a non-viral gene therapy strategy for CHM and USH2A-related inherited eye diseases using Scaffold Matrix Attachment Region DNA plasmid vectors. - Talk ECR symposium meeting 2022 -

Toualbi L, Toms M, Vingadas-Almeida P, Harbottle R, Moosajee M Poster. Developing a non-viral gene therapy strategy for USH2A-related retinitis pigmentosa using Scaffold Matrix Attachment Region DNA plasmid vectors. – Poster presentation ECR symposium meeting 2021 -

Toualbi L, Toms M, Vingadas-Almeida P, Harbottle R, Moosajee M. Using non-viral S/MAR DNA vectors to restore protein expression in models of Choroideremia - Poster presentation ARVO symposium 2022 –

Toualbi L, Toms M, Vingadas-Almeida P, Harbottle R, Moosajee M. Developing a non-viral gene therapy strategy for choroideremia using Scaffold Matrix Attachment Region DNA plasmid vectors - Poster SenSyT Symposium 2019 –

Updates on Choroideremia in our lab, Talk to a patient meeting for France Choroideremia 2023

Table of contents

List of figures

List of tables

Abbreviations

AAV	Adeno-associated virus
AON	Antisense oligonucleotide
CDS	Coding sequence
cGas	Cyclic guanosine monophosphate
DAMPs	Damage-associated molecular patterns
Dpf	Days post fertilization
DsDNA	Double-stranded DNA
DsRNA	Double-stranded RNA
EB	Embryoid body
EMA	European Medicine Agency
FA	Food and Drug Administration
GCL	Ganglion cell layer
GGTaseII	Geranyl-geranyl transferase 2 complex
GFP	Green Fluorescent Protein
HEK293	Human embryonic kidney 293
hIPSC	Human induced pluripotent stem cell
HDF	Human dermal fibroblasts
IRD	Inherited retinal dystrophy
INL	Inner nuclear layer
IPL	Inner plexiform layer
IS	Inner segment
IRF	Interferon response factor
ITR	Inverted terminal repeats
IFN	Leber congenital amaurosis
LCA	Melanoma differentiation associated protein
MAVS	Mitochondrial antiviral signalling protein
mpf	Months post postfertilization
MyD88	Myeloid differentiation primary response protein 88
mOPS	Murine opsin promoter
NLS	Nonsense mediated decay
NF-κB	Nuclear factor κ-light-chain-enhancer of activated B cells
OS	Outer segment
PMC	Periciliary membrane complex
PR	Photoreceptor
PTC	Premature termination codons
PE	Pseudo-exon
REP1	Rab-escorted protein 1
REP2	Rab-escorted protein 2
RPE	Retinal pigmented epithelium
RP	Retinitis pigmentosa
RIG-I	Retinoic acid-inducible gene-I
RdCVF	Rod-Derived Cone Viability Factor
ssRNA	Single-stranded RNA
S/MAR	Scaffold Matrix attachment Regions
SAF-A	Scaffold attachment factor protein A
STING	Stimulator of Interferon genes
SLN	Solid lipid nanoparticles
TLR	Toll-like receptor
TAT	Transactivator of transcription
UTMD	Ultrasound-targeted microbubble destruction

Chapter 1. Introduction

1.1 The eye, the organ of vision

The eye allows us to be aware of the world around us by perceiving colour, shape, motion, and light. These properties are supported by the neural retina: a 0.2-mm-thick tissue lining the internal surface of our eyes, which is responsible for the transformation of light signals into nervous impulses. The neural retina is organised in a laminar fashion, with six major types of neurons. The first layer formed by photoreceptors (PR) interdigitating with the supporting monolayer of retinal pigment epithelium (RPE), an intermediate layer of interneurons such as horizontal, bipolar and amacrine cells and a final layer of retinal ganglion cells (RGC), the axons of which form the optic nerve and transmit signals to the brain for visual processing (Hoon et al. 2014) (Figure 1).

1.1.1 The photoreceptors

The human retina contains approximately 130 million PRs divided into two types: rods and cones (Kennedy et Malicki 2009). The rods are responsible for vision in dim light with low spatial acuity called scotopic vision whereas cones mediate photopic vision in bright light and trichromatic vision, with 3 cone subtypes: blue-opsin (short wavelength), green-opsin (medium wavelength), or red-opsin (long wavelength).

To be able to convert the light stimuli into a biochemical cascade and communicate the information to the downstream neurons. PRs have

developed unique morphological features, starting with a highly specialized ciliary tripartite compartment formed of the basal body (BB), the connecting cilium (CC) and the outer segment (OS). The basal body is a structure composed of microtubule triplets, from which arise the axoneme. BBs are attached to the periciliary membrane (PCM), the area between the ciliary membrane and the cell membrane (Seo et Datta 2017). These membranes serve as docking points for proteins that go to the ciliary compartment. PR OS, an extension of the CC, is filled with stacks of disks full of light-sensitive G-protein coupled receptors (GPCR), containing a transmembrane opsin protein and an 11-cis-retinal chromophore. Photons can trigger 11-cis-retinal chromophore photoisomerization into an all-trans configuration. This modification leads to the activation of the transducin, which initiates a phosphodiesterase resulting in decreasing GMPc concentration in the OS, closed sodium channels, and ultimately cell hyperpolarization (Goldberg, Moritz, et Williams 2016).

1.1.2 The retinal pigmented epithelium (RPE)

The retinal pigmented epithelium is a continuous monolayer of epithelial cells at the interface with the PR outer segments and choroidal blood supply. It plays an essential role in retinal homeostasis. RPE cells possess long and thin microvilli in close contact with PR outer segments. RPE phagocytic abilities allow recycling of shed PR outer segments, which contain Vitamin A derivatives and lipids (Baehr et al. 2003). Besides, RPE contains many melanosomes to absorb light and enhance visual acuity

(Boulton et Dayhaw-Barker 2001). In addition, RPE contributes to immune regulation of the retina. As a matter of fact, it expresses factors and receptors to sense pathogens and create an adequate pro or anti-inflammatory microenvironment (Wong et al. 2022).

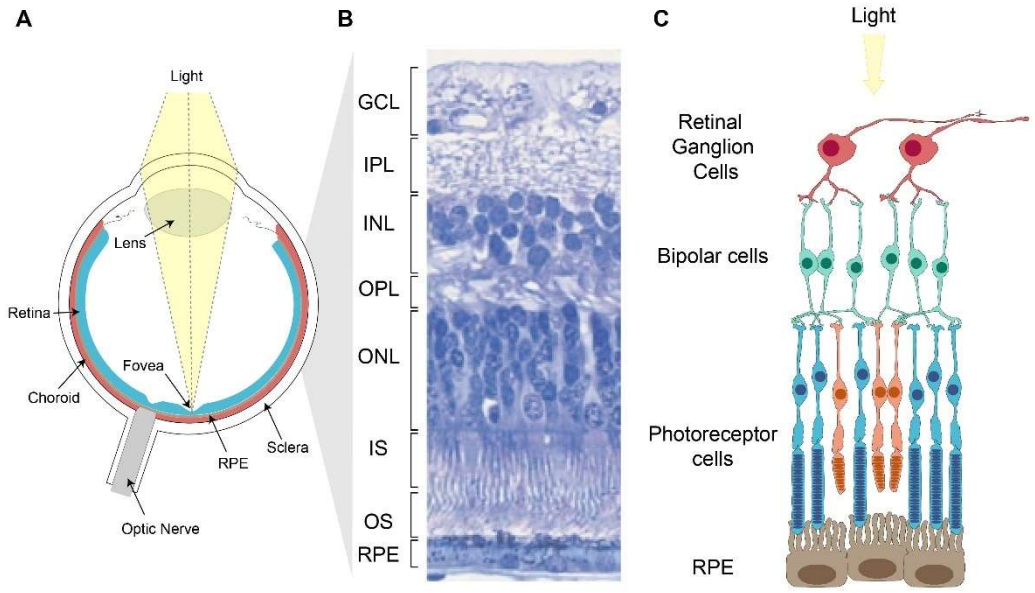

Figure 1. The eye and the retinal structure.
The eye (A) focuses light onto the neural retina. Ganglion cell layer (GCL). Inner plexiform layer (IPL) Inner nuclear layer (INL) Outer plexiform layer (OPL) Outer nuclear layer (ONL) Inner segments (IS) Outer segments (OS) Retinal pigmented epithelium. Adapted from (Kennedy et Malicki 2009).

1.2 Inherited retinal dystrophies (IRD)

Loss of photoreceptors and/or RPE leads to progressive blindness, which is the case in inherited retinal dystrophies (IRD) such as retinitis pigmentosa (RP). Approximately 1 in 3000 people develop an IRD, which leads to sight loss (Liew, Michaelides, et Bunce 2014). So far, more than 250 genes have been identified as causative of IRD (Figure 2). In RP, rod cells are lost first, leading to night blindness (nyctalopia) in early stages, followed by constriction of the peripheral visual field. The cones situated in the periphery, then lose their outer segments and die. Cones survive for longer in the macula, especially the fovea due to their density, however, in

end-stage disease these will be lost leading to complete blindness. Several therapeutic windows of opportunity could improve the patient's life, depending on the stage of the pathology. However, the wide heterogeneity of mutations involved in this pathology makes it challenging to treat (Verbakel et al. 2018a). Moreover, gene replacement therapy, pharmacotherapy and neuroprotection cannot treat the late stages of RP, because of the PR loss.

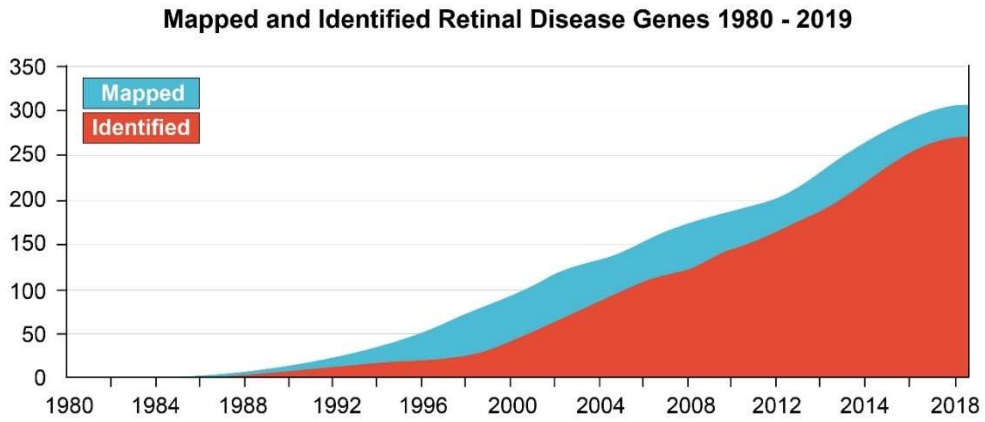

Figure 2. Mapped and identified retinal disease genes since 1980 (adapted from https://sph.uth.edu/retnet/sum-dis.htm#D-graph).

1.3 Gene therapy for inherited retinal dystrophies

1.3.1 Challenges and limitations of retinal gene therapy

The eye offers many advantages as a target for gene therapy. It is small, relatively immune-privileged, and easily accessible for therapeutic interventions, which makes it possible to inject small amounts of vectors directly *in-situ*. In addition, non-invasive *in vivo* imaging techniques allow reliable monitoring of the time course of degeneration and treatment safety

and efficacy for clinical trials. Altogether, these features place the retina at the forefront of translational gene therapy. Currently, there are over 40 gene therapy clinical trials for inherited retinal dystrophies from Phase I to Phase III trials, and recently the first gene replacement therapy has been approved for Leber congenital amaurosis (LCA) type 2, caused by biallelic mutations in the *RPE65* gene. However, challenges need to be addressed, such as expanding the carrying capacity of vectors, ensuring long-term transgene expression and keeping inflammatory reactions to a minimum. Therefore, the development of alternative vectors is crucial to broaden the gene therapy possibilities for genetic eye diseases.

1.3.1.1 Toxicity and immune response

The eye benefits from having a relative “immune privilege”, leading to reduced immune-mediated inflammation. The eye was described as such by Sir Peter Medawar, who reported that allografts can survive without rejection when implanted into the anterior chamber of the eye (Medawar 1948). This immune exception prevents any uncontrolled inflammatory responses, sparing precious non-regenerative retinal cells, and therefore protecting the sense of vision. However, the eye is not completely void of immune cells and resident T cells and circulating monocytes enter the eye (Wu et al. 2024). Inflammatory and immune responses can occur in the eye. A better understanding of ocular immune response, especially to

gene vectors and transgenes, would ensure safer and more efficient gene therapies for inherited retinal dystrophies.

Several challenges need to be taken into account to ensure the safety of gene therapy, especially immunogenicity of the vector, which is when a transgene or its product triggers a harmful immune response, and phenotoxicity due to overexpression or ectopic expression of the transgene (Khabou et al. 2018). Phenotoxicity can occur in gene therapy when the translated protein or its overexpression induces a cellular stress. For instance, Khabou and collaborators reported that AAV vectors encoding GFP were significantly more toxic compared to a non-coding control capsid in mice retina. Intracellular pathways such as endoplasmic reticulum stress can lead to apoptosis of transfected cells, and therefore reduce efficiency of the treatment (Khabou et al. 2018).

Most of the current clinical trials are using viral vectors, and more specifically adenoviral-associated viral (AAV) vectors. Until now, they remain the vector of choice for retinal/ocular gene therapy. They have so far demonstrated the best transduction efficacy, with a relatively good safety profile (Trapani et Auricchio 2019). In addition, the risk of insertional mutagenesis is minimal. However, several AAV clinical trials reported cases of inflammation in treated eyes. For instance, a dose-dependent inflammatory response to a high dose of AAV2-*RPE65* was reported in 5 of 8 participants, displaying intraocular inflammation, which was resolved under steroid treatments (Bainbridge et al. 2015). Similarly, one serious adverse event of presumed intra-retinal inflammation resulting in severe

functional and structural impairment was observed in a clinical trial treating choroideremia patients with AAV2-REP1 (Dimopoulos et al. 2018). Similarly, Zhai and colleagues reported intraretinal inflammation triggered by AAV2-REP1 subretinal injection, which resulted in permanent damage to the retinal structure (Zhai et al. 2023). Furthermore, preclinical studies in non-human primates displayed an innate and adaptive immune response following the subretinal injection of clinical-grade AAV8 (expressing the human *CNGA3* cDNA sequence and driven by the cone-specific human arrestin 3 promoter) under concomitant steroid treatment (Felix F. Reichel et al. 2017) . It activated all three main recognition pathways of innate immunity (1) Toll-like (2) NOD-like and (3) RIG-I-like (Felix F. Reichel et al. 2017). These receptors play the role of microbial sensors, to bacterial or viral products and nucleic acids, and mediate the innate immune response. Inflammatory response to AAV seems to occur in a dose-dependent fashion, encouraging the development of more efficient AAV capsids to use lower doses of vector (Khabou et al. 2018).

Viral and bacterial nucleic acids can trigger an innate immune response (Shirley, de Jong, et al. 2020) mediated by TLR. For instance, DNA plasmid vectors induce a proinflammatory response. It is mediated by TLR9 and result in the activation of the NFkB pathway (Figure 3).

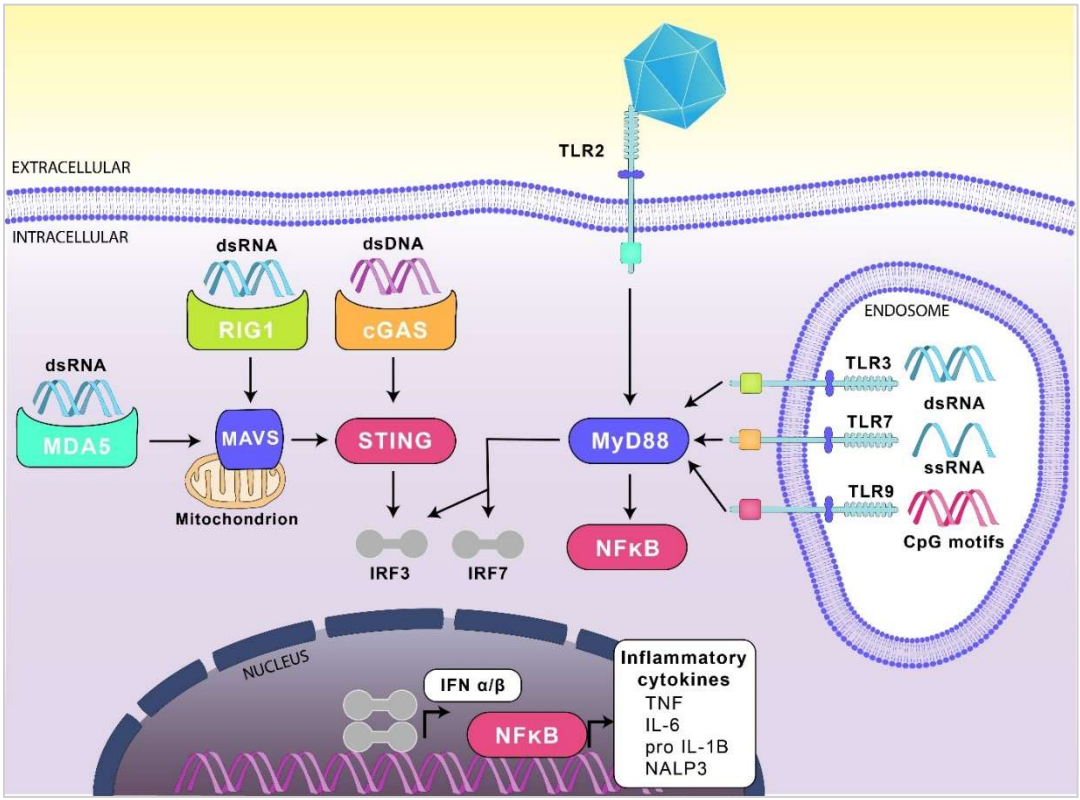

Figure 3. Innate Immune sensing and signalling pathways to viral and bacterial component.

Adapted from (Shirley, de Jong, et al. 2020). This figure is not exhaustive and shows the most common pathways for immune sensors to foreign DNA or RNA. TLR2 recognizes a wide range of ligands such as viral capsids and bacterial products. TLR3, TLR7 and TLR9's main ligands are dsRNA, ssRNA and CpG motifs, respectively. TLR activation switches on both the MyD88/NFKB and MyD88/IRF3/IRF7 signalling pathways, resulting in IFNα/β and pro-inflammatory cytokines production (TNF, IL6, pro IL1B and NALP3). DsRNAs are also direct ligands of MDA5 and RIG1, which activate the MAVS/STING/IRF3/IRF7 pathway. Additionally, dsDNAs (self or foreign dsDNA) are also direct ligands of the cGAS/STING/IRF3/IRF7 signalling pathway.

TLR =Toll-like Receptor dsRNA= double-stranded RNA, dsDNA=double-stranded DNA, ssRNA=single-stranded RNA, MDA5=melanoma differentiation associated protein, RIG-I=retinoic acid-inducible gene-I, MAVS=mitochondrial antiviral signalling protein, STING= Stimulator of Interferon genes, IRF= interferon response factor, cGAS=cyclic guanosine monophosphate-AMP synthase, IFN = interferon, MyD88=myeloid differentiation primary response protein 88, NF-κB=nuclear factor κ-light-chain-enhancer of activated B cells.

1.3.2 S/MAR technology

S/MAR are defined as DNA sequences found in eukaryotic genomes anchoring the chromatin to the nuclear matrix (Argyros, Wong, et Harbottle 2011a). These sequences are 300 to 5000 bp-long with 70% AT-rich content (Jurgen Bode et al. 2000). The first report of these motifs was published about 30 years ago in drosophila DNA and suspected to play a role in chromatin loop organization (Mirkovitch, Mirault, et Laemmli 1984; R Richardson et al. 2017). Several S/MAR sequences have been characterized in the human genome such as *APOB* matrix attachment region associated to the human apolipoprotein B locus or the *IFNB1* MAR associated to the human Interferon Beta 1 locus (J Bode et al. 1992). S/MAR elements occur in the human genome, contributing to DNA structure, loop domain partitions, replication, and transcriptional activity regulation.

The AT-rich content of S/MAR has been shown to favour DNA strands unwinding, increasing its availability to transcriptional factors. Additionally, S/MAR sequences have been found to play an insulator-like role by protecting genes from being silenced (Jenke et al. 2002). Additionally, S/MAR sequences serve as binding sites for scaffold attachment factor protein A (SAF-A), a RNA-binding protein that interacts with the nuclear phosphoprotein p300, a transcription factor regulating gene transcription (Martens et al. 2002). Several other transcription activator recruitment is facilitated by S/MAR sequences such as SAF-B, SATB1 and ARBP

(Argyros, Wong, et Harbottle 2011b) (Figure 4). The valuable properties of S/MAR sequences, such as episomal maintenance and silencing protection, have been exploited to tailor a novel kind of episomal vector.

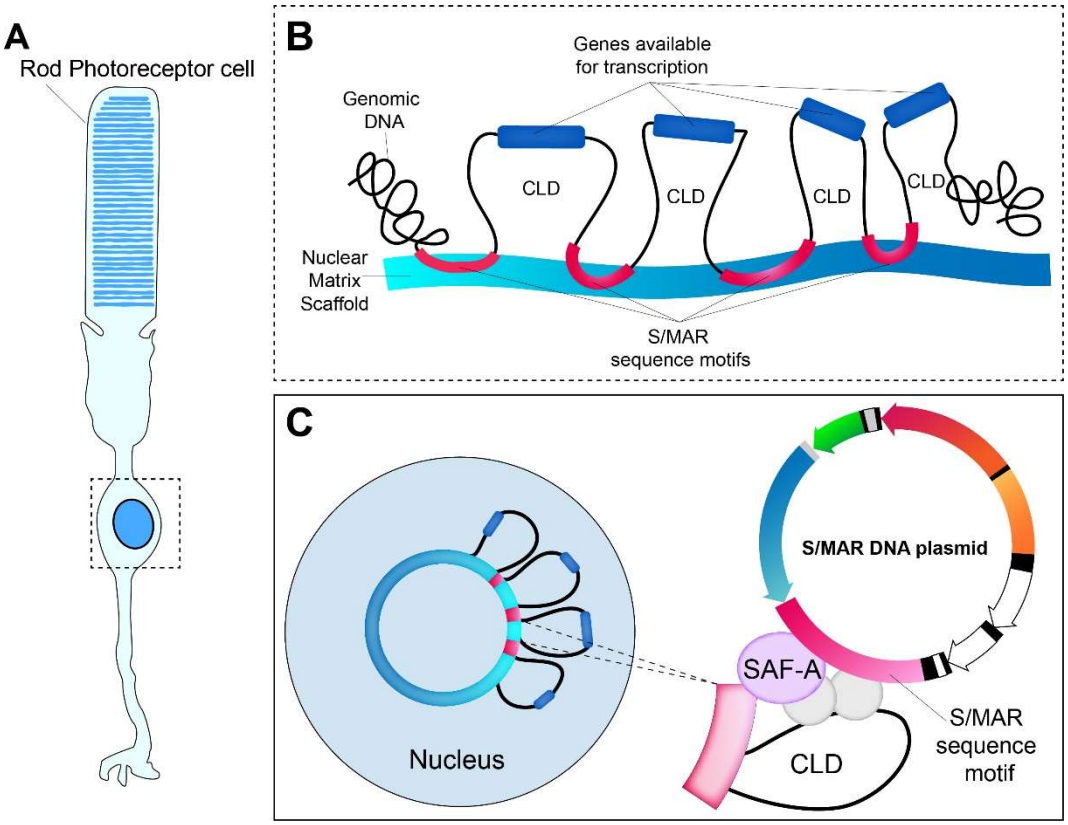

Figure 4. S/MAR motifs in the human genome organize chromatin. (A) Rod photoreceptor cell with a nucleus containing genomic DNA. (B) The S/MAR motifs in red interacts with the nuclear matrix allowing the formation of the chromatin loop domain (CLD). This chromatin organisation makes genes in blue more available for transcription factors, allowing higher expression. (C) DNA plasmids containing a S/MAR sequence reaching the nucleus, bind sites for scaffold attachment factor protein A (SAF-A), a RNA-binding protein that interacts with the nuclear phosphoprotein p300. Adapted from (Argyros, Wong, et Harbottle 2011a)

1.3.2.1 Episomal vectors using S/MAR

The first episomal vectors exploiting S/MAR sequence properties is the pEPI vector (Piechaczek et al. 1999). It represents the first virus-free episomal vector replicating in eukaryotic cells (CHO cells). The cloned 2kb-S/MAR fragment in this vector comes from the 5' region of the human *interferon β-gene* and is responsible for a stable expression maintained over more than 100 generations without selection pressure (Piechaczek et al. 1999). Following this work, the development of a minimally sized S/MAR vector, produced by cutting off the bacterial backbone of pEPI, allowed a higher and more sustained expression both *in vitro* and *in vivo.* This pEPI minicircle contains the expression cassette of interest and a 2kb S/MAR fragment (Argyros et al. 2011). Since then, many improvements have been made by Dr Richard Harbottle's team (DKFZ, Germany) in collaboration with Nature Technology Corporation, such as the addition of insulating elements (Ele40) and the production of spliced versions of the vectors with a minimal bacterial backbone to increase vector expression and establishment (Argyros et al. 2011; Bozza et al. 2020; Roig-Merino et al. 2022; Bozza et al. 2021). These DNA plasmid vectors present several advantages for gene therapy such as (1) persistence of expression and episomal maintenance without insertional mutagenesis (2) unlimited cloning capacity that can accommodate the cDNA of large genes, such as *USH2A* (3) no potentially toxic viral components (4) great versatility and accessible production.

1.3.2.2 Proof of concept in eye disease models

S/MAR DNA vectors have shown some promising results in animal models of eye disease, especially RPE-based diseases. Koirala and colleagues developed a promising non-viral approach, exploiting S/MAR DNA vector properties in a LCA mouse model. They used a S/MAR plasmid expressing the human *RPE65* cDNA driven by the *VMD2* promoter, which allows RPE-specific expression. RPE65-S/MAR DNA plasmids nanoparticles were formulated and introduced into *Rpe65*$^{-/-}$ mice, by subretinal injection. In 15-month post-injection mice, expression of RPE65 protein in the RPE, functional rescue of the protein, and improvement of cone ERG amplitudes were detected (Koirala et al. 2013; Koirala et al. 2013a). In addition, another study assessed the sustained expression of several S/MAR vectors such as pEPI and its significantly reduced derivative pEPIto (60% less CpG motifs compared to pEPI) islands in mouse retina and demonstrated transgene expression up to 32 days post-injection (Calado et al. 2014; Haase et al. 2010).

1.4 Applications in two inherited retinal dystrophies

1.4.1 Choroideremia (CHM)

With an estimated prevalence of between 1 in 50,000-100,0000 people (MacDonald et al. 2015), CHM is the most common inherited X-linked chorioretinal dystrophy. Caused by mutations within the *CHM* gene encoding the Rab-escorted protein 1 (REP1), it is characterized by the degeneration of choriocapillaris, RPE and the PR layer. Affected males present with night blindness in their first or second decade of life followed by the gradual loss of peripheral vision leading to legal blindness during the fifth or sixth decade of life. Female carriers usually remain asymptomatic with good visual acuity throughout their lifetime, although mild progressive vision loss has been observed with nyctalopia and pigmentary changes (Coussa et Traboulsi 2012). CHM pathogenesis remains unclear, especially regarding its exact site. However, it is generally accepted that pathogenic *CHM* mutations are loss-of-function mutations, which makes it an ideal candidate for gene augmentation therapy. Additionally, no known dominant-negative effects have been reported and *CHM* cDNA is small enough (1.9kB) to fit into an AAV vector. Thus, expression of even a small amount of healthy functional protein is predicted to be therapeutic. Several promising clinical trials using AAV vectors are currently underway.

1.4.1.1 Genetics of CHM

The *CHM* gene (OMIM 303390) is located on chromosome X at position Xq21.2 and consists of 15 exons encoding a 653-amino acid (aa) protein, the ubiquitously expressed Rab escort protein-1 (REP1) (Sorsby et al. 1952; Cremers et al. 1990). REP1 plays a key role in the intracellular trafficking pathways of vesicles and prenylation of Rab proteins. Loss of function or absence of REP1 leads to choroideremia (Moosajee et al. 2014; Furgoch et al. 2014). To date, 297 unique pathogenic variants among 348 variants have been reported (*CHM* LOVD Database, accessed 03/05/23). These mutations span across the entire *CHM* gene and consists of nonsense, missense, frameshifts, in-frame deletions and insertions, duplications and deep-intronic mutations. Most *CHM* pathogenic variants are null, either caused by deletions leading to non-functional REP1 or nonsense mutations resulting in premature termination codons (PTC) and therefore, termination of protein translation. Some rare cases of unusual mutations have been reported such as missense variants, deep-intronic and a variant in the promoter region, but still with absence of REP1 expression (Simunovic et al. 2016; Carss et al. 2017; Radziwon et al. 2017) (Figure 5).

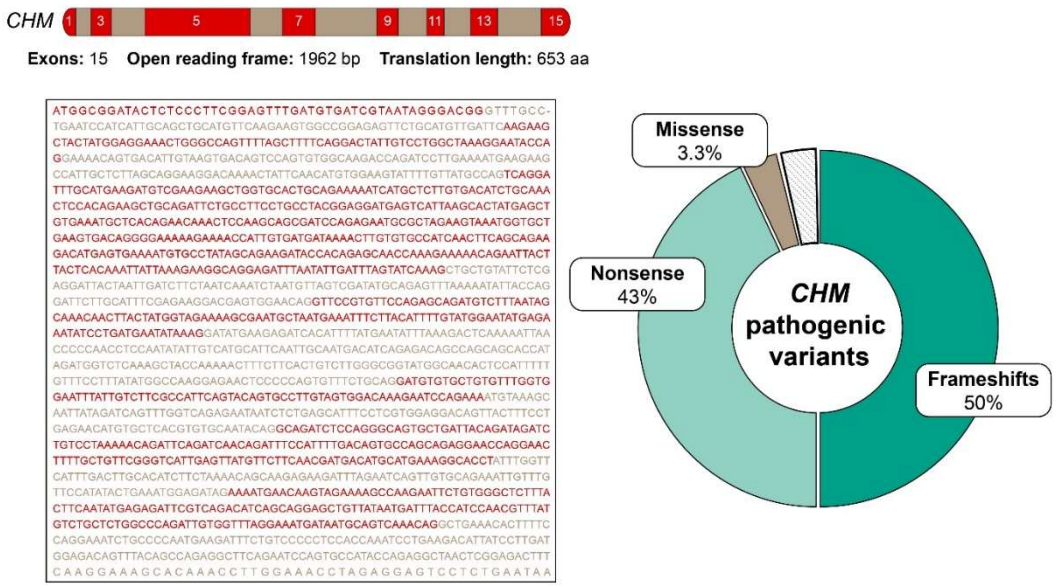

Figure 5. *CHM* gene and variants.

CHM gene contains 15 exons for an open-reading frame of 1.9kb, translating into REP1, a 653aa-long protein. Most *CHM* pathogenic variants are null with 50% frameshifts, 43% nonsense and 3.3% missense mutations (LOVD Database, accessed 03/05/2023).

1.4.1.2 Role of REP1 and pathogenesis

REP1 modifies small GTP-binding proteins called Rab proteins. Rab proteins act as key regulators of intracellular trafficking (Miguel C. Seabra, Mules, et Hume 2002; Miguel C. Seabra et Wasmeier 2004). There are over 50 Rab proteins expressed in all cells. In the retina, they play a central role in guiding melanosomes within the RPE and help phagocytosis of disc membranes shed from the photoreceptor cells. REP1 escorts Rab proteins in the cytosol to the geranyl-geranyl transferase 2 complex (GGTase2). This tripartite complex allows the addition of geranyl-

geranyl groups to Rab proteins, anchoring them to the bilayer lipidic membranes ensuring correct addressing to the target compartment (Corbeel et Freson 2008) (Figure 6). The absence of REP1 in *CHM* patients leads to a reduction in prenylation levels in various cell types of the body, but the disease phenotype remains restricted to the retina, suggesting that a mechanism could compensate REP1 absence (Miguel C. Seabra, Brown, et Goldstein 1993). This discrepancy led to the identification of the *CHM*-Like (*CHML*) gene (OMIM 118825) encoding REP2, a second isoform of REP1. REP2 is also an ubiquitously expressed protein, which shares 75% identity with REP1, and can ensure the escorting of Rab proteins to GGTase2 (Cremers et al. 1994). The characterisation of REP2 and its properties supported the hypothesis of a partial redundancy. However, REP1 and REP2 showed different activities of prenylation towards a subset of Rab proteins, especially Rab27A. Rab27A is expressed in the RPE and the choroid and demonstrated to accumulate in its unprenylated state in the cytosol of *CHM* patient cells (M. C. Seabra, Ho, et Anant 1995). In addition, Rab27A is less efficiently prenylated by REP2 than it is by REP1 (Rak et al. 2004). Finally, it has been shown that REP2 activity towards Rab27A is blocked in *CHM* cells due to the competition with high-affinity Rab proteins. Therefore, absence of REP1 is thought to result in unprenylated low-affinity Rab proteins, which could explain pathogenesis in the retina (Mitsios, Dubis, et Moosajee 2018).

The pathogenic mechanism of unprenylated Rab proteins leading to cell death in *CHM* patients has not yet been elucidated. Evidence of dysfunctional phagocytosis in the RPE of *CHM* mouse and zebrafish models has been reported, as well as abnormal melanosome transport (Wavre-Shapton et al. 2013; van Wijk et al. 2006; Krock, Bilotta, et Perkins 2007). This may be a cell-autonomous process due to the ubiquitous expression but also a cell-dependent contribution as PR are intimately dependent on RPE health and normal function.

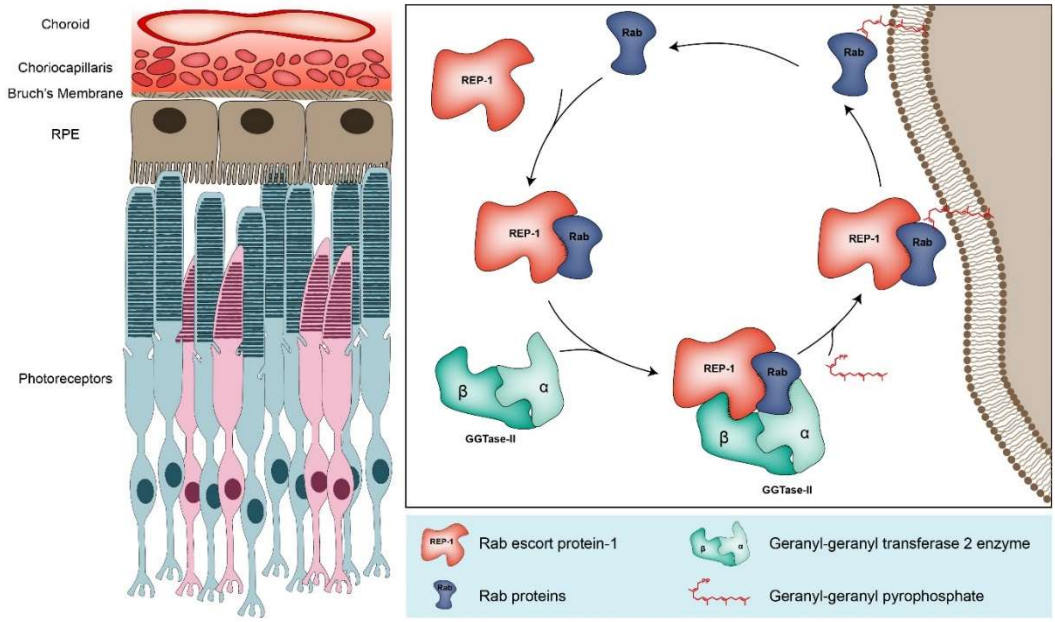

Figure 6. REP1 role in Rab proteins prenylation in the retina.

Photoreceptor cells, RPE and choroid are degenerating in Choroideremia. REP-1 ensures the escorting of Rab proteins to the Geranyl-geranyl transferase 2 enzyme. The GGTase-II is responsible for the addition of geranyl-geranyl pyrophosphate groups to the Rab proteins. REP1 also guides newly prenylated Rab proteins to their target compartment.

1.4.1.3 Therapeutic strategies

Gene therapy is currently the most promising therapeutic strategy for choroideremia (Cehajic Kapetanovic, Patrício, et MacLaren 2019). In principle, restoration of REP1 expression should result in improvement of the disease phenotype. *CHM* has a relatively short cDNA sequence of 1.9kb, allowing delivery of the transgene vector and REP1 cDNA by AAV vectors. However, recently, the phase 3 clinical trial did not meet the primary or secondary endpoints, and triggered harmful ocular inflammation (Zhai et al. 2023).

Amongst all public *CHM* pathogenic variants, 37% are caused by nonsense mutations (LOVD Database, Accessed 05/03/2023). Nonsense mutations result in premature termination codons (PTC) and trigger nonsense mediated decay (NMD). The NMD pathway acts as a control quality mechanism by eliminating transcripts containing PTCs. However, some of these PTC-containing transcripts can escape surveillance, leading to the expression of partially truncated protein. Translational Readthrough Inducing Drugs (TRIDs) exploit these PTC-containing transcripts by allowing readthrough of the PTC, resulting in the restoration of full-length protein. Such strategies have been explored in the *chm*^{ru848} zebrafish model and *CHM* patient cells using the drug ataluren (PTC124) and its analogue PTC414, and provided partial rescue of REP1 expression and function (Moosajee et al. 2016; Rose Richardson et al. 2017).

1.4.2 USH2A-retinopathy, for large gene replacement therapy

Retinitis pigmentosa (RP) has a prevalence of 1 in 4000, the most common cause of blindness amongst working age adults. *USH2A* mutations alone are the leading cause of non-syndromic retinitis pigmentosa (nsRP) accounting for 12-25% of cases (Pagon 1988; Verbakel et al. 2018b; Hartong, Berson, et Dryja 2006).

USH2A mutations represent the most frequent cause of Usher syndrome, an autosomal recessive disorder involving dual sensory impairment of the visual and audiovestibular systems. It was first described in 1858 by Albrecht Von Graefe (Graefe 1858) and classified as an inherited disorder in 1914 by the Scottish ophthalmologist Charles Usher (Usher 1914). It is the most common cause of deaf-blindness with an estimated prevalence of 3-6 in 100,000 people worldwide (Toms et al. 2015). Patients with Usher syndrome have congenital sensorineural hearing loss with or without vestibular dysfunction, and visual loss in the form of RP. These symptoms allowed clinicians to classify the disease into three clinical subtypes depending on the severity of hearing loss as well as the presence of vestibular symptoms (Smith et al. 1994; Toms et al. 2020).

Usher syndrome type 1 is the most severe subtype characterised by severe-to-profound congenital deafness, vestibular dysfunction and prepubertal onset of RP in the first decade of life. So far, nine gene loci

have been identified as involved in Usher type 1; USH1B (*MYO7A*, myosin VIIa), USH1C (*USH1C,* harmonin), USH1D (*CDH23*, cadherin-23), USH1E (*USH1E,* unknown), USH1F (*PCDH15,* protocadherin-15), USH1G (*USH1G,* SANS), USH1H (*USH1H,* unknown), USH1J (*CIB2,* CIB2) and *USH1K* (*USH1K*, unknown) (Toms et al. 2015).

Usher syndrome type 2 is the most common form accounting for more than 50% of all cases and exhibits a milder phenotype with moderate-to-severe hearing defects without vestibular dysfunction, and later onset of RP in the second decade of life. In total, three gene loci have been reported as associated with Usher type 2; USH2A (*USH2A*, usherin) the most prevalent accounting for around 57-79% (Lentz et Keats 1993) of this subtype, USH2C (*ADGRV1*, ADGRV1 also known as VLGR1 or GRP98) and USH2D (*WHRN*, Whirlin) (Figure 7)

Lastly, Usher type 3 is the rarest form of Usher Syndrome, involving progressive hearing loss, variable vestibular dysfunction and onset of RP symptoms. Only one gene locus has been described for this subtype, USH3A (*CLRN1*, Clarin-1).

1.4.2.1 Genetics of USH2A

The *USH2A* gene (OMIM: 608400) is located on the long arm of chromosome 1q41, and codes for two usherin transcripts due to an

alternative splicing: a short isoform (a) containing 21 exons leading to a 1546-aa secreted protein (Eudy et al. 1998) and a very large isoform (b) with 51 additional exons (van Wijk et al. 2004). Isoform (b) is predominant in the retina and the cochlear, giving rise to a 5202-aa matrix protein with a predicted total molecular weight of 570 kDa. The long isoform b contains an intracellular region which interacts with the Usher protein network, a short transmembrane domain and a very long extracellular domain with several motifs associated with extracellular matrix proteins such as laminin and fibronectin repeats (van Wijk et al. 2006; 2004). In addition to these two isoforms, a modified exon 71 encoding an additional 24-aa peptide restricted to the inner ear, has also been described (Adato et al. 2005).

The mutation spectrum is very heterogenous and includes over 1500 mutations with more than 600 variants presumed to be pathogenic (LOVD Database, accessed on May 03th, 2023) which span the whole *USH2A* gene, consisting of nonsense, missense, deletions, duplications, splicing variants and pseudo-exon inclusion variants, with no crucial hotspots (Baux et al. 2014). Most are solitary, but several are more prevalent such as the recurrent c.2299delG, pGlu767Serfs*21 (rs80338903) variant (Eudy et al. 1998; X.-Z. Liu et al. 1999; Weston et al. 2000). This is the most frequent pathogenic mutation (Le Quesne Stabej et al. 2012) and responsible for approximatively 24.5% (606/2484) of pathogenic variants in *USH2A* (LOVD database, accessed on 03/05/2023). The c.2299delG mutation has been reported in patients from Northern and Southern

Europe, North America, South America, North and South Africa, and China (Baux et al. 2014) with a particular high allelic frequency of 30.6% in Scandinavia (Dreyer et al. 2008). Investigating the reasons underlying its exceptionally high prevalence through haplotype studies has found evidence of a European common ancestor (Aller et al. 2010; Dreyer et al. 2001). This single pair deletion in exon 13, coding for the fifth laminin-type epidermal growth factor-like domain, results in a PTC presumed to result in a truncated protein and/or target of nonsense-mediated mRNA decay (NMD). Additionally, it has been demonstrated to induce an exonic splicing defect leading to the skipping of exon 13 or both exons 12 and 13 (Lenassi et al. 2014).

Another common pathogenic variant, also located in exon 13 coding for the fifth laminin domain, is the missense mutation c.2276G>T, p.Cys759Phe (rs80338902) accounting for 7.6% of pathogenic variants (LOVD database). The replacement of a cysteine by a phenylalanine has been predicted to disrupt a presumed disulphide bond or lead to the rearrangement of a key region promoting interactions with the extracellular matrix, impairing the function of usherin (Rivolta, Berson, et Dryja 2002; Pérez-Carro et al. 2018). A further relatively frequent mutation driving a diseased phenotype by a different mechanism is the deep-intronic c.7595-2144A>G mutation (rs786200928) in intron 40 of *USH2A*. It induces the addition of a 152 bp pseudo-exon (PE) into the mature *USH2A* transcript between exon 40 and 41 (Vaché et al. 2012). The *USH2A* transcript

containing the aberrant exon is then subjected to the NMD pathway and further degradation (Radulfus WN Slijkerman et al. 2016a).

Apart from *USH2A* pathogenic variants, mutations in *PDZD7* gene (PDZ domain-containing 7) have been suspected to act as a retinal disease modifier in *USH2A* patients, supporting a digenic inheritance model of Usher Syndrome explaining the frequently observed variability of the visual phenotype (Ebermann et al. 2010) but no further studies have found evidence for digenic inheritance (Le Quesne Stabej et al. 2012).

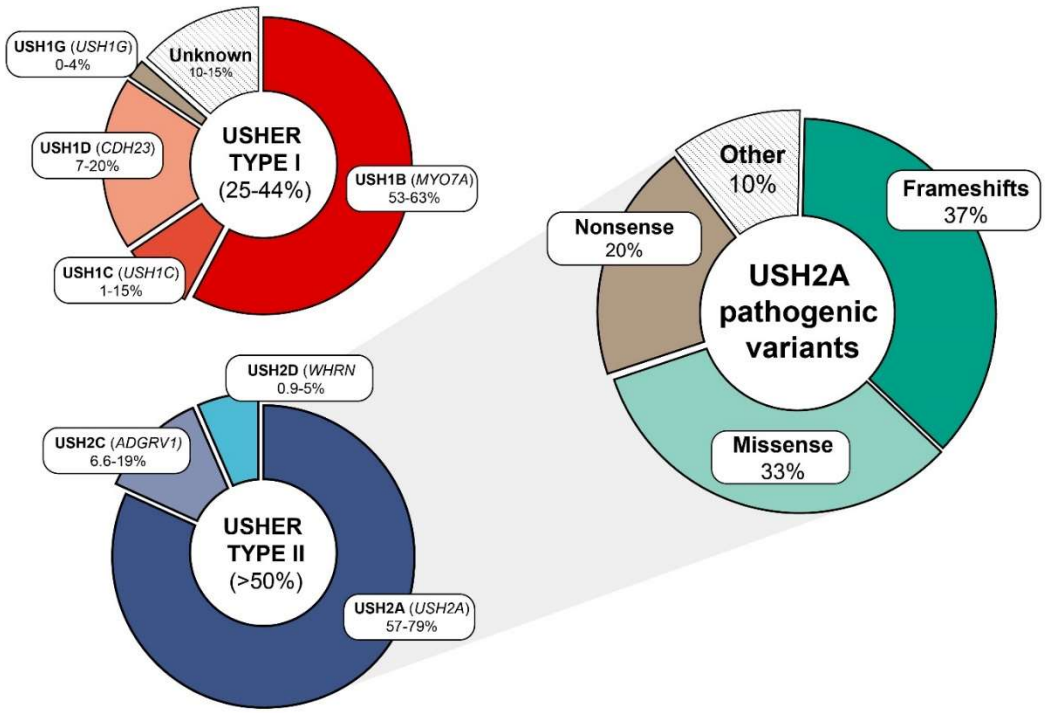

Figure 6. Diagram summarizing the repartition of Usher Syndrome types and *USH2A* pathogenic variants.

1.4.2.2 Understanding USH2A genotype phenotype correlations

Mutations in *USH2A* are responsible for both Usher syndrome type 2 and nsRP, which are distinguished by impaired and preserved hearing function, respectively. Both disorders show autosomal recessive inheritance and therefore, patients must carry two pathogenic allelic variants to drive a diseased phenotype. Accordingly, genotype-phenotype studies have been conducted to understand whether specific mutations were more likely to preserve hearing or to produce a more severe phenotype. Lenassi and colleagues have proposed a model of an allelic hierarchy, where the presence of at least one retinal disease specific *USH2A* allele results in the preservation of normal hearing and leads to nsRP. Retinal disease specific alleles were more likely to be those where some protein function may be preserved. Thus, considered as phenotypically dominant to Usher syndrome type 2 alleles, for instance, carriers of at least one copy of c.2276G>T, p.Cys759Phe (rs80338902) missense mutation are associated with nsRP with preserved hearing function (Lenassi, Vincent, et al. 2015).

In addition to these considerations, the onset and severity of the symptoms have also been investigated. The presence of two null alleles has been described as likely to cause more severe hearing loss and retinal degeneration (Pierrache et al. 2016). In a large *USH2A* patient cohort, nsRP patients were found to become visually impaired 13 years later, based on visual field, and 18 years later, based on visual acuity, than

Usher syndrome type 2 patients. In addition, other studies have shown that the combination of two truncating mutations in *USH2A* causes more severe and progressive hearing impairment compared to the presence of one or two non-truncating mutations (Hartel et al. 2016; Abadie et al. 2012). Overall, it seems that remnant usherin protein function could attenuate both retinal and hearing symptoms. However, a recent study investigating the patterns of degeneration between syndromic and non-syndromic RP patients, relying on autofluorescence ring, area horizontal diameter and ellipsoid width, showed no significant differences between the two groups (Dubis AM, et al. Invest Ophthalmol Vis Sci. 2019;60:ARVO E-Abstract 5172).

Interestingly, differences in cone functionality have been identified when comparing electroretinogram (ERG) responses of syndromic and non-syndromic *USH2A*-related RP. (Sengillo et al. 2017). The Usher type 2 patients displayed a more attenuated 30 Hz-flicker amplitude of 17 μV compared to 2.1 μV in nsRP patients, indicating a reduced cone function in Usher 2 patients compared to those with nsRP. Nevertheless, an identical *USH2A* genotype may also lead to very different phenotypes between patients. A case report of two siblings carrying the same *USH2A* mutations displayed a surprising clinical heterogeneity; the first was diagnosed as having Usher Syndrome 2 while the second sibling had completely preserved visual function, which made it the first reported *USH2A*-related non-syndromic deafness (Lenassi, Robson, et al. 2015).

This intra-familial genotype-phenotype discrepancy raises questions about the role of protective environmental, genetic and epigenetic factors.

1.4.2.3 Usherin protein

In addition to retinal and cochlear expression, it has been shown that usherin isoforms are also expressed in other tissues. The short isoform is secreted in the extracellular matrix and has been described in testis, small and large intestines, uterus and ovary, while the long isoform has been reported in heart and kidneys (Pearsall et al. 2002; Bhattacharya et al. 2002; van Wijk et al. 2004) (Figure 9). More recently, Schwaller and colleagues reported presence of usherin long isoform in mouse hair follicles and Meissner corpuscles (Schwaller et al. 2021).

The usherin long isoform b is predominantly expressed in the adult retina where it localises to the photoreceptor cells (van Wijk et al. 2004; Huang et al. 2002; Eudy et al. 1998). The photoreceptor, the light-sensitive cell of the retina, is composed of an inner segment and an outer segment. The inner segment is mainly responsible for the cell metabolism and protein production while the outer segment is a highly specialized cilia filled with stacks of discs containing photosensitive transmembrane proteins called opsins. The connecting cilium is a narrow collar wrapping the photoreceptor ciliary axoneme. Here, Liu and colleagues were the first to show evidence of a specific usherin long isoform expression in murine photoreceptors, which was spatially restricted to the periciliary membrane

complex (PMC), a structure wrapping the photoreceptor connecting cilium (X. Liu et al. 2007). Similarly, usherin has been specifically localized to the PMC of both cone and rod macaque photoreceptors (Sahly et al. 2012), zebrafish and Syrian hamster photoreceptors (Zou et al. 2019; Dona et al. 2018) (Figure 8).

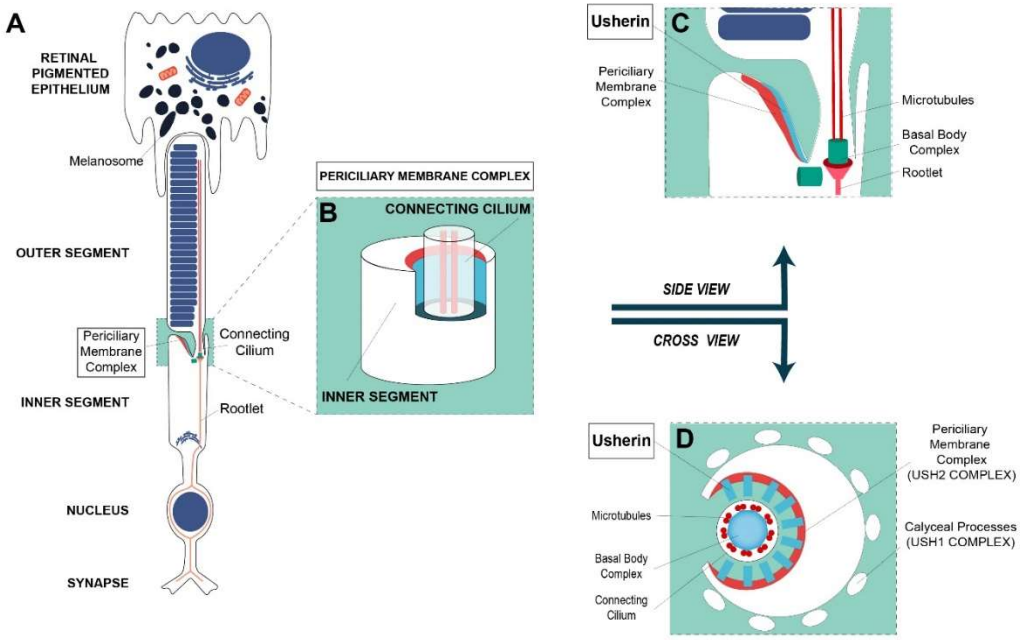

Figure 7. Schematic diagram of usherin localisation in photoreceptors

(A) Cellular organisation of a photoreceptor. The photoreceptor possesses an inner segment and an outer segment, a highly specialised cilia responsible for light detection. The inner segment is followed by the connecting cilium and the outer segment. (B) The connecting cilium is wrapped in the periciliary membrane complex, where the usherin long isoform is spatially restricted. (C) Side view and section (D) of the periciliary membrane complex.

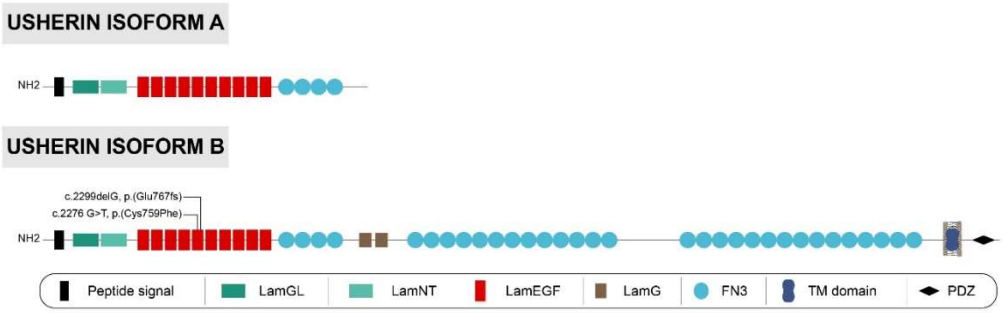

Figure 8. Usherin isoforms in photoreceptor cells.
Usherin isoform a consists of 1 LamG-like jellyroll fold domain (LamGL), 1 Laminin N-terminal domain (LamNT), 10 laminin EGF-like domains and 4 fibronectin type III repeats. Additionally to these domains, usherin isoform b is composed of 2 laminin G domains (LamG), 28 fibronectin type III repeats, a transmembrane domain and an intracellular PDZ-binding domain. The 2 most common mutations (c.2299delG, p.Glu767Serfs*21 and c2276.)

The Usher interactome includes Usher type 2; usherin, the ADGRV1 (USH2C) and whirlin (USH2D). In vitro and in vivo experiments showed that whirlin physically interacts with both usherin isoform b and ADGRV1 isoform b through the association of the whirlin PDZ domain with usherin and ADGRV1 PDZ-binding domains (Reiners et al. 2006). This Usher 2 complex has been localized to the photoreceptor PMC in mice (Yang et al. 2010), zebrafish (Dona et al. 2018) and macaque models (Sahly et al. 2012).

Additionally, it was shown that removal of whirlin long isoform in a murine model resulted in the disruption of Usher 2 complex associated with usherin and ADGRV1 mislocalisation, and reduced usherin expression. Consistently, AAV-mediated whirlin replacement in this whirlin-knockout

mouse model rescued both whirlin expression and Usher 2 complex localization to the PMC (Zou et al. 2011). Furthermore, not only does whirlin play a central role in Usher 2 complex formation but also integrates the Usher 1 protein network by interacting with the unconventional actin-based motor protein myosin VIIa (USH1B), cadherin-23 (USH1D) and protocadherin-15 (USH1F), the scaffold protein SANS (USH1G) and the calcium/integrin binding-protein CIB2 (USH1J). Harmonin (USH1C), SANS (USH1G) and PDZD7, as well as whirlin, are key assembler scaffold proteins at the centre of the Usher protein network (Ralph WN Slijkerman, Kremer, et van Wijk 2017). Harmonin interacts with all Usher 1 proteins (except CIB2) and is linked to the Usher 2 complex via ADGRV1 and usherin binding (Reiners et al. 2005). Similarly, SANS interacts with the same Usher 1 proteins but in addition, binds to both scaffold proteins whirlin and harmonin. Moreover, SANS has been recently described as being part of a protein complex in the photoreceptors involving usherin and whirlin (Sorusch et al. 2017) (Figure 10). Sorusch and colleagues hypothesized that SANS is involved in two distinct functions in photoreceptors; firstly, scaffolding the usher protein complex for intracellular transport through the inner segment and secondly, regulating the cargo transfer from the transport machinery of inner segment to the ciliary transport module at the base of the photoreceptor cilium (Sorusch et al. 2017).

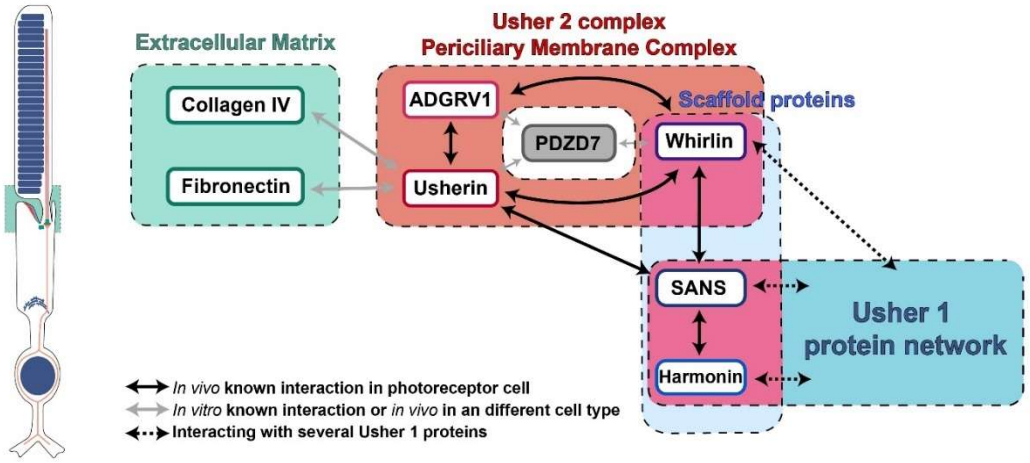

Figure 9. Usherin interacting partners in photoreceptors.

Interacting partners have been divided into 4 groups: the Usher 2 complex periciliary membrane complex (red), the extracellular matrix partners (green), the scaffold proteins (magenta) and the Usher 1 protein network (blue).

In light of *USH2A*-related hearing symptoms, the subcellular distribution of the usherin isoform b has been characterized in the ciliated sensory cells of the cochlea, known as hair cells. Located within the inner ear, sensory hair cells accommodate a mechano-transduction system converting sound-induced vibrations in electric signals (Schwander, Kachar, et Müller 2010). A set of highly specialized microvilli (known as stereocilia) protruding from their apical surfaces, the hair bundle, is responsible for hair cells mechano-sensitivity. Vibration-induced deflection of these stereocilia leads to the opening of a mechano-sensitive ion channel, resulting in depolarization of the hair cell. Usherin isoform b has been localized in the ankle links of the developing cochlear hair cells (X. Liu et al. 2007; Adato et al. 2005; Michalski et al. 2007). The ankle links

form transient fibrous structures spanning between the bases of growing stereocilia, essential for correct development and organisation of the hair bundle. In the developing mouse hair cells, their development occurs at P0-P2 and persists until P9. By P12, the ankle links are no longer detectable (Goodyear et al. 2005). Consistently, several studies have reported similar transient expression patterns of usherin long isoform and ankle links (Adato et al. 2005). Similar observations have been described in cochlear hair cells, with the three proteins being interdependent for preservation of normal subcellular localization at the hair cell ankle links (Adato et al. 2005). The scaffolding protein PDZD7 has also been localized to the stereociliary ankle links of developing hair cells (Grati et al. 2012) coupled with in vitro affinity properties for Usher 2 proteins complex (Chen et al. 2014). Hence, PDZD7 appears as a potential component of Usher 2 complex, especially when considered with the finding that a frame-shift mutation in PDZD7 combined with homozygous *USH2A* mutations was associated with a more severe USH2A-related phenotype (Ebermann et al. 2010).

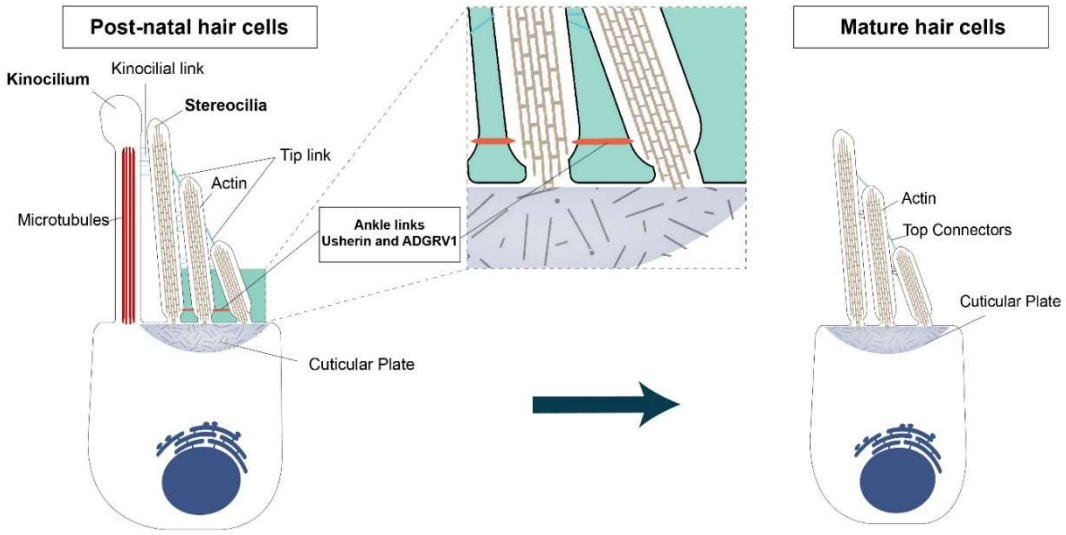

Figure 10. Schematic diagram of usherin localisation in cochlear hair cells.

Hair cells are the ciliated sensory cells of the cochlea responsible for the transformation of sound-induced vibrations in electric signals. The usherin is localised in the ankle link of developing hair cells.

The two main cell types involved in USH2A-related disorders are sensory-ciliated cells. In hair cells, the stereocilia on their apical surface are microvilli-structures while the genuine axonemal cilium is the kinocilium, which degenerate during hair cell development. It plays a critical role in hair bundle formation and polarization (Schwander, Kachar, et Müller 2010) (Figure 11). Similarly, two comparable structures are found in photoreceptors, where the true cilium is the outer segment while the microvilli are the calyceal processes forming a collar around the base of the outer segment. Interestingly, the calyceal processes are conserved in frog, zebrafish and primate photoreceptors. The Usher 1 complex has been localized to the photoreceptor calyceal processes, suggesting a role

in retinal structure maintenance (Sahly et al. 2012). Similar to its role in ankle links for the correct development of hair bundles, usherin could span between the apical inner segment and the connecting cilium internal membrane to strengthen or arrange a proper spacing, ensuring correct maintenance of connecting cilium and outer segment. Additionally, associations with extracellular matrix components could be involved in its structural maintenance function. Supporting this idea, interactions of Usherin LE domain with type IV collagen 7S domain and fibronectin have been characterized (Bhattacharya et al. 2004; Bhattacharya et Cosgrove 2005).

Since Usher syndrome has been proposed to act as a ciliopathy, investigations towards other ciliated cells have been conducted. For instance, sperm abnormalities have been observed in patients with Usher Type 2 associated with atypical axoneme leading to decreased sperm motility and velocity, although contradictory studies have been reported since (van Aarem et al. 1999). However, a study from 1986 suggested cilia axoneme impairment in Usher Syndrome pathogenesis (Hunter et al. 1986). Further evidence suggesting that Usher Syndrome can be classified as a ciliopathy is an accelerated age-related olfactory decline among Usher patients (Ramos et al. 2019; Ribeiro et al. 2016). Additionally, a recent study showed a cilia defect in *USH2A* patient-derived human dermal fibroblasts (HDF) compared to a healthy control, suggesting a role of usherin in ciliogenesis (Samanta et al. 2019).

It remains unknown why the rod photoreceptors degenerate before cones even though usherin is expressed in both. Recently, single-cell RNA sequencing from adult human retinas revealed *USH2A* expression was photoreceptor-specific, but surprisingly was higher in the cones (Cowan et al. 2019). Whether usherin function in cone photoreceptors is less essential to their long-term maintenance compared to rods, or usherin function in rods can be compensated for by cones remains to be found. The discrepancy between the two cell types may help understand the pathogenesis behind *USH2A*-related RP. Further characterisation of usherin protein interacting partners, their function and subcellular localisation will aid in understanding the role of usherin and *USH2A*-related pathogenesis mechanisms.

1.4.2.4 USH2A models

1.4.2.4.1 Cell models

The accumulated knowledge regarding the genetic and clinical characterization of USH2A-related disease has allowed the generation of cell and animal models. Such models have provided invaluable insights into the *USH2A*-related retinal pathogenesis and are essential tools to assess new therapeutic strategies.

To circumvent the limited supply of *USH2A* patient retinal primary cells, human induced pluripotent stem cell (hiPSC) technology offers an unlimited source of retinal tissue preserving a human and patient genetic background. hiPSCs are pluripotent stem cells generated from patient-derived somatic cells, which have the ability to generate retinal cells (Takahashi et Yamanaka 2006). To achieve this, several *in vitro* differentiation protocols of hiPSCs towards a retinal fate have been optimized, leading to the generation of 3D self-organizing optic cup-like structures, known as retinal organoids (Llonch, Carido, et Ader 2018). These *in vitro* models gave rise to organized laminated layers containing all major retinal cell types. Furthermore, the retinal organoids not only follow the naturally occurring *in vivo* retinal development in a stepwise fashion (Meyer et al. 2009) but also display the same transcriptional signature as a normal developing human retina (Cowan et al. 2019; Welby et al. 2017). Significantly, the generated cone and rod photoreceptors contain rudimentary outer segment-like structures, capable of light-responses (Zhong et al. 2014; Hallam et al. 2018). Overall, these elements suggest that retinal organoids are relevant models for human retina.

The derivation of hiPSCs from patients with *USH2A*-related disease offers the opportunity to create the ‘disease in a dish’ and thus dissect the molecular mechanisms and screen innovative therapies. To date, only two publications have reported generation of *USH2A*-retinal cells derived from

hiPSCs. The first study conducted by Tucker et al used a 3D/2D protocol to produce eye-cup-like structures derived from keratinocytes cells from a patient carrying the deep-intronic c.7595-2144A>G mutation (rs786200928) in intron 40 of *USH2A* and the c.12575G>A mutation (rs199605265) *in trans*. While there were no obvious differences indicative of early developmental abnormalities in *USH2A*-derived retinal cells compared to control, they displayed an increased GRP78 and GRP94 expression protein levels, suggesting that ER stress could be involved in *USH2A* pathogenicity in photoreceptors (Tucker et al. 2013).

The second report from Guo et al derived retinal organoids from reprogrammed urine cells of a patient with nsRP carrying the c.9127-9129delTCC and c.8559-2A > G (rs397518039) mutations in *USH2A*. In contrast to the previous study, the investigators found reduced laminin expression, defective retinal progenitor cell differentiation and disorganized neural retina, higher expression of pro-apoptotic and decreased expression of cilium associated genes in patient-derived retinal organoids compared to wild-type controls (Guo et al. 2019). However, these findings were produced from 12-week-old retinal organoids, and usherin expression has not been demonstrated at this time point. In addition, no evidence of interaction between the usherin and its partners such as whirlin or ADGRV1 has been provided. More mature retinal organoids would have been more relevant as supported by single-cell transcriptomic data analysis of retinal organoids exhibiting a high *USH2A* gene expression in 24-week -old retinal organoids (Cowan et al. 2019).

Although limited *USH2A*-related patient-derived retinal organoids have been published, several retinal organoids modelling ciliopathy-related retinal diseases have successfully recapitulated key features of patient retinal phenotype, such as *CEP290*-LCA related ciliopathy (Parfitt et al. 2016), *RP2*-related *RP* (N. Schwarz et al. 2017) and *RPGR*-associated *RP* (Deng et al. 2018). Although they have great potential for advancing our knowledge of *USH2A*-related retinal disease, many challenges remain to be addressed to improve retinal organoid models. Firstly, the generated photoreceptors are not fully developed, with limited OS formation and disc organization, which hampers the understanding of molecular mechanisms and architectural maintenance of photoreceptor cells. In addition, hiPSCs display a high variability to produce layered retinal organoids with photoreceptor cells, depending on the patient, the hiPSC clone and the retinal differentiation protocol (Cowan et al. 2019; Mellough et al. 2019).

1.4.2.4.2 Animal models

Mouse models are a very valuable tool in ophthalmology research, according to the several retinal degenerative mice models that have been characterized (Veleri et al. 2015). Mice are nocturnal animals with a similar retinal organisation to humans. However, the murine retina contains fewer cone photoreceptors than the human retina, and do not possess any enriched cone regions such as the fovea found in primate retina.

1.4.2.4.2.1 Mouse models

An *Ush2a*-null mouse model has been described, displaying complete depletion of both usherin isoforms in the retina and the cochlear (X. Liu et al. 2007). *Ush2a*-null mice exhibited a late-onset photoreceptor degeneration and a non-progressive moderate hearing loss at high frequencies without vestibular dysfunction, recapitulating the main symptoms found in the patients with Usher type 2. Loss of outer hair cells bundles and mislocalisation of usherin partners such as whirlin, PDZD7 and ADGRV1 were observed in the mutant cochlea (Zou et al. 2015). Up to 10 months of age, no phenotypic differences in retinal structure and function were observed in *Ush2a*-null mice compared to wild-type, although Müller cell activation in the mutant retina was described as early as 2 months postnatally, indicative of early retinal stress. By 20 months of age, the photoreceptor nuclei were reduced by half and accordingly, ERG responses were significantly reduced compared to the age-matched wild-type mice, demonstrating a late-onset progressive retinal degeneration. Interestingly, further studies showed red-green cone opsin mislocalisation at P80 in the *Ush2a* mutant mice, prior to wide spread degeneration; however, the mechanisms underlying the retinal disease were not elucidated in this mouse model (Lu et al. 2010).

Another Usher-like mouse model named $KM^{USH/USH}$, displaying spontaneous RP and moderate hearing loss, showed decreased expression in both *Pde6b* and *Ush2a* gene (Yao et al. 2016). The several

point mutations identified in the *Ush2a* gene suggested a causative role of usherin in the *KM*$^{USH/USH}$ usher-like phenotype. However, further studies showed that a base deletion occurring in *Adgrv1* resulting in a nonsense mutation was responsible from the hearing loss phenotype of this model (Yan et al. 2018).

Even if the retinal degeneration has been reproduced in an *Ush2a*-null model, a high phenotypic discrepancy has been described when comparing human patients and other Usher mutant mice. Accordingly, only Ush2a-null and Whirlin-null mutant mice displayed obvious retinal degeneration (Toms et al. 2015). One of the main reasons for the discrepancy between Usher patients and mice could be the absence of calyceal processes in murine photoreceptors, where Usher 1 proteins have been localized and suspected to form an adhesion belt from the apical inner segment to the outer segment basal region in primate retinas (Sahly et al. 2012; Toms et al. 2015)

1.4.2.4.2.2 Zebrafish

Zebrafish (*Danio rerio*) are alternative vertebrate models becoming increasingly popular for research into ocular disease. Human and zebrafish eyes share several common features; the structural organization of the retina is well-conserved with a cone-enriched retina (R Richardson et al. 2017) responsible for acuity and colour vision. In addition, 70% of human genes have at least one zebrafish orthologue, allowing the

recapitulation of disease phenotypes in mutant models (Howe et al. 2013). Regarding the *USH2A* gene, the zebrafish and human usherin protein sequences show 52% identity and 68% similarity with the same domain structure (Dona et al. 2018), supporting a conserved role of usherin between these species.

To date, five different *ush2a* zebrafish models have been generated. Dona and colleagues characterised two *ush2a* zebrafish lines (*ush2a*^{rmc1} and *ush2a*^{b1245}) with protein-truncating mutations, generated using CRISPR/Cas9 (Dona et al. 2018). The mutant zebrafish retinas showed a complete ablation of usherin expression along with a reduction of the other Usher 2 proteins, adgrv1, whirlin A and B, at the photoreceptor PMC. In addition, ERG responses were reduced at 5 days post-fertilization (dpf) compared to age-matched wild-type zebrafish. The photoreceptor degeneration in the larval retina was exacerbated by constant high-level light exposure of 3000 lux up to 8 dpf. Similarly, Han and colleagues reported another *ush2a*-null zebrafish (*ush2a*^{hzu6}) generated using TALEN technology, displaying early retinal dysfunction (at 6-7 days post-fertilization) demonstrated by ERG recordings (Han et al., 2018). Furthermore, levels of rod-specific proteins rhodopsin were reduced from 7 months and shortening of photoreceptor outer segments was described from 12 months. Surprisingly, in contrast to all previous studies, usherin expression in wild-type zebrafish was detected in the ganglion cell layer as well as the photoreceptors. Additionally, *ush2a*^{hzu6} larvae showed

decreased acoustic startle responses indicative of early impaired auditory function.

Recently, the novel CRISPR/Cas9-generated *ush2a*^{u507} zebrafish mutant line was described; unlike the previously reported mutants (*ush2a*^{rmc1}, *ush2a*^{b1245} and *ush2a*^{hzu6}) displaying early defects, this line presented a slowly progressive adult retinal degeneration, with increased apoptotic photoreceptor levels from 6 months post-fertilization. Rhodopsin and blue opsin mislocalisation with lysosome-like structures in the photoreceptors were also observed from 6 months post-fertilization. Following these results, further characterisation of the *ush2a*^{rmc1} revealed a similar pattern in photopigment mislocalisation with elevated autophagy levels at 6 dpf. Defective photopigment trafficking is consistent with the hypothesis of the Usher 2 complex playing a role in docking and fusion of transport vesicles through the connecting cilium to the outer segment (Toms et al. 2020).

In addition, the four *ush2a*-knockout models described, a humanized zebrafish knock-in model for the deep-intronic c.7595-2144A>G mutation in *USH2A* has been generated (R. Slijkerman et al. 2018). Even though only 7.4% of *ush2a* transcripts contained the human pseudo-intron and did not reveal phenotypic changes compared to wild-type zebrafish, antisense-morpholino treatment was able to partially correct the *ush2a* aberrant splicing. Collectively, these zebrafish models are invaluable tools

to better understand USH2A-related pathogenesis and to provide preclinical proof-of-concept for the development of efficient and safe treatments.

1.4.2.5 Therapeutic strategies

To date, no approved treatments are available to alleviate the retinal symptoms of *USH2A*-related disease. Potential therapeutic strategies can be divided in two main types: *USH2A*-targeted therapy, which manipulate levels of *USH2A*; and *USH2A*-independent therapy, which aims to prevent retinal degeneration or through targeting common disease pathways such as cell death or oxidative stress.

It has been almost 50 years since the concept of introducing genetic material into a host cell for therapeutic purposes was formulated by researchers. Gene therapy has had to overcome many pitfalls to reach the clinic, and still has many challenges to address. Regarding the treatment of inherited eye diseases, the eye benefits from its immune-privileged status, accessibility and compartmentalization allowing a restricted spread of the delivered drug.

1.4.2.5.1 Viral approaches

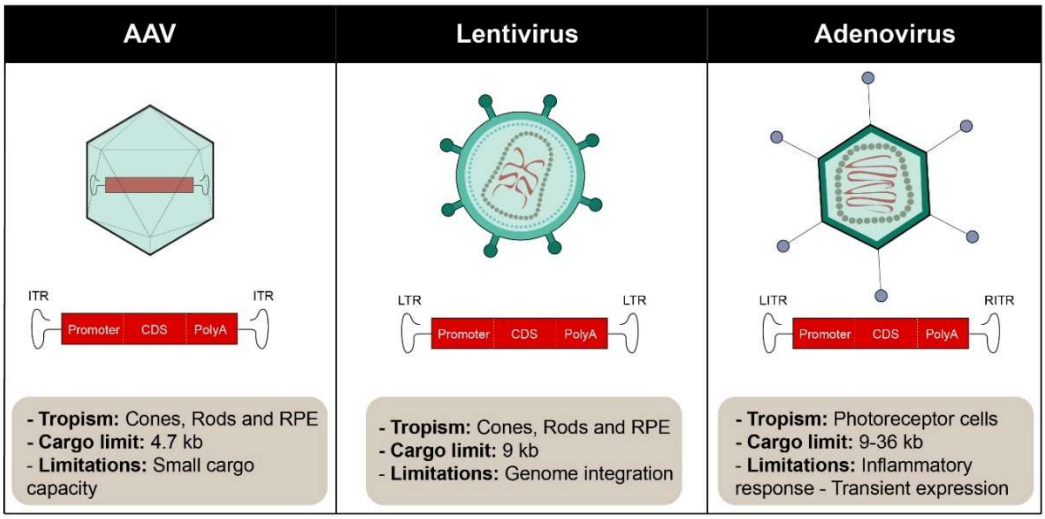

Figure 11. Viral vectors for eye gene therapy.

Although several engineered AAVs transduction efficacy with “enhanced” capsids towards photoreceptor cells have been well documented, the AAV cargo limit is still 4.7 kb (Figure 12). Single AAV particles cannot carry the full USH2A coding sequence (15.6 kb). Therefore, several strategies have been investigated and optimized to overcome AAV carriage limitations. The use of dual and triple AAV has expanded AAV transfer capacity from 4.7 kb to a maximal transfer capacity of 14 kb (Trapani et al. 2014; Maddalena et al. 2018). However, this technology displays a limited efficiency reaching 40% efficacy of a single AAV photoreceptor transduction in pig retina, and still does not spare enough capacity for USH2A cDNA. Recently, Maddalena and colleagues used intein-mediated protein trans-splicing to expand AAV transfer capacity in the retina. Inteins are genetic elements leading to the production of splice-sites in the proteins (Maddalena et al. 2018). They allow the protein to excise itself to

produce a full-length protein without leaving any amino-acid modifications in the final product or without an external energy source. This technology allowed them to efficiently restore *ABCA4* (6.8 kb-long transcript) and CEP290 (7.4 kb-long transcript) protein levels in the retina of two corresponding mouse models. A higher efficiency of transduction was achieved compared to the triple AAV strategy. Nevertheless, intein-mediated protein transplicing via AAV vectors requires the use of cis-regulatory sequences in each AAV, limiting its actual capacity. To translate this strategy to USH2A, more than 5 AAV particles transducing the same photoreceptor cell to produce the full usherin protein would be needed (Figure 13).

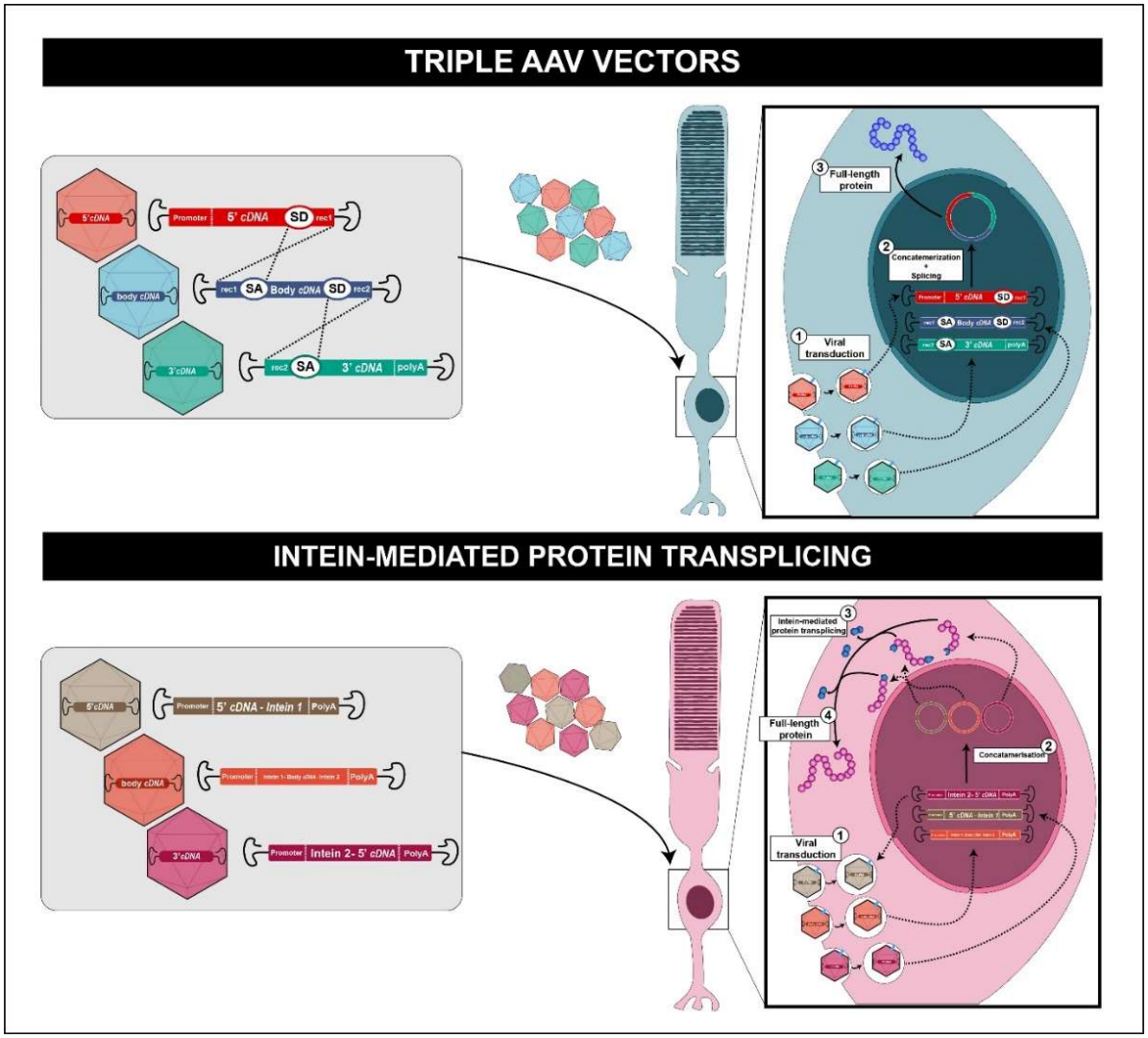

Figure 12. Expanding AAV vector capacity for large gene transfer.

The scheme represents two strategies that allow the successful transfer of large genes. The first strategy on the left panel is based on the concatemerisation and splicing of three transgenes to reconstitute the full-length coding sequence of interest. AAV vectors carrying the three different transgenes transduce the photoreceptor cell. The transgenes concatemerise and splice into a single episome in the nucleus allowing the production of the full-length protein of interest. The second strategy consists of intein-mediated transplicing allowing the reconstitution of the full-length protein. Similarly to the previous strategy, AAV vectors carrying three different transgenes transduce the targeted cell. However, it forms three distinct episomes. The three proteins resulting from these episomes by intein-mediated transplicing, lead to the full-length protein. AAV,adeno-associated virus; CDS, coding sequence; SD, splicing donor; SA, splicing acceptor; rec, recombinogenic region.

To accommodate the full-length USH2A coding sequence, a viral vector with a large carrying capacity would be required. Lentiviral vectors have been investigated for gene therapy, resulting in the terminated clinical trial evaluating the use of recombinant EIAV-based lentiviral vector UshStat for treating USH1B (*MYO7A*) patients (NCT01505062). However, they have a gene size limit of 9 kb and therefore are not able to accommodate the full-length USH2A coding sequence (Lee et al. 2017). Additionally, this clinical trial has been halted due to safety. Alternatively, adenoviral vectors display a sufficient cargo capacity (8 – 36 kb) to carry the full USH2A cDNA, and so would be an ideal candidate for gene replacement. Furthermore, they can efficiently transduce mouse and human retinal cells, such as the Helper-dependent Adenovirus 5 (Puppo et al. 2014; I. C. Han et al. 2019). However, adenoviral vectors are prone to elicit a harmful inflammation response leading to retinal damage (Leikas, Ylä-Herttuala, et Hartikainen 2023). Developing strategies to circumvent innate immune responses would improve the translational development of such viral vectors for large transgene expression in ocular gene therapy.

Another approach for large gene sizes has been applied for Duchenne muscular dystrophy caused by the dystrophin gene (DMD) mutations (11 kb-long coding sequence) where shorter synthetic dystrophin versions, known as microdystrophins, have been developed, allowing to be

transduced by AAV vectors (Le Guiner et al. 2017; D. Duan 2018). This strategy requires an extensive knowledge of the crucial protein domains to ensure a functional protein is produced.

The limitations of viral vectors for gene therapy have encouraged efforts towards the development of alternative strategies. Non-viral synthetic vectors are easier to produce, less immunogenic and most importantly, suitable for larger transgenes. For instance, nanoparticles can accommodate DNA plasmid vectors up to 20 kb and do not limit effective in vivo gene transfer (Fink et al. 2006), which would accommodate the USH2A coding sequence. The use of compacted DNA nanoparticles formulated with polyethylene glycol-substituted polylysine (CK30PEG) containing the *ABCA4* cDNA cassette (6.8 kb) was able to improve the phenotype of an abca4-deficient mouse model, when delivered subretinally (Koirala, Makkia, et al. 2013). Additionally, the carrying capacity of nanoparticles allows the addition of cis-regulatory elements such as promoters, insulators and scaffold-matrix attachment region (S/MAR) sequences (Planul et Dalkara 2017). However, despite extensive research, non-viral methods remain less efficient at transducing cells compared to viral vectors.

1.4.2.5.2 CRISPR-Cas9 editing

As an alternative to gene augmentation therapy, the CRISPR/Cas9 breakthrough has paved the way for the use of gene-editing strategies for

inherited diseases through correction of point mutations and small indels or exon-skipping. It provides a promising option for treating diseases caused by large genes such as *USH2A* whether by correcting the *USH2A* mutation directly in the patient retina or by correcting IPSC-derived photoreceptors for future transplantation.

To date, CRISPR/Cas9 targeting of USH2A involved in vitro editing of the recurrent c.2299delG, p.Glu767Serfs*21 mutation (rs80338903) and c.2276 G>T, p.Cys759Phe (rs80338902) in HEK cell models, patient-derived fibroblasts and hiPSC (Fuster-García et al. 2017; Sanjurjo-Soriano et al. 2019) (Figure 14).

Additionnally, the CRISPR toolbox was enriched with new generations of editing tools such as base editing, which uses an enzyme allowing precise nucleotide transitions, or such as the prime editing, which uses a Cas nickase to nick the targeted DNA strand (Major, McClements, et MacLaren 2023).

Despite proof-of-concept in vitro, for clinical translation there remains many challenges such as eliminating off-targets, and increasing in vivo editing efficiency in post-mitotic cells such as photoreceptors (Burnight et al. 2018).

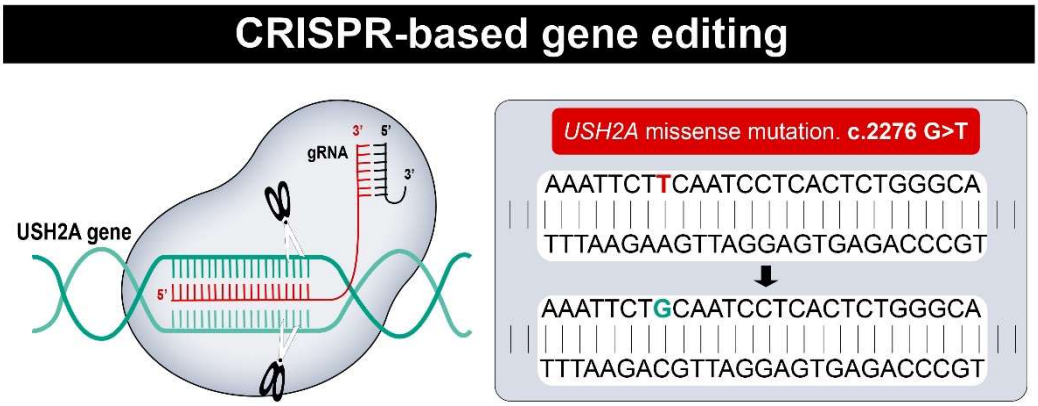

Figure 13. CRISPR-Cas9 editing as a strategy for *USH2A* missense mutation c.2276 G>T.

1.4.2.5.3 Nonsense suppression

As 20% of USH2A pathogenic variants are nonsense mutations, USH2A-related diseases are an ideal target for small translational read-through molecules (TRIDs). The introduction of a premature termination codon leads to either degradation of the mRNA by NMD or premature termination of the translation leading to a non-functional protein. Small compounds, such as ataluren (PTC124) or designer aminoglycosides (NB84), induce ribosomal translation infidelity allowing a near cognate amino acid to compete with a release factor. This allows the premature termination codon to be bypassed, resulting in restored translation with synthesis of up to 25% of full-length protein (Figure 15). This approach has been

investigated in Usher type 1 models (Welch et al. 2007; Rebibo-Sabbah et al. 2007). Notably for USH1C (harmonin) nonsense mutations, the designers NB30, NB54 and PTC124 efficacy were investigated in vitro in HEK cells and in ex vivo mice retinal cultures allowing partial restoration of full-length protein synthesis and its function (Tobias Goldmann et al. 2012; T. Goldmann et al. 2011).

For USH2A-related disease, Neuhaus and colleagues applied PTC124 to a HEK cell model containing a cDNA fragment from c.12550-15996 of usherin long isoform containing the p.Trp3955* mutation and showed a 3.3 fold increase of USH2A expression compared to a DMSO control (Neuhaus et al. 2017). Further studies demonstrated PTC124 efficacy in restoring usherin expression and primary ciliogenesis capability in USH2A patient-derived fibroblasts with the p.Gly3142* (rs397518048) mutation (Samanta et al. 2019). Additionally, the European Medicine Agency (EMA) and the U.S Food and Drug Administration (FDA) has granted Ataluren orphan drug designation for the treatment. Therefore, TRIDs show promise as a safe and cost-effective strategy to treat a range of USH2A nonsense mutations.

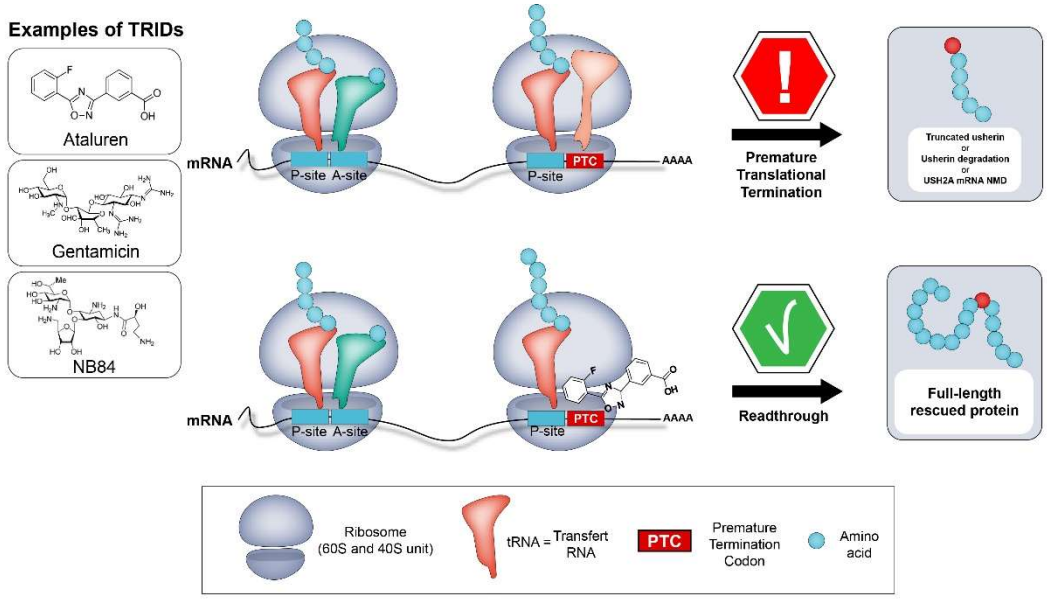

Figure 14. Translational Readthrough Inducing Drugs mechanism of action.

Mutation leading to premature stop codons can result in truncated protein, protein degradation by the proteasome or RNA nonsense-mediated decay. Molecules such as ataluren, gentamicin and NB84, allow readthrough of premature stop codon resulting in the restoration of full-length protein. A-site (aminoacyl) is the first binding site in the ribosome. During protein translation, the P-site holds the tRNA binding to polypeptide chain.

1.4.2.5.4 Antisense oligonucleotides (AON)

Antisense oligonucleotides (AON) are small and versatile RNA molecules that can interfere with mRNA splicing by specifically blocking aberrant splice sites and therefore allowing restoration of correct splicing. Investigations into using AONs for the treatment of inherited retinal diseases have yielded encouraging results (Figure 16). A clinical trial was underway in which QR-110, an RNA antisense oligonucleotide for intravitreal injection, was being tested in patients with Leber congenital amaurosis carrying the deep-intronic mutation c.2991+1655A>G in the

ciliopathy gene centrosomal protein 290 (CEP290) (NCT03140969). The c.2991+1655A>G mutation causes a splicing defect leading to a premature stop codon. QR-110 treatment showed restoration of the correct splicing and resulted in vision improvement at 3 months (Cideciyan et al. 2019). However, although the QR-110 treatment demonstrated statistically significant improvements in visual acuity and retinal sensitivity were reported, it did not meet phase III trial primary endpoints (Russell et al. 2022).

Such strategies are applicable for USH2A patients carrying the deep-intronic c.7595-2144A>G mutation (rs786200928) in intron 40 of USH2A, which introduces a pseudo-exon PE40 (Vaché et al. 2012). Slijkerman and colleagues demonstrated that administration of engineered AON to USH2A patient fibroblasts carrying the c.7595-2144A>G mutation partially restores correct splicing of USH2A mRNA (Radulfus WN Slijkerman et al. 2016b). In addition to the correction of deep-intronic mutations, an AON candidate (QR-421a) has been designed to exclude the whole exon 13 of the USH2A mature transcript (https://www.proqr.com/qr-421a-for-usher-syndrome-type-2/). Given that two of the most common pathogenic USH2A mutations are in exon 13 (LOVD Database), it has been hypothesized that QR421a treatment will result in restoration of a slightly shorter but functional usherin protein. A clinical trial was ongoing in phase 2 in patients with RP due to mutations in USH2A exon 13 (NCT03780257). However, the clinical trial has been halted due to financial constraints.

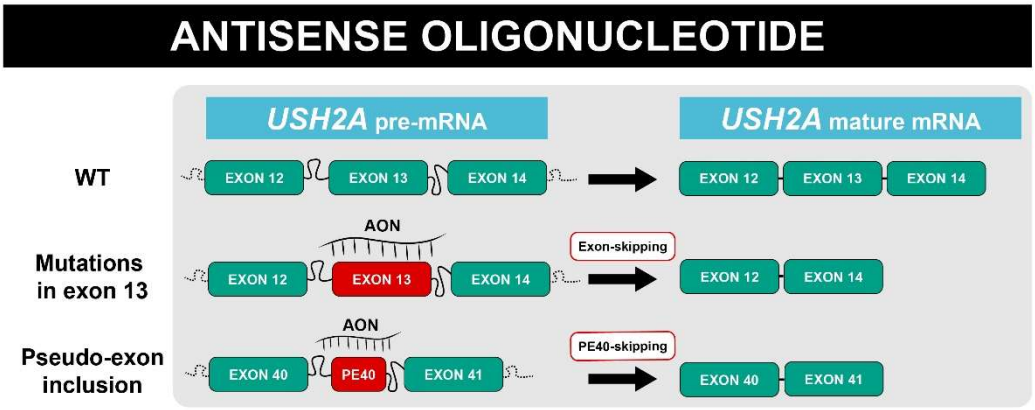

Figure 15. Antisense oligonucleotide for *USH2A* exon 13 skipping

1.4.2.5.5 Other strategies

Retinitis pigmentosa ultimately lead to irreversible degeneration of photoreceptors, first the rods, followed by cones. Gene independent strategies are being considered, which operate by either slowing down the degenerative process or by restoring retinal photosensitivity.

1.4.2.5.5.1 Neuroprotection

Neuroprotective strategies have been investigated to prevent photoreceptors degeneration in several models (Pardue et Allen 2018). For instance, the Rod-Derived Cone Viability Factor (RdVCF), has been shown to slow the rate of cone cell death and to improve cone function in rat and murine models of retinal disease (Byrne et al. 2015) . RdCVF, a truncated thioredoxin-like protein encoded by the nucleoredoxin-like-1 gene (*NXNL1*), is endogenously secreted by rod photoreceptors and promotes retinal cone survival by facilitating glucose uptake and

metabolism. Therefore, loss of rods occurring in the first stage of RP results in cone death. By restoring RdCVF secretion, the cone photoreceptors responsible for the visual acuity of patients would be preserved. This approach would be a gene therapy, amenable by AAV vectors.

Similarly, ciliary neurotrophic factor (CNTF) has been found to prolong photoreceptor survival in mouse and rat models of retinal degeneration (Y. Li et al. 2010; Liang et al. 2001; LaVail et al. 1998). Currently, retinal implantation of capsules containing human NTC-201 cells releasing CNTF is in a phase 2 clinical trial for patients with RP (NCT00447980) (MacDonald, Sauvé, et Sieving 2007; Talcott et al. 2011). However, the neuroprotective strategies for USH2A-related patients are only relevant in the early stages of RP. Once the photoreceptor layer is fully degenerated, strategies to replace photoreceptor function are required.

1.4.2.5.5.2 Optogenetic therapies

Among the different approaches, optogenetic therapies consist of the introduction of light-sensitive proteins, named optogenes, into the remaining cells of the degenerative retina. It has already been shown that targeting the remaining cone cell bodies (Busskamp et al. 2010) with hyperpolarizing optogenes, bipolar cells or retinal ganglion cells (Sengupta et al. 2016; Macé et al. 2015; Berry et al. 2019) with depolarizing optogenes or middle-wave opsin, restores visual responses in mouse models of RP and post-mortem retina of macaque. However, targeting the

remaining cone cell bodies with optogenes does not prevent the cell degenerating. Therefore, a combined neuroprotective strategy such as RdCVF may be of benefit. Currently, two clinical trials are underway using AAV vectors to deliver the optogenes to the cells of interest (NCT02556736 for advanced RP, and NCT03326336 for nsRP).

1.4.2.5.5.3 Cell therapy

Finally, the accessibility of the eye makes it an ideal candidate for cell therapy and retinal prostheses for patients with advanced retinal degeneration. Embryonic stem cell and iPSC technology as well as the extensive research that has led to the optimisation of retinal differentiation protocols, has improved the availability of tissue for transplantation. Photoreceptor transplantation aims to rebuild the photoreceptor layer by grafting in vitro generated photoreceptors (Gagliardi, Ben M'Barek, et Goureau 2019) but many challenges such as the cell product manufacturing and the maintenance of the transplant light-sensitive properties must be addressed. Innovative strategies such as the transplantation of optogenetically engineered photoreceptors demonstrated promising results to ensure a reliable light-sensitive properties of the graft (Garita-Hernandez et al. 2019).

Hypothesis. S/MAR plasmid vectors have the potential to provide persistent transgene expression and rescue the disease phenotype in inherited retinal dystrophies.

1.5 Project aims

Project. To design S/MAR episomal plasmids and assess their efficacy and toxicity in CHM and USH2A human cellular models.

Main aims.

- Clone and validate a S/MAR DNA plasmid vector toolbox for CHM and USH2A
- Rescue CHM model phenotype using CHM S/MAR DNA plasmid vector. In HDF derived from CHM patient. In CHM-hiPSC derived RPE. Rescue USH2A model phenotype using USH2A S/MAR DNA plasmid vector. In HDF derived from USH2A patient. In USH2A-hIPSC derived retinal organoids

Chapter 2. Material and methods

2.1 Cell culture

2.1.1 Human Dermal Fibroblasts (HDFs)

Wild-type (WT), *USH2A*$^{-/-}$ and *CHM*$^{Y42X/y}$ (HDFs) were purchased from Coriell Repository or obtained from skin biopsies. Targeted *USH2A* sequence analysis of the patient cells confirmed compound heterozygosity for the c.2299del p.(Glu767Serfs*21) and c.3187_3188del p.(Gln1063Serfs*15) variants. Cells were cultured in Dulbecco's modified Eagles medium (DMEM) high glucose (Gibco #41966029), 15% foetal bovine serum (FBS) (Gibco #10500064), 1% Penicillin/Streptomycin (pen/strep) (Gibco #15140122). Cells were kept at 37°C, under 5% CO_2 /95% air atmosphere, and 20% Oxygen tension and 80-85% of humidity. When reaching 80% of confluency, cells were passaged using TrypLE Express Enzyme (Gibco™ #12605028) and media was changed twice a week.

2.1.2 Human embryonic kidney 293 cells (HEK293)

Human embryonic kidney 293 (HEK293) cells were cultured in the same conditions as HDFs but with a 10% FBS concentration. When reaching 80% of confluency, cells were passaged using TrypLE Express Enzyme (Gibco™ #12605028) and media was changed twice a week.

2.1.3 Human induced pluripotent stem cells

hiPSCs clones were cultured with mTesR™ Plus (Stemcell Technology™ #05825) in 60mm dish or 6 well-plate coated with Matrigel (Corning® #734-1440) or Geltrex™ (Thermo Fisher Scientific, #A1413302) and passaged once a week using ReLeSR™ (Stemcell Technology™, #05872) when reaching 70-80% of confluency.

2.2 hiPSC reprogramming

HDF were reprogrammed using integration-free episomal vectors from Addgene™: pCXLE-hOCT3/4-shp53-F (Addgene™ #27077), pCXLE-Hsk (Addgene™ #27078), pCXLE-Hul (Addgene™ # 27080) and pCXWB-EBNA1 (Addgene™ ID#37624) (Table 1). Reprogramming protocol was based on a previously described protocol with minor modifications (Okita et al. 2011; N. Schwarz et al. 2015). 1 x 10^6 HDFs were electroporated with 1 µg of each episomal vector using NEON™ transfection system. Electroporated HDFs were plated on 0.1% gelatin-coated 100 mm dish and cultured in HDF media, supplemented with 0.5 mM sodium butyrate (Sigma-Aldrich™ #B5887) until day 7 post-electroporation. Then, HDFs were passaged and plated at a density of 200 000 cells per well on Matrigel (Corning® #734-1440) coated 6 well-plate in mTesR™ Plus. Medium was then changed every 1-2 days until hiPSC colonies appeared

3 to 4 weeks later. Clonal hiPSC were isolated mechanically, and manually passaged for the first four passages.

Episomal Plasmid	Addgene ID	Expression
pCXLE-Hsk	27078	SOX2 and KLF4
pCXLE-Hul	27080	L-MYC and LIN28
pCXLE-hOCT3/4-shp53-F	27077	OCT3/4 and shRNA against p53
pCXWB-EBNA1	37624	transient EBNA-1

Table 1. Episomal plasmids with Yamanaka factors to reprogram HDF to hIPSCs.

2.3 Karyotyping and Short tandem repeat (STR) analysis

DNA was extracted using QIAamp DNA Micro Kit (Qiagen). For low-pass whole-genome sequencing (WGS), libraries were produced using Illumina DNA Prep library prep kit and sequenced on Illumina HiSeq 4000 with paired 100 bp reads. After alignment, copy number estimation was performed using the QDNASeq package (Scheinin et al., 2014). Short Tandem Repeat (STR) profiling was obtained for each cell line with Promega PowerPlex16HS system and was compared back to any available commercial cell banks.

2.4 Random differentiation of embryoid bodies

Embryoid bodies (EB) from hIPSC were generated to the differentiation potential of hIPSC line into the 3 germ layers. iPSCs were passaged and plated in Aggrewell medium (Stemcell Technology™, # 05893), supplemented with 10 µM Y27632 (Sigma-Aldrich™ #B1293), in low adherence plates until they formed EBs in 7 to 10 days. EBs were plated on gelatine-coated plates in DMEM/20% FBS medium and cultured for 2 weeks. Immunostainings were performed, using markers for each of the germ layers (AFP as an endoderm marker, Vimentin as a mesoderm marker and PAX6 as an ectoderm marker).

2.5 Retinal organoid differentiation

HiPSCs were first differentiated into retinal organoids following a previously described protocol A (Gonzalez-Cordero et al. 2017) and into RPE following another one (Reichman et al. 2017).

Briefly, hiPSCs were grown to reach 80-90% confluency At this point, defined as day 0 of differentiation, mTesR™ Plus was replaced by Essential 6TM (Gibco™ #A1516401).

- From day 0 to 2, cells are cultured in Essential 6TM (Gibco™ #A1516401).
- From day 2 to 28, the differentiating cells were subjected to a neural induction medium composed of Essential 6TM, 1% N2

supplement (Stemcell Technology™ #17502048) and 0.1% Pen/Strep.

- From day 21 to day 28, neural retina-like structures emerged from the cell layer and were manually dissected at day 28 using a 21G needle.
- From day 28 to day 35, the isolated 3D retinal-like structures were then further cultured in 6 well-plate in a maturation media composed of DMEM/F12 (Gibco™ #21331020), 1% MEM NEAA (Gibco™ #10370021), 2% B27 supplement (Gibco™ #12587010), 10ng/mL FGF2 (Peprotech™ #100-18B) and 0.1% Pen/Strep. At D28, the dishes containing the 2D cell layer were further cultured for RPE maturation and mechanically expanded.

Then, a new optimized protocol B was used, and resulted in more efficient retinal organoids production for *USH2A* hIPSC clones. The first 2D step was changed.

- From day 0 to day 2, hiPSC were cultured in DMEM high glucose supplemented with 20% KOSR, 10mM Nicotinamide, and 0.1% P/S. From D2 to D28, N2 supplemented was added.
- From day 5 to day 9, KOSR was decreased to 15% KOSR concentration
- At day 7, Nicotinamide is withdrawn from the differentiation media.
- From day 9 to day 28, KOSR concentration is decreased to 10%. The 3D step of protocol B is similar to protocol A. Brightfield images

of differentiating organoids were acquired using an EVOS™ XL Core Cell Imaging System.

2.6 RPE differentiation

hiPSCs were differentiated to hiRPE following a previously reported protocol (Regent et al. 2019). Briefly, hiPSCs were cultured until 80% of confluency, and submitted a to 3 sequential differentiation steps. From day 0 to 7, cells were cultured in DMEM (Thermofisher™ #11965092) supplemented with 20% KSR (Thermofisher™ #108280) and 10mM Nicotinamide (Sigma™ #N3376-100G). Then, Nicotinamide was changed for 100ng/mL Activin A (Stemcell Technology™ #78001) from day 7 to 14. Lastly, Activin A was stopped for 3 µM CHIR99021 (Stemcell Technology™ #72052) from day 14 to 42. On day 42, cells were passaged and further cultured on Matrigel-coated dishes or µ-Slide 8-Well (Ibidi™ #80821) in DMEM/ 4% KSR maintenance media.

2.7 Molecular biology

2.7.1 Polymerase Chain Reaction (PCR)

REP1 cDNA, NA65p and VMD2 sequences were amplified by PCR using CloneAmp HiFi PCR Premix (Takara-Bio #639298) and primers with 15 bp overhangs at their ends allowing the homologous recombination with linearized backbone vector. Reagents were mixed as described in Table 2.

The 25 µL Master Mix was then vortexed and briefly centrifuged before being transferred into 8 individual PCR tubes. The thermal cycles were run as described in Table 2. Finally, PCR fragments were excised and extracted using QIAquick PCR Purification Kit (Qiagen #28104), according to manufacturers' instructions. DNA concentration was measured using Nanodrop 2000C (ThermoFisher scientific #ND-2000C).

Reagent	Volume per reaction	Final concentration
CloneAmp hifi PCR Premix	12.5µl	1X
Primer forward	1µl	0.2µm
Primer reverse	1µl	0.2µm
DNA template	X µl	0.4ng/µl
dH2O	Up to 25µl	-
Total volume	25µl	-

Program	Temperature	Time	Number of cycles
Preheat lid	110°C	-	-
Initial denaturation	95°C	2min	-
Denaturation	98°C	10s	30 cycles
Annealing	Gradient 60°C ± 10°C	15s	
Elongation	72°C	Xs	
Final elongation	72°C	10min	-
Final hold	4°C	Hold	-

Table 2. PCR reaction protocol

2.7.2 Enzymatic restriction digestions

Enzymatic restriction digestions were used to linearized S/MAR plasmid backbones, and as quality control of the recombined plasmids. Briefly, the following reagents volumes (see Table 3) were mixed into a 1.5 mL reaction Eppendorf tube and incubated for 1-4h at 37°C in a heating block, depending on restriction enzymes.

Reagent	Quantity	Volume
S/MAR vector	2-4 µg	-
Restriction enzyme 1	1-3 UI	1-3 µL
Restriction enzyme 2	1-3 UI	1-3 µL
10X Digest Buffer	-	5 µl
dH2O	-	Up to 50 µL
Total	-	50µL

Table 3. Restriction enzyme digestion. (UI = international unit)

2.7.3 Gel electrophoresis

Agarose gels were prepared dissolving agarose in 1X TAE buffer supplemented with peqGreen DNA/RNA dye solution (VWR #732-3196) (see Table 3). PCR fragments and digested vectors were run at 100-120 V for 0.5-1h on 0.8-1.2% agarose gels depending on their size (Table 4).

Reagent	**0.8% agarose gel**	**1.2% agarose gel**
Agarose	4g	6g
1X TAE buffer	50mL	50mL
pegGreen DNA/RNA	6µL	6µL

Table 4. Agarose gel components

2.7.4 In-Fusion Cloning reaction

First, 1-3µg of vector backbone were digested with 1-3 Units of the desired restriction enzyme(s) for 1h at 37°C. The insert was amplified by PCR using specific primers containing 15 bp of homology with the vector as described above, with the CloneAmp HiFi PCR Premix (Takara-Bio #639298). To proceed with the recombination reaction, 100 ng of vector and 50 ng of the insert were mixed with water containing the 5x InFusion mix, containing the appropriate buffer and enzyme to allow homologous recombination between the 15 bp of homology. It was essential that the volume of insert+vector did not exceed 7 µl. In such case, the InFusion reaction volume was doubled. The recombination reaction took place in a water bath at precisely 50°C for 15 minutes. Meanwhile, a 50µl aliquot of *E.coli* Stellar Competent cells was thawed on ice for the transformation (Table 5 and 6).

USH2A cDNA (15606bp) was cloned into S/MAR vector backbones as previously described with several optimizations due to its very large size. *USH2A* cDNA was kindly provided by Professor Luk Vandenberghe. Briefly, *USH2A* cDNA was amplified by PCR using Phusion™ High-Fidelity DNA Polymerase (Thermofisher scientific #F530S) into five fragments of equal size for further in-fusion cloning, piece by piece. In-fusion cloning was optimized to 2:1 vector/insert ratio. The cloning was repeated five times to get the complete *USH2A* cDNA insert in the vector backbone. Finally, enzyme restriction digestions and sequencing of the insert were performed as quality controls.

Gene primers (Cloning)	Sequence 5'-3'	Amplicon size (bp)
REP1_Forward **REP1_Reverse**	aagcaggccggcgacgtggaggaaaaccctgggcccatggcggatactctcccttcg tatcatcgagctcgagttattcagaggactcctctaggtttccaag	2014
NA65_Forward **NA65_Reverse**	ttgattattgactagtagatcttcgaaatactctcagagtgcca caataaagctactagtccaactgcagaatgaagaaggaagtt	761
VMD2_Forward **VMD2_Reverse**	ttgattattgactagtaattctgtcattttactagggtgatgaaattccc caataaagctactagtggtctggcgactaggctg	623
USH2A_1_Forward **USH2A_1_Reverse**	aagcaggccggcgacgtggaggaaaaccctgggcccatgaattgcccagttctttcat cttcgccagatctcgagctcgatgataatgaatgtctaagttaatgcagaaacggagagaca	3234
USH2A_2_Forward **USH2A_2_Reverse**	ccttttgctcacatgtggcattgattattgactagttattaatagtaatcaattacgggg cgccgaggccagatctttattcttcaccggcatctgcatccg	2923
USH2A_3_Forward **USH2A_3_Reverse**	ggggtaccgaagccgctagcatggagagcgacgagagc tatcatcgagctcgagttattcttcaccggcatctgcatccgg	3031
USH2A_4_Forward **USH2A_4_Reverse**	ttgacatgcatgggacgcggaacccctatttgtttatttttc tctcctccctttgcaaaagcctaggcctcc	3030
USH2A_5_Forward **USH2A_5_Reverse**	cttcgccagatctcgagctcgatgataatgaatgtctaagttaatgcagaaacggagagaca tatcatcgagctcgagtcaaacacacttaccagtgaagtctg	3390

Table 5. In-fusion cloning primers

Reagent	Quantity	Volume
Digested S/MAR vector backbone	50-200 ng	-
PCR Fragment	100-200 ng	-
In-Fusion HD Enzyme Premix 5X	-	2 µL
dH2O	-	Up to 10µL
Total	-	10 µL

Table 6. In-fusion cloning reaction mix

2.7.5 Transformation of competent cells

Stellar competent cells (*E. coli* HST08 Strain) were thawed on ice before use. Fifty microlitres of the cell suspension were placed into an Eppendorf tubes. The In-Fusion reaction mix containing the plasmid product was placed on ice and 2.5 µl were added to the competent cells. The cells were incubated on ice for 30 minutes, heat shocked at 42˚C for 45 seconds and then immediately placed on ice for 2 minutes. 450 µl of SOC medium (Invitrogen #15544034) were added to the reaction tube and incubated for 1h at 37˚C (with gentle shaking) to allow their recovery. 100µL of the transformed Stellar competent cell were then spread on Kanamycin LB-agar plates and incubated overnight at 37°C.

2.7.6 DNA isolation and purification

The day after, 3 isolated colonies were picked using a loop and inoculated in Kanamycin LB round-bottomed tubes. The tubes were then incubated overnight at 37° in a shaking incubator. Then, the QIAGEN Plasmid Mini or Maxi Kit (Qiagen #12125) was used to isolate and purify plasmids from bacteria, according to manufacturer's instructions.

2.7.7 Sanger and Plasmidsaurus sequencing

Isolated genomic DNA or plasmids were sent to SourceBioscience for Sanger sequencing or Plasmidsaurus (Plasmidsaurus Inc. Eugene, Oregon) for whole plasmid sequencing. The sequencing primers used are listed in Table 7.

USH2A_seq1	TACTACAGCTTCGTGGTGGACAGC
USH2A_seq2	GAAAGTATTCAGTTCTGTACCCAG
USH2A_seq3	TTGCATCTGGTACTGTGCAAATAG
USH2A_seq4	TTTGCCAGGAATTGTGGTGC
USH2A_seq5	CCTTGTCAATGCAACAGCCATTC
USH2A_seq6	ATGATGTTGGATGTGAGCCC
USH2A_seq7	ACATTACCTGGGACCATTTGTGAC
USH2A_seq11	CTGGAGTCCACCTGATTCTC
USH2A_seq12	CCCAAAGACTAAGTCCACCTAAG
USH2A_seq13	AGCTGTTGCACACTGCTAAATC
USH2A_seq14	GGGTCACCAGTGGAAGTAAC
USH2A_seq15	ATTGACCTTCCGGTTAAATACCAG
USH2A_seq16	AAAGAGCAGAGTGTTTACGAG
USH2A_seq17	GTACTGTTTATACATGGATGGGAG
USH2A_seq18	CCCAAAGCCCACTCATATTCAC
USH2A_seq19	TATTTCAAATAGCCAAGGCAGC
USH2A_seq20	TACTTGAGAACTCCTGGAAATGTC
USH2A_seq21	CACTCATCCAGAACGGAGAC
USH2A_seq22	TTTACACCGAGCCGAGAAGTG
USH2A_seq23	TCTGAGAGACCTGTCTCCCTTCAC
USH2A_seq24	GCTGTCCAGATGAACAGCAC
USH2A_seq25	ATGGAAGCCACAGAACATTG
USH2A_seq26	TGTGCCACCAGTAGCAAGGTAG
USH2A_seq27	AGCCCAATAGCAGATACACTTAC
USH2A_seq28	GCTGGCATTGAAGAGGAGTCTG
USH2A_seq29	TAGAACAGAAAGAGAATGGCCGGG
USH2A_seq30	AGCTGGGCATACCTGTAGCTCTTG
USH2A_seq31	TGCAGCCTTACTCTCAGTATAAC
USH2A_seq32	AGCTGAAGCCATTTCACAGG
USH2A_seq33	CCCACGTTCCATGTGATCTC
USH2A_seq34	TGAGAGTGGTGGCACACAAC
USH2A_seq35	TCCACAAAGAGCCATATATCAGAG
USH2A_seq36	AAGCTGTTTGTTAACTTGCCAACC
REP1_seq1	CATTGCTCTTAGCAGGAAGG
REP1_seq2	TTCGAGAAGGACGAGTGGAACAG
REP1_seq3	TGCAGGATGTGTGCTGTGTTTG
REP1_seq4	GAATTCTGTGGGCTCTTTACTTC
CRB1_c2548GA_seq1	CAGATTTGGCCAGGATGACT
CRB1_c2548GA_seq2	TGATGGAAATGTCCACTTGA
CRB1_c4006-10AG_seq1	GCTTGCTCTGGTTGGTCTTC

Table 7. Sequencing primers list

2.8 Transfections

Transfection of HDFs were carried out using the Neon Transfection System 100 µL kit (Neon Electroporation System # MPK10025). Briefly, cells were dissociated using TrypLE Express and counted using Countess II Automated cell counter. For each transfection, 1 million cells were resuspended in 100 µl buffer R and mixed with DNA plasmid ranging from 1.5 to 10µg and electroporated with the following parameters: 1350V-20ms-2 pulses or 1700V-20ms-1 pulse. GFP expression was monitored by fluorescent microscopy. Media was changed 24 hours after electroporation.

2.9 qRT-PCR

RNA was extracted from HDF or RPE using the RNeasy Plus mini or micro kit from (QIAGEN #74136), according to manufacturer's instructions. cDNA was synthesised from 1 µg of RNA using High-Capacity RNA-to-cDNA™ Kit (ThermoFisher #4387406), according to the manufacturer's instructions. qRT-PCR were performed using SYBR Green Master Mix (ThermoFisher #4309155) on a StepOne Real-Time PCR system (Applied Biosystems), under standard cycling conditions. All samples were assayed in triplicate. The qRT-PCR primers used are listed in Table 8.

Gene primers	Sequence (5'-3')
OCT4 forward	CCCCAGGGCCCCATTTTGGTACC
OCT4 reverse	ACCTCAGTTTGAATGCATGGGAGAGC
KLF4 forward	ACCCATCCTTCCTGCCCGATCAGA
KLF4 reverse	TTGGTAATGGAGCGGCGGGACTTG
SOX2 forward	TTCACATGTCCCAGCACTACCAGA
SOX2 reverse	TCACATGTGTGAGAGGGGCAGTGTGC
LIN28 forward	AGCCATATGGTAGCCTCATGTCCGC
LIN28 reverse	TCAATTCTGTGCCTCCGGGAGCAGGGTAGG
LMYC forward	GCGAACCCAAGACCCAGGCCTGCTCC
LMYC reverse	CAGGGGGTCTGCTCGCACCGTGATG
OCT3/4 plasmid forward	CATTCAAACTGAGGTAAGGG
OCT3/4 plasmid reverse	TAGCG AAAAGGAGCAACATAG
KLF4 plasmid forward	CCACCTCGCCTTACACATGAAGA
KLF4 plasmid reverse	TAGCGTAAAAGGAGCAACATAG
SOX2 plasmid forward	TTCACATGTCCCAGCACTACCAGA
SOX2 plasmid reverse	TTTGTTTGACAGGAGCGACAAT
L-MYC plasmid forward	GGCTGAGAAGAGGATGGCTAC
L-MYC plasmid reverse	TTTGTTTGACAGGAGCGACAAT
LIN28 plasmid forward	AGCCATATGGTAGCCTCATGTCCGC
LIN28 plasmid reverse	TAGCGTAAAAGGAGCAACATAG
EBNA-1 forward	ATCAGGGCCAAGACATAGAGATG
EBNA-1 reverse	GCCAATGCAACTTGGACGTT
PEDF forward	AATCCATCATTCACCGGGCTCTCT
PEDF reverse	TGCACCCAGTTGTTGATCTCTTGC
MERTK forward	AAGGCCGCATTGCTAAGAT
MERTK reverse	CGCGTAGCTATTTCCCACAT
TYR forward	ACTTACTCAGCCCAGCATC
TYR reverse	GGTTTCCAGGATTACGCC
PMEL forward	GCCTGGCAGTGGTCAGCACC
PMEL reverse	CGGGGTAGACGCAGCCAGTGA
ADGRV1_ex8-9 forward	TTGGGTGTTGACACGGAACA
ADGRV1_ex8-9 reverse	CTTTTGCTTGCAAGGGGTCC
ADGRV1_ex27-28 forward	CAAGCACCCTGTGCCATCTT
ADGRV1_ex27-28 reverse	GTGCAGGATCATCAACAGACAG
USH2A_ex13 forward	CCTCCCTGGGACTGTCTGTA
USH2A_ex13 reverse	CAGTTGCAAGGCAGACAGAG
USH2A_ex39 forward	CAGCGGAGAAGAGACAAACC
USH2A_ex39 reverse	TCAAGCTGCCTTGGCTATTT
USH2A_ex69-70 forward	GCTTGGACACCACCCTCTAC
USH2A_ex69-70 reverse	CCCTGGGAGTAGGTTAGGCT
WHRN_ex1 forward	CCCATGCTTCGTCTGGTCAT
WHRN_ex1 reverse	CCTGGTTCCACCAGAGACAC
WHRN_ex6-7 forward	CACGCCAAGTTCTCACTCCT
WHRN_ex6-7 reverse	GGATGAACCCGTGTCACTGT
coGFP forward	GCCGCATGACCAACAAGATG
coGFP reverse	GTTGCTGTGCAGCTCCTCCA

hGAPDH forward **hGAPDH reverse**	GCTGCATTCGCCCTCTTA GAGGCTCCTCCAGAATATGTGA
RPE65 forward **RPE65 reverse**	AGCACTGAGTTGAGCAAGCA GGCCTGTCTCACAGAGGAAG
BEST1 forward **BEST1 reverse**	GTCAGAGGCTCCTCCTTCCT TCTGCTCCACCAGTGTTCTG
MITF forward **MITF reverse**	CCGGGTGCAGAATTGTAACT GGACAATTTTGGCATTTTGG
CRALBP forward **CRALBP reverse**	CACGCTGCCCAAGTATGATG CCAGGACAGTTGAGGAGAGG
USH2A_exon11-15 forward **USH2A_exon11-15 reverse**	AGTTGGTGCAGATCCTTCGG CTTGCACTGGGAACACAAGC

Table 8. qRT-PCR primers list

2.10 Western Blot

Cells were washed with cold PBS twice and lysed with a RIPA cell lysis buffer (ThermoFisher #10017003) supplemented with 1X Protease and Phosphatase Inhibitor Cocktail (ThermoFisher #78441). Cell lysate was centrifuged at 4°C for 15min at 13,000rpm. The protein supernatant was collected, and the concentration was measured using the BCA Protein Assay Kit (ThermoFisher #23227). 15-30µg of each protein sample were boiled at 95 °C for 5 minutes with Nupage sample buffer (ThermoFisher #NP0007) and Nupage reducing agent (ThermoFisher #NP0009). Gel electrophoresis was performed using SDS–polyacrylamide gel (Biorad Laboratories #4569035) and transferred onto an Immuno-Blot PVDF membrane (Biorad Laboratories #1620177). For usherin western blot, gel electrophoresis was performed using NuPAGE Tris-Acetate SDS Running Buffer gel, which was then wet-transferred onto an Immuno-Blot PVDF membrane for 16 hours at 25 V at 4°C. The membrane was incubated in

blocking buffer solution (5% dry milk/0.1%PBS-T) for 1H before incubation overnight at 4°C under agitation with primary antibody diluted in blocking buffer. The membrane was then washed 3 times with PBS/0.1%Tween and further incubated with the secondary antibody diluted in the blocking solution for 1h at room temperature under agitation. The membrane was washed 3 times again before chemiluminescent detection the ClarityTM ECL Western Blotting Substrate (Biorad Laboratories #1705061) and the ChemiDoc MP Imaging system. ImageJ was used to analyse the results.

2.11 Prenylation assays

Cells were placed on ice and washed three times with ice-cold PBS. Then, cells were scraped in PBS supplemented with 1X protease and phosphatase inhibitor cocktails, pelleted in 1.5mL Eppendorf tube and centrifuged 5min at 1500G. The cell pellet was then frozen in liquid nitrogen and kept at -80°C. The cell pellet was then lysed for 15min on ice in a degassed buffer containing 25 mM final HEPES, 50 mM NaCl,2 mM MgCl2, 2 mM DTE (Gebu Biotechnik GmbH #1007), 20 µM GDP (Sigma-Merck #20-177), 1× complete mini EDTA-free protease inhibitors (Roche #11836170001). Cell lysates were then sonicated 3 times for 45 seconds at 40Hz. Then, cell lysates were centrifuged 5min at 1500G and the supernatant transferred to 1.5-ml polyallomer microcentrifuge tubes (Beckman #357448). The collected supernatants were centrifuged at 100,000G for 1h at 4°C using a TLA45 rotor in a Optima MAX-E Beckman Coulter to obtain cytosolic protein extracts. The prenylation assay was performed on the freshly prepared lysate using 5 mM biotin-labelled geranyl pyrophosphate (Jena Bioscience #LI-015) as a prenyl group donor, 0.5 mM recombinant REP1 (Jena Bioscience #PR-105), 0.5 mM recombinant Rab geranylgeranyl transferase (Jena Bioscience #PR-103) and 20 mM GDP in prenylation/lysis buffer at 37°C for 1h [13,57,58]. The prenylation reaction was stopped by adding 6X SDS loading buffer, boiled at 95 °C for 5min and biotin incorporation analysed by western blot.

2.12 Transfection and electroporation

Both electroporation and chemical transfections were used. Electroporation was performed with the 10µL or 100µL Neon transfection kit (Invitrogen # MPK1025) was used. Chemical transfections were performed with JetOptimus Chemical reagent (Polyplus transfection #117-01). Briefly, 200,000-400,000 cells were seeded in 6-well plate or 50,000-100,000 cells in 24 well-plate and left in culture for the next day. DNA plasmids vectors were diluted in JetOptimus Buffer. JetOptimus Reagent was then added and vortexed. The mix was then incubated for 10min at room temperature. The DNA/Jet Optimus solutions were distributed dropwise in the well.

2.13 Ciliation assays

HDFs were cultured to reach 70% of confluency in a T75 flask and then subjected to a 48h-long serum starvation. Cells were then passaged and seeded in 12-well plates on sterilised coverslips. 24h later, cells were washed in PBS 2 times and fixed in ice-cold methanol for 10min. Fixed cells were then washed 3 times in PBS/0.1% tween and permeabilized 1 hour in PBBS/0.5%triton. Then, cells were incubated overnight at 4°C with primary antibodies. The day after several washes with PBS/T, cells were incubated one hour with the secondary antibody, washed again, the coverslips were mounted using Diamond Antifade Prolong Mounting medium with DAPI (Invitrogen # P36962). Cells were imaged using a Zeiss

LSM510 upright confocal microscope. Cilia were counted and measured on ImageJ using 3 independent experiments.

2.14 Immunostaining of hiRPE

hiRPE cells were fixed in 4% paraformaldehyde (PFA) for 10 min at room temperature and washed 3 times for 10min with PBS/0.1% Tween. After 1h in blocking solution (10% FBS in 0.1% Triton PBS) at RT, cells were incubated with primary antibodies overnight at 4 °C. After 3 washes of PBS/0.1% Tween, cells were incubated with fluoroconjugated secondary antibodies and DAPI for 1h at room temperature. Further washes PBS/0.1% Tween were performed. Images of hiRPE were acquired using an EVOS™ XL Core Cell Imaging System or a Leica LSM 710 confocal microscope.

2.15 Cryosections and immunostaining

Retinal organoids were washed in PBS and fixed in 4% PFA for 15min at 4°C. Fixed organoids were incubated in a PBS/30% sucrose solution overnight at 4°C and embedded in a solution of PBS/7.5% gelatin/10% sucrose. Gelatin blocks included with OCT were then frozen in isopentane at -50°C. 10 µm-thick cryosections were processed using a Leica CM1850 Cryostat and mounted on SuperFrost Plus™ Adhesion slides (VWR™ # 631-0108).For immunostaining, cryosections were washed in PBS, permeabilized in 0.5 % Triton X-100/PBS for 1h at RT and blocked in 0.2% gelatin/0.25% Triton X-100/PBS for 1h at RT. Sections were incubated with

primary antibodies (Table 9) overnight at 4°C, followed by 3 washes in Tween 0.2%/PBS and an incubation with fluorochrome-conjugated secondary antibodies for 1 h at RT. After several washes in Tween 0.2%/PBS, the sections were mounted and counterstained using ProLong™ Diamond Antifade Mountant with DAPI (Invitrogen™ #P36962). The slides were imaged using a Leica LSM 710 confocal microscope and were analyzed using ImageJ software.

Antibody	Species	Supplier	Application	Dilution
Arl13b	Rabbit	Thermo	IS	1/500
VSX2	Mouse	Santa-Cruz	IS	1/500
PAX6	Rabbit	Biolegend	IS	1/500
Whirlin	Guinea Pig	Van Wijk Lab	IS	1/300
B-actin	Mouse	Sigma	WB	1/5000
Vinculin	Mouse	Santa-Cruz	WB	1/2000
RHO 4D2	Mouse	Abcam	IS	1/500
ZO-1	Rabbit	Abcam	IS	1/500
MITF	Mouse	Invitrogen	IS	1/500
OCT4	Mouse	Santa-Cruz	IS	1/100
SSEA3	Rat	Millipore	IS	1/50
Vimentin	Mouse	Santa-Cruz	IS	1/300
RCVN	Rabbit	Sigma	IS	1/300
OTX2	Rabbit	R&D Systems	IS	1/500
REP1	Mouse	Santa-Cruz	WB	1/1000
CRX	Mouse	VWR	IS	1/1000
GNAT1	Mouse	Insight Biotech	IS	1/300
Acetylated Tubulin	Mouse	Sigma	IS	1/1000
PNA	Lectin	Vector Lab	IS	1/1000
GD3	Mouse	Abcam	IS	1/300
AFP	Mouse	Santa-Cruz	IS	1/100

Table 9. List of antibodies. IS= Immunostaining WB= Western blot

2.16 Statistical analysis

Statistical analysis was performed using GraphPad Prism 8. All data are expressed as mean ± SD of when at least three independent experiments. Shapiro-Wilk normality test was initially carriedout to determine if data is normally distributed, and appropriate statistical test was chosen. Paired or unpaired t-test were performed to compare two groups, depending on experimental design. $p < 0.05$ was considered significant.

Chapter 3. Design and validation of REP1-S/MAR and USH2A-S/MAR vectors

3.1 Introduction and aims

Gene therapy starts with a reliable and relevant DNA design. This is the case for viral and non-viral strategies. DNA vector components are crucial for transgene expression level and duration, but also its toxicity. Promoters, cis-regulatory elements, size of the DNA vectors, bacterial backbones for plasmid-based strategies or inverted terminal repeats (ITRs) for AAV strategies, must be chosen carefully, as they are decisive in the development of an efficient and safe gene therapy.

The aim of this study to create a S/MAR DNA toolbox for *CHM* and *USH2A* retinopathies in collaboration with Pr. Richard Harbottle's team (DKFZ, Germany). His research focuses on tailoring the best DNA vectors for the genetic modifications of cells. One of the key aspects of their plasmid-based vectors are the use of S/MAR sequences (see Introduction).

The aim of this chapter was to successfully insert the *CHM* coding sequence (CDS) (1,962bp) or the *USH2A* CDS (15,609bp) into S/MAR vector backbones with several promoters to tailor an alternative to viral gene therapy for Choroideremia or Usher syndrome type 2A retinopathies. As depicted in the graphical abstract (Figure 17), the S/MAR backbones

were digested with XhoI and BmgBI restriction enzymes, cutting out the Puromycin resistance cassette (the white cassette on Figure 19). The gene of interest (GOI) coding sequence (CDS) was then inserted in the digested S/MAR plasmid backbones using an in-fusion cloning kit.

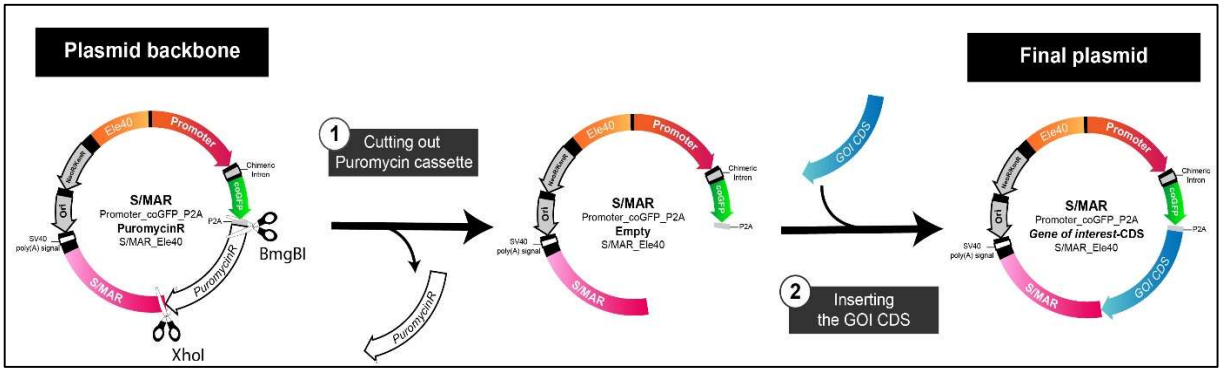

Figure 16 Graphical abstract of cloning process to develop a S/MAR DNA vector toolbox CHM and USH2A retinopathies.

Plasmid backbones containing a promoter, a chimeric intron, coGFP coding sequence, P2A self-cleaving peptide, a puromycin cassette, a S/MAR, a SV40 polyA signal, an insulator Ele40 and a bacterial backbone containing an Ori and a Neo/Kan resistance cassette. The first step of the process is cutting out the puromycin cassette and the second one to insert the gene of interest coding sequence (GOI CDS).

3.2 Inserting the human *CHM* CDS into S/MAR vectors

The *CHM* CDS is translated into the REP1 protein. For a better understanding, the plasmids containing the *CHM* CDS will be referred as REP1-S/MAR plasmids. To clone these vectors, the CMV-PuroR-S/MAR and CAG-PuroR-S/MAR backbones were digested using XhoI and BmgBI. As described in Figure 20, the Puromycin resistance cassette was discarded in both backbones (600bp-long fragment). *CHM* CDS (1962bp) was then amplified by PCR with primers containing 15-bp overhangs and cloned into the CMV-S/MAR and CAG-S/MAR backbones. The in-fusion cloning reaction was incubated for 15 min at 50°C and transformed into Stellar competent cells (*E.coli* HST08 strain). The competent cells were then grown on LB Agar plate with 50µg/ml Kanamycin, to select the clones.

Then, putative CMV-REP1-S/MAR vectors and CAG-REP1-S/MAR were digested using HindII and ran on an 0.8% agarose gel. As expected, digested CMV-REP1-S/MAR and CAG-REP1-S/MAR displayed the expected band sizes (Figure 18):

- For CMV-REP1-S/MAR: 9339bp, 1826bp and 1230bp-long bands
- For CAG-REP1-S/MAR: 9339bp, 2651bp, 1826bp and 1230bp-long bands

These vectors were then maxiprepped and were sent for Sanger sequencing.

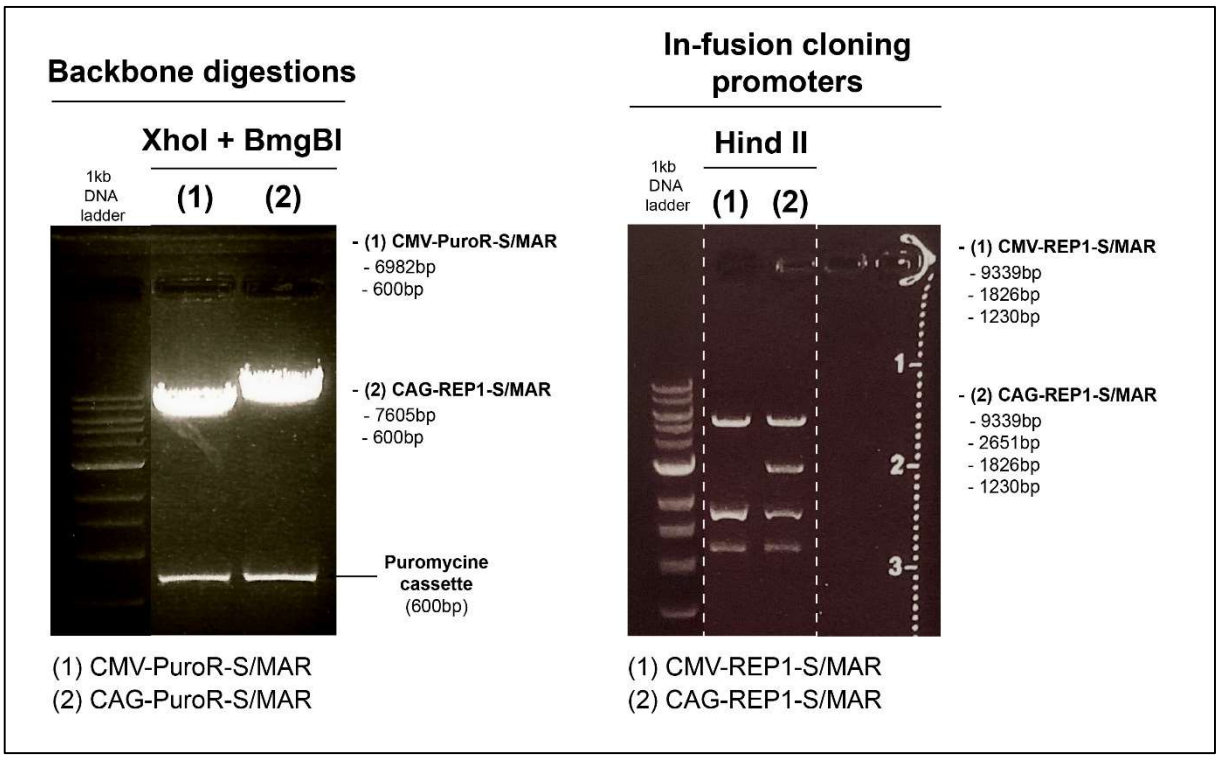

Figure 17. In-fusion cloning of CMV-REP1-S/MAR vectors and CAG-REP1-S/MAR.

CAG and CMV-PuroR-S/MAR were digested using XhoI and BmgBI to cut out the puromycin resistance cassette (600bp) and ran on a 0.8% TAE-agarose gel to separate the two bands. *CHM* CDS was cloned into these backbones, and the resulting plasmids were digested with HindII as a quality control.

To clone REP1-S/MAR vectors with RPE-specific promoters, both NA65 and VMD2 sequences were successfully amplified by PCR (Figure 19). NA65 and VMD2 amplicons were 761bp and 623bp-long respectively.

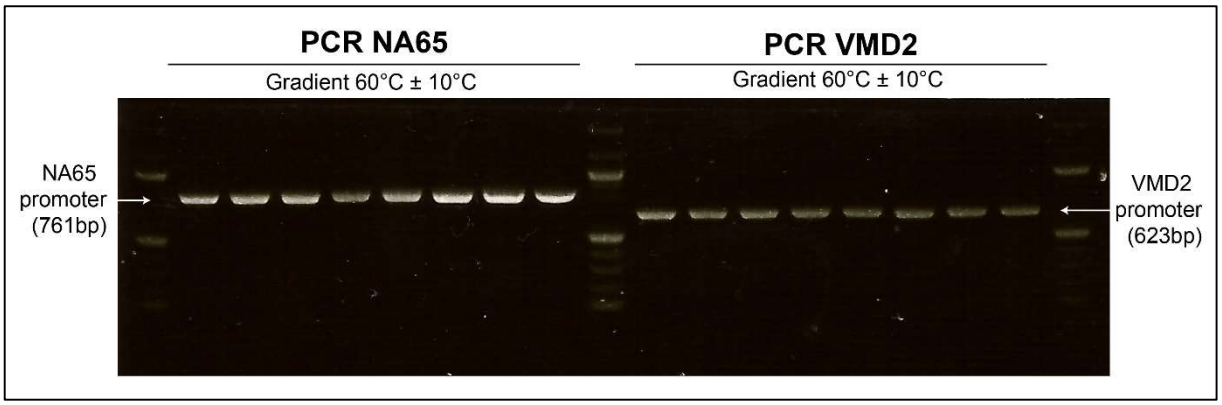

Figure 18. PCR amplification of NA65 and VMD2 promoter sequences.

PCR amplified fragments were ran on 1.2% agarose gel. A gradient of 60°C ±10°C was applied for the PCR annealing temperature. NA65 and VMD2 promoter are 761bp-long and 623bp-long respectively.

CMV-REP1-S/MAR and CAG-REP1-S/MAR were digested using BcuI, in order to cut out the CMV (591bp) and CAG (1620bp) promoters from the backbones (Figure 20). The two fragments (7956bp and 7943bp) were harvested using a gel extraction kit and purified for further in-fusion cloning. The in-fusion cloning was performed using a molar ratio of 1 vector for 1 insert (NA65 or VMD2 fragment). To validate the NA65-REP1-S/MAR and VMD2-REP1-S/MAR vector sequences, the plasmids were digested using EcoNI restriction enzymes. The digestions produced the expected bands (Figure 20):

- For NA65-REP1-S/MAR: 6215bp and 2501bp-long bands.
- For VMD2-REP1-S/MAR: 6185bp and 2393bp-long bands

These vectors were then maxiprepped and were sent for Sanger sequencing.

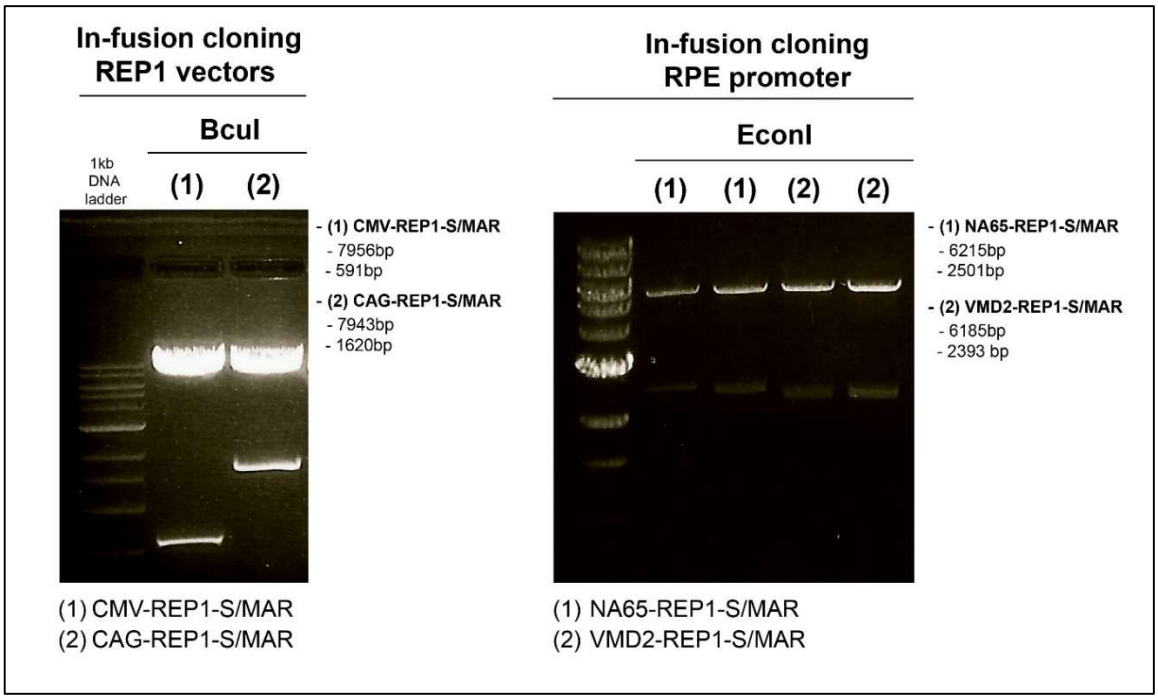

Figure 19. In-fusion cloning of NA65-REP1-S/MAR vectors and VMD2-REP1-S/MAR.
CAG and CMV-REP1-S/MAR were digested using BcuI to cut out the CMV (591bp) or the CAG (1620bp) promoter and ran on a 0.8% agarose gel to separate the two bands. PCR-amplified NA65 and VMD2 were cloned into these backbones, and the resulting plasmids were digested with EconI as a quality control.

Additionally, following the same process depicted in Figure 20, CHM CDS was cloned in several S/MAR vectors backbones. The 17 resulting REP1-S/MAR plasmids are listed in Table 10.

CHM S/MAR plasmids								
		Promoter						
		CMV	CAG	hPGK	EF1a	CHMp	NA65	VMD2
S/MAR sequence	INFb S/MAR Spliced	8,607 bp	9,625 bp	8527 bp	8661 bp	7850 bp	8716bp	8578bp
	ApoL/MAR Spliced	7,449 bp	8,467 bp	7369 bp	7503 bp	6692 bp		
	ApoL/MAR Core Spliced	7,175 bp	8,193 bp	7095 bp	7229 bp	6418 bp		
	INFb S/MAR Spliced	7,369 bp	8,387 bp	7289 bp	7423 bp	6612 bp		
	ApoL/MAR Spliced	6,211 bp	7,229 bp	6131 bp	6265 bp	5454 bp		
	ApoL/MAR Core Spliced	5,937 bp	6,955 bp	5857 bp	5991 bp	5180 bp		

Table 10. REP1-S/MAR toolbox. 3 different S/MAR sequences and 7 promoters have been used in this toolbox.

3.3 Inserting the full-length human *USH2A* cDNA into S/MAR vectors

The aim of these experiments was to successfully insert *USH2A* cDNA (15,606bp) into S/MAR vector backbones with ubiquitous promoters (CAG and CMV). S/MAR DNA plasmid vectors can accommodate the full *USH2A* coding sequence and so, is a potential method for *USH2A*-related gene augmentation therapy. However, the full-length *USH2A* cDNA sequence is 15,609 bp, which is challenging to amplify without any mutations and to clone into a plasmid DNA vector. *USH2A* CDS was kindly provided by Professor Luk Vandenberghe from a plasmid template (pUC57-CMV-hUSH2A). The cloning process went through several optimizations due to its very large size. Different approaches were considered. The first one was to clone the full USH2A CDS in one cloning, similarly to what has been performed for the REP1-S/MAR plasmids. However, performing an efficient PCR of 16kb-long amplicon without mutation has been challenging, most attempts failed (Figure 21).

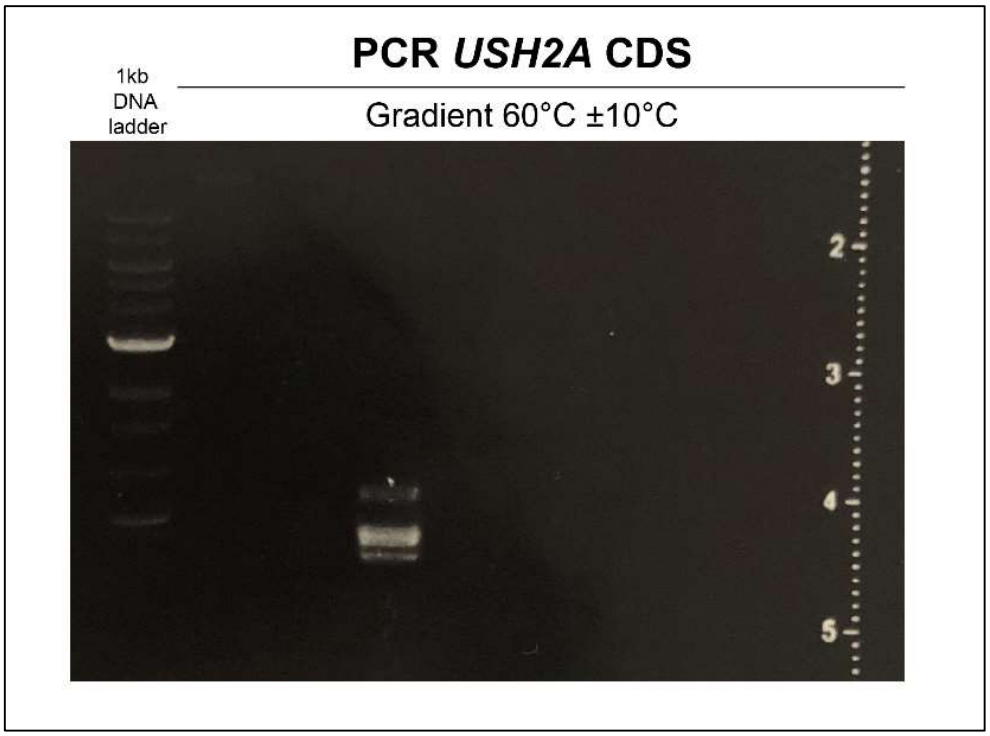

Figure 20. Failed PCR amplification of full USH2A CDS.
PCR amplified fragments were ran on 0.7% agarose gel. A band at 15,6-kb-long was expected, but no amplicons were produced. A gradient of 60°C ±10°C was applied for the PCR annealing temperature.

The second approach was to insert the S/MAR backbone in the *USH2A* CDS as described in Figure 22. The rationale was to change the insert/backbone ratio as the *USH2A* CDS (15.6kb) was 2.5 larger than the actual S/MAR backbone (6.5kb).

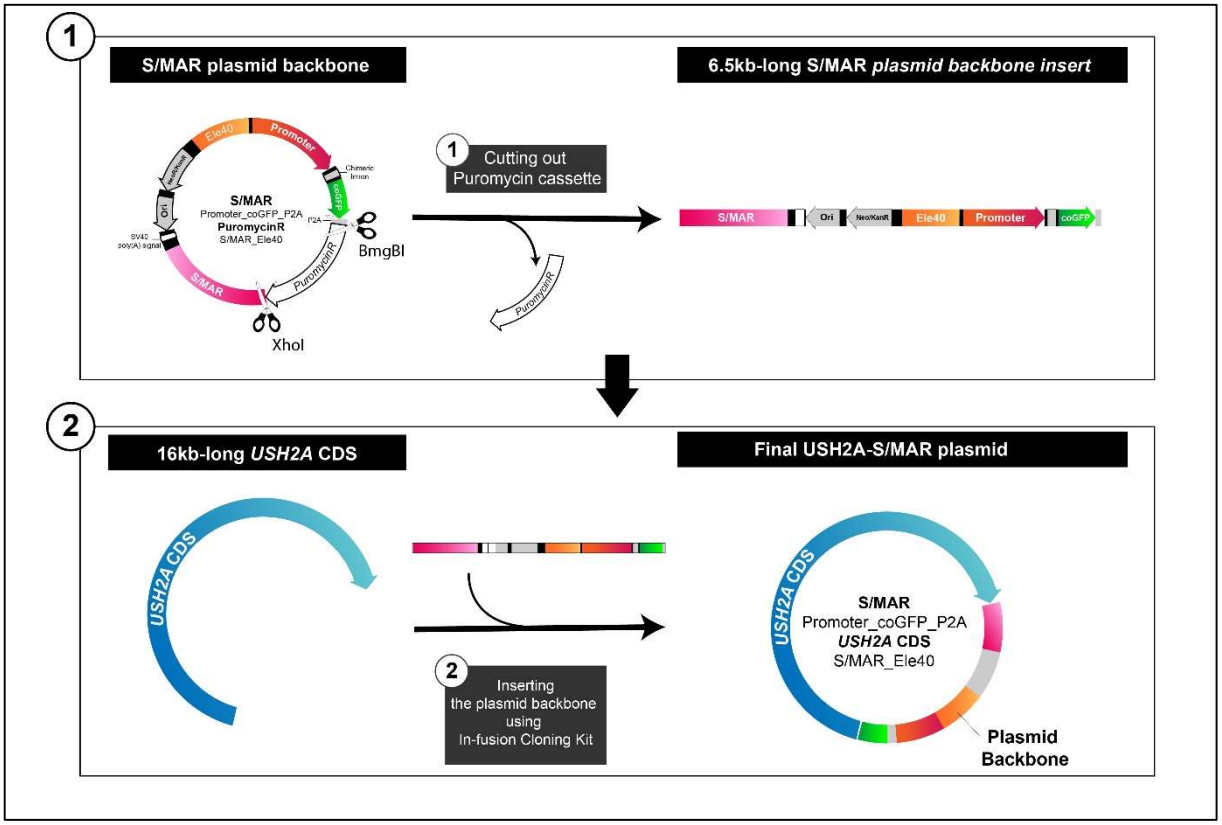

Figure 21. Strategy 2 to clone a USH2A-S/MAR DNA vector.
Plasmid backbones containing a promoter, a chimeric intron, coGFP coding sequence, P2A self-cleaving peptide, a puromycin cassette, a S/MAR, a SV40 polyA signal, an insulator Ele40, considered as a 6.5kb-long insert, and a 16kb-long *USH2A* CDS backbone.

The third approach was to amplify the *USH2A* CDS by PCR using Phusion™ High-Fidelity DNA Polymerase (Thermofisher scientific #F530S) into five fragments of equal size (~3000 bp) using primers with overhangs (Figure 23) allowing efficient in-fusion cloning recombination and introducing enzymatic restriction sites into S/MAR vector backbones previously digested with XhoI+BmgBI.

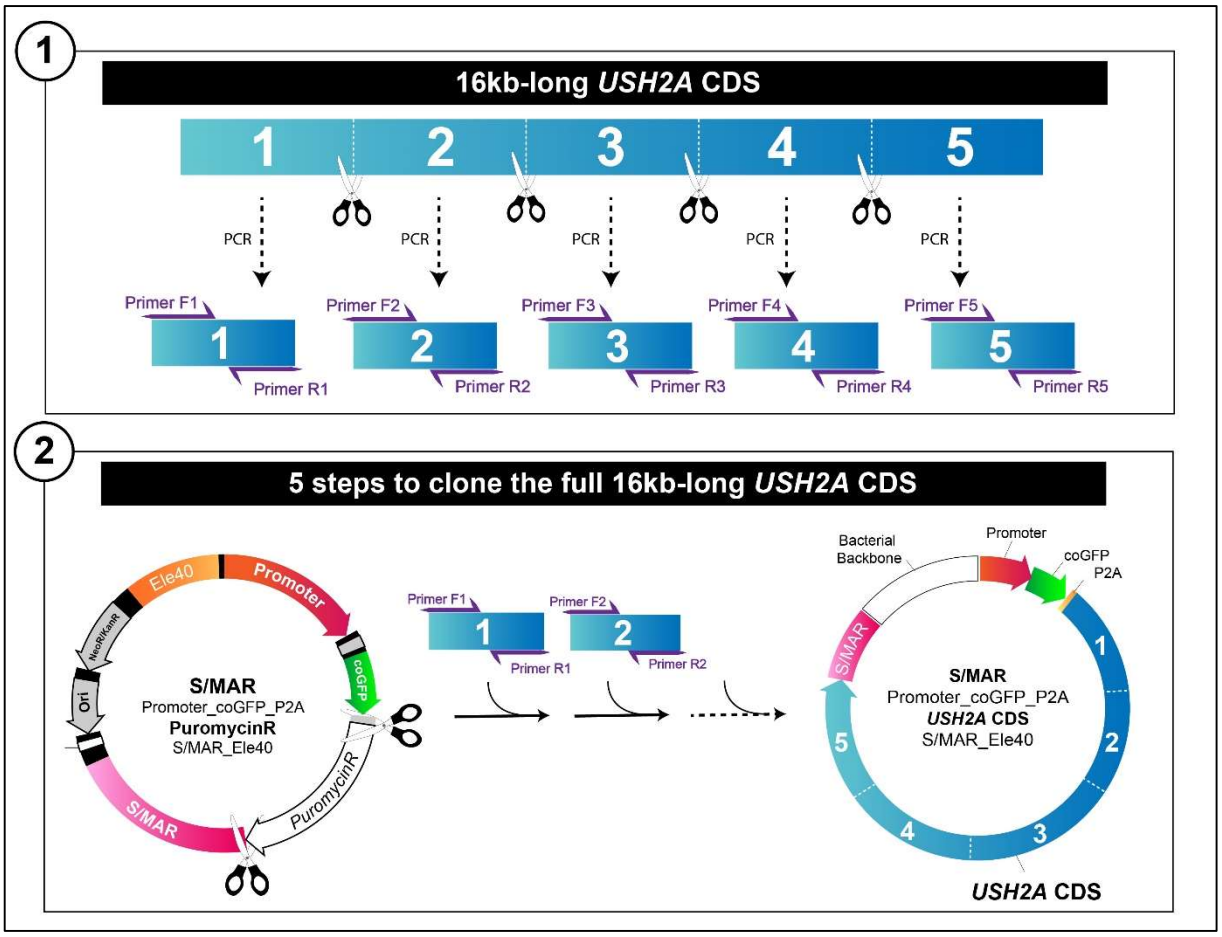

Figure 22. Strategy 3 to clone a USH2A-S/MAR DNA vector
(1) PCR was performed to amplify each *USH2A* fragment. (2) USH2A S/MAR vectors were generated in 5 five cloning steps by inserting a fifth of the 16kb-long *USH2A* CDS in the S/MAR backbone at each step.

The first primers efficiently amplified the fragment 1, 2 and 3 but fragment 4 and 5 failed at first. New primers were ordered, and I manage to amplify fragment 4 and 5 (Figure 24).

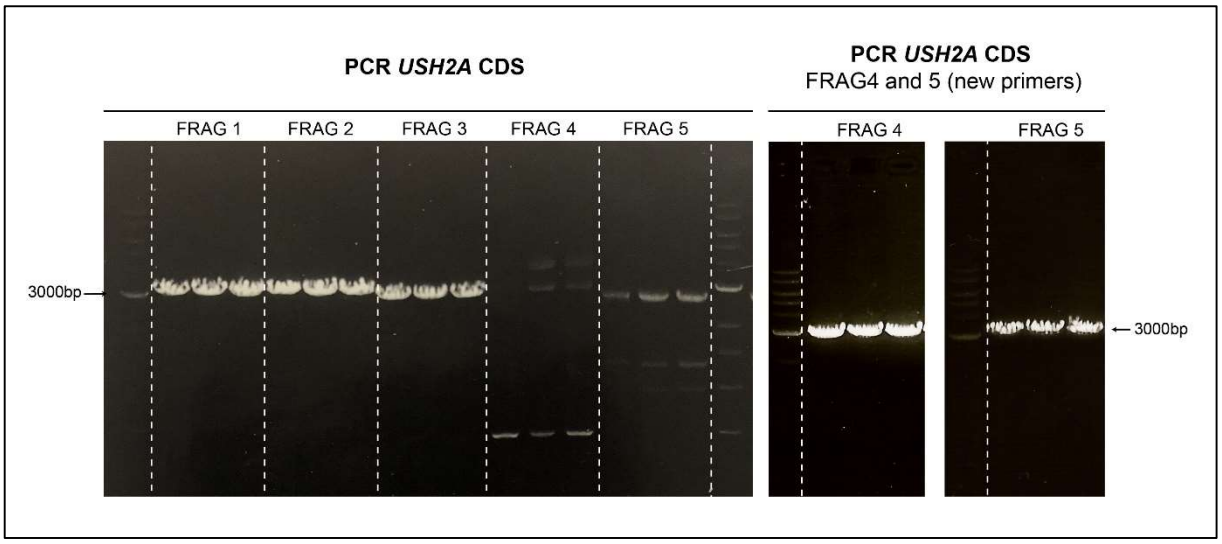

Figure 23. PCR amplification of *USH2A* CDS fragments.

PCR amplified fragments were ran on 0.8% agarose gel. Amplicons at the expected sizes were observed for Fragment 1, 2 and 3 but not for Fragment 4 and 5.

In-fusion cloning was optimized to a 2:1 vector/insert ratio. The cloning was repeated five times to get the complete *USH2A* cDNA insert in the vector backbone, as described in Figure 25. The two vectors generated either had ubiquitous CAG (CAG-*USH2A*-S/MAR) or CMV (CMV-*USH2A*-S/MAR) promoters. The vectors also contained the green fluorescent protein (GFP) gene from the copepod species *Pontellina plumata* (also known as copGFP). CAG-*USH2A*-S/MAR and CMV-*USH2A*-S/MAR were 22.2kb and 23.2kb in size, respectively, as described in Table 11.

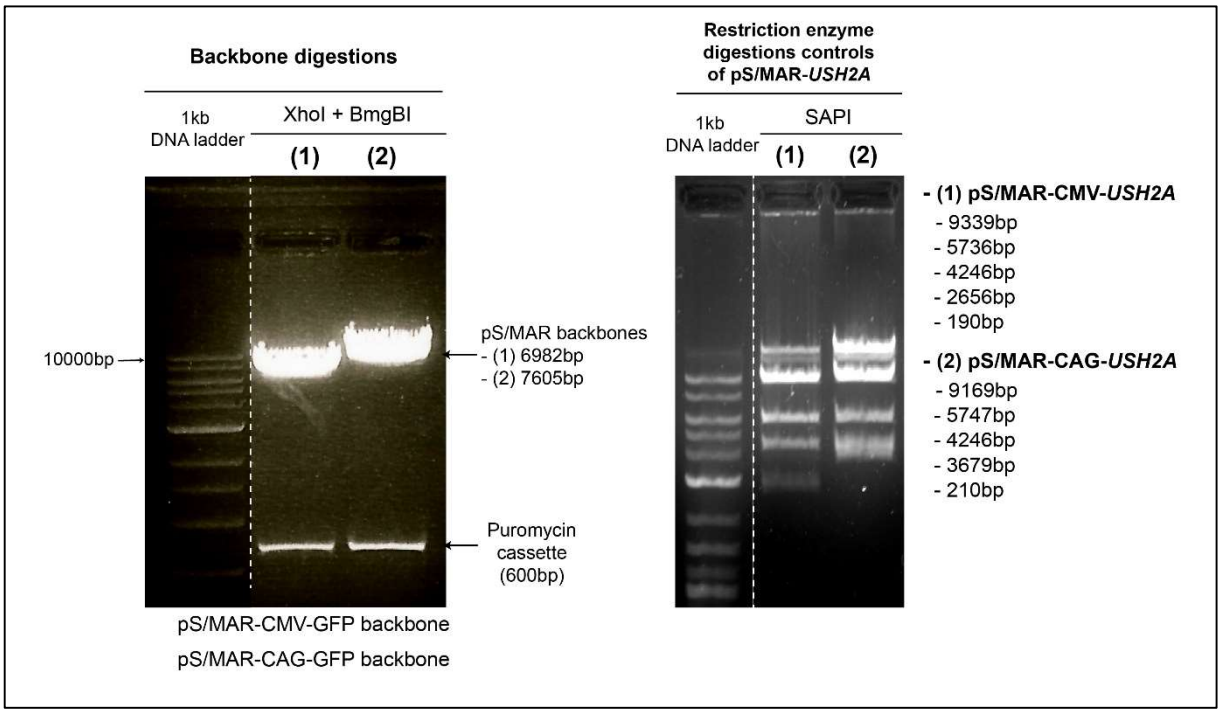

Figure 24. Inserting the full-length human USH2A cDNA into pS/MAR vectors.

S/MAR backbone digestion cut out the puromycin cassette and restriction enzyme digestion controls of the pS/MAR-USH2A vectors using SAPI. (1) pS/MAR-CMV-USH2A (2) pS/MAR-CAG-USH2A. 0.8% agarose gel concentration.

Once the cloning steps were performed, the vectors were digested with SAPI restriction enzyme, and run on an agarose gel as a first quality control, as shown in Figure 27 bands were expected (Figure 25):

- For pS/MAR-CMV-*USH2A*: 9339bp, 5736bp, 4246bp, 2656bp and 190bp-long bands.
- For pS/MAR-CAG-*USH2A*: 9169bp, 5747bp, 4246bp, 3679bp and 210bp-long bands

All the bands were observed at the correct size. However, further Sanger sequencing revealed one single mutation located on the nucleotide 6987 C>A leading to a change from an alanine to a glutamic acid residue in usherin. The mutation was corrected by cutting out the *USH2A* cDNA fragment containing the mutation and replacing it with a corrected fragment.

The *Plasmidsaurus* platform, which uses Oxford Nanopore long reads, was used to sequence the full-length plasmid including the *USH2A* insert. Every new maxi-prepped batch was sent for sequencing for quality control before further experimental work.

USH2A S/MAR plasmids						
		Promoter				
		CMV	CAG			
S/MAR sequence	INFb S/MAR Spliced	22254bp	23272bp			

Table 11. USH2A-S/MAR toolbox. 2 different promoters have been used in this toolbox.

PROMOTER	UBIQUITOUS	**CMV**	The CMV viral promoter is extensively used in molecular biology to drive strong constitutive expression of transgenes in a broad range of cells. However, CMV promoter is susceptible to silencing, and can vary considerably among different cell types (Qin et al., 2010).
		CAG	The CAG promoter is a strong hybrid mammalian promoter, containing the CMV early enhancer and chicken β-actin promoter. It drives strong constitutive expression of transgenes in a broad range of cells.
		hPGK	The hPGK promoter is a mammalian promoter originating from the *PGK* gene. It usually drives a milder transgene expression.
		EF1α	The human eukaryotic translation elongation factor 1 alpha (EF1α) promoter is constitutively active in a broad range of cells. Using this promoter in an optimized version of the pEPI plasmid vector, Wang and colleagues showed an increased in transfection efficiency, transgene expression, and the copy number of the episomal vector in long-term culture in CHO cells (Wang et al. 2017).
	CELL-SPECIFIC	**hCHM**	The human endogenous promoter of the *CHM* gene has been identified as the region encompassing nucleotides c.-119 to c.-76 by Radziwon and colleagues. Using the human endogenous promoter would be a promising approach as it would drive an expression level similar to the endogenous one.
		NA65	NA65 promoter is 0.8kb-long shortened version of the 1.6kb-long native RPE65 promoter, which drives RPE-specific expression.
		VMD2	The VMD2 promoter is a 0.6kb-long RPE-specific promoter cloned from human *BEST1* gene (Alexander and Hauswirth 2008).
		hIRBP	The human interphotoreceptor retinoid-binding protein (hIRBP) promoter is a 1.3-kb promoter fragment of the human *IRBP* gene driving expression in both rod and cone photoreceptors (Beltran et al 2017).
		hRK1	The human rhodopsin kinase (hRK1) promoter drives transgene expression exclusively in photoreceptors (Khani et al 2007).
S/MAR SEQUENCE		**INFβ S/MAR**	The cloned 2kb-S/MAR fragment in this vector comes from the 5' region of the human interferon β-gene and used in the pEPI plasmid vector (Piechaczek et al., 1999).
		ApoL S/MAR	The cloned 0.8kb-S/MAR fragment in this vector comes from the core repetitive domain of the matrix-attachment region of the ApoB gene. Dr. Matthias Bozza in Pr. Richard Harbottle team showed that ApoL S/MAR when cloned in a plasmid vector could efficiently drive episomal maintenance and transgene expression.
		ApoLC S/MAR	ApoLC S/MAR is a spliced version of the ApoL S/MAR fragment previously described and developed by Pr. Richard Harbottle's team.
OTHER SEQUENCES		**Ele40**	Anti-repressor element 40 (ele40) is originally located on the human chromosome 22 upstream of the *IL17R* gene. It is a known insulator element, and has been used by Richard Harbottle's team in S/MAR vectors as boundaries between the bacterial backbone and the expression cassette.
		P2A	The self-cleaving 2A peptide P2A originates from porcine tescovirus-1 and allows from one mRNA to produce 2 separated proteins. For instance, in our case, there is one protein of interest produced for one GFP produced.
		GFP	The vectors contain the green fluorescent protein (GFP) CDS from the copepod species *Pontellina plumata* (also known as copGFP).

Table 12. S/MAR plasmid components used in this study.

3.4 Discussion

Drawbacks raised by clinical trials for LCA and Choroideremia with viral gene therapy, call attention to the design of vectors for retinal gene therapy. Not only in terms of non-viral or viral carriers of the transgene, but also in regard to the transgene itself. DNA design importance has probably been overlooked in the gene therapy field.

DNA vector components are crucial for transgene expression level and duration, but also its toxicity. Promoters, cis-regulatory elements, size of the DNA vectors, bacterial backbones for plasmid-based strategies or inverted terminal repeats (ITRs) for AAV strategies, must be chosen carefully, as they are decisive.

Here in this chapter, valuable DNA S/MAR plasmids for Choroideremia and *USH2A*-related retinopathies have been cloned and validated. For Choroideremia, ubiquitous and RPE-specific promoters have been inserted into the REP1-S/MAR. This toolbox will allow us to assess the best promoters on different Choroideremia models, in terms of level and duration of transgene, and functional rescue.

For *USH2A*-S/MAR, only two promoters have been inserted, as the cloning process have been challenging. It is the first vector, in our knowledge, containing the full *USHA* CDS for gene therapy. It is the first time such a large gene has been successfully cloned for an ophthalmic disease.

Although the S/MAR plasmids can theoretically accommodate any gene insert size, the larger the plasmid, the more toxic and inefficient the transfection. That is why, strategies to limit plasmid sizes or mini-gene approaches would be beneficent for large gene therapies such as *USH2A* or *ABCA4*. Besides, the size of our USH2A-S/MAR plasmid (23kb) can make it more fragile, and must be handle with care. Quality controls must ensure the purity and the dominant peak size such as the ones provided by Plasmidsaurus. Furthermore, mutations can arise from bacterial transformation and would need frequent sequencing.

However, production of plasmid-based vectors (complexed with nanoparticles or not) is cheaper, more efficient, and versatile compared to AAV-based gene therapy. It would allow safer and more affordable gene therapies.

Several S/MAR vectors applications have been achieved by Richard Harbottle's team in different areas (Bozza et al. 2020; Roig-Merino et al. 2022).

For example, Roig-merino and colleagues achieved stem cell reprogramming using S/MAR reprogramming plasmids, instead of using integrating vectors. They developed this non-viral, non-integrating and autonomously replicating S/MAR based plasmids to persistently modify stem cells and their differentiated progeny. Moreover, Bozza and colleagues used similar S/MAR vectors to manufacture recombinant T cells. Using this technology, they quickly generated chimeric antigen

receptor (CAR)-T cells at clinical scale. A clinical trial has been recently set up for the latter example (Bozza et al. 2021).

More work is being done, especially regarding the development of minicircles, which are plasmids devoid of bacterial backbones, or with a minimally sized one. Not only it decreases plasmid size, but it also reduces innate immune response due CpG islands contained in bacterial backbones. Such minicircles were produced in collaboration with Richard Harbottle's lab and Nature Technology company for CMV-REP1-S/MAR an CAG-REP1-S/MAR (Bozza et al. 2021).

More recently in the ophthalmic field, Sun and colleagues generated stable PEG-ECO*/pGRK1-ABCA4-S/MAR* nanoparticles producing specific and prolonged expression of ABCA4 in the photoreceptors of *Abca4* $^{-/-}$ mice and significantly inhibit accumulation of toxic A2E in the eye. The 11.6 kb-long plasmid showed very encouraging results supporting the development of non-viral retinal gene therapies.

Overall, this work has allowed the production of a valuable DNA vector toolbox for Choroideremia and *USH2A*-related retinopathies, which will be further assessed in cell and animal models.

Chapter 4. S/MAR vectors in cell models of Choroideremia

4.1 Introduction and aims.

The generated and validated REP1-S/MAR vectors in the previous chapter do not exceed 9.6kb. *CHM* cDNA is relatively short, 1.9kb in length and so can be accommodated by AAV vectors. However, among several clinical trials for *CHM* AAV therapy, a phase I/II trial (NCT02341807) did not report differences in visual acuity between injected and un-injected eyes at 2 years post-surgery, and a phase III multicentre study (NCT03496012) failed to meet the primary endpoints and key secondary endpoints after 12 months post-treatment (Sarkar et Moosajee 2022). Furthermore, intraocular inflammation was reported in two CHM patients (Dimopoulos et al. 2015; Xue et MacLaren 2018), which has also been noted in AAV studies for other IRD genes, including *RPE65* and *CNGB3* (Ye et al. 2016). More recently, Voretigene neparvovec has reported to cause RPE atrophy with consequent photoreceptor loss in and outside of the bleb area, raising concern for viral-based retinal gene therapy (Reichel et al. 2022). Therefore, non-viral strategies are needed to pave the way to new therapeutic avenues.

In this study, 3 cell models have been used. First, we used HEK293 cells as they are easy to grow and to transfect with a DNA vectors, in order to

confirm that REP1-S/MAR plasmids were efficiently driving REP1 expression.

The second cell is primary HDF from Choroideremia patients. WT and *CHM* patient dermal fibroblasts harbouring the homozygous c.126C>G, p.(Y42*) were used. HDF are a relevant *CHM* cell model as WT HDF express REP1 protein, while *CHM* patient-derived HDF do not. Moreover, a prenylation defect in *CHM* patient derived HDF have been well documented in the literature and levels of unprenylated Rabs can be used as a functional assay.

Finally, we moved to human induced pluripotent stem cells reprogrammed from *CHM* patient fibroblasts. These hIPSC were then differentiated into RPE to recapitulate a retinal context and to assess the REP1-S/MAR vectors in a more relevant model (Figure 26).

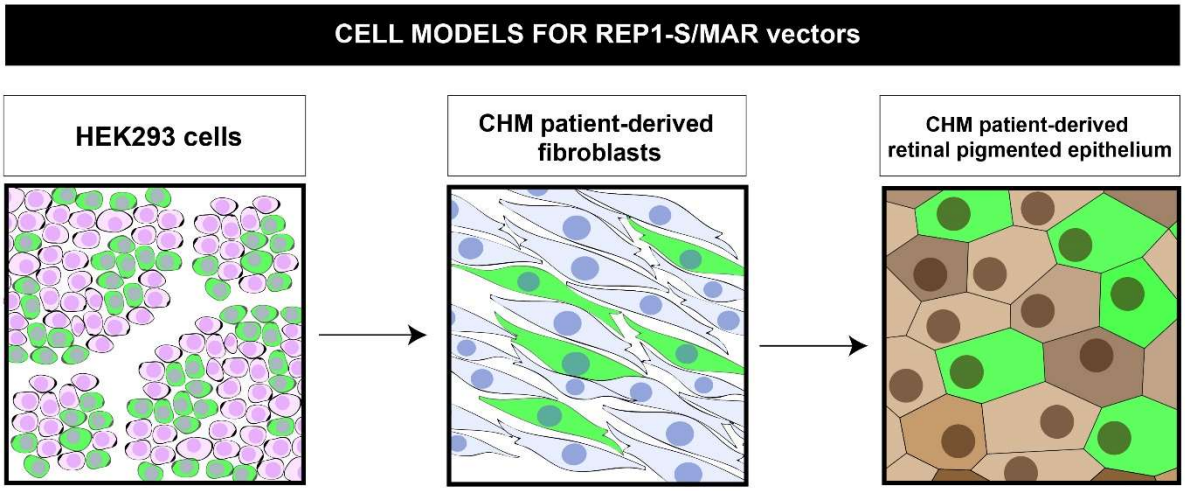

Figure 25. Graphical abstract of cell models used to assess *CHM*-S/MAR plasmids.
HEK293 cells, *CHM* patient-derived fibroblasts and RPE have been cultured. Transfected cells expressing a GFP reporter are depicted in green.

4.2 HEK293 cells transfection with REP1-S/MAR

After cloning and validating by Sanger sequencing a REP1-SMAR plasmid toolbox with several promoters (CMV, CAG, EF1a, hPGK and CHMp), HEK293 cells were transfected with vectors to determine whether they drove REP1 protein overexpression. Cells were transfected with 1µg of either vector complexed with Lipofectamine 2000. After 48 hours, GFP fluorescence and REP1 protein expression was analysed. Transfected HEK cells displayed varying levels of GFP fluorescence, (Figure 27) at 48h and later 7 days post transfection.

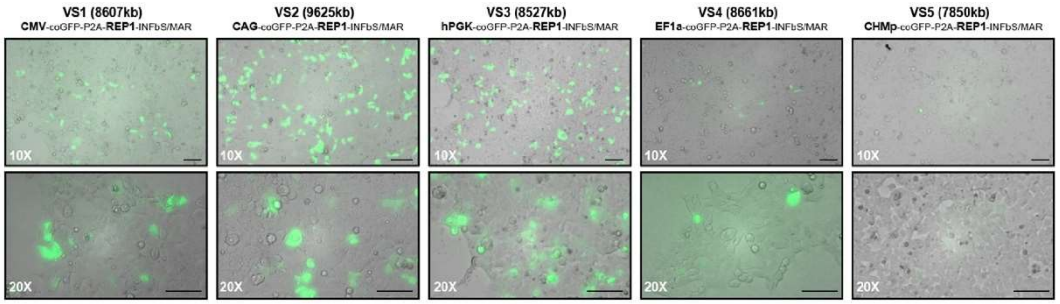

Figure 26. REP1-S/MAR-generated expression of human REP1 in HEK293 cells.
REP1-S/MAR toolbox with ubiquitous promoters (CMV, CAG, hPGK and EF1a) and specific promoter (CHMp). GFP fluorescence 48-hours post-transfection in HEK293 cells. (Scale bar = 50µm)

Additionally, protein lysates of transfected HEK cells were collected 48 hours after transfection. Western blots demonstrated an important overexpression of REP1 for V1 (CMV-REP1-S/MAR), V2 (CAG-REP1-S/MAR), V3 (hPGK-REP1-S/MAR) and V4 (EF1a-REP1-S/MAR) compared to non-transfected cells. Interestingly, use of the endogenous *CHM* promoter did not drive REP1 overexpression, although sparse GFP positive cells were observed for V5 (CHMp-REP1-S/MAR). The V5 vector would be an interesting vector to study in the future as it should drive a REP1 level similar to the endogenous one. Among the 5 vectors tested, the ones with CMV and CAG promoters showed the highest level of REP1 expression (Figure 28). Therefore, V1 (CMV) and V2 (CAG) vectors were taken forward for further study.

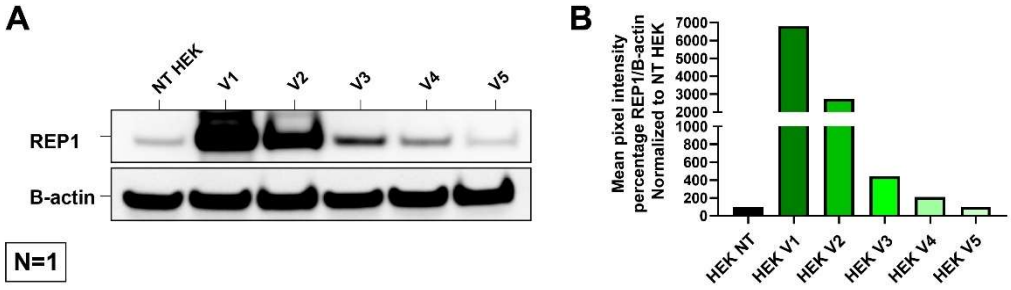

Figure 27. Western blot analysis of REP1 protein expression in HEK293 cells. (A) Western Blot analysis. Non-transfected (NT) HEK293 cells, and V1 (CMV), V2 (CAG), V3 (hPGK), V4 (EF1a) and V5 (CHMp) transfected HEK293 cells. (B) Y-axis of the graph is the mean pixel intensity percentage of REP1/B-actin, normalized to actin protein expression. (N=1)

4.3 CHM HDF cells electroporation with REP1-S/MAR

To determine whether REP1-S/MAR plasmid vectors restored a persistent REP1 expression in HDF, western blots were undertaken on WT, *CHM*$^{Y42X/y}$ and (CAG-REP1-S/MAR) V2 electroporated *CHM*-HDF. First, *CHM*$^{Y42X/y}$ HDF electroporation were optimized. For 1 million electroporated HDF cells, the use of 6µg of V2 showed the best results in terms of efficacy and toxicity. To produce enough cell material, 10 million *CHM*$^{Y42X/y}$ HDF were electroporated and 800,000 GFP-positive cells were FACS sorted 7 days post-electroporation (Figure 29). Western blot after one passage at day 11 and two passages at day 35 showed persisting expression of REP1 (N=3).

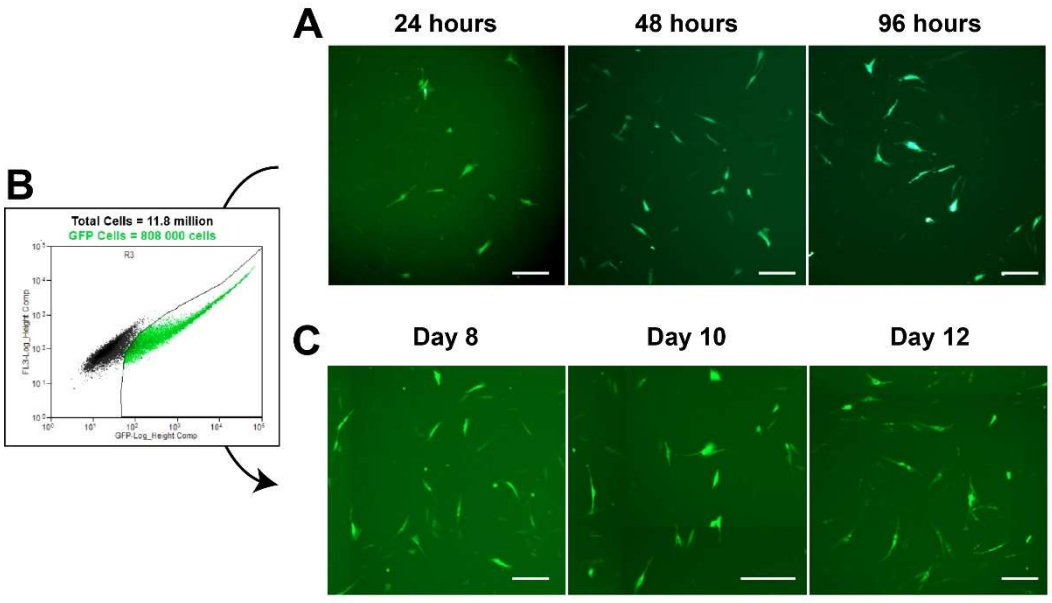

Figure 28. CAG-REP1-S/MAR electroporated in *CHM* patient fibroblasts. (A) GFP fluorescence of CAG-REP1-S/MAR electroporated CHM patient fibroblasts 24h, 48h and 96h after electroporation. (B) GFP positive cells were selected using FACS. (C) GFP fluorescence of CAG-REP1-S/MAR FACS sorted cells at day 8, 10 and 12 after electroporation. (Scale bar = 50µm)

CHM HDF expressed significantly less REP1 than the WT, with 28.65% of WT REP1 expression (SD = 8.64%), as expected. However, this significant difference of expression was rescued in V2 electroporated HDF with 116.60% of WT (SD = 27.28%) at Day 11 post-FACS and 66.87% of WT (SD = 25.22%) at Day 35 post-FACS. However, a 50% decrease in REP1 expression was observed between day 11 post-FACS and day 35 post-FACS (Figure 30). This could be explained by either the silencing of the transgene or a toxicity driven by its expression. Vector silencing is a major challenge that needs to be addressed for gene therapy.

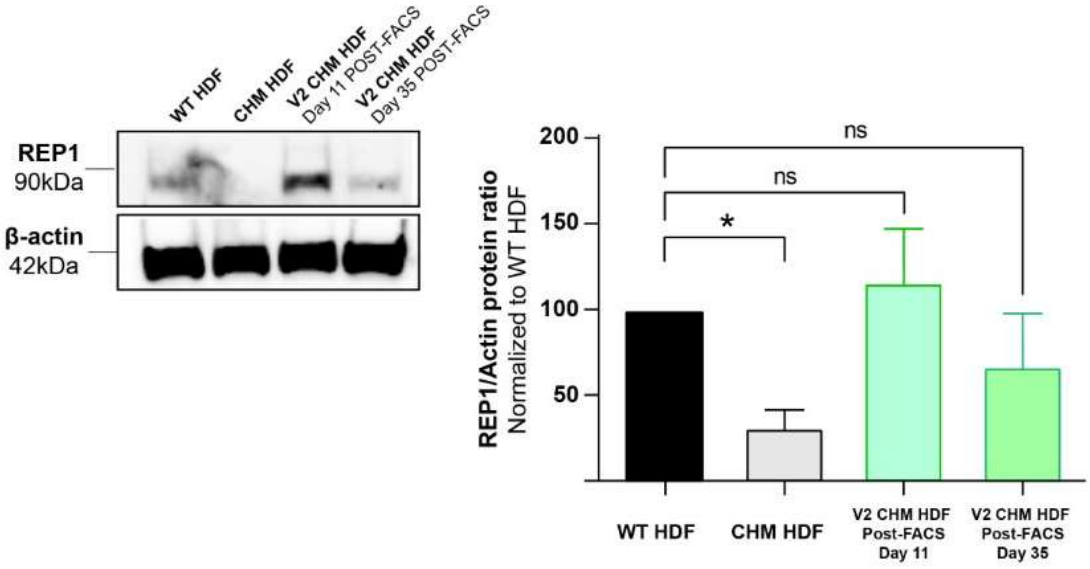

Figure 29. Western blot of *CHM* HDF transfected with CAG-REP1-S/MAR.

Western blot analysis of REP1 protein expression in WT and *CHM* fibroblasts, and V2 electroporated *CHM* patient fibroblasts. (ns=non-significant) (* $p<0.05$) (N=3).

4.4 Prenylation function in REP1-S/MAR electroporated CHM HDF

REP1 plays an essential role in lipid modification of Rab proteins and facilitates their intracellular membrane transport trafficking by binding to the hydrophobic prenylation motifs at the C termini; when REP1 is absent, a population of unprenylated Rabs (especially Rab27A) builds up in the cells. By rescuing REP1 expression in *CHM* fibroblasts, we would expect the level of unprenylated Rabs to decrease if exogeneous REP1 is functional. Therefore, prenylation function was investigated by measuring the pool of unprenylated Rabs in transfected and non-transfected cells using an in vitro assay. Briefly, Rabs proteins were collected from the protein lysates. Then, an *in vitro* prenylation reaction was performed by adding an exogeneous REP1 protein, the GGTase-II enzyme, and Biotinylated Geranyl pyrophosphate. The unprenylated Rabs fraction was then prenylated with a Biotin function, allowing western blots analysis and measurement of the initial unprenylated Rabs fraction (Figure 31).

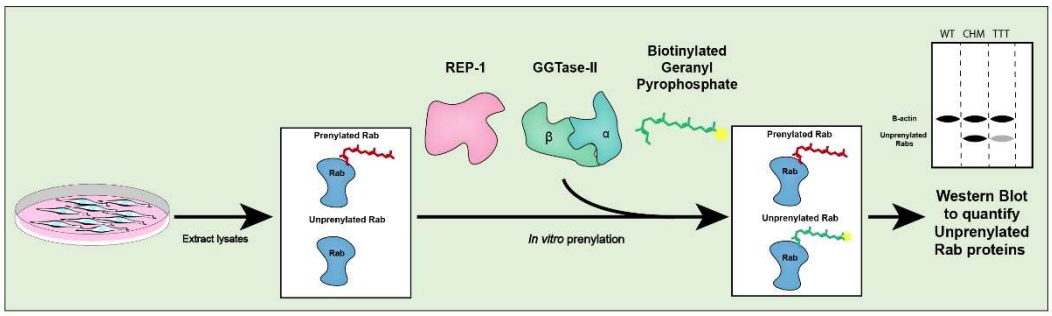

Figure 30. Outline of prenylation assays process.
3 main steps : (1) extract lysates, (2) In vitro prenylation reaction and (3) western blot to quantify unprenylated Rab proteins.

At 7 days post-electroporation, it was found that transfected *CHM* fibroblasts showed a 75% (SD=11.7) ($p < 0.05$) decrease in unprenylated Rabs compared to non-transfected CHM cells (Figure 32). Unprenylated Rabs were not detected in the wild-type fibroblasts, as expected. This rescue means that the REP1 proteins produced by CAG-REP1-S/MAR is functional, and can efficiently add a prenyl group to the unprenylated Rabs.

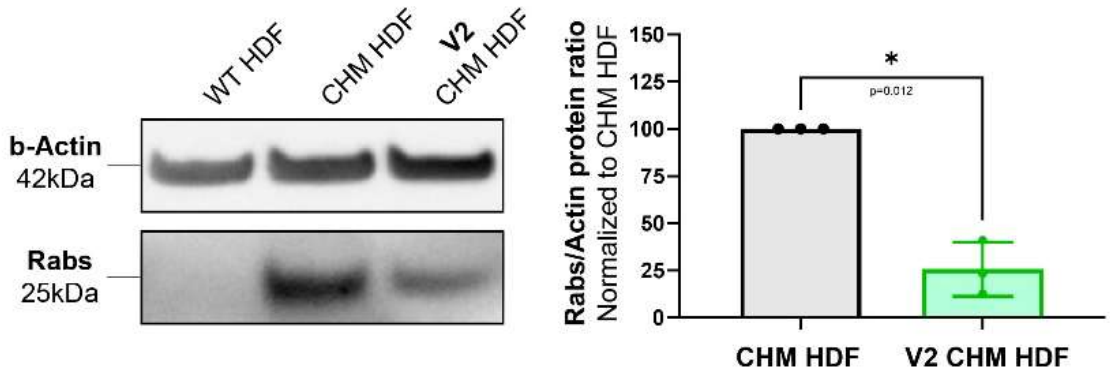

Figure 31. Prenylation assays in *CHM* patient fibroblasts.

Prenylation assays in WT and *CHM*$^{Y42X/y}$ patient fibroblasts, and V2 electroporated *CHM* patient fibroblasts. (A) Western blot analysis with Rabs proteins (25kDa) and b-Actin (42kDa). Student t-test was performed to compare the groups (* $p<0.05$) (n=3).

4.5 Retinal pigmented epithelium (RPE) differentiated from hIPSC

4.5.1 Optimization of RPE differentiation protocol

After HDF reprogramming into hIPSC, hiPSC-derived RPE cell model was cultured and characterized. First, hIPSC were differentiated into RPE following the protocol optimized by Reichman and colleagues (Reichman et al. 2017). As described in Figure 33, this differentiation protocol is divided into 2 steps. hIPSC are cultured to reach 90% confluency. mTESR hIPSC maintenance medium is replaced by E6 medium devoid of FGF2 and TGFb. Withdrawal of these factors stops the pluripotency machinery and encourages the spontaneous differentiation of hIPSC. This step is defined as Day 0 (D0). At D2, the medium is changed to a pro-neural medium containing E6 supplemented with N2, until D28. At D28, the medium was changed to a RPE maturation medium until the end of the differentiation. At D42, pigmented RPE patches were mechanically dissected and further culture in 24-well Geltrex-coated plates. RPE were then passaged at D56 (P1) and around D70. However, this undirected protocol was not very efficient, and needed extensive work with the mechanical isolation of RPE patches. Therefore, Regent and colleagues protocol was used (Regent et al. 2019). This protocol starts with a 3-step protocol. hIPSC are cultured to reach 90% confluency. Briefly, a sequential use of nicotinamide (D0-D7), activin A (D7-D14) and Chir99021 (D14-D42) are improving RPE differentiation. Further passaging, without mechanical isolation of RPE patches results in mature RPE.

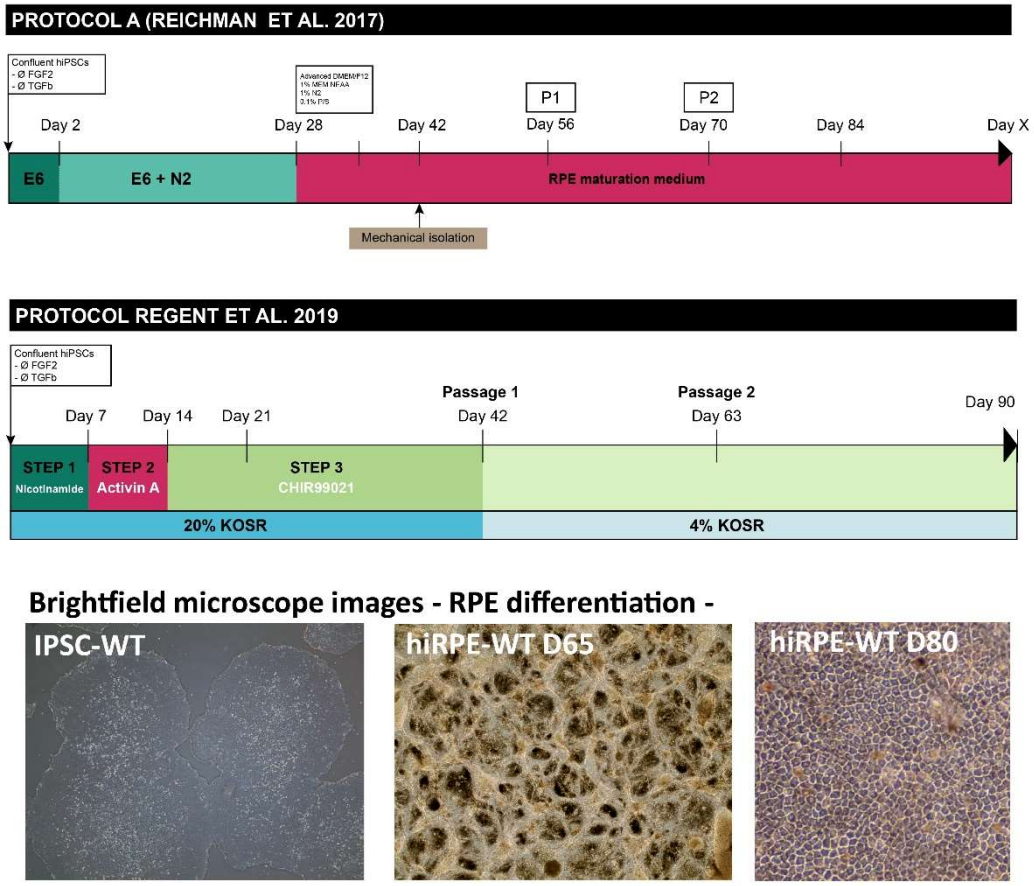

Figure 32. RPE differentiation protocol.

Two different protocols were used for RPE differentiation (A) from Reichman et al., 2017 and (B) from Regent et al., 2019.

As shown in Figure 34A, the tight junction marker Zonula-Occludens 1 (ZO-1) reveals a nice regular cobblestone organization of the differentiated WT RPE after one passage. In addition, it displays a clear baso-lateral polarisation with the tight junctions localizing at the apical part of the cells, as shown with the RPE orthogonal view (Figure 34C). Melanocyte inducing transcription factor (*MITF*) (Figure 34 in green), a RPE marker, was well expressed colocalizing with the DAPI (Figure 34 in blue) in the cell nuclei. In conclusion, the differentiation protocol worked efficiently to yield differentiated RPE, with a typical cobblestone morphology.

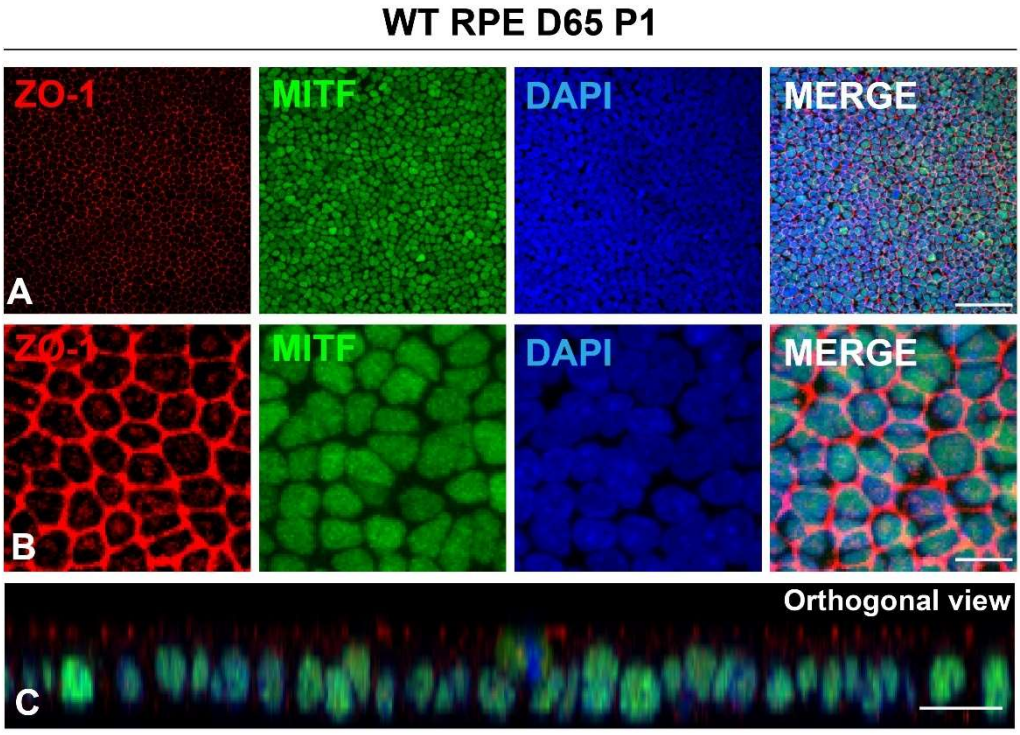

Figure 33. WT RPE characterisation and morphology using Regent and colleagues protocol.

WT RPE at day 65 of differentiation was stained against ZO-1 (Zonula-Occludens 1) in red, Melanocyte inducing transcription factor in green (MITF), and nuclei were counterstained with DAPI in blue. An orthogonal view of the RPE was captured allowing a better understanding of the baso-apical distribution of ZO-1 and the nuclei. (Scale bars: A= 50µm; B=10µm C=20µm).

4.5.2 WT vs CHM RPE characterisation

Differentiation protocol from hIPSC to RPE was applied to WT and CHM hIPSC. Both *CHM* and WT control, produced RPE patches with typical cobblestone morphology at the brightfield microscope. However, it was noted that *CHM* RPE displayed a less pigmented phenotype than the WT control. It could be noticed comparing the dishes but also when centrifuged in 15mL plastic tube (Figure 35). That difference can be clone-specific or related to *CHM* phenotype. More work needs to be undertaken to explore this anomaly.

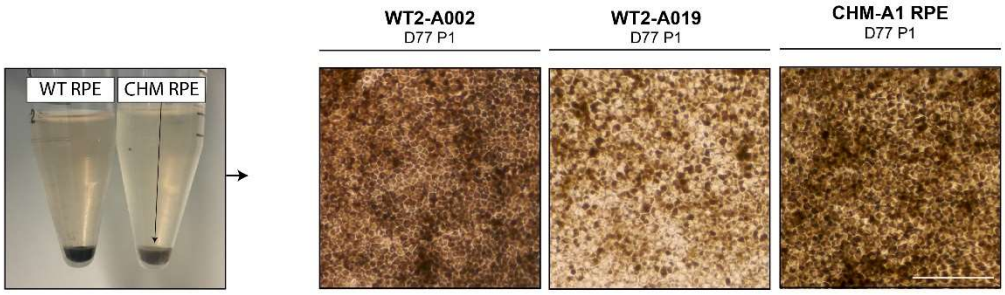

Figure 34. *CHM* and WT hiRPE morphology. WT and CHM RPE pellets in 15mL falcons. WT seems more pigmented than CHM. Brightfield images of typical RPE cobblestone morphology (Scale bar = 100µm).

Protein lysates of WT and *CHM* hIPSC and RPE were collected. Western blots were performed and showed loss of REP1 protein in *CHM* hIPSC and RPE, which confirms absence of REP1 in the patient cells (Figure 36).

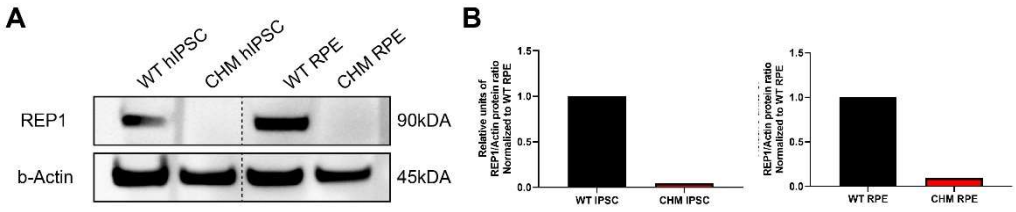

Figure 35. Western blot analysis of CHM and WT IPSC and RPE cells. (A) Western Blot analysis. WT hiPSC, CHM hiPSC, WT RPE and CHM RPE cells. (B) Y-axis of the graph is the mean pixel intensity percentage of REP1/B-actin, normalized to WT REP1/b-Actin (N=1).

Expressions of RPE specific markers in WT and CHM RPE (D63) were analyzed by RT-qPCR and normalized to mRNA expression at day 0. Expression of *OCT4,* a pluripotency gene, was downregulated in WT and CHM RPE differentiated cells, with a 4.1-fold and 1.2-fold decrease, respectively. *MITF*, *BEST1*, *RPE65* and *CRABLP*, which are genes specifically expressed in mature RPE were upregulated in both conditions WT and CHM RPE. Upregulation of these markers in both lines supports the idea of an efficient differentiation of WT and CHM hIPSC in mature RPE cells (N=2) (Figure 37).

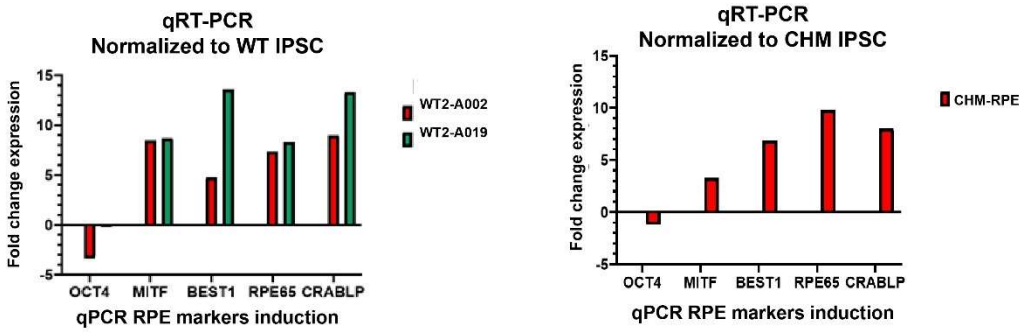

Figure 36. qPCR of WT and *CHM* RPE.
It displays expression of *MITF*, *BEST1*, *RPE65* and *CRABLP*, which are genes specifically expressed in mature RPE.

Additional, immunostaining of ZO-1 an MITF in WT and *CHM* RPE at day 90 of differentiation, showed similar morhology (Figure 38). Both display a nice cobblestone morphology, and strong specific MITF signal.

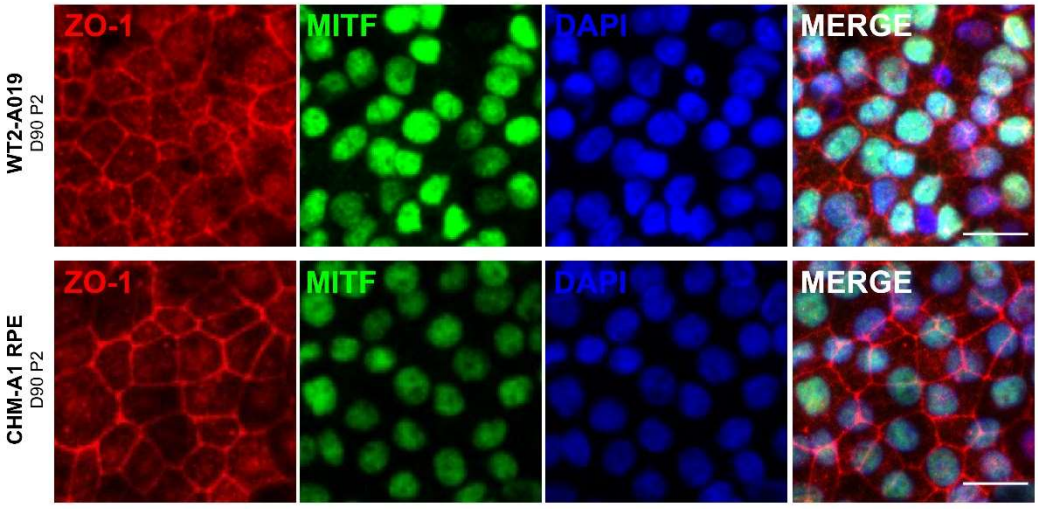

Figure 37. CHM and WT RPE characterisation.
Day 90 WT and CHM RPE immunostaining showing MITF expression (in green) and cobblestone morphology of RPE cells. (Scale bar 10µm).

4.6 Discussion

With an estimated prevalence of between 1 in 50,000-100,0000 people (MacDonald et al. 2015), CHM is the most common inherited X-linked chorioretinal dystrophy. Caused by mutations within the *CHM* gene encoding the Rab-escorted protein 1 (REP1), it is characterized by the degeneration of choriocapillaris, RPE and the PR layer. It is generally accepted that pathogenic *CHM* mutations are loss-of-function mutations, which makes it an ideal candidate for gene augmentation therapy. Additionally, no known dominant-negative effects have been reported and *CHM* cDNA is small enough (1.9kB) to fit into an AAV vector. Thus, expression of even a small amount of healthy functional protein is predicted to be therapeutic. However, recent reports from Phase III clinical trials failed to meet primary and secondary endpoints. Furthermore, intraretinal inflammation was triggered by AAV2-REP1 subretinal injections,and resulted in permanent damage to the retinal structure (Zhai et al. 2023). These concerning results, cast doubt on AAV-REP1 as an efficient gene therapy strategy for CHM patients. Therefore, the development of non-viral gene augmentation therapy strategies is needed.

In this chapter we have assessed S/MAR plasmid vectors carrying the human *CHM* coding sequence to produce functional human REP1 expression in *CHM* patient-derived resulting in a significant functional rescue of Rabs prenylation. Such results are very promising for the therapeutic potential of S/MAR vectors as non-viral alternatives for CHM retinal gene therapy.

The REP1-S/MAR toolbox containing CAG, CMV, EF1a and hPGK drove high expression of REP1 protein in HEK293. CAG and CMV promoters drove the highest expression, and showed similar results in CHM HDF. However, CMV-REP1-S/MAR, although driving a higher expression in the first 2 days, was more prone to silencing, while CAG-REP1-S/MAR drove more sustainable expression in CHM HDF. Additionally, CAG promoter is the one used in retinal gene therapy for Choroideremia using AAV2 (NCT01461213). CAG promoter has been shown to drive long-lasting transgene expression in RPE, with voretigene neparvovec for RPE65-mediated LCA. Therefore, work has been carried out using the CAG promoter.

CAG-REP1-S/MAR electroporated CHM HDF displayed sustained expression after 3 passages, 35 days post-electroporation. Nonetheless, the expression was not stable and decreased between Day 11 and Day 35. Electroporated cells could be silenced or dying. Investigating apoptotic levels among the electroporated cells would be valuable. High sustained expression of an exogenous REP1 and GFP, could be toxic to the cell.

That is why, alternative promoters such as the endogeneous *CHM* promoter are relevant to drive suitable REP1 expression a cell. Besides *CHM* promoter is shorter than the CAG promoter, which would save 1.775kb in the plasmid vector.

At 7 days post-electroporation, it was found that transfected CHM fibroblasts showed a 75% (SD=11.7) ($p < 0.05$) decrease in unprenylated

Rabs compared to non-transfected CHM cells. This result shows an *in vitro* “proof-of-concept” on CHM patient-derived cells using non-viral REP1-S/MAR plasmids. However, this functional rescue resulted from CHM HDF electroporation, which is not translatable to *in vivo* model. One of the major challenge for retinal gene therapy, is the DNA vehicle by which, the transgene will reach the nucleus of the targeted cell.

CHM HDF were successfully reprogrammed and differentiated into RPE cells derived from patient hiPSC. This technology remarkably improved the availability of human RPE tissue, to recapitulate the “disease-in-a-dish” but also, to test innovative drugs and gene therapy (reviewed in Rohowetz et al., 2023). Here, WT and CHM RPE was produced and partially characterized by immunostaining, qRT-PCR and Western blot. No major differences were noticed so far, but more work should be undertaken. Interestingly, CHM RPE cells seem overall less pigmented than WT RPE cells. It could be a clone-dependent feature, but could also be caused by diseases. As a matter of fact, REP1 is involved in the prenylation of Rab proteins and is essential for intracellular trafficking of vesicles. Many targets can be disrupted by hindered intracellular trafficking of vesicles, such as melanosomes found in the RPE (Sarkar et Moosajee 2022).

Chapter 5. S/MAR vectors in cell models of *USH2A*

5.1 Introduction and aims.

The generated and validated USH2A-S/MAR vectors in chapter 3, are very large, approaching 23kb. To our knowledge, these *USH2A*-S/MAR plasmids are the first DNA vectors containing the full human *USH2A* coding sequence. In this chapter, we aim to assess if these vectors can drive *USH2A* expression and produce functional usherin protein. To do so, three cell models have been used (i) HEK293 cells, (ii) patient dermal fibroblasts, and (iii) human *USH2A*-iPSC and retinal organoids. HEK293 cells were primarily used as they are easy to grow and transfect with DNA vectors. HEK293 cells are derived from human embryonic kidney cells. This cell line displays a reliable growth and performs a high transfection efficiency. In addition, they contain efficient protein production machinery, more likely to handle the large usherin protein.

Primary HDFs were obtained from a patient with Usher syndrome type 2A. It is a more relevant disease model, as it originates from an *USH2A* patient. Targeted *USH2A* sequence analysis of the patient cells confirmed compound heterozygosity for the c.2299del p.(Glu767Serfs*21) and c.3187_3188del p.(Gln1063Serfs*15) variants. However, primary human

dermal fibroblasts are difficult-to-transfect cells, and less resilient than HEK293 cells.

Human induced pluripotent stem cells (hIPSC) were reprogrammed from the *USH2A* patient fibroblasts. These hIPSC were then differentiated into retinal organoids to recapitulate a retinal context and to assess the USH2A-S/MAR vectors for potential future clinical translation (Figure 39).

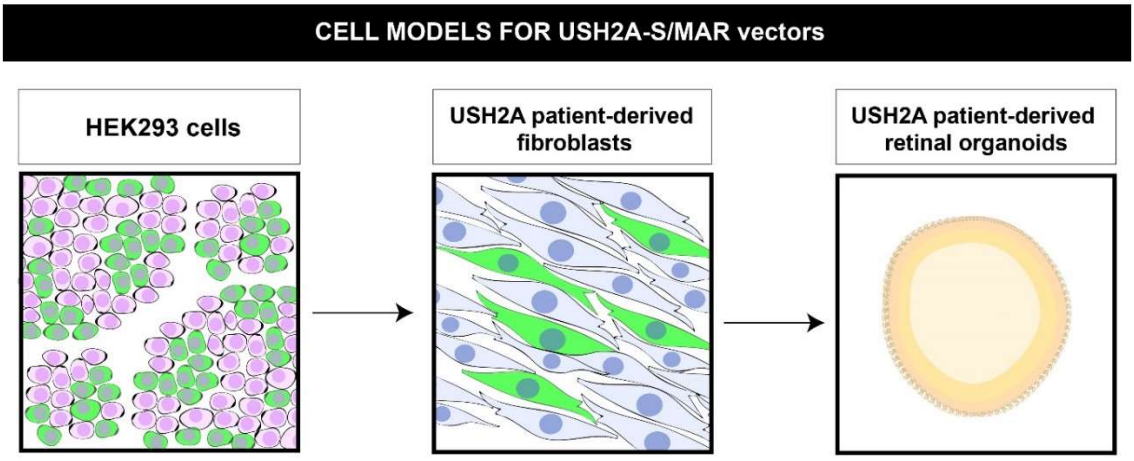

Figure 39. Graphical abstract of cell models used to assess *USH2A*-S/MAR plasmids.
HEK293 cells, USH2A patient derived fibroblasts and retinal organoids have been cultured. Transfected cells expressing a GFP reporter are depicted in green.

5.2 Optimization of HEK293 cells transfection with *USH2A*-S/MAR

5.2.1 Using Jet-Optimus Reagent

The *USH2A*-S/MAR vectors designed in this study are very large vectors exceeding 20kb. To allow the uptake of large DNA vectors, transfection optimizations were conducted. Chemical transfection was first performed using JetOptimus reagent, which is a commercially available branched PEI-based chemical reagent for highly efficient transfection in hard-to-transfect cells. 100,000 HEK293 cells were seeded on 12-well plate and transfected 24h later with the conditions described in Table 13. GFP expression was monitored by fluorescent microscopy 48 hours post-transfection to assess its efficacy. Three DNA plasmid quantities (500ng, 1000ng and 1500ng) were tested. Additionally, 2 different DNA/Jet-Optimus reagent ratios of 1:1 to 1:1.5 were tested.

	DNA/jetOPTIMUS® ratios					
	1:1			1:1.5		
	DNA quantities					
	500ng	1000ng	1500ng	500ng	1000ng	1500ng
CMV-*USH2A*-S/MAR	-	-	-	+	+++	++
CAG-*USH2A*-S/MAR	-	-	-	+	++	++

Table 13. HEK293 cell transfection optimization with JetOPTIMUS reagent coupled with USH2A-S/MAR plasmids.
2 DNA/jetOPTIMUS® ratios, 3 DNA quantities and 2 different promoters were assessed.

Only the ratio 1:1.5 resulted in GFP expression. All conditions were performed for both CMV-*USH2A*-S/MAR and CAG-*USH2A*-S/MAR. For both CMV-USH2A-S/MAR and CAG-USH2A-S/MAR, 500ng and 1500ng showed similar GFP expression but the higher dose was leading to significant cell death. The most efficient condition was 1000ng of CMV-USH2A-S/MAR with a DNA/Jet-Optimus ratios of 1:1.5. However, a lot of cell death occurred 48h-post transfection. The combination of a very large plasmid and a branched PEI-based chemical reagents resulted in significant cell toxicity (Figure 40).

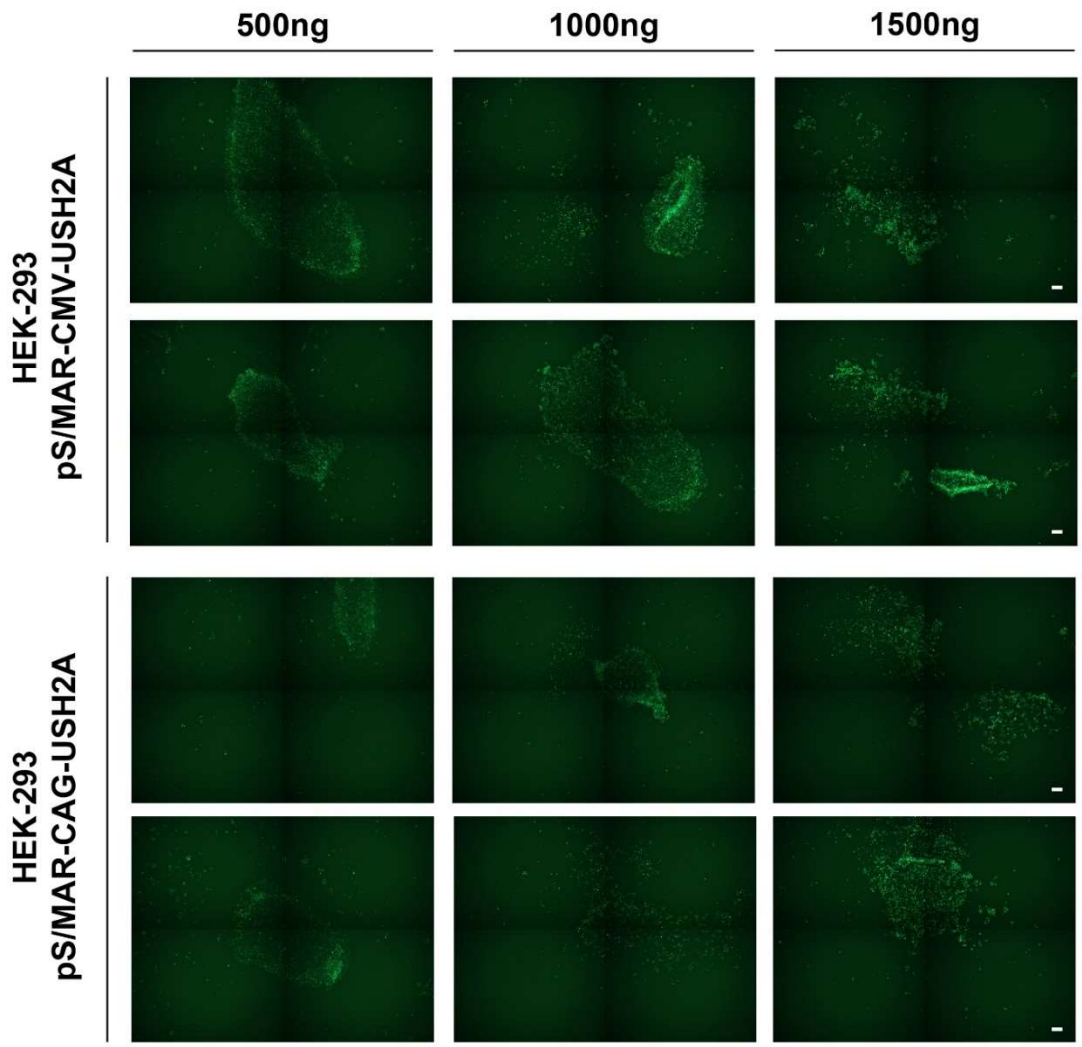

Figure 40. HEK293 cell transfection optimization with Jet-Optimus reagent coupled with USH2A-S/MAR plasmids.
3 DNA quantities and 2 different promoters were assessed. (Scale = 100µm).

5.2.2 Using Neon electroporation system

Next 100,000 HEK293 cells were collected, electroporated and seeded on 12-well plate with the conditions described in Table X. GFP expression was monitored by fluorescent microscopy 48 hours later to assess electroporation efficiency. Three DNA plasmid quantities (500ng, 1000ng

and 1500ng) were tested. Additionally, 2 different NEON electroporation programs were tested: 1450V - 10ms -1 pulse and 1450V - 20ms - 2 pulses. All conditions were performed for both CMV-*USH2A*-S/MAR and CAG-*USH2A*-S/MAR. The most efficient condition was 1000ng of CMV-USH2A-S/MAR using the 1400V - 20ms - 2 pulses program. Significant cell death occurred, but after 1 week, GFP-positive cells recovered and expanded (Table 14).

	NEON ELECTROPORATION PROGRAM					
	1450V-10ms-1 pulse			1400V-20ms-2 pulses		
	DNA quantities					
	500ng	1000ng	1500ng	500ng	1000ng	1500ng
CMV-*USH2A*-S/MAR	+	++	+	+	+++	++
CAG-*USH2A*-S/MAR	+	++	+	+	++	++

Table 14. HEK293 cell electroporation optimization with USH2A-S/MAR plasmids using Neon electroporation system.
2 neon electroporation programs, 3 DNA quantities and 2 different promoters were assessed. (+ = level of GFP signal).

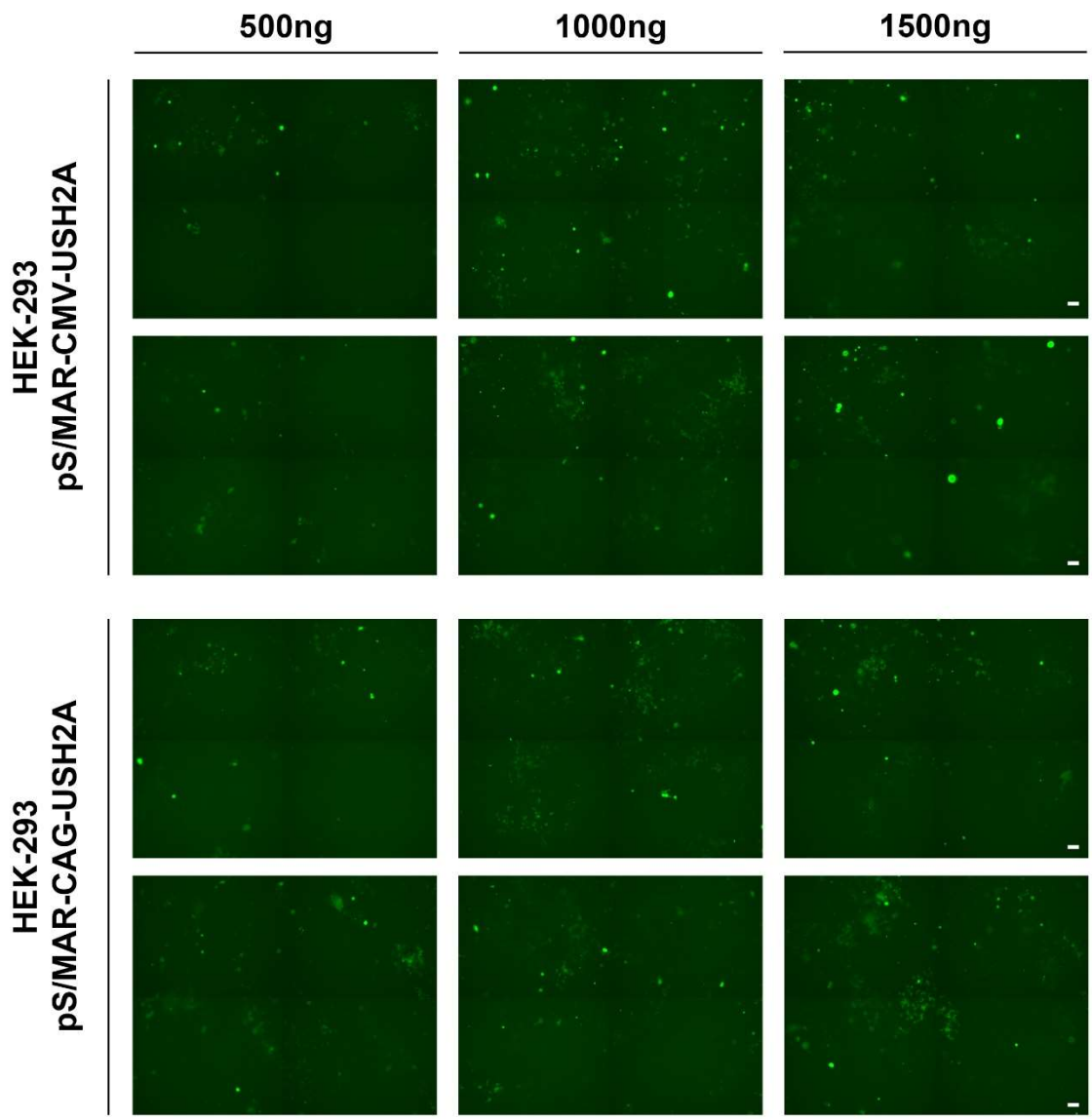

Figure 381. HEK293 cell transfection optimization with NEON electroporation system with USH2A-S/MAR plasmids.
3 DNA quantities and 2 different promoters were assessed. (Scale = 100µm).

Interestingly, HEK293 expressing USH2A-S/MAR plasmids displayed an altered morphology with long and thin neurite-like processes. As showed in Figure 47, some GFP-positive cells grew 2 to 3 neurite-like processes of 50-70µm each. Such phenotype was not observed in HEK293 expressing GFP only or REP1-S/MAR plasmids (Figure 41). These morphologic changes could be caused by the stress induced by such a big transgene transfection or could be driven by exogenous usherin overexpression. Similar morphological changes in HEK cells, have been reported by Koch and colleagues when transfecting HEK cells with a 7kb-long NRSE dsRNA-expressing vectors. They observed an altered morphology leading to the formation of comparable thin processes and induced the expression of neurofilament-68. Also, they found that it was enhancing neurite outgrowth in primary retinal ganglion cells, and it was caused by the sequestration REST1 (Koch et al. 2011). Therefore, some mechanisms can trigger neurite outgrowth in HEK cells. More work should be done to investigate this effect by measuring the length of neurite-like processes compared to a GFP plasmid control. It could provide more insights into the role of usherin function in cells, and therefore a better understanding of Usher syndrome type 2A pathomechanism.

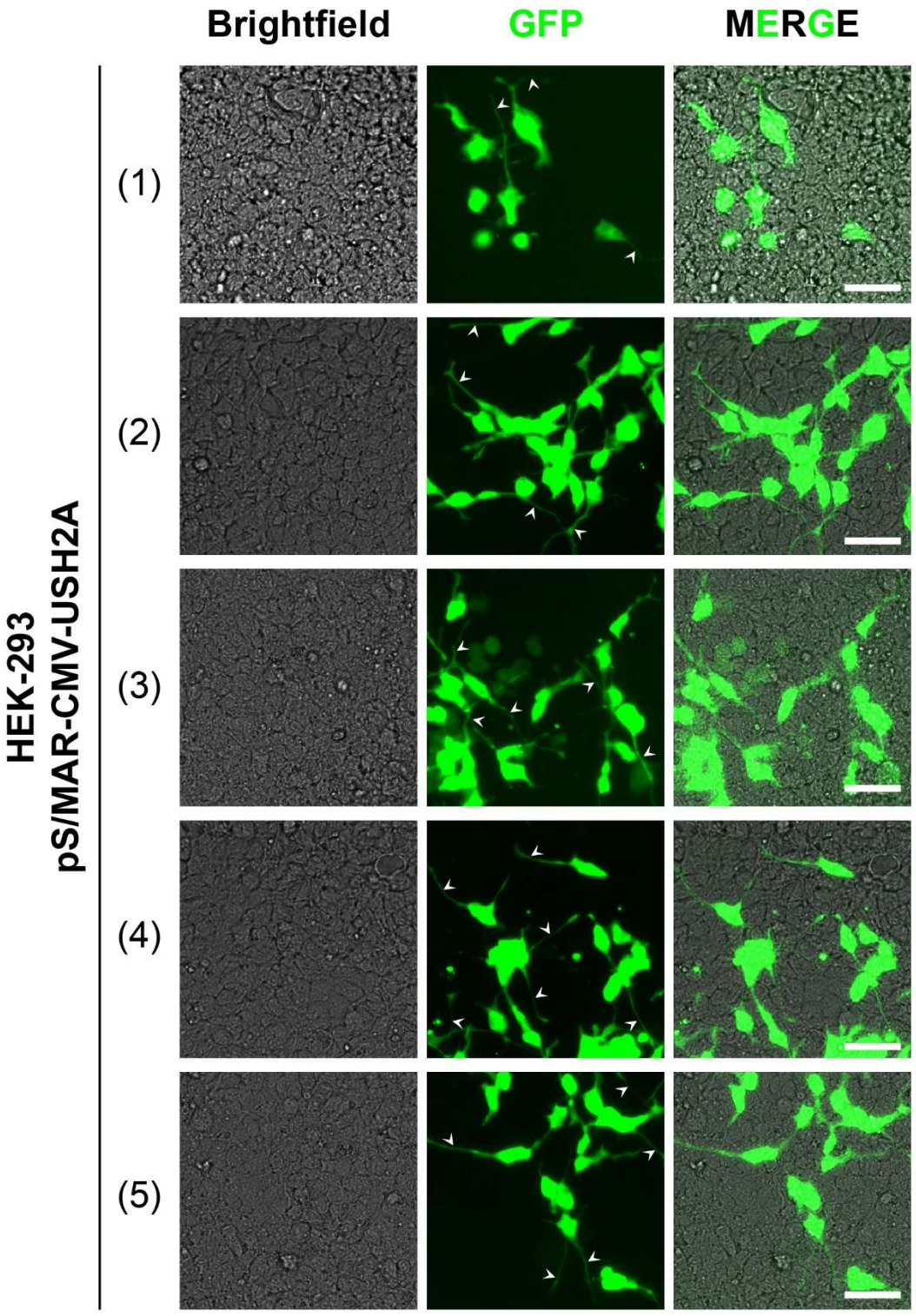

Figure 42. USH2A-S/MAR transfected HEK293 cells display neurite-like processes.
HEK293 were transfected with CMV-USH2A-S/MAR. They displayed neurite-like processes after 7-days post electroporation. White arrows show examples of neurite-like processes. (Scale bar 50μm).

5.3 *USH2A*-S/MAR electroporated HEK293 cells overexpress usherin

HEK293 cells were then electroporated with the most efficient condition using the 1450V - 20ms - 2 pulses NEON program. However, to produce enough cell material, the electroporation was scaled up. 1,000,000 HEK293 cells were electroporated with 10µg of CMV-USH2A-S/MAR or CAG-USH2A-S/MAR in a cultured in 6-well plate. Once electroporated, GFP expression was monitored by fluorescent microscopy 96-, 110- and 240-hours post-transfection. GFP-positive cells attached to the well, 24 hours post-electroporation. As shown in Figure 42, after 240 hours, cells reached 90% confluency, with dense islands of GFP-positive cells. Two wells of a 6 well-plate was then collected for Western blot.

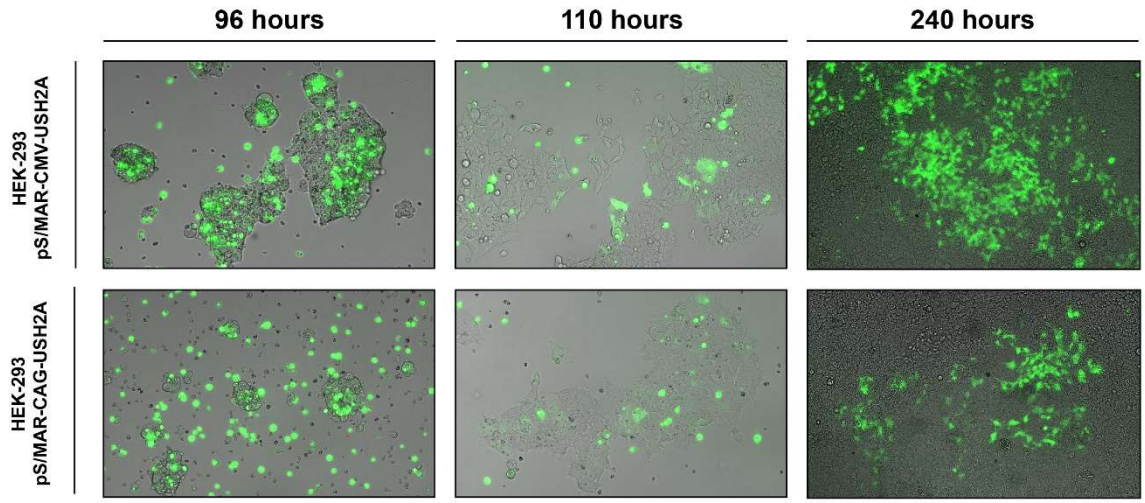

Figure 43. Transfection HEK293 cells with pS/MAR-CAG-USH2A or pS/MAR-CMV-USH2A vector.

Fluorescent microscope images showing GFP expression in HEK293 cells electroporated with pS/MAR-CAG-USH2A vector or pS/MAR-CMV-USH2A vector, at 96- 110- and 240- hours post-electroporation.

Western blot of a 570-kda protein such as the usherin, is challenging and has required a lot of optimisation. Gel electrophoresis was performed using NuPAGE Tris-Acetate SDS Running Buffer gel, which provides a better separation of large molecular weight. 40µg proteins was loaded on each well. Wet transfer was used instead of semi-dry transfer, for 16 hours at 25 V and 4°C. The quality of protein transfer was assessed with a Red ponceau staining. In addition, different lysis buffers were tested:

- Lysis buffer 1. RIPA cell lysis buffer supplemented with 1X Protease and Phosphatase Inhibitor Cocktail
- Lysis buffer 2. 50 mM Tris-HCl pH 7.5, 150 mM NaCl, 0.5% Triton X-100, 5 mM EDTA, 1 X Protease inhibitor, 1 mM DTT, 5% CHAPS (Yu et al., 2020)
- Lysis buffer 3. 50 mM Tris-HCl pH 7.5, 150 mM NaCl, 0.5% Triton X-100, 5 mM EDTA, 1 X Protease inhibitor, 1 mM DTT, 1% NP-40 (Yu et al., 2020)
- Lysis buffer 4. 50 mM Tris-HCl pH 7.5, 150 mM NaCl, 0.5% Triton X-100, 5 mM EDTA, 1 X Protease inhibitor, 1 mM DTT, 1% Triton X-10 (Yu et al., 2020)

All the lysis buffers displayed comparable efficiency, therefore the Lysis buffer 1 was chosen. Finally, 4 different antibodies (from collaborators and commercially available) directed against the usherin were assessed (Table 15)..

Antibody	Providers	Lowest dilution used	Results
Anti-Usherin	Origene	1/100	Non-specific
Anti-Usherin	Wolfrum Lab	1/100	Non-specific
Anti-Usherin	Van Wijk Lab	1/100	Non-specific
Anti-Usherin	Amraoui Lab	1/100	Worked

Table 15. List of Usherin antibodies tested for stainings and Western Blot analysis.

Western blot of HEK-293 cells electroporated with CMV-USH2A-S/MAR and CAG-USH2A-S/MAR detected expression of GFP, with an expected band at 25 kDa, such as the GFP-positive control band. Similarly, usherin isoform b (570kDa) was observed at the right size (See Figure 49). Usherin expression was also detected in the non-transfected HEK-293 cells at lower levels, which was unexpected. CMV-USH2A-S/MAR transfected HEK cells showed a significant increase of 47.0 % (SD = 3.8%), while CAG-USH2A-S/MAR transfected HEK cells displayed a non-significant increase (p=0.18) of 31.9% (SD = 29.4%). To confirm these results, we used two different positive controls reported to express the usherin. CORL24, a small lung cancer cell line and NCI-H2106, a large cell lung carcinoma (https://depmap.org/portal/gene/USH2A?tab=characterization&characterization=expression). As shown on the blot membrane, both are expressing usherin isoform b (Figure 44).

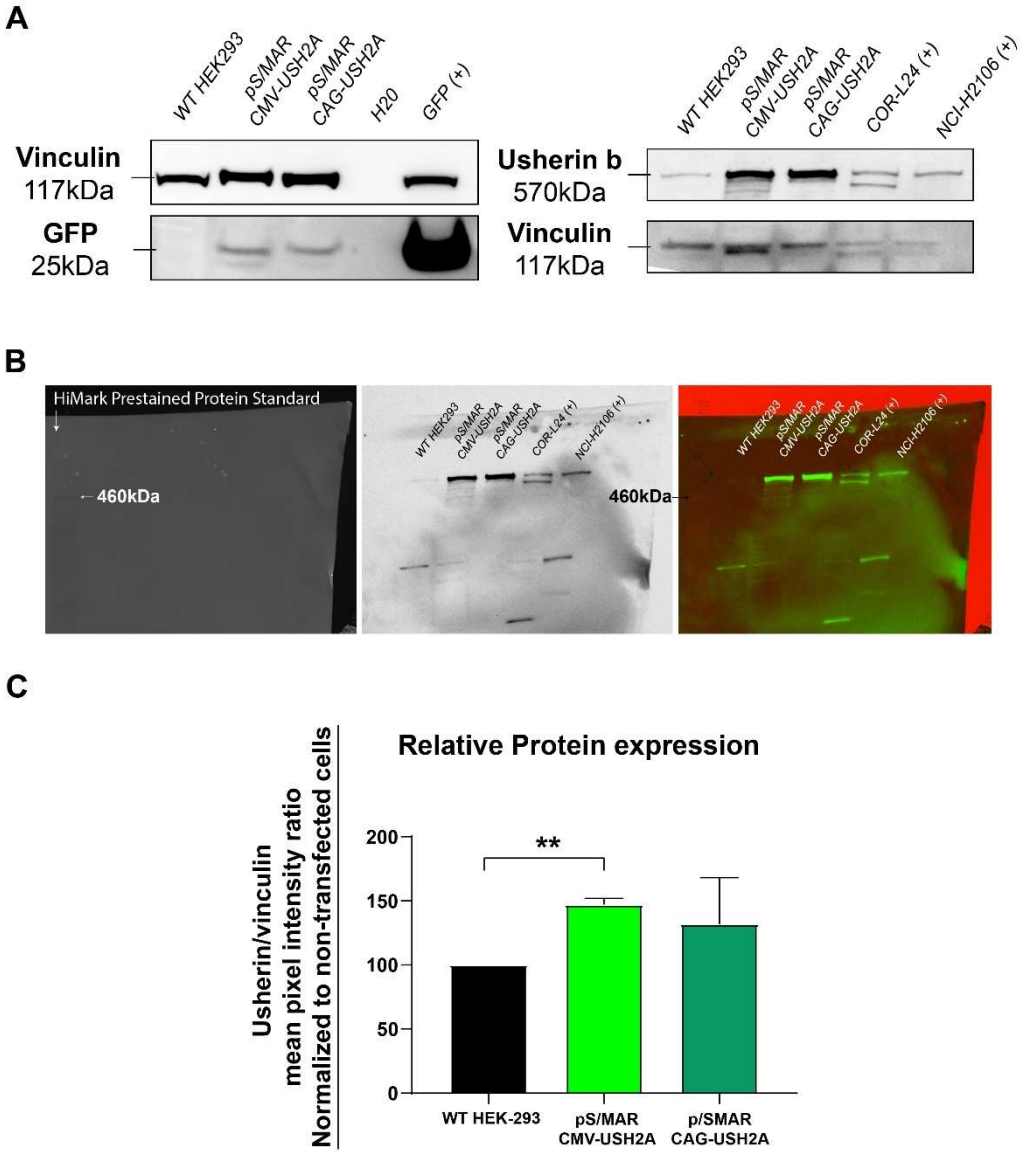

Figure 394. Western blot of transfected HEK293 cells with pS/MAR-CAG-USH2A or pS/MAR-CMV-USH2A vector.
(A) Western blot analysis of non-transfected WT HEK cells, pS/MAR-CMV-USH2A, pS/MAR-CAG-USH2A transfected HEK293 cells, COR-L24 and NCI-H2106 two cancer cell lines reported to express usherin used as positive controls. (B) Full membrane for usherin western blot, localizing above th 460kDa marker of the HiMark Prestained Protein Standard (C) Usherin/vinculin ratio normalized to non-transfected cells graph (** $p<0.01$) (n=3).

5.4 *USH2A*-S/MAR vectors drive usherin expression in transfected human dermal fibroblasts (HDF)

5.4.1 Electroporation in HDF

Primary HDFs from patient with Usher type 2A were electroporated with 10µg of CAG-USH2A-S/MAR, using the NEON program 1650V - 10ms - 3 pulses. Significant cell death occurred at 24-hour post-electroporation as showed in Figure 50, but some cells recovered 5 days later. CAG-USH2A-S/MAR was used as this was found to generate more persistent GFP expression, after 5 days. GFP expression was monitored using a fluorescent microscope. GFP positive HDFs were collected 120-hour post-electroporation. As protein lysates did not yield enough protein for usherin western blot, qRT-PCR of *USH2A* was performed. It confirmed significantly higher levels of *USH2A* expression in transfected HDF compared to non-transfected cells, with a 13.5-fold increase in expression (SD=1.196; p=0.0039) (Figure 45).

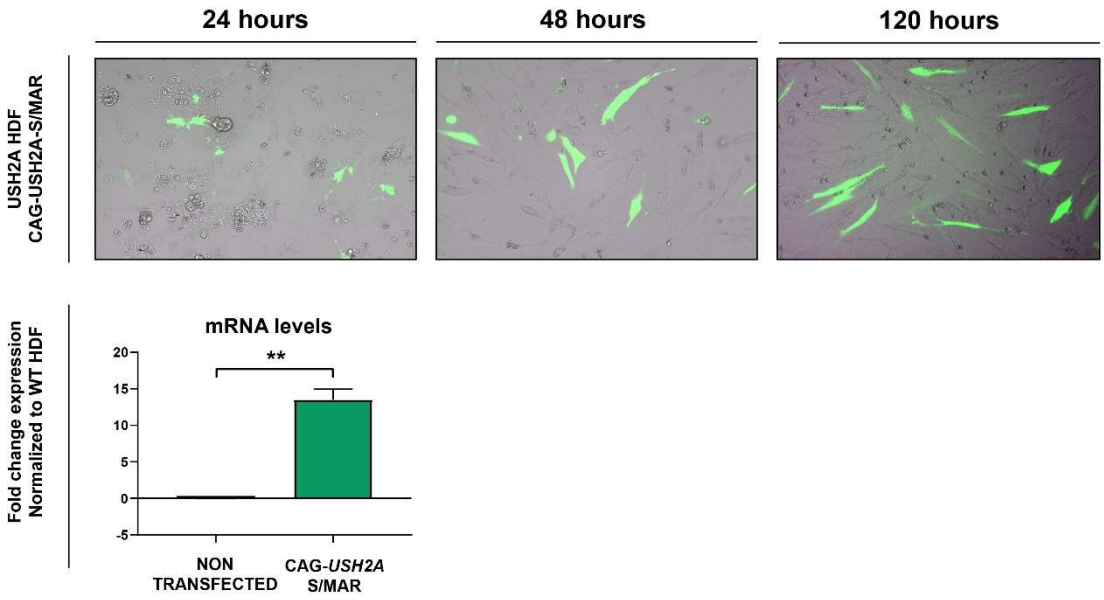

Figure 45. Transfection of USH2A HDF cells with CAG-USH2A-S/MAR.

Fluorescent microscope images showing GFP expression in USH2A patient-derived human dermal fibroblasts electroporated with CAG-USH2A-S/MAR vector. Fold change gene expression of USH2A in non-transfected wild-type and USH2A patient fibroblasts, and CAG-USH2A-S/MAR transfected USH2A fibroblasts. (n=3) (** $p<0.01$)

5.4.2 Immunostaining of usherin in dermal fibroblasts transfected with USH2A-S/MAR

Given that HDF cells are a valuable cell model for *USH2A*-related disorders, usherin protein expression was investigated in HDF cells and USH2A-S/MAR transfected HDF. Previous studies reported *USH2A* expression at RNA and protein level in fibroblasts by western blot and immunostaining (Samanta et al. 2019; Radulfus WN Slijkerman et al. 2016b). Additionally, Pendse and colleagues showed localisation of usherin at the primary cilium base of OC-k1 cell line (Pendse et al. 2019) while Samanta and colleagues observed the protein all over the cell membrane. Therefore, we sought to investigate the localisation of the usherin near the primary cilia of fibroblasts (Figure 46). However, no convincing specific signal was observed for the usherin using the antibodies kindly provided by Pr. Uwe Wolfrum's team or Pr. Aziz Amraoui's team (Figure 46). Also, we stained USH2A-S/MAR transfected fibroblasts. Despite GFP expression, still no specific signal was observed for the usherin (Figure 46).

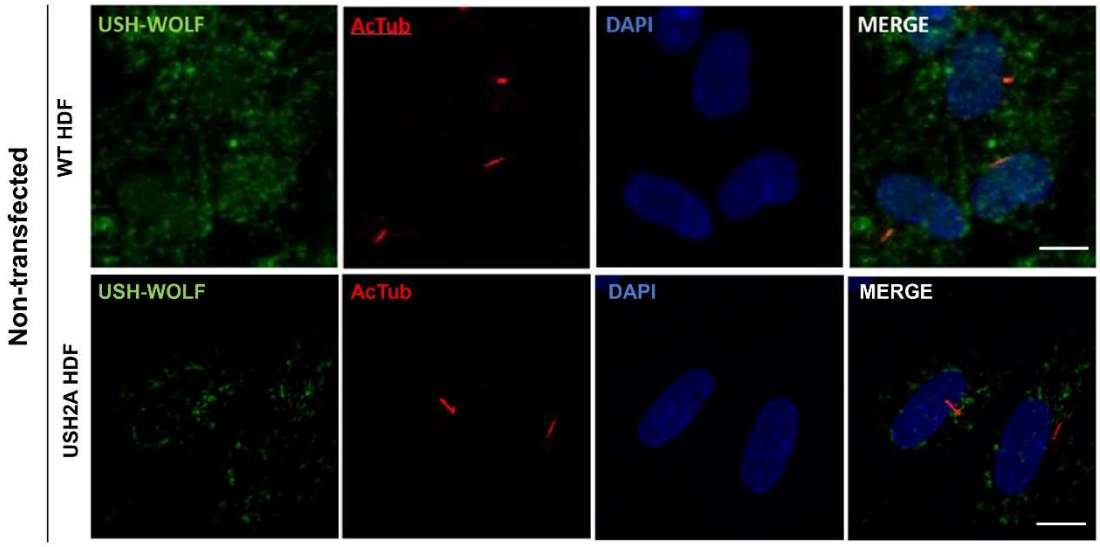

Figure 46. Usherin expression in non-transfected WT and USH2A human dermal fibroblasts.

WT and USH2A HDF were immunostained with an anti-usherin antibody from Wolfrum's team (in green). Cilia were stained using an acetylated tubulin antibody (in red) and dapi nuclei stain (blue) was used. (Scale bars = 10 µm).

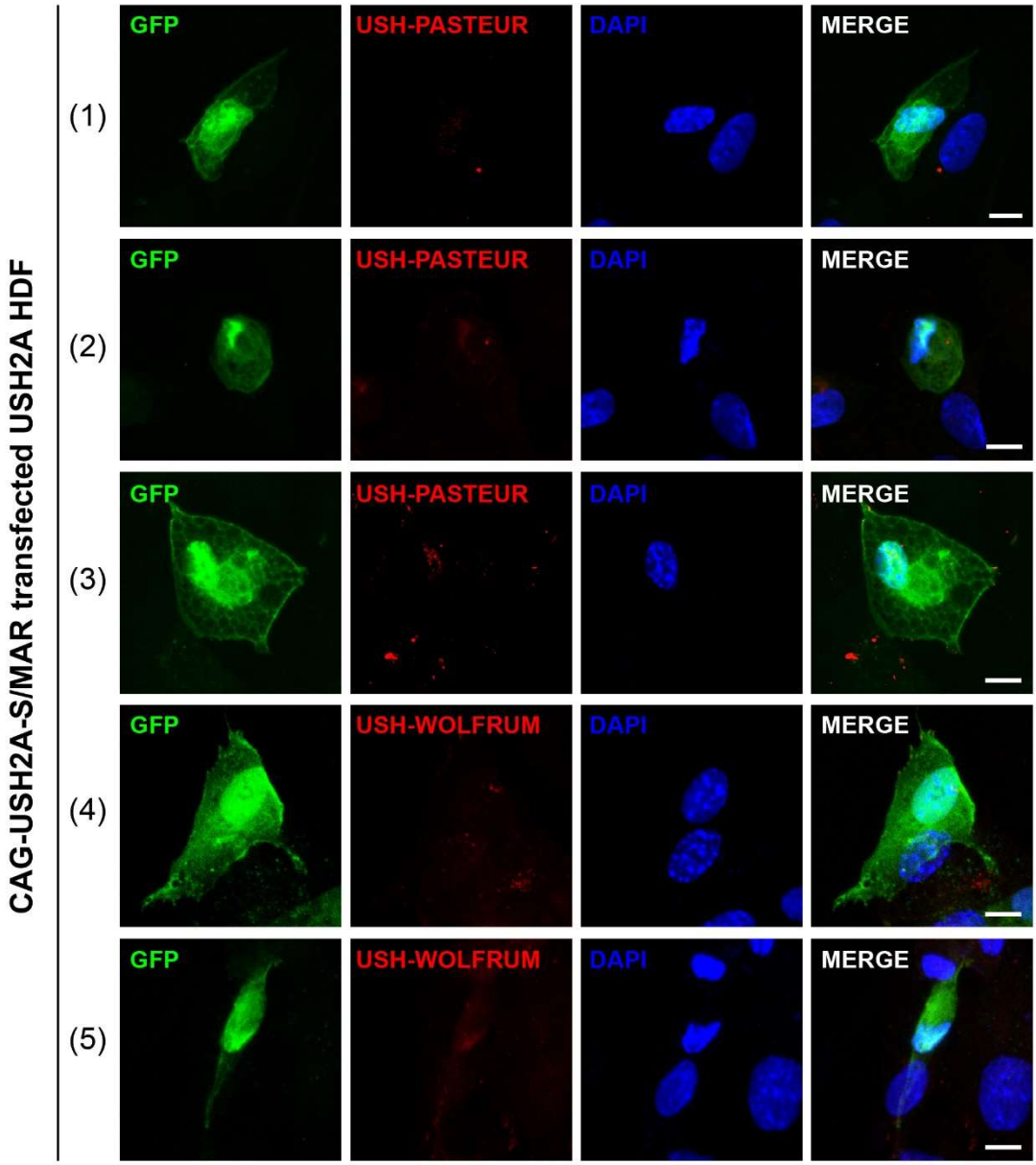

Figure 47. Unsuccessful immunostaining of overexpressed usherin in dermal fibroblasts transfected with CAG_USH2A-S/MAR.
USH2A patient-derived dermal fibroblasts, transfected with CAG-USH2A-S/MAR, were immunostained with anti-usherin (red). GFP (green) was also detected and dapi nuclei stain (blue) was used. (Scale bars = 10 μm).

An antigen retrieval step was then added to the immunostaining protocol. The fixed cells were boiled in hot citrate buffer allowing the breakage of PFA cross links during the fixation step. Following this new protocol, immunostaining of WT and *USH2A* HDF was performed to detect usherin expression (Figure 48). In HDF transfected with *CAG-USH2A-S/MAR*, a specific and novel expression pattern of usherin could be observed compared to background levels of the protein or non-specific staining observed in the control fibroblasts. GFP-positive cells displayed an usherin signal localising to the cell borders, resembling the site of focal adhesions (Figure 48). Focal adhesions are clustered-integrin receptors interacting with the extracellular matrix. They play a role in adhesion, migration and mechano-sensing (Burridge, Chrzanowska-Wodnicka, et Zhong 1997). Similarly, a recent study showed expression of ADGRV1, a protein part of the Usher 2 complex, at the focal adhesions of several cell lines such as hTERT-RPE1, mouse embryonic fibroblasts, and mouse astrocytes, showing a similar pattern to the usherin overexpression (Kusuluri et al. 2021).

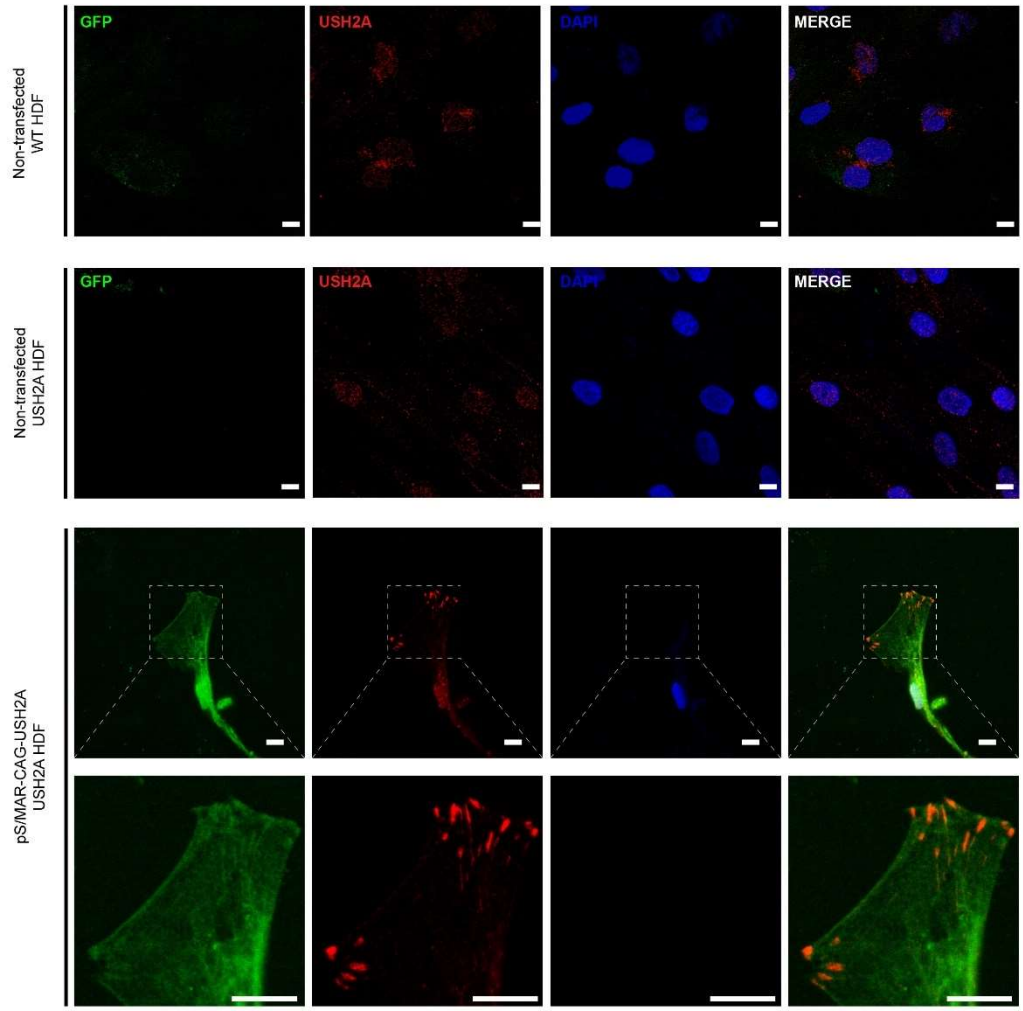

Figure 48. Optimized immunostaining of overexpressed usherin in dermal fibroblasts transfected with CAG-USH2A-S/MAR.

USH2A patient-derived dermal fibroblasts, non-transfected or transfected with pS/MAR-CAG-USH2A, were immunostained with anti-usherin (red). GFP (green) was also detected and DAPI nuclei stain (blue) was used. (Scale bars = 10 µm).

In line with this finding, focal adhesion and usherin localization were investigated, however, staining of F-actin (Figure 49) and Vinculin (not shown) failed and need to be repeated. Similarly, immunostaining of ADGRV1 and Whirlin, two usherin partners were performed but were unsuccessful within the timeframe of this study (not shown). Hence, further

work should be undertaken to study usherin partner and focal adhesion proteins in USH2A-S/MAR transfected HDF.

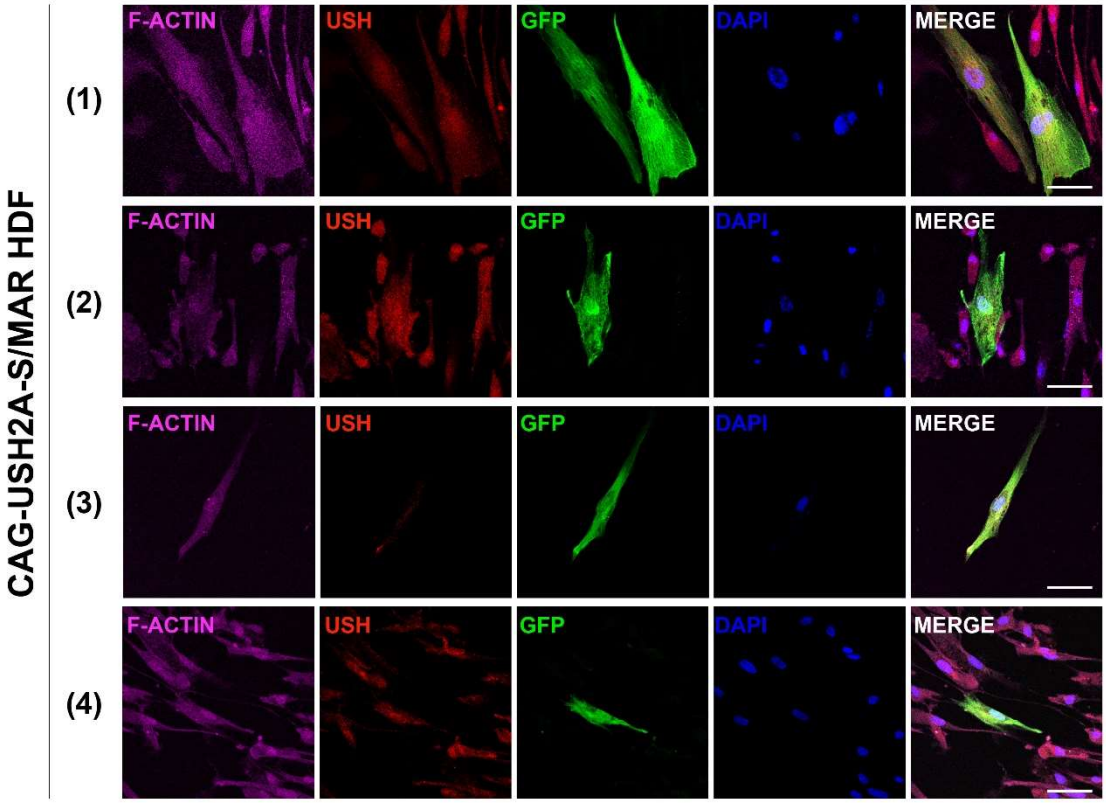

Figure 49. Investigation of focal adhesions in in dermal fibroblasts transfected with USH2A-S/MAR.

USH2A patient-derived dermal fibroblasts, non-transfected or transfected with pS/MAR-CAG-USH2A, were immunostained with phalloidin targeting F-actin (magenta) and anti-usherin (red). GFP (green) was also detected and dapi nuclei stain (blue) was used. (Scale bars = 10 μm).

5.5 USH2A HDF display a cilium defect.

Several recent studies suggested that Usher Syndrome is a ciliopathy (May-Simera, Nagel-Wolfrum, and Wolfrum 2017). Recent evidence showed a significant decrease of 29% in the number of ciliated cells in USH2A patient-derived fibroblasts compared to a healthy control

(Samanta et al. 2019). Similarly, Pendse and colleagues showed that ablation of *Ush2a* affects the ciliogenesis in OC-k1 cell line, with a significant reduced cilia length. Using a similar protocol, WT and USH2A HDF were serum-starved for 72 hours to initiate ciliogenesis of primary cilia. Cilia were double stained against Arl13b and Acetylated tubulin, colocalizing to the primary cilium (Figure 50). Three independent experiments were performed. No significant differences were found when comparing percentage of ciliated cells for WT (69%) and USH2A HDF (64%). However, USH2A-derived fibroblasts displayed significantly ($p<0.001$) shortened cilia (4.1µm) compared to the control (6.2µm); this 2.1 µm decrease in cilia length represents a 33% reduction compared to of WT cells. Cilium length differences in this cell model could be used as a reliable endpoint to assess the functional rescue efficacy driven by USH2A-S/MAR vectors or other potential treatments. This finding has only been determined in one *USH2A* patient cell line with c.2299del p.(Glu767Serfs*21) and c.3187_3188del p.(Gln1063Serfs*15) variants. This phenotype could be specific to these variants, hence investigating cilia length in another patient line with different *USH2A* mutations would be desirable.

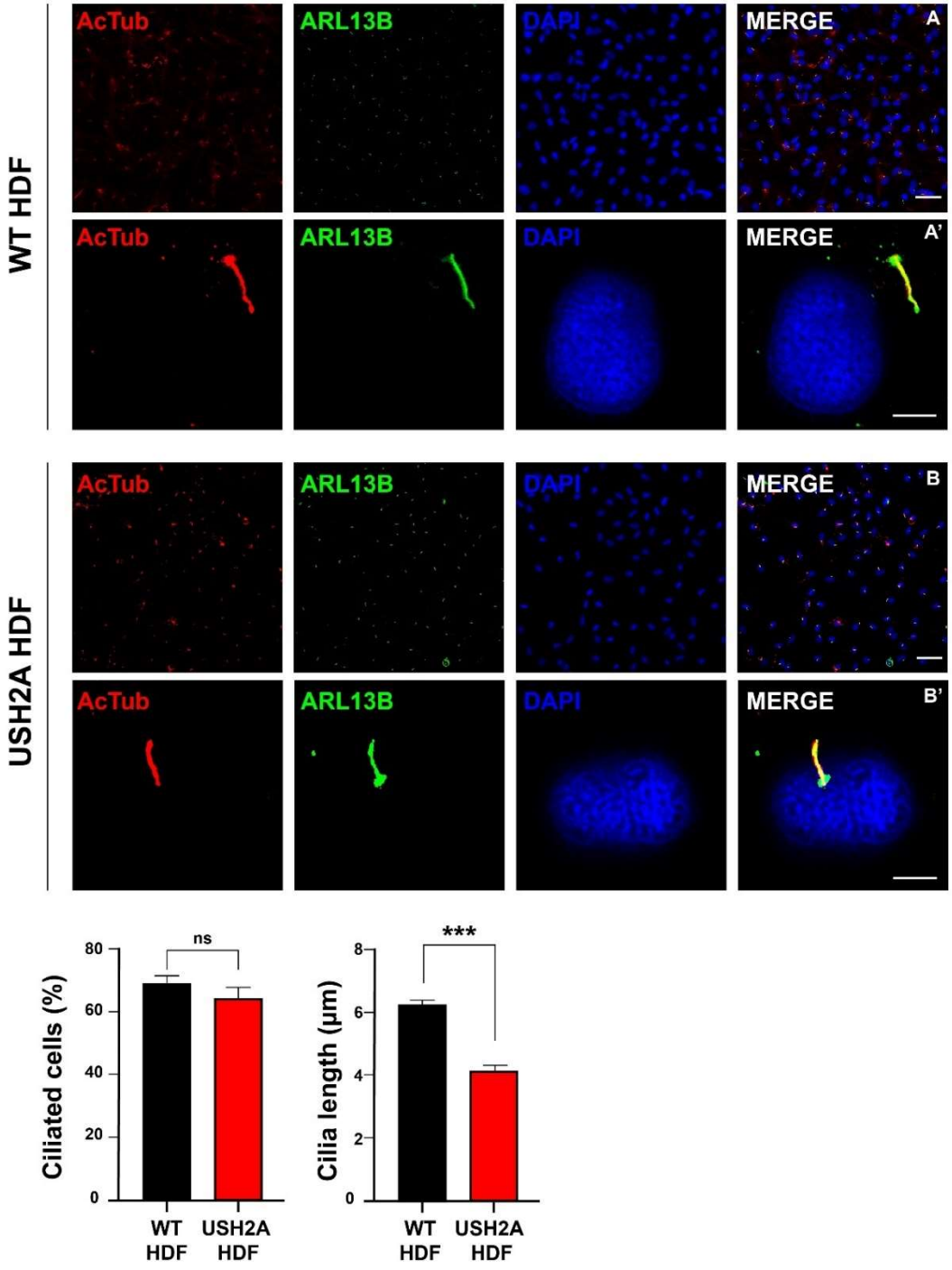

Figure 50. Ciliation assay in USH2A HDF.

Cilia were double stained against ARL13B (in green) and acetylated tubulin (in red). Three independent experiments were performed, the ciliated cell percentage were counted, and cilia length measured. ns=non-significant ***=p<0.001. Scale bars: 50µm (A and B) ; 5µm (A' and B').

Following these results, cilia length rescue was going to be assessed in transfected cells expressing the CAG-USH2A-S/MAR. However, the combination of CAG-USH2A-S/MAR electroporation and 72-hour long serum-starved medium lead to dramatic cell death and disrupted cilia formation. Further time is required to optimise this protocol in order to use cilia as an endpoint in transfected HDF (see Figure 51).

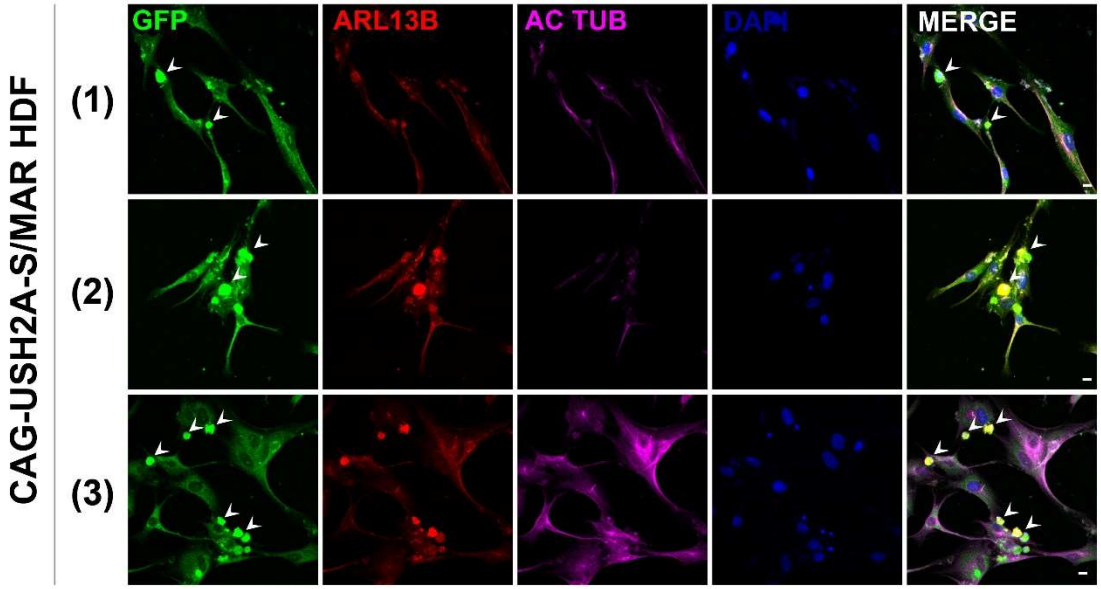

Figure 51. Ciliation assay in electroporated USH2A HDF with CAG-USH2A-S/MAR.

Cilia were double stained against ARL13B (in n) and acetylated tubulin (in red). Three independent experiments were performed, the ciliated cell percentage were counted, and cilia length measured. Arrows showing dying cells. ns=non-significant ***=p<0.001. Scale bars: 50μm (A and B) ; 5μm (A' and B').

5.6 Human IPSC reprogramming

5.6.1 Reprogramming

Human Dermal Fibroblasts (HDFs) from the USH2A patient with c.2299del p.(Glu767Serfs*21) and c.3187_3188del p.(Gln1063Serfs*15) variants, were reprogrammed using integration-free episomal vectors. Reprogramming protocol was based on a previously described protocol with minor modifications (Okita et al. 2011; N. Schwarz et al. 2015). Using this reprogramming protocol, more than 40 clones were mechanically isolated and the 5 best ones were expanded (See Figure 52). hIPSC colonies should display a highly compact morphology with well-defined edges. Cell morphology resembles that of ESCs with a high nuclei/cytoplasm area ratio. The three clones displaying the best morphology and growing rate were selected for future experiments: clone USH2A-A4b, USH2A-A6b and USH2A-C2.

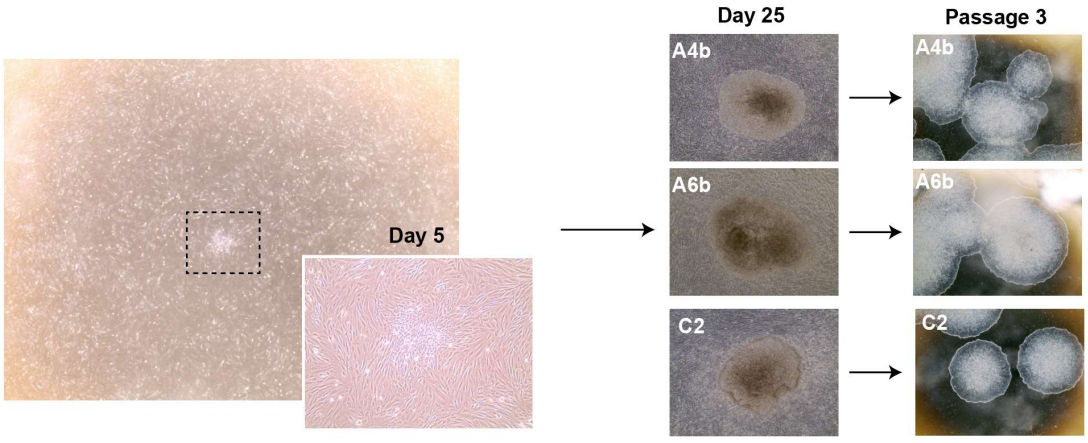

Figure 402. Reprogramming of USH2A patient derived human dermal fibroblasts.
Several hIPSCs colonies emerged from the cell layer, the three clones with the best morphology were selected for future characterisation and experiments (A4b, A6b and C2).

5.6.2 hIPSC Characterisation

As shown in Figure 53A, hIPSC colonies were compact, flat and with a large nuclei/cytoplasmic ratio. An alkaline phosphatase staining was performed to evaluate undifferentiated state of the cells. Colonies were positive (Figure 53A), displaying an intense purple staining. Additionally, colonies were expressing pluripotency markers: OCT4 (red in Figure 53A), and SSEA3 (green in Figure 53A). Upregulation of pluripotency genes in hIPSC such as *OCT4*, *SOX2*, *L-MYC* and *LIN28* compared to HDF controls was observed by qRT-PCR (Figure 53B). Embryoid body formation was used to investigate hIPSC ability to give rise to the 3 germ layers. Immunostainings of random undirected hIPSC differentiation showed presence of ectoderm marker PAX6, mesoderm marker Vimentin (VIM) and endoderm marker AFP (Figure 53C). Low-pass whole genome sequencing analysis of iPSCs displayed a normal female 46,XX karyotype (see Figure 53D). This *USH2A* hIPSC line can act as a tool for disease modelling of *USH2A*-related retinopathy through differentiation into retinal organoids or other potential cell types of interest.

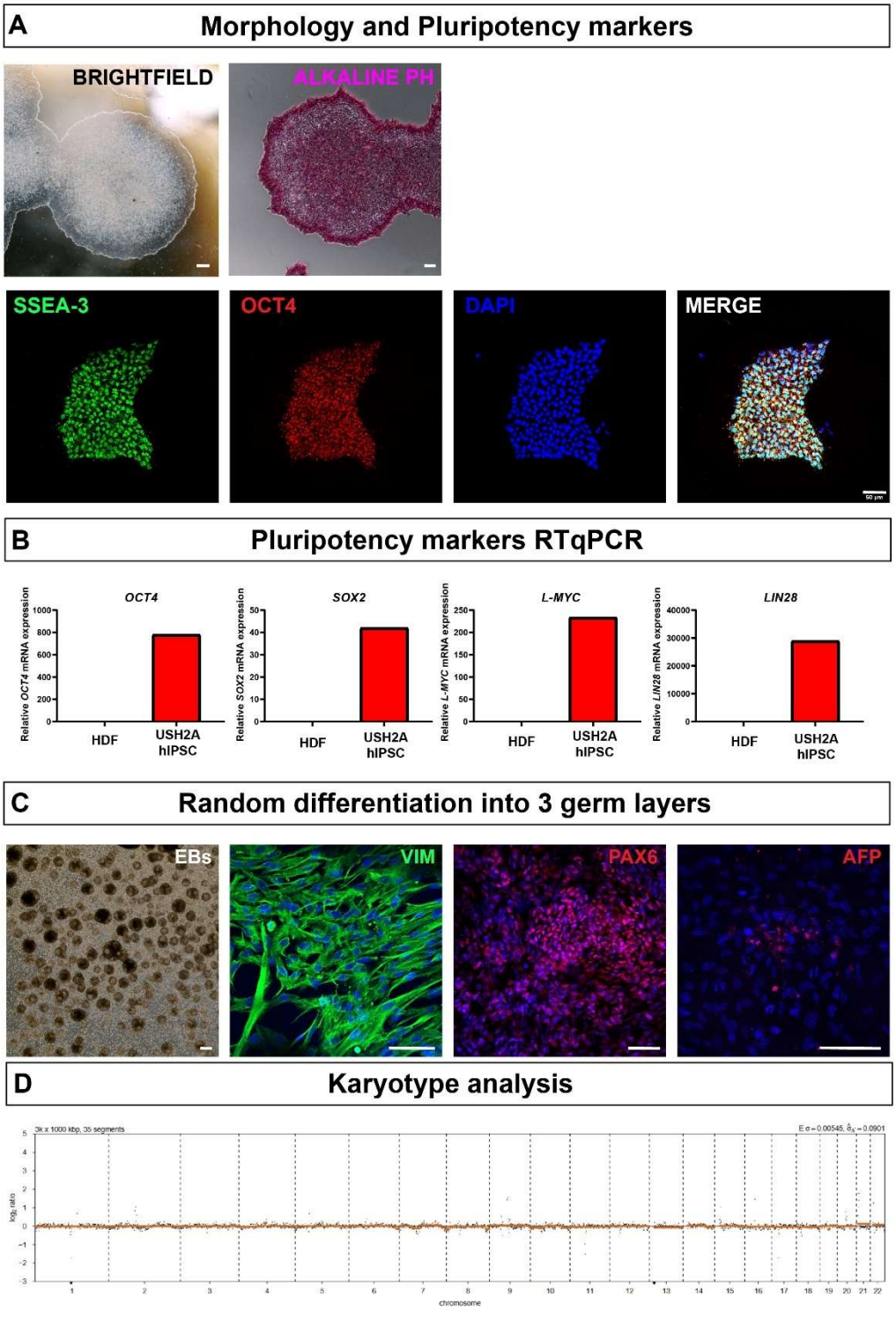

Figure 53. USH2A hiPSC characterisation.

(A) Brightfield image of an *USH2A* hiPSC colony. hiPSC colony positive to the alkaline phosphatase staining (purple). Immunostaining of hiPSC for pluripotency markers such as OCT4 (Red) and SSEA3 (green). (B) RT-

qPCR of pluripotency markers in hiPSC gene expression of pluripotency markers compared to HDF : *OCT4*, *SOX2*, *L-MYC* and *LIN28* (C) Embryoid bodies (EB) formation to differentiate into the three germ layer : ectoderm marker PAX6, mesoderm marker Vimentin (VIM) and endoderm marker AFP. (D) Low pass whole genome sequencing revealed normal chromosomal structure for USH2A hiPSC line (scale bar = 50µm).

5.6.3 Cilia in hIPSC

Similarly, to HDF, ciliogenesis function was investigated in USH2A hiPSC vs WT hiPSC. However, no serum-starvation process was performed as hIPSC need mTeSR supplement to survive and maintain their pluripotency state. Cilia were stained against ARL13B, localizing to the primary cilium (Figure 54). Two independent experiments were performed. Cilia were too short to be reliably measured. As shown in Figure 54, 61% of WT hIPSC were ciliated, compared to 25.3% for USH2A hiPSC (N=2). Further work needs to be undertaken to check if this 35.6% decrease in ciliogenesis is reproducible.

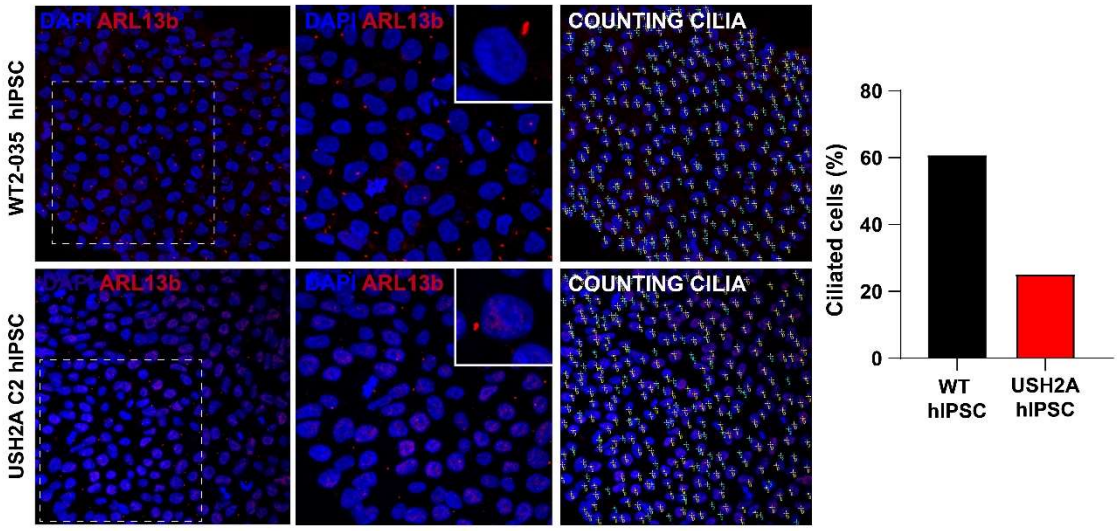

Figure 414. Ciliation assay in WT and USH2A hiPSC. Cilia were double stained against ARL13B (in green) and acetylated tubulin (in red). (n=1) (scale bar = 50µm)

Cilia were stained against ARL13B (in red) and nuclei counterstained with DAPI (in blue). Only two independent experiments were performed, the ciliated cell percentage were counted.

5.7 Retinal organoids model

5.7.1 Optimization of differentiation protocol

After cell line pluripotency validation, hiPSC-derived retinal organoids models were cultured and characterized. First, hIPSC were differentiated into retinal organoids following the protocol optimized by Gonzalez-Cordero and colleagues (Gonzalez-Cordero et al. 2017). As described in Figure 60, the differentiation protocol A is divided into 2 main steps. The first step is in 2-dimensions (2D), while the second step is in 3-dimensions (3D). hIPSC are cultured to reach 90% confluency. mTESR hIPSC maintenance medium is replaced by E6 medium devoid of FGF2 and TGFb. Withdrawal of these factors stops the pluripotency machinery and encourages the spontaneous differentiation of hIPSC. This step is defined as D0. At D2, the medium is changed to a pro-neural medium containing E6 supplemented with N2. After 3 weeks, neuroepithelial structures arises from the 2D layer. At D28, these structures are mechanically isolated and further cultured in 3D. From D28 to D35, isolated 3D retinal structures are further cultured in Advanced DMEM-F12 / B27 supplement / MEM NEAA/ Glutamax 2mM / 0.1% Penicillin/Streptomycin / FGF2 5µM. Then, from D35 to D70, this medium was supplemented with 10%FBS / Taurine 100µM. From D70 to D84, 1µM retinoic acid was added for photoreceptor maturation. From D84 to D250, retinoic acid was decreased to 0.5µM and N2 supplement was added.

However, USH2A hIPSC clones were not producing retinal organoids using the first protocol. In parallel, the use of Regent et al. 2019 protocol described in the previous chapter for RPE differentiation produced similar neuroepithelial structures as the one expected with protocol A. Therefore, a new optimized protocol was used, and resulted in more efficient retinal organoids production for USH2A hIPSC clones. The first 2D step was changed. From D0 to D2, hIPSC were cultured in DMEM high glucose supplemented with 20% KOSR, 10mM Nicotinamide, and 0.1% P/S. From D2 to D28, N2 supplemented was added. KOSR was decreased to 15% KOSR concentration (D5-D9) and 10% KOSR (D9-D28). Nicotinamide was withdrawn at D7. The 3D step of protocol B is similar to protocol A.

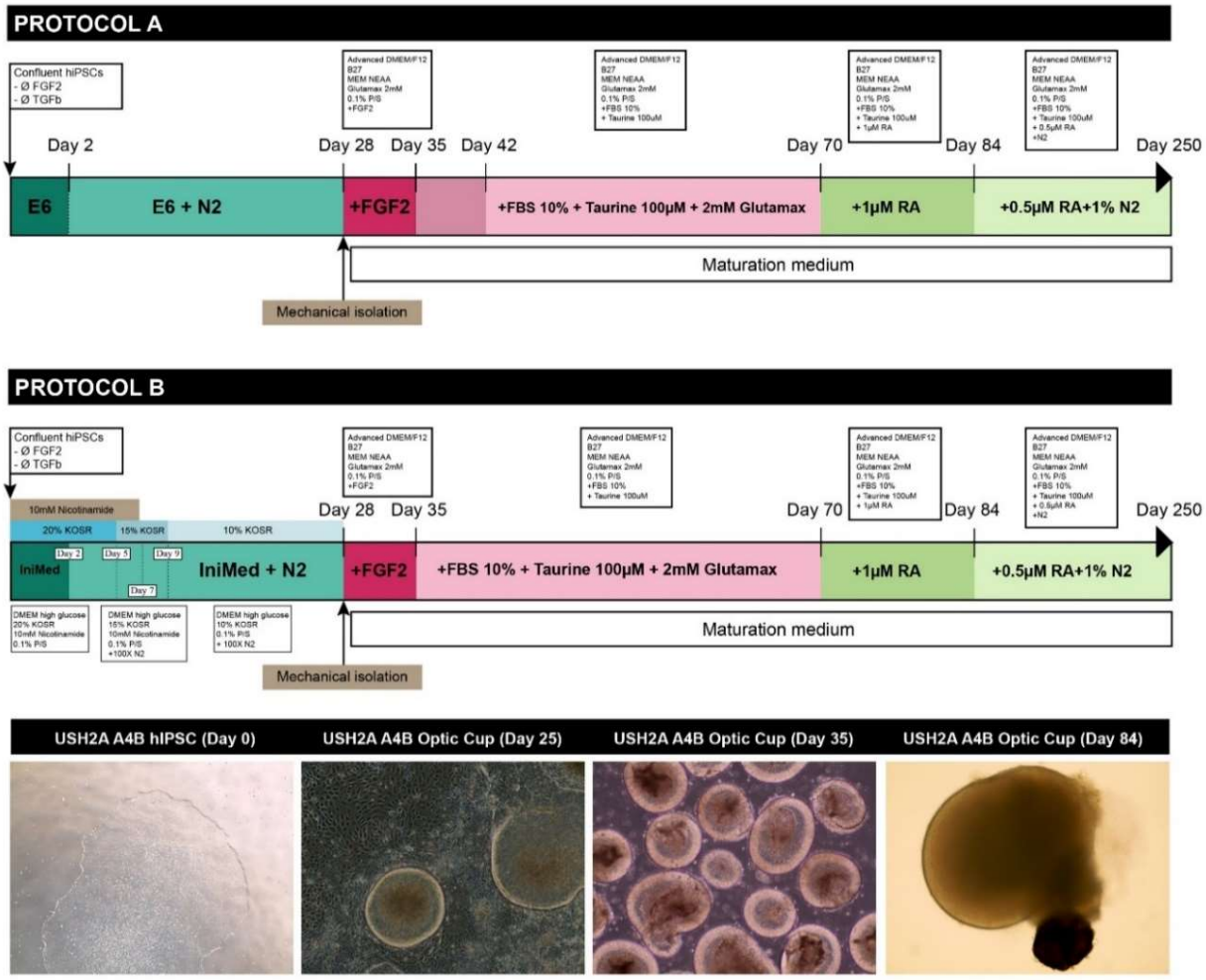

Figure 425. Retinal organoids differentiation protocol.
2 different protocols were used for retinal organoids differentiation (A) and (B). Brightfield images of hIPSC, retinal neuro-epithelial structures, 3D early retinal organoids, late retinal organoids (Scale bars = 100µm).

5.7.2 Cilia in day-35 retinal organoids

WT and USH2A retinal organoids were cultured until Day 35 of maturation. Similarly to HDF and hIPSC, ciliogenesis and cilia length was measured. At Day 35, cryosections of retinal organoids were stained against *VSX2*, a retina-specific transcription factor to identify photoreceptor progenitor cells. A VSX2-positive cell layer was well-defined to the retinal organoid border. ARL13B was also stained to investigate cilia length. Interestingly, ARL13B staining showed that VSX2-positive cell cilia at the outer part of the retinal organoid, were polarized radially (Figure 56). These cilia may develop to form nascent photoreceptor outer segments.

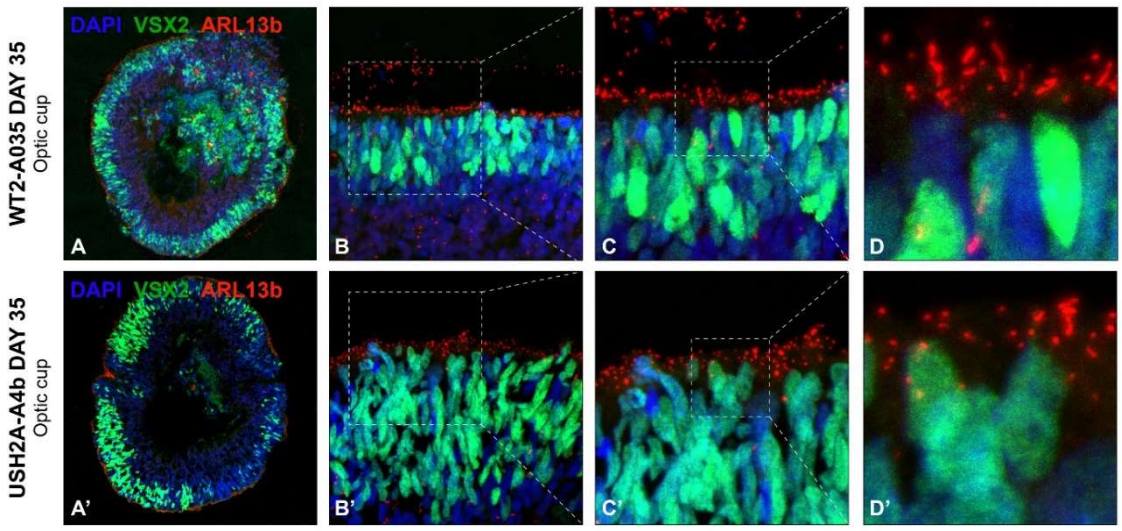

Figure 56. USH2A retinal organoids at Day 35.

WT (A,B,C and D) and USH2A (A',B',C' and D') retinal organoids at Day 35 stained VSX2 (green) and ARL13B (red). Cilia length of VSX2-positive cells in USH2A organoids seemed to be shorter, however higher resolution was required for precise measurement.

As shown in Figure 57, the cilia density at the retinal organoid outer part was preventing a reliable cilia length measurement. Therefore, higher magnification confocal pictures were acquired using Airyscan module on the Zeiss LSM 710S confocal microscope. Z-stacks were projected on the same plan using a temporal-color code (Fire), allowing a better differentiation of each cilium. Day-35 old WT organoids displayed an average length of 1.59µm compared to an average length of 0.95µm for Day-35 old USH2A organoids. This significant decrease of 0.64µm (N=3, p<0.001) accounts for 39% of WT cilium length. Similarly, to 5.4.1, this finding has been performed with one *USH2A* patient cells with c.2299del p.(Glu767Serfs*21) and c.3187_3188del p.(Gln1063Serfs*15) variants. So, the phenotype could be specific to these variants.

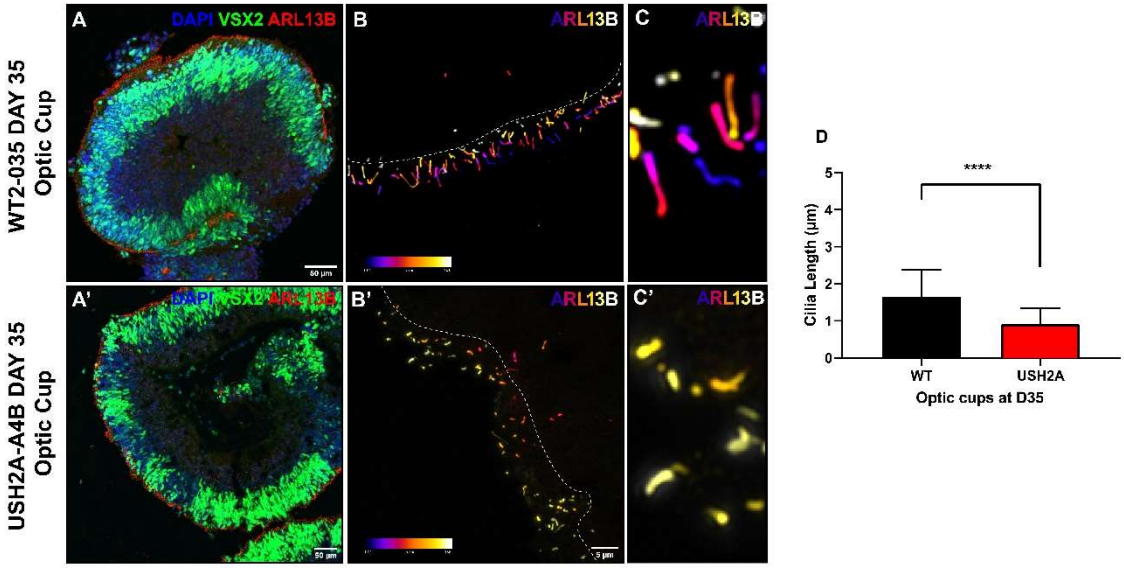

Figure 57. Higher resolution of USH2A retinal organoids at Day 35 displayed cilia formation defects.

WT (A) and USH2A (A') retinal organoids at Day 35 stained VSX2 (green) and ARL13B (red). WT (B,C) and USH2A (B',C') Z-stack projection of ARL13B. Measurement of cilia length of VSX2-positive cells in WT and USH2A retinal organoids (D) (n≤3, mean ± SEM). ****p<0.001.

5.7.3 Retinal organoids at week 11

USH2A retinal organoids were then further cultured to later timepoints of differentiation. However, an important amount of retinal organoids has lost its laminated organisation, forming rosette-like structures. Eleven-week-old retinal organoids were stained against Cone-Rod Homeobox (CRX) and Recoverin (RCVN), which are expressed later in the developmental timing of the retina. Both were well expressed as shown in Figure 58. However, CRX and RCVN were expressed in rosette structures. RCVN-positive cells being expressed at the internal part of the rosettes while CRX-positive nuclei were localized at its external border, and at the retinal organoid edges. These immunostainings confirmed the retinal nature of these organoids, expressing retinal-specific markers such CRX, OTX2 or RCVN.

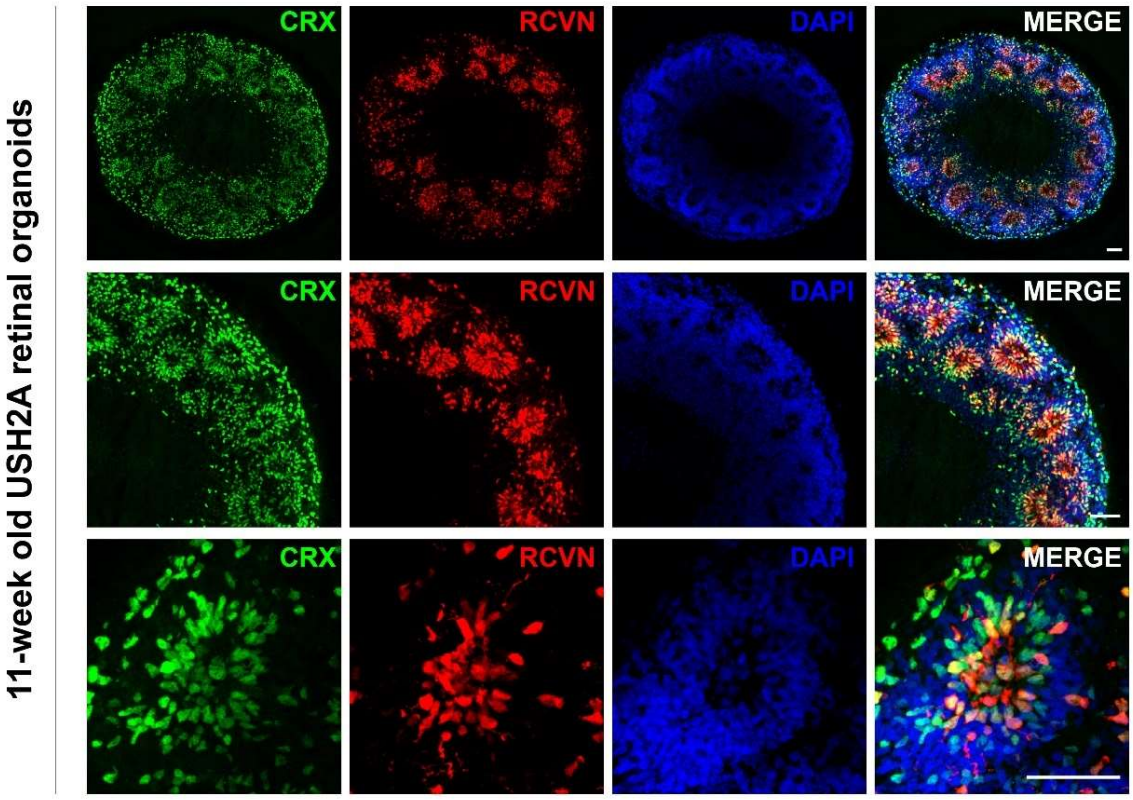

Figure 58. Rosette formation in 11-week-old USH2A retinal organoids.

USH2A retinal organoids at Week 11 stained against CRX (Cone-Rod Homeobox) in green and recoverin (RCVN) in red. Some of the retinal organoids in culture lost their lamination and formed rosette-like structures. Scale bar: 50μm.

More immunostainings were performed on other retinal organoids, some of them displayed a preserved laminated structure, as shown in Figure 64. These 11-week-old retinal organoids were stained for similar markers: CRX, OTX2 and RVCN. These data are preliminary, and more work should be undertaken, to study mature retinal organoids compared to WT, especially to investigate usherin expression, localisation and known partners, which has never been reported in the literature so far.

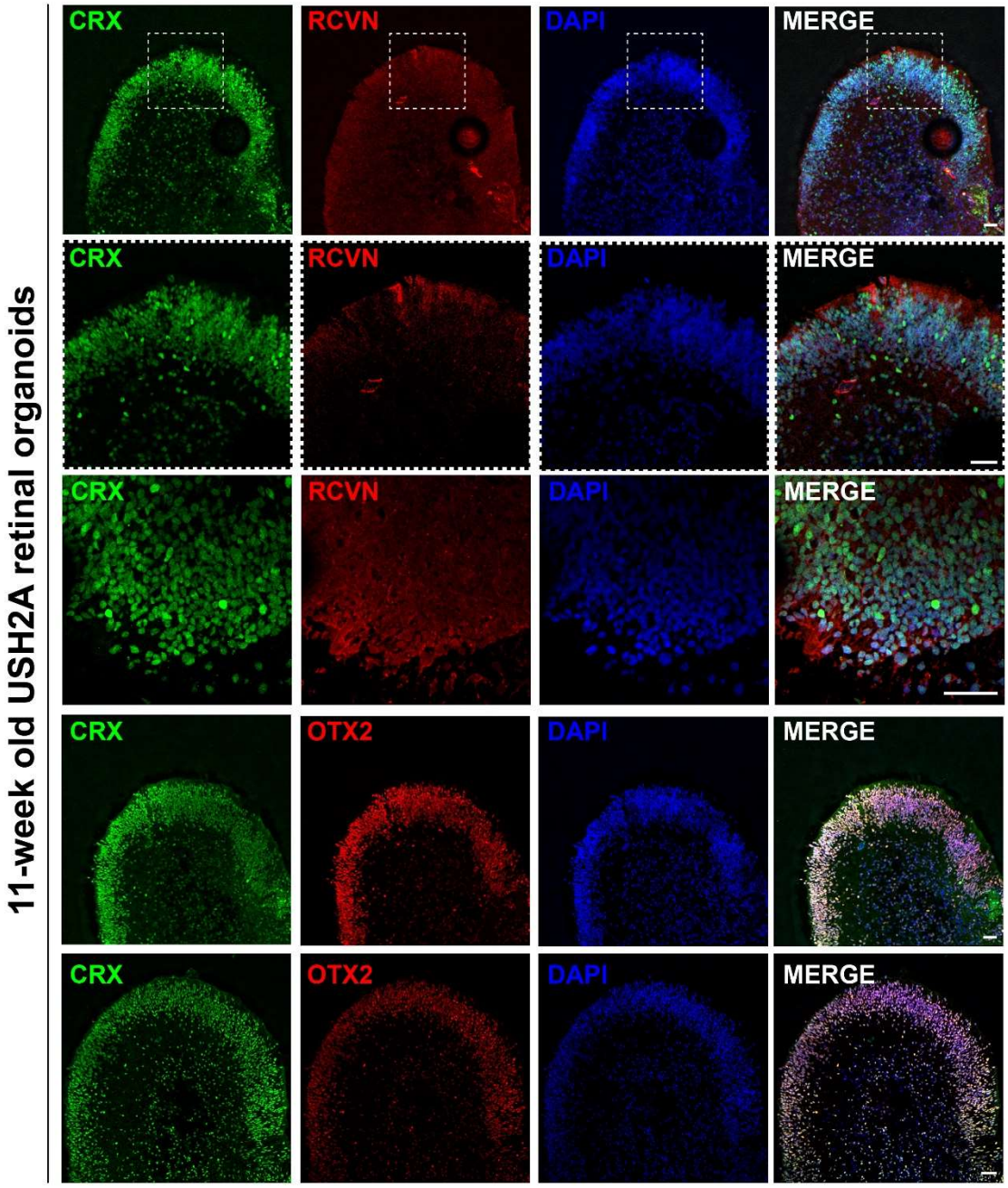

Figure 59. 11-week-old USH2A retinal organoids with preserved lamination.
USH2A retinal organoids at Week 11 stained against CRX (Cone-Rod Homeobox) in green, recoverin (RCVN) or Orthodenticle Homeobox 2 (OTX2) in red. Some of the retinal organoids in culture lost their lamination and formed rosette-like structures. Scale bar: 50μm

5.7.4 Usherin in mature WT organoids

Cowan et al. single-cell transcriptomic data of retinal organoids, suggests that usherin and whirlin is well expressed after 24 weeks of differentiation. Therefore, we performed an immunostaining on cryosections of a 42 week-old retinal organoids to test the specificity of the usherin antibody used in this study. Following the protocol B of differentiation, 42 week-old retinal were produced. These organoids were fixed, frozen and cryosectioned as described in the methods. They were used as positive control for usherin and whirlin expression. As showed in Fig 60, Rhodopsin staining in red displayed a shaped at the nascent outer segment of developing rod photoreceptors cells. These retinal organoids preserved a nice laminated organization. Whirlin, one of usherin partner in the Usher 2 complex, in green displays a diffuse localisation in the photoreceptor cells, in the body cell part, whereas usherin in magenta showed a dotty pattern at the base of the nascent outer segments. Usherin localisation is in line with his expected localisation in mature photoreceptors at the periciliary membrane complex. Additionally, a control staining without the primary antibodies have been performed. This finding supports the idea of specific targeting of usherin antibody used in our study.

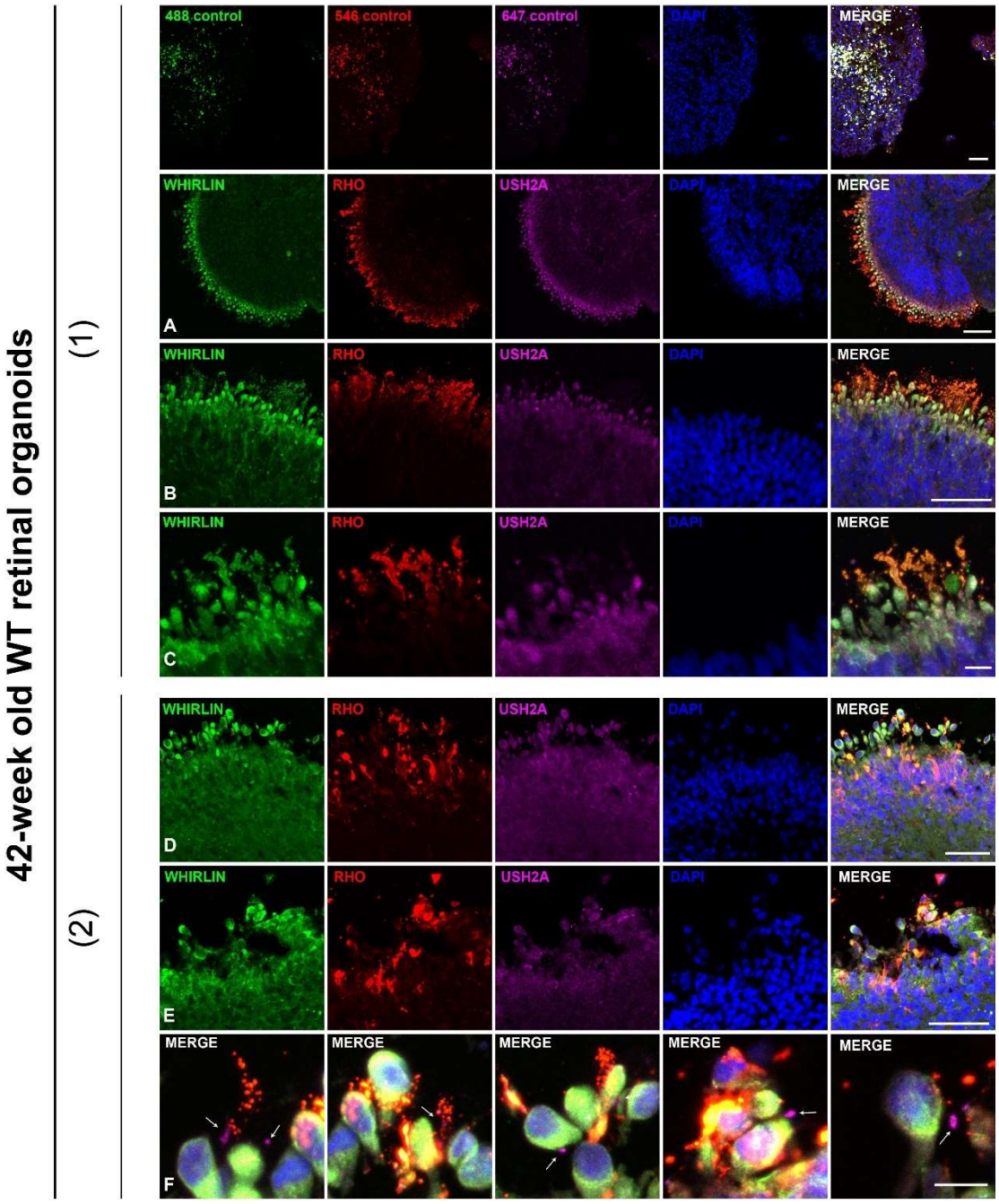

Figure 60. 42-week-old WT retinal organoids with preserved lamination.

WT retinal organoids at Week 42 stained against Usherin (in magenta) in green, whirlin (in green) or Rhodopsin (in red) in red. Arrows points to dotty signal of usherin staining in the photoreceptor cells. (Scale bars: A,B,D,E= 50µm C,F=10µm).

5.8 Discussion

Bilallelic variants in the *USH2A* gene can cause a significant proportion of Usher syndrome type 2A and non-syndromic retinitis pigmentosa (RP). In both disorders, the retinal phenotype involves progressive rod photoreceptor loss resulting in nyctalopia and a constricted visual field, followed by cone degeneration. This leads to the loss of central vision and severe visual impairment.

The *USH2A* gene raises many challenges for researchers and clinicians due to a broad spectrum of mutations, a large gene size hampering gene therapy development and limited knowledge on its pathogenicity. Patients with Usher type 2 may benefit from hearing aids or cochlear implants to correct their hearing defects, but there are currently no approved treatments available for the retinopathy. Viral gene therapies for IRDs in recent years have reached clinical trials and been approved for clinical use in patients (such as voretigene neparvovec for biallelic *RPE65* variants). However, drawbacks of viral strategies still need to be addressed, for example, limits on gene size carrying capacity and reports of inflammatory responses in treated patients suggest the need for alternative gene augmentation strategies.

In this work, the *USH2A* coding sequence (15.6kb) has successfully been cloned into non-viral S/MAR plasmid vectors. It is the first time reported

that the full human *USH2A* coding sequence has been cloned into a vector. Only Yu and colleagues have cloned a plasmid vector with the full-length mouse usherin with its own signal peptide and examined its expression in FreeStyle™ 293-F, Expi293F™, and COS-7 cells. They detected usherin expression by western blots, but at very low concentrations not useful for functional rescue. However, they did transfect COS-7 and with an extracellular portion of usherin (F19-F32), which localized at the plasma membrane, with no usherin aggregates observed in the cytoplasm.

In this chapter, *USH2A*-S/MAR vectors were introduced into HEK-293 cells using electroporation. Persistent GFP expression was detected more than 10 days after electroporation, and usherin protein (570kDa) was detected by western blot analysis. This successful overexpression of the human usherin protein *in vitro* is novel, but still needs further optimization to decrease cell toxicity.

Interestingly, as reported in Figure 42, HEK293 expressing USH2A-S/MAR plasmids showed an altered morphology with neurite-like processes. GFP-positive cells grew 2 to 3 neurite-like processes of 50-70μm each. Such phenotypes were not observed in HEK293 expressing GFP only or REP1-S/MAR plasmids. These morphologic changes could be caused by the stress induced by such a big transgene transfection or be driven by

exogenous usherin overexpression. Similar morphological changes in HEK cells, have been reported by Koch and colleagues when transfecting HEK cells with a 7kb-long NRSE dsRNA-expressing vectors. They observed an altered morphology leading to the formation of comparable thin processes and induced the expression of neurofilament-68. Also, they found that it was enhancing neurite outgrowth in primary retinal ganglion cells, and it was caused by the sequestration of REST1 (Koch et al. 2011). Therefore, some mechanisms can trigger neurite outgrowth in HEK293 cells. This mechanism would need to be explored. These modifications in HEK293 morphology could provide new insights into usherin long-isoform functions such as cell migration and neurite outgrowth, which requires a complex interplay with the extracellular matrix. As a matter of fact, usherin long-isoform contains a very long extracellular domain with several motifs associated with extracellular matrix proteins such as laminin and fibronectin repeats. It has been reported that Usherin LE domain interacted with type IV collagen 7S domain and fibronectin. However, few studies have been investigating the relationship of usherin extracellular domains and the surrounding extracellular matrix.

USH2A-S/MAR vectors were also introduced in primary HDF from patient with Usher type 2A using electroporation. Primary HDF are hard-to-transfect cells. The use of commercially available branched PEI-based chemical reagent did not lead to reproducible GFP expression. Therefore, NEON electroporation system was used. qRT-PCR of *USH2A* was

performed and confirmed significantly higher levels of *USH2A* expression in transfected HDF compared to non-transfected *USH2A* HDF cells.

The lack of cell material to confirm usherin presence by western blot could be addressed by electroporating a higher number of cells, which would be FACS sorted. Then, a stable-expressing USH2A-S/MAR HDF cell line would allow to collect enough cell material for western blot analysis functional assays (Roig-Merino et al., 2022).

To confirm usherin protein production, immunostainings were performed. Exogenous usherin produced by CAG-*USH2A*-S/MAR in HDF appears to localize to a specific part of the cell, which has been hypothesised as the focal adhesions. Focal adhesions are clustered-integrin receptors interacting with the extracellular matrix. They play a role in adhesion, migration and mechano-sensing (Burridge, Chrzanowska-Wodnicka, et Zhong 1997). This is the first time such localisation of usherin is reported. Similarly, a recent study reported expression of ADGRV1, a protein part of the Usher 2 complex, at the focal adhesions of several cell lines such as hTERT-RPE1, mouse embryonic fibroblasts, and mouse astrocytes, showing a similar pattern to the usherin overexpression (Schwaller et al. 2021) (Kusuluri et al., 2022; Guler et al 2023). They showed that ADGRV1 (also known as VLGR1) is a vital component of focal adhesions serving as

a metabotropic mechanoreceptor controling cell spreading, migration and focal adhesions assembly and turnover.

In line with this finding, this novel localisation of Usherin at focal adhesions provide valuable information to a better understanding of usherin role in photoreceptor cells. This idea is also consistent with the altered morphology of USH2A-S/MAR electroporated HEK cells. However, more work should be undertaken to confirm this hypothesis. For instance, colocalization of overexpressed usherin with focal adhesions proteins such as F-actin, Vinculin or Paxillin in the USH2A-S/MAR electroporated HDF would be needed to support this hypothesis.

Usherin and its Usher 2 complex partners (Whirlin and ADGRV1) roles are still poorly understood. However, several recent studies suggest a role in mechanotransduction. Schwaller and colleagues reported that absence of usherin in mice and humans is associated with deficit in vibration perception. They reported that usherin is present in adult skin sensory end-organs, where it plays a role in vibration sensing, precisely in mouse hair follicles and Meissner corpuscles. Loss of usherin may lead to changes in the stiffness of elements within Meissner's corpuscle, which could be due to changes in cellular stiffness or the stiffness of physical connections between the sensory ending and Schwann cells within the end-organ (Schwaller et al., 2021). This idea of stiffness of physical

connections is reminiscent of usherin role in the ankle links of the developing cochlear hair cells. It could be an unexplored role of Usher 2 complex in photoreceptor cells.

Accordingly, in photoreceptor cells, Verschueren and colleagues used super-high resolution expansion microscopy to study the cytoskeleton and Usher proteins architecture in the primate photoreceptors. They described the link between inner segment an outer segment as formed by the Usher 2 complex proteins at the very base of the cilium and then above by Usher 1 complex proteins. Therefore, they sought that outer segment/inner segment continuity is probably reinforced by Usher 2 proteins and suggests a functional mechanical role (Verschueren et al. 2022).

Besides, Usherin and partners are thought to play a role in docking and fusion of transport vesicles through the connecting cilium to the outer segment (Toms et al., 2020). Absence of usherin in u*sh2a*^{rmc1} zebrafish model leads to an increased number of autophagosomes in the inner segment of u*sh2a*^{rmc1} photoreceptor cells and elevated autophagy markers by qRT-PCR. Similarly, examination of the retinal ultrastructure of the *ush2a*^{u507} revealed presence lysosomal-like structures around the photoreceptor inner and outer segment boundary and at the synaptic termini (Toms et al., 2020). Similarly, Linnert and colleagues performed whole transcriptome sequencing of the retinae of the Vlgr1/del7TM mouse

model revealed altered expression profiles of gene-related autophagy. Moreover, they reported increased autophagy in VLGR1-deficient hTERT-RPE1 cells and USH2C patient-derived fibroblasts (Linnert et al. 2023). Altogether, these results suggest that Usher 2 complex disruption leads to an activation of autophagy. Therefore, autophagy markers should be examined in Usher 2 models.

Several studies suggested that Usher Syndrome is a ciliopathy (May-Simera, Nagel-Wolfrum, and Wolfrum 2017). Recent evidence showed a significant decrease of 29% in the number of ciliated cells in USH2A patient-derived fibroblasts compared to a healthy control (Samanta et al. 2019). Similarly, Pendse and colleagues showed that ablation of *Ush2a* affects the ciliogenesis in OC-k1 cell line, with a significant reduced cilia length. Interestingly, fibroblasts from USH1C pigs or USH1C patients showed a significantly elongated primary cilia, supporting the idea that usher syndrome is a ciliopathy.

In this work, ciliogenesis and cilia length were investigated. In HDF, no significant differences were found when comparing percentage of ciliated cells for WT (69%) and USH2A HDF (64%), unlike Samanta and colleagues study. However, similarly to Pendse and colleagues work in OC-k1 cell line, USH2A-derived fibroblasts displayed significantly ($p<0.001$) shortened cilia (4.1µm) compared to the control (6.2µm); this

2.1 µm decrease in cilia length represents a 33% reduction compared to of WT cells. Cilium length differences in this cell model could be used as a reliable endpoint to assess the functional rescue efficacy driven by USH2A-S/MAR vectors or other potential treatments. This finding has only been determined in one *USH2A* patient cell line with c.2299del p.(Glu767Serfs*21) and c.3187_3188del p.(Gln1063Serfs*15) variants. This phenotype could be specific to these variants, hence investigating cilia length in another patient line with different *USH2A* mutations would be desirable.

USH2A HDF were reprogrammed in hIPSC, allowing their differentiation into retinal organoids. This model has allowed us to access to a human retinal-like tissue and therefore to a more relevant disease cell model. Retinal organoids were grown to day 35 of differentiation, and showed early defect in cilia length. It is the first time reported, that early USH2A retinal organoids display such defects. This finding has been performed with only one *USH2A* patient cells with c.2299del p.(Glu767Serfs*21) and c.3187_3188del p.(Gln1063Serfs*15) variants. So, the phenotype could be specific to these variants. However, our study lacks investigation of usherin and its partners level of expression in early retinal organoids. qRT-PCR, immunostainings, and western blots would be needed. Additionally, more mature organoids have to be characterised at week 24 and later, as available transcriptomic data suggests strongest expression at these timepoints in WT retinal organoids (Cowan et al. 2019). So far, only two publications have reported generation of *USH2A*-retinal cells derived from

hiPSCs. The first study conducted by Tucker et al used a 3D/2D protocol to produce eye-cup-like structures from a patient carrying the deep-intronic c.7595-2144A>G mutation (rs786200928) in intron 40 of *USH2A* and the c.12575G>A mutation (rs199605265) *in trans*. While there were no obvious differences indicative of early developmental abnormalities in *USH2A*-derived retinal cells compared to control, they displayed an increased GRP78 and GRP94 expression protein levels, suggesting that ER stress could be involved in *USH2A* pathogenicity in photoreceptors (Tucker et al. 2013). The second report from Guo et al derived retinal organoids from reprogrammed urine cells of a patient with nsRP carrying the c.9127-9129delTCC and c.8559-2A > G (rs397518039) mutations in *USH2A*. In contrast to the previous study, the investigators found reduced laminin expression, defective retinal progenitor cell differentiation and disorganized neural retina, higher expression of pro-apoptotic and decreased expression of cilium associated genes in patient-derived retinal organoids compared to wild-type controls (Guo et al. 2019). However, these findings were produced from 12-week-old retinal organoids, and usherin expression has not been demonstrated at this time point. In addition, no evidence of interaction between the usherin and its partners such as whirlin or ADGRV1 has been provided. More mature retinal organoids would have been more relevant as supported by single-cell transcriptomic data analysis of retinal organoids exhibiting a high *USH2A* gene expression in 24-week -old retinal organoids.

Retinal organoids are a valuable tool to assess retinal gene therapies. For example, it has allowed to test several AAV capsids for gene therapy and different promoters to tailor cell-specific and efficient transgene expression (Gonzalez-Cordero et al., 2018; Garita-Hernandez et al. 2018; Tornabene et al., 2019; Garita-Hernandez et al. 2020; Achberger et al. 2021; Volkner et al., 2021). Similar experiments could be performed for non-viral retinal gene therapies, such the USH2A-S/MAR DNA vectors. However, retinal organoids models have limitations. First, the differentiation process is variable, batch, clone and protocol-dependent. In addition, the photoreceptor cells generated in a dish, do not display fully functional outer segments. Also, to reduce inter-individual variation, isogenic line generated by CRISPR/Cas9 are desirable, which has not been undertaken for this study as yet.

To assess *USH2A*-S/MAR expression *in vivo*, the previously CRISPR/Cas9-generated *ush2a*^{u507} zebrafish was used, which shows loss of usherin protein and retinal defects including reduced ERG responses and progressive rod cell degeneration (Toms et al., 2020). Dr Maria Toms undertook this work in Prof Mariya Moosajee's lab (one-cell stage micro-injections, zebrafish maintenance, breeding and tissue processing and imaging. *USH2A*-S/MAR was injected at the one-cell stage. GFP was detected in the developing embryos, including the retinal photoreceptor cells. Photoreceptor expression of GFP was detected up to 12 mpf, although fluorescent photoreceptors became sparser with age due to the

continued growth of the zebrafish retina from the ciliary marginal zone. There was a mosaic expression pattern of GFP throughout the zebrafish larval body, which showed preferential expression in certain cell types and was likely silenced by certain lineages during the development. Assessing different promoters may improve the range of expression or using a mammalian animal model may be more suitable. In addition, direct injection of the S/MAR DNA into the zebrafish eye may improve expression.

The step further for the development of USH2A-S/MAR is to move to other animal models. Several *USH2A* mouse models have been reported, but the most recent one, a knock-in mouse model for one of the most common mutations in USH2A (c.2299delG), exhibited a retinal phenotype comparable to USH2A patients with the c.2299delG mutation (Tebbe et al. 2023). It could be a valuable model to assess functional rescue with USH2A-S/MAR. Additionally, an *USH2A* knock-out rabbit model has been reported and characterized (Nguyen et al,. 2023). At 4 months of age, *USH2A* mutant rabbits exhibit hyper-autofluorescent signals on fundus autofluorescence and hyper-reflective signals on optical coherence tomography images, which indicate retinal pigment epithelium damage. At 7 months to 22 months of age, electroretinography signals of rod and cone function were decreased in the *USH2A* mutant rabbits, indicating progressive photoreceptor degeneration. *USH2A* mutant rabbits would be

a very valuable model for gene therapy assessment, before translating to non-human primate and patients.

Chapter 6. Final discussion and future work

Five years ago, voretigene neparvovec was approved by the Food and Drug Administration for gene replacement therapy for Leber congenital amaurosis (LCA) type 2, caused by biallelic mutations in *RPE65* gene. This first gene therapy of this kind was available for patients. Since then, no further retinal gene therapies have reached the market. In contrast, many retinal gene therapy trials failed to meet their primary endpoints such as for choroideremia (Zhai et al. 2023), X-linked RP (NCT03116113) and X-linked retinoschisis (NCT02416622).

AAV vectors remain the vector of choice in terms of retinal cell transduction capabilities. However, safety concerns have been overlooked, especially ocular inflammation triggered by AAV vectors. Real-world experience of voretigene neparvovec has revealed drug-induced chorioretinal atrophy at the site of the treatment from 2 weeks post-surgery (Gange et al. 2022; Felix Friedrich Reichel et al. 2022) (1,2). These factors call for safer and more applicable strategies for gene replacement. Moreover, AAV have a limited carrying capacity, that cannot accommodate large genes such as *USH2A*, *ABCA4* or *CEP290*. Here a non-viral alternative is proposed, using S/MAR DNA plasmids, allowing episomal maintenance, long-lasting expression and virtually unlimited cloning capacity. REP1-S/MAR and USH2A-S/MAR have been successfully clones and showed promising proof-of-concept in patient-cell derived and

zebrafish models. These tailored DNA vectors will be valuable to develop alternative strategy.

However, they can still be improved. For example, the development of minicircles, which are plasmids devoid of bacterial backbones, or with a minimally sized one. Not only it decreases plasmid size, but it also reduces innate immune response due CpG islands contained in bacterial backbones. Additionally, cis-regulatory elements must be carefully evaluated: several S/MAR sequences, promoters and reporters can be tested.

To address innate immune response to foreign DNA or a viral vehicle, gene therapy could be combined with immunomodulatory ligands. Chan and colleagues demonstrated that linking specific immunomodulatory non-coding sequences could reduce innate immune and T cell responses and enhanced gene expression when using AAV in mouse and pig model in different tissue such as the retina. In their study, they antagonize TLR9 activation directly into the vector genome (Chan et al. 2021). Such approaches could translate to non-viral strategies as well.

Still, the major bottleneck of non-viral gene therapy and especially for large DNA vectors, is the vehicle that will allow the DNA uptake, to

ultimately reach the nucleus. To date, there are a limited number of studies using non-viral vectors for the therapeutic delivery of large genes.

The efficiency of naked DNA transfection is very low and therefore, several synthetic carriers have been developed to use in combination with nucleic acids to assist cell entry (Figure 2). Nanoparticles are cationic structures capable of forming a complex with polyanionic nucleic acids. This complex facilitates cell uptake from the endosomal cellular system to the nucleus and protects the transgene from endonucleases. Several synthetic vectors have been developed based on liposomes, polymers, solid lipids, and niosomes.

Liposomes are nanoparticles made of a phospholipid bilayer allowing molecule encapsulation. For transfection of the retina, Rajala and colleagues developed an innovative lipo-some-based protamine complex with improved efficiency and long-term expression. Their next-generation lipoplex contained (1) a liposome consisting of a cationic lipid DOTAP (1, 2-dioleoyl-3- trimethylammonium-propane), a neutral lipid DOPE (1,2-dioleoyl-sn-glycero-3-phosphoethanolamine), and cholesterol, (2) protamine to compact the DNA and protect it from endonucleases, and (3) cell penetrating transactivator of transcription (TAT) and nuclear localization signalling (NLS) peptides to promote plasmid entry in the nucleus and its expression. Subretinal injection of this liposome-based nanocarrier, coupled with an *Rpe65* DNA plasmid, successfully resulted in

the efficient transfection of photoreceptor and RPE cells of a *Rpe65*$^{-/-}$ mouse, partially rescuing the disease phenotype. GFP expression was reported at 3 months post-injection (Rajala et al. 2014). Following this work, Wang and colleagues performed liposome-based retinal transfections using cell-specific promoters; they achieved specific gene expression in the RPE with the VMD2 promoter, ganglion cells with the thymocyte antigen promoter, and finally rod and cone photoreceptors with the mouse rhodopsin and red opsin promoters respectively (Rajala et al. 2014). Overall, these liposome-based complexes provide a promising alternative to viral vectors for retinal gene therapy, but assessment in larger animal models is necessary.

Among the polymer nanoparticle formulations investigated for retinal gene therapy, poly-L-lysin peptides have shown convincing results. Naash's group have used compacted rod-shaped DNA nanoparticles formulated with 30-mer poly-L-lysin peptides conjugated to polyethylene glycol 10000K (CK30PEG) in a number of investigations; they have successfully shown efficient transfection of photoreceptors and RPE cells, which improved the phenotype of several retinal mouse disease models such as retinitis pigmentosa (Cai et al. 2010) and Leber congenital amaurosis, with up to 2 years of persistent transgene expression (Koirala, Conley, et al. 2013b). In another study, CK30PEG nanoparticles were enhanced with a cell penetrating TAT peptide sequence and demonstrated partial improvement of visual function in the *Rho*$^{P23H/P23H}$ knock-in mouse model of retinitis pigmentosa (Rajendra Narayan Mitra et al. 2018a).

Furthermore, CK30PEG containing the large *ABCA4* cDNA cassette (6.8 kb) was able to drive sustained expression for up to 8 months after injection and to improve the phenotype of an *Abca4*-deficient Stargardt disease mouse model when delivered subretinally (Z. Han et al. 2012). Plasmids as large as 20 kb have been effectively transfected using CK30PEG for in vivo mice lung gene transfer (Fink et al. 2006), which is promising for large transgene delivery in the eye. Encouragingly, translation in a non-human primate eye showed safe and efficient transfection of CK30PEG when injected subretinally and intravitreally (Kelley et al. 2018). In addition, anionic span-based poly-L-arginine nanoparticles have been used to deliver a *PRFP31* plasmid and partially rescue the retinal phenotype in *Prpf31*$^{A216P/+}$ mouse model of retinitis pigmentosa (Pensado et al. 2016).

More recently, a combined strategy using a lipo-peptide nanoparticle showed efficient plasmid DNA delivery into retinal cells. These so-called ECO nanoparticles consist of a protonable ethylenediamine (E) head group, two cysteine (C) functional linkers and two oleoyl (O) lipophilic tails (Malamas et al. 2013). In the eye, these nanoparticles, self-assembled by the multifunctional pH-sensitive amino lipid ECO and a therapeutic bovine rhodopsin promoter-driven *ABCA4* plasmid, delayed the phenotype of a *Abca4*$^{-/-}$ Stargardt mouse model for at least 6 months (Sun et al. 2019). The 16 kb plasmid is the largest reported for non-viral gene therapy in the eye. Prolonged *ABCA4* expression for at least 8 months was observed in the photoreceptor outer segments of subretinally injected mice. ECO-

based nanoparticles can also be chemically modified with targeting ligands; the addition of a retinylamide or its analogue ACU4429 produced increased RPE expression in *Rpe65*$^{-/-}$ LCA model mice and *Abca4*$^{-/-}$ mice respectively (Sun et al. 2017; 2020). More recently, Sun and colleagues generated stable PEG-ECO*/pGRK1-ABCA4-S/MAR* nanoparticles producing specific and prolonged expression of ABCA4 in the photoreceptors of *Abca4* $^{-/-}$ mice and significantly inhibit accumulation of toxic A2E in the eye. They also performed repeated administrations without major side effects (Sun et al. 2022).

Alternative biopolymers such as chitosan have shown valuable properties as nanoparticle building blocks. Chitosan is a biodegradable non-toxic cationic polysaccharide. It is produced by alkaline deacetylation of chitin, which is a component commonly found in the cell walls of fungi and crustacean shells. Chitosans are composed of N-acetyl-D-glucosamine and D-glucosamine units and vary in molecular weight (50 to 2000 kDa) and in the degree of deacetylation (40 - 99%). The cationic nature of chitosan derivatives is an exception among the usual polysaccharides, which makes it an invaluable polymer as a non-viral gene vector component. Regarding ocular gene therapy applications, Puras and colleagues assessed the efficiency of highly deacetylated (99%) low molecular weight (5.7 kDa) oligochitosan-DNA nanoparticles in the rat retina. Subretinal injection led to GFP expression in the RPE cells, while intravitreal injection induced GFP expression in the retinal ganglion cells (Puras et al. 2013). Similarly, Mitra and colleagues designed a chitosan-

based nanoparticle (250 kDa, 82% of deacetylation degree) with glycol moieties to improve its solubility. Subretinal injections of 5.7 kb-long GFP plasmid DNA glycol chitosan nanoparticles in albino wild-type mice resulted in GFP expression in the RPE cells, without any safety concerns (Rajendra N. Mitra et al. 2014). The safe profile of chitosan-derived nanoparticles makes them a strategy of interest for retinal gene therapy, however modification and optimization still needs to be explored to improve the low efficiency (A. V. V. Oliveira, Silva, et Chung 2015; A. V. Oliveira et al. 2016).

Similarly, solid lipid nanoparticles (SLNs) have displayed promising results as vectors for gene delivery. SLNs are 10 - 1000 nm-diameter nanocarriers with a rigid core lipid matrix (Iafisco et al. 2020). They offer many advantages compared to liposomes and polymeric nanoparticles such as (1) their biodegradability (2) their stability and large-scale production feasibility and (3) the possibility of ligand additions (Y. Duan et al. 2020). Apaolaza and colleagues designed a solid lipid-based formulation consisting of DOTAP, protamine and a polysaccharidic ligand such as hyaluronic acid or dextran. The protamine is a cationic peptide with nuclear localization signals enhancing DNA condensation (Brewer, Corzett, et Balhorn 1999), while hyaluronic acid contributes to better plasmid DNA cell delivery and the final structure of the SLNs (Paola Stephanie Apaolaza et al. 2014). SLNs coupled with an RS1 plasmid driven by the murine opsin promoter (mOPS) successfully induced long-lasting photoreceptor-specific expression of RS1 (3 months) in a X-linked

juvenile retinoschisis mouse model when injected intravitreally, resulting in an improved phenotype (P. S. Apaolaza et al. 2015; 2016). The SLNs capability to reach the photoreceptors and RPE when injected intravitreally makes these nanoparticles a very promising feature for retinal gene therapy.

Niosome-based nanoparticles are similar to liposomes, except the phospholipid is replaced by non-ionic surfactants (reviewed in (Grijalvo et al. 2019)). Niosomes are usually composed of 3 key elements: a non-ionic surfactant as its main component, a cationic lipid interacting with the plasmid DNA, and a neutral lipid helper. In the eye, several studies have been conducted using various niosome-based plasmid DNA carriers; initially, a cationic niosome formulation with 2,3-di(tetradecyloxy)propan-1-amine cationic lipid, combined with 2% of squalene and 0.5% of polysorbate 80, was optimized for compact delivery of a 5 kb-long pCMS-eGFP DNA plasmid (Puras et al. 2014). Following subretinal injection in rats, RPE cells were modestly transfected while intravitreal injection led to GFP expression in the inner retinal layers. The addition of protamine to the formulation improved nucleus targeting and allowed transfection of a small proportion of photoreceptor cells following subretinal injection, although the transfection efficiency remained very modest. Several combinations have been assessed by changing the non-ionic surfactant, the lipid helper or the cationic lipid.

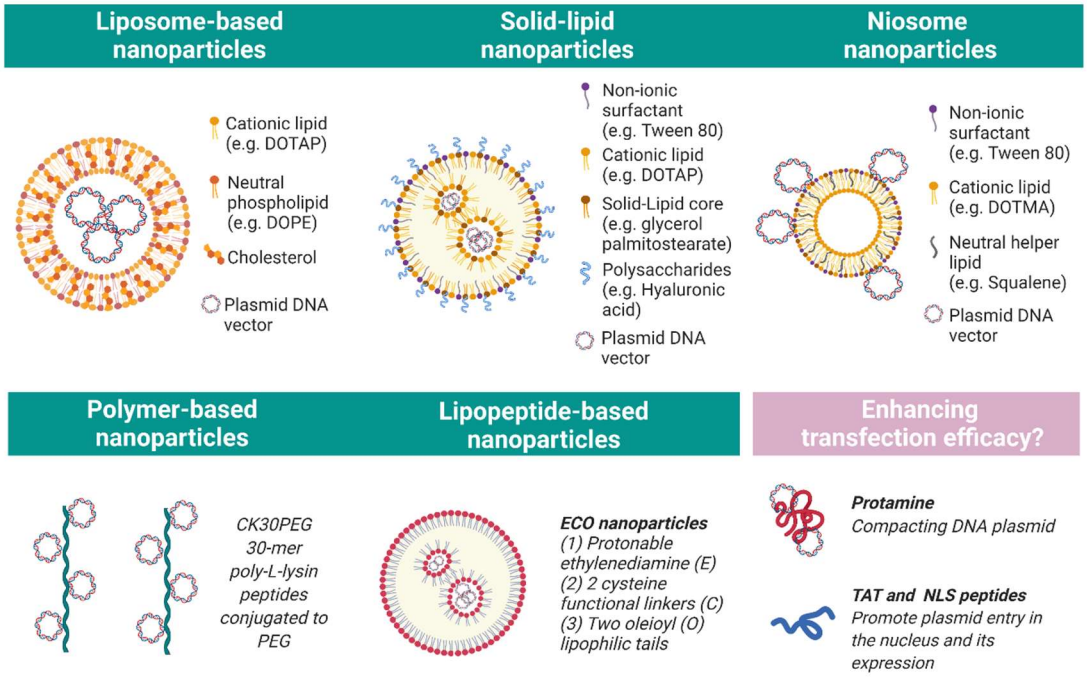

Figure 61. Key nanoparticles of interest for retinal non-viral gene therapy.
Several chemical vehicles have been developed as plasmid DNA carriers, such as nanoparticles based on liposomes, solid lipids, niosomes, polymers and lipopeptide.

To facilitate cell entry of non-viral gene therapies, several physical methods have been developed to allow plasmids to efficiently cross cell barriers and be expressed. Among those reported to increase transfection in retinal cells are iontophoresis, electrotransfection, ultrasound-targeted microbubble destruction (UTMD) and optoporation.

Iontophoresis is a non-invasive drug delivery technology enhancing the permeation of ionized molecules across biological barriers using a continuous low-level electrical field (Souied et al. 2008). This strategy has been proved useful for transdermal drug delivery to facilitate percutaneous penetration (Hasan et al. 2020; Ita 2016) and became an attractive option for drug and gene delivery in the eye (Jung et al. 2018). Several studies have assessed transcorneal and transscleral iontophoresis-assisted plasmid DNA transfer for non-viral ocular gene therapy; however, limited expression was produced, especially in the photoreceptor cells (Souied et al. 2008; Asahara, T; Shinomiya, Kayo; Naito, Takeshi; Siota 2001). Asahara and colleagues applied iontophoresis to transfect a 4.7 kb-long CMV-GFP plasmid in rabbit eyes and showed expression in the cornea, the anterior chamber angle and the ciliary subepithelial tissues, but not in the retina. In contrast, Souied and colleagues demonstrated that transscleral iontophoresis of *β-pde6b* cDNA plasmid driven by human *PDE6B* promoter in rd1 mice could penetrate photoreceptor cells and consequently showed partial rescue of photoreceptor morphology and ERG measurements (Souied et al. 2008). For both studies, the positive electrode was placed at the back of the animal while the negative

electrode was inserted into an applicator containing the plasmid solution bathing the cornea, the limbus and the adjacent sclera. Overall, the safety profile and non-invasive aspects of iontophoresis are ideal for non-viral retinal gene delivery strategies and would allow safe repetitive applications, such as those performed in rd1 mice by Souied et al. However, no novel studies using this technique have been reported in the last decade and it would still require extensive optimization regarding its low plasmid transfection in retinal cells. This technology appears to be most suitable for small molecules and short nucleic acids (Bordet et Behar-Cohen 2019).

Electrotransfection, also known as electroporation, is an additional method exploiting electric fields that has been explored for non-viral gene delivery. Unlike iontophoresis, electrotransfection relies on a high voltage pulsed electric field applied to the surrounding cells, which transiently permeabilizes their cell membranes, allowing plasmid DNA entry. In the retina, successful plasmid electrotransfection following a subretinal injection has been performed in newborn mouse and rat (P0) retinal cells (Matsuda et Cepko 2004; 2007; de Melo et Blackshaw 2011; 2018) and in adult mouse RPE cells (Nickerson et al. 2012; Johnson et al. 2008). Alternative routes of delivery, such as injection of plasmid DNA solution into the suprachoroidal space followed by electrotransfection, displayed transfection of choroid, RPE and a proportion of photoreceptor cells in the adult rat (Touchard et al. 2012). Altogether, these studies demonstrate the valuable features of electrotransfection such as (1) its efficiency of

transfection (2) the possibility for repetitive administrations and (3) its cost effectiveness compared to viral vectors. However, the therapeutic use of electrotransfection would require invasive surgical procedures and extensive optimization to ensure safety in patients. In addition, the application of a safe and adapted electric field to the large 1094 mm2 human retinal surface is a challenge that will need to be addressed. To date, no proof-of-concept investigations in large animal eyes have been reported. Retinal electrotransfection would benefit from alternative approaches using innovative electrotransfection tools to address these issues (D. Schwarz et Schaefer 2020).

Other physical methods under investigation include ultrasound-targeted microbubble destruction (UTMD). This involves loading plasmid DNA into microbubbles, which are small gas-filled spherical voids stabilized with phospholipids or synthetic polymers. Gene-carrier microbubbles are injected and subjected to ultrasounds; the microbubbles act as cavitation nuclei by focusing ultrasound energy, causing cell membrane permeabilization and plasmid uptake (Wan, Li, et Li 2015). UTMD is non-invasive, allows repetitive administrations and displays low toxicity, but with limited transfection in RPE and photoreceptor cells (Sonoda et al. 2012; Zhou et al. 2009).

More recently, optoporation has been investigated as a method of gene transfer in the retina. Laser-induced optoporation allows the introduction of small molecules or plasmid DNA by transiently permeabilizing cell membranes using continuous or pulsed laser waves (Schneckenburger

2019). Batabyal and colleagues have successfully used this strategy to efficiently deliver a 7.9 kb-long plasmid in rd10 mouse retinal ganglion cells. They designed a two-step strategy: the first step is an intravitreal injection of the plasmid of interest and gold nanorods conjugated with concanavalin A to the target cell membrane; the following step is a 800-1064 nm laser irradiation, allowing site-specific cell permeabilization (Batabyal et al. 2020; 2019). Additionally, no evidence of a harmful immune response or other safety issues were apparent, making optoporation-based gene delivery a promising tool for retinal gene therapy.

Overall, a number of physical methods have shown great potential as delivery strategies for non-viral gene therapy but improving their transfection efficiency and translation to larger animal models is essential. Several of these techniques can also be used as an adjuvant method to increase viral vectors penetrance or transduction efficiency. For instance, intravitreal injection of AAV vectors combined with iontophoresis significantly improved penetration of the internal limiting membrane and increased transduction of cells in the outer retina (Song et al. 2019; 2020). Similarly, several studies showed that UTMD-mediated delivery of AAV improved their transduction in rodent retinas in vivo (Zhou et al. 2009; Xie et al. 2010).

The main limitation of non-viral strategies for gene augmentation therapy is their lack of transfection efficiency in targeting the photoreceptor cells and RPE. So far, non-viral strategies still do not outperform the AAV

transduction rates. Han and colleagues performed a comparative analysis of CK30PEG, AAV2 and AAV5 efficacies with subretinal injections in mice (Z. Han et al. 2012). They showed that the AAV vectors (10^9 vg) were more efficient per vector genome than CK30PEG (6.9^{11} vg), but CK30PEG still drove a comparable level and longevity of gene expression. However, AAV capsids have been subsequently improved, such as the engineered AAV2.7m8 capsid (Dalkara et al. 2013), allowing highly efficient transduction after both subretinal and intravitreal injection.

Although non-viral methods are less likely to trigger significant inflammatory responses because they lack the viral capsid, the potential responses still require investigation. For instance, double-stranded DNA can trigger an innate immune response mediated by the Toll-like receptor pathway or cGAS pathway (Shirley, De Jong, et al. 2020). Furthermore, physical methods of transfection can lead to inflammation through damage-associated molecular patterns (DAMPs), by releasing intracellular proteins, extracellular matrix or non-protein molecules like ATP (Bucher et al. 2020). Altogether, these safety issues need to be assessed in a relevant retinal context. Similar to AAV therapy, steroid administration may be necessary alongside the non-viral gene therapy to reduce potential inflammatory responses.

Investigation into non-viral methods for retinal gene therapy should be intensified to overcome its current limitations and reach the clinical stage. To date, only one study assessed DNA nanoparticles in non-human primate eyes (Kelley et al. 2018). No adverse events were reported in the injected baboons, with no systemic or inflammatory reaction subsequent to the injections. However, the efficiency was not as high as current AAV capsids used in clinical trials. Similarly, none of the non-viral physical transfection methods have reached the clinical stage for IRDs. However, the Evesensys electroporation system is currently being trialled for electroporating the eye ciliary muscle in patients with uveitis, allowing transfected cells to produce and secrete therapeutic proteins of interest (NCT03308045). The company is aiming to use the same technology to treat patients with degenerative retinal diseases.

The development of gene augmentation therapy has created a highly promising avenue for treating a range of IRDs, which will greatly impact the quality of life of affected patients. With the first approved ocular gene therapy and a number of ongoing clinical trials, the development of enhanced strategies is of interest more than ever. Non-viral vectors offer a relatively cost-effective and safe alternative option, with greater packaging capacities compared to viral vectors. Currently, the common limitation for non-viral IRD treatment is the low transfection efficiency in the key retinal cells of interest, the photoreceptors. There are various aspects of the non-viral therapeutic strategy that can be targeted for optimisation, including

DNA plasmid design, chemical delivery vehicles and injection techniques. Innovative improvements, and assessing different gene transfer methods in combination, will be necessary to ensure a sufficient transfection efficiency in the retina, with safe long-term expression. Further non-viral therapeutic studies in larger animal models will also aid clinical translation.

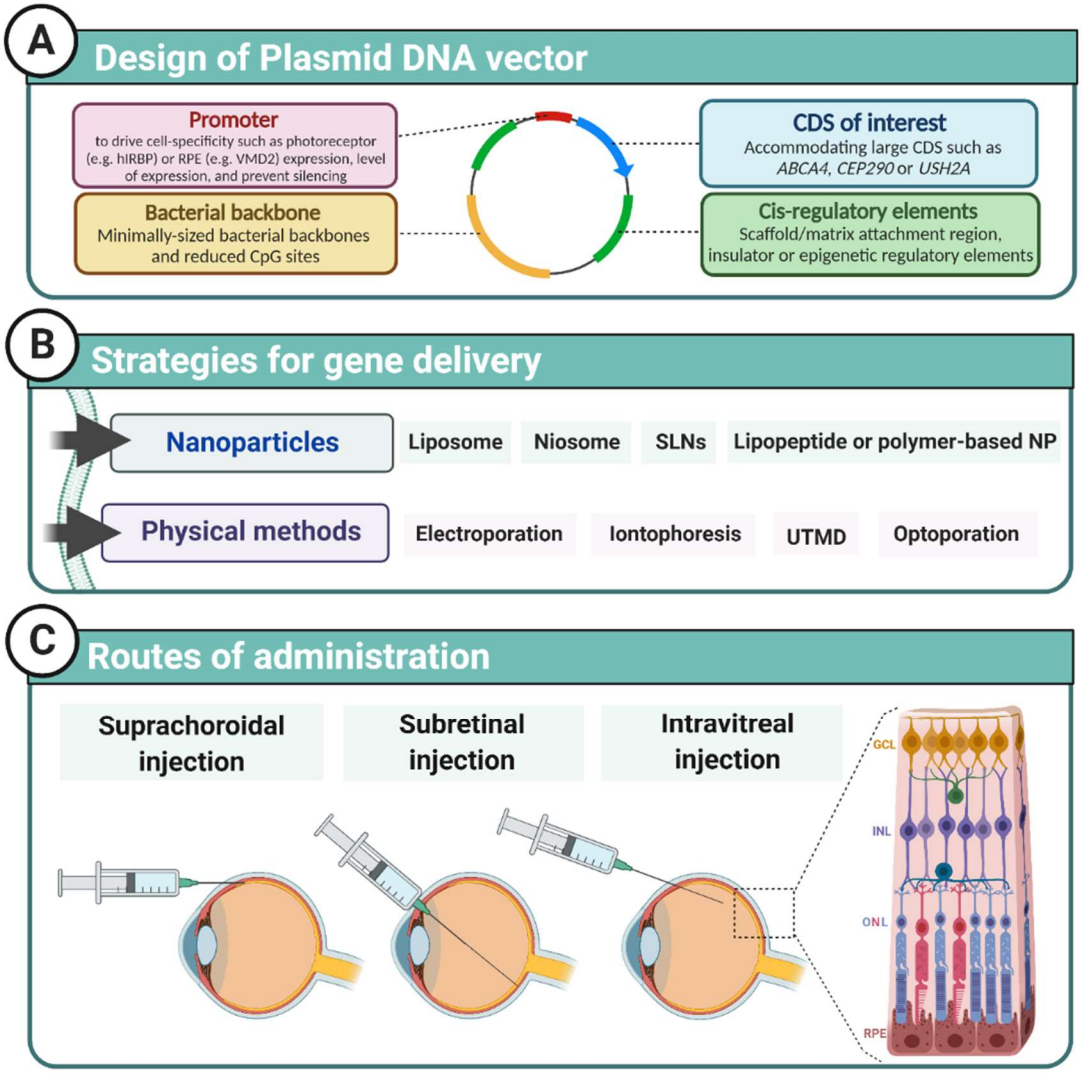

Figure 62. Retinal non-viral gene therapy.

Plasmid DNA vectors are designed to ensure cell-specific, long-lasting, and safe expression of the transgene of interest. (B) Different physical or chemical strategies can be applied to aid DNA transfection in the necessary cells (C) Different routes of administration can be used depending on the gene delivery strategy and the targeted cells. CDS, coding sequence; GCL. ganglion cell layer; INL, inner nuclear layer; ONL, outer nuclear layer.; SLNs, solid-lipid nanoparticles; UTMD, ultrasound-targeted microbubble destruction.

To our knowledge the largest plasmid vector delivered *in vivo* was 20.2 kb; this luciferase plasmid with CMV promoter was transfected into the mouse liver using polyethylene glycol-substituted lysine 30-mers (CK30PEG) (Fink et al. 2006). For retinal work, vectors of either approximately 12 kb, 14 kb or 16 kb (Sun et al. 2019) in size containing the *ABCA4* coding sequence have been used successfully to transfect the *Abca4*$^{-/-}$ mouse retina, producing months of protein expression and improvements in the disease phenotype compared to untreated mice. All studies packaged the plasmids into nanoparticles, CK30PEG (Rajendra Narayan Mitra et al. 2018b) or multifunctional pH-sensitive amino lipid ECO nanoparticles (Sun et al. 2019), to increase the transfection rate. Some nanoparticles, including ECO (Sun et al. 2020; 2017), can be modified with ligands to aid in cell targeting, making them an attractive option. That is why, collaborations with Pr. Zheng-Rong Lu (Case Western Reserve University, Cleveland, Ohio) and Pr. Stephen Hart (UCL, London) developing ECO nanoparticles and liposomes respectively, have been instigated, to incorporate REP1- and USH2A-S/MAR plasmids with these carriers.

Another approach to optimising targeted cell entry of the S/MAR vectors is utilising the unique glycome signature of retinal cells. Dr. Cécile Méjécase.

In our team has been characterising the glycan-binding protein patterns in human photoreceptor cells, in order to modify nanoparticles for targeting the photoreceptor cell inner segment. As shown in Figure 70, human retinal sections were stained with peanut agglutinin (PNA), a lectin bound to the glycans that localised to the inner and outer segment of cone photoreceptors. Ganglioside GD3, did not display specific staining in the human retinal sections.

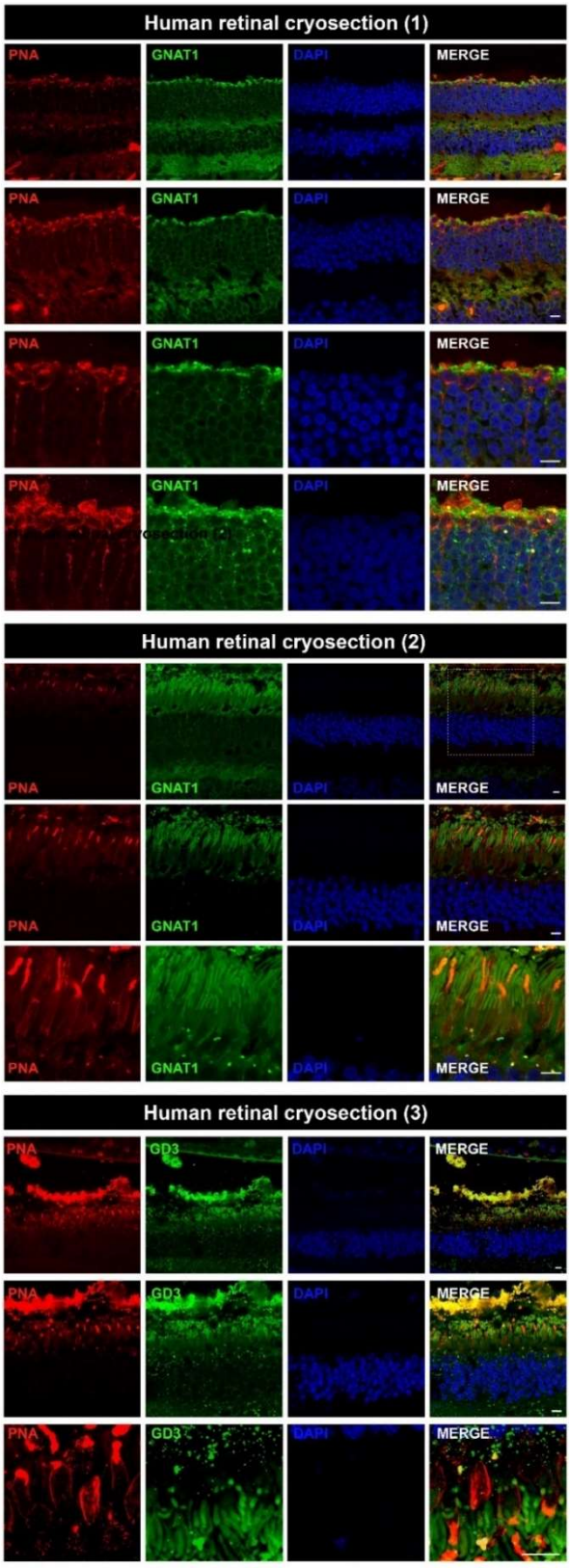

Figure 63. Glycan-binding proteins pattern in human adult retina.

PNA (in red) is located at inner segment and outer segment of cone photoreceptors, GNAT1 (in green) is expressed in rod photoreceptors. (Scale bar = 10μm)

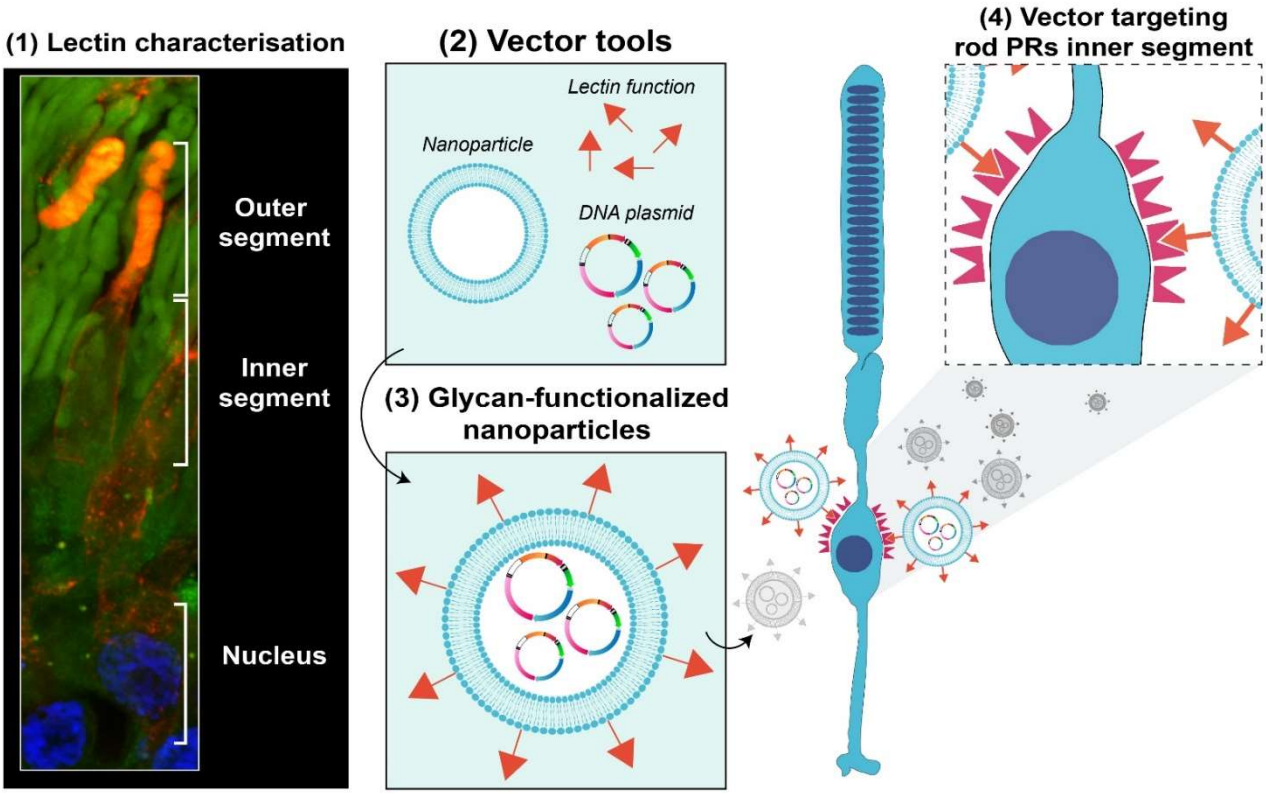

Figure 43. Developing glycan-functionalized nanoparticles to target human photoreceptor cells.

(1) Using lectins binding to specific glycans on human retinal sections. Peanut-agglutinin (PNA in red), GD3 (in green) and DAPI (in blue). (2) Vector toolbox to form DNA plasmids – glycan-functionalized nanoparticles. (4) Glycan-functionalized nanoparticles to target the photoreceptor inner segments.

In conclusion, the full *USH2A* coding was successfully cloned into a non-viral episomal S/MAR vectors and demonstrated the potential of these vectors in replacing large protein expression in different *in vivo* and *in vitro* disease models. Although further optimisations to improve efficiency in the larger animal models and mammalian retina is needed. It is a major step for the development a safe and effective non-viral large gene therapy will be hugely beneficial to a significant proportion of retinal disease patients requiring functional genes that exceed the AAV limit.

References

Aarem, A. van, M. Wagenaar, E. Tonnaer, S. Pieke Dahl, J. Bisseling, H. Janssen, B. Bastiaans, W. Kimberling, et C. Cremers. 1999. « Semen Analysis in the Usher Syndrome Type 2A ». *ORL* 61 (3): 126-30. https://doi.org/10.1159/000027656.

Abadie, C, C Blanchet, D Baux, L Larrieu, T Besnard, P Ravel, R Biboulet, et al. 2012. « Audiological findings in 100 USH2 patients ». *Clinical Genetics* 82 (5): 433-38. https://doi.org/10.1111/j.1399-0004.2011.01772.x.

Adato, Avital, Gaëlle Lefèvre, Benjamin Delprat, Vincent Michel, Nicolas Michalski, Sébastien Chardenoux, Dominique Weil, Aziz El-Amraoui, et Christine Petit. 2005. « Usherin, the defective protein in Usher syndrome type IIA, is likely to be a component of interstereocilia ankle links in the inner ear sensory cells. » *Human molecular genetics* 14 (24): 3921-32. https://doi.org/10.1093/hmg/ddi416.

Aller, Elena, Lise Larrieu, Teresa Jaijo, David Baux, Carmen Espinós, Fernando González-Candelas, Carmen Nájera, et al. 2010. « The USH2A c.2299delG mutation: dating its common origin in a Southern European population. » *European journal of human genetics : EJHG* 18 (7): 788-93. https://doi.org/10.1038/ejhg.2010.14.

Apaolaza, P. S., A. del Pozo-Rodríguez, M. A. Solinís, J. M. Rodríguez, U. Friedrich, J. Torrecilla, B. H.F. Weber, et A. Rodríguez-Gascón. 2016. « Structural recovery of the retina in a retinoschisin-deficient mouse after gene replacement therapy by solid lipid nanoparticles ». *Biomaterials* 90 (juin):40-49. https://doi.org/10.1016/j.biomaterials.2016.03.004.

Apaolaza, P. S., A. Del Pozo-Rodríguez, J. Torrecilla, A. Rodríguez-Gascón, J. M. Rodríguez, U. Friedrich, B. H.F. Weber, et M. A. Solinís. 2015. « Solid lipid nanoparticle-based vectors intended for the treatment of X-linked juvenile retinoschisis by gene therapy: In vivo approaches in Rs1h-deficient mouse model ». *Journal of Controlled Release* 217 (novembre):273-83. https://doi.org/10.1016/j.jconrel.2015.09.033.

Apaolaza, Paola Stephanie, Diego Delgado, Ana Del Pozo-Rodríguez, Alicia Rodríguez Gascón, et M. Ángeles Solinís. 2014. « A novel gene therapy vector based on hyaluronic acid and solid lipid nanoparticles for ocular diseases ». *International Journal of Pharmaceutics* 465 (1-2): 413-26. https://doi.org/10.1016/j.ijpharm.2014.02.038.

Argyros, Orestis, Suet Ping Wong, Constantinos Fedonidis, Oleg Tolmachov, Simon N. Waddington, Steven J. Howe, Marcello Niceta, Charles Coutelle, et Richard P. Harbottle. 2011. « Development of S/MAR minicircles for enhanced and persistent transgene expression in the mouse liver ». *Journal of Molecular*

Medicine 89 (5): 515-29. https://doi.org/10.1007/s00109-010-0713-3.

Argyros, Orestis, Suet-Ping Wong, et Richard P Harbottle. 2011a. « Non-viral episomal modification of cells using S/MAR elements ». *Expert Opinion on Biological Therapy* 11 (9): 1177-91. https://doi.org/10.1517/14712598.2011.582035.

———. 2011b. « Non-viral episomal modification of cells using S/MAR elements ». *Expert Opinion on Biological Therapy* 11 (9): 1177-91. https://doi.org/10.1517/14712598.2011.582035.

Asahara, T; Shinomiya, Kayo; Naito, Takeshi; Siota, Hiroshi. 2001. « Induction of Gene into the Rabbit Eye by Iontophoresis Preliminary Report ». *Japanese Journal of Ophthalmology* 45 (1): 31-39. https://doi.org/10.1016/S0021-5155(00)00291-4.

Baehr, Wolfgang, Samuel M. Wu, Alan C. Bird, et Krzysztof Palczewski. 2003. « The retinoid cycle and retina disease ». *Vision Research*. Elsevier Ltd. https://doi.org/10.1016/j.visres.2003.10.001.

Bainbridge, J. W.B., M. S. Mehat, V. Sundaram, S. J. Robbie, S. E. Barker, C. Ripamonti, A. Georgiadis, et al. 2015. « Long-term effect of gene therapy on Leber's congenital amaurosis ». *New England Journal of Medicine* 372 (20): 1887-97. https://doi.org/10.1056/NEJMoa1414221.

Batabyal, Subrata, Sivakumar Gajjeraman, Sulagna Bhattacharya, Weldon Wright, et Samarendra Mohanty. 2019. « Nano-enhanced Optical Gene Delivery to Retinal Degenerated Mice ». *Current Gene Therapy* 19 (5): 318-29. https://doi.org/10.2174/1566523219666191017114044.

Batabyal, Subrata, Sivakumar Gajjeraman, Kissaou Tchedre, Adnan Dibas, Weldon Wright, et Samarendra Mohanty. 2020. « Near-Infrared Laser-Based Spatially Targeted Nano-enhanced Optical Delivery of Therapeutic Genes to Degenerated Retina ». *Molecular Therapy - Methods and Clinical Development* 17 (juin):758-70. https://doi.org/10.1016/j.omtm.2020.03.030.

Baux, David, Catherine Blanchet, Christian Hamel, Isabelle Meunier, Lise Larrieu, Valérie Faugère, Christel Vaché, et al. 2014. « Enrichment of LOVD-USHbases with 152 *USH2A* Genotypes Defines an Extensive Mutational Spectrum and Highlights Missense Hotspots ». *Human Mutation* 35 (10): 1179-86. https://doi.org/10.1002/humu.22608.

Berry, Michael H., Amy Holt, Autoosa Salari, Julia Veit, Meike Visel, Joshua Levitz, Krisha Aghi, et al. 2019. « Restoration of high-sensitivity and adapting vision with a cone opsin ». *Nature Communications* 10 (1). https://doi.org/10.1038/s41467-019-09124-x.

Bhattacharya, Gautam, et Dominic Cosgrove. 2005. « Evidence for functional importance of usherin/fibronectin interactions in retinal basement membranes. » *Biochemistry* 44 (34): 11518-24. https://doi.org/10.1021/bi050245u.

Bhattacharya, Gautam, Raghu Kalluri, Dana J Orten, William J Kimberling, et Dominic Cosgrove. 2004. « A domain-specific usherin/collagen IV interaction may be required for stable integration into the basement membrane superstructure. » *Journal of cell science* 117 (Pt 2): 233-42. https://doi.org/10.1242/jcs.00850.

Bode, J, Y Kohwi, L Dickinson, T Joh, D Klehr, C Mielke, et T Kohwi-Shigematsu. 1992. « Biological significance of unwinding capability of nuclear matrix-associating DNAs. » *Science (New York, N.Y.)* 255 (5041): 195-97.

Bode, Jurgen, Craig Benham, Angela Knopp, et Christian Mielke. 2000. « Transcriptional Augmentation: Modulation of Gene Expression by Scaffold/Matrix-Attached Regions (S/MAR Elements) ». *Critical Reviews™ in Eukaryotic Gene Expression* 10 (1): 18. https://doi.org/10.1615/CritRevEukarGeneExpr.v10.i1.90.

Bordet, Thierry, et Francine Behar-Cohen. 2019. « Ocular gene therapies in clinical practice: viral vectors and nonviral alternatives ». *Drug Discovery Today* 24 (8): 1685-93. https://doi.org/10.1016/j.drudis.2019.05.038.

Boulton, Mike, et Pierrettc Dayhaw-Barker. 2001. « The role of the retinal pigment epithelium: Topographical variation and ageing changes ». *Eye* 15 (3): 384-89. https://doi.org/10.1038/eye.2001.141.

Bozza, Matthias, Edward W. Green, Elisa Espinet, Alice De Roia, Corinna Klein, Vanessa Vogel, Rienk Offringa, James A. Williams, Martin Sprick, et Richard P. Harbottle. 2020. « Novel Non-integrating DNA Nano-S/MAR Vectors Restore Gene Function in Isogenic Patient-Derived Pancreatic Tumor Models ». *Molecular Therapy - Methods and Clinical Development* 17 (juin):957-68. https://doi.org/10.1016/j.omtm.2020.04.017.

Bozza, Matthias, Alice De Roia, Margareta P. Correia, Aileen Berger, Alexandra Tuch, Andreas Schmidt, Inka Zörnig, Dirk Jäger, Patrick Schmidt, et Richard P. Harbottle. 2021. « A nonviral, nonintegrating DNA nanovector platform for the safe, rapid, and persistent manufacture of recombinant T cells ». *Science Advances* 7 (16): 1333-47. https://doi.org/10.1126/sciadv.abf1333.

Brewer, Laurence R., Michele Corzett, et Rod Balhorn. 1999. « Protamine-induced condensation and decondensation of the same DNA molecule ». *Science* 286 (5437): 120-23. https://doi.org/10.1126/science.286.5437.120.

Bucher, Kirsten, Eduardo Rodríguez-Bocanegra, Daniyar Dauletbekov, et M. Dominik Fischer. 2020. « Immune responses to retinal gene therapy using adeno-associated viral vectors – Implications for treatment success and safety ». *Progress in Retinal and Eye Research*. Elsevier Ltd. https://doi.org/10.1016/j.preteyeres.2020.100915.

Burnight, Erin R., Joseph C. Giacalone, Jessica A. Cooke, Jessica R. Thompson, Laura R. Bohrer, Kathleen R. Chirco, Arlene V. Drack, et al. 2018. « CRISPR-Cas9 genome engineering: Treating inherited retinal degeneration ». *Progress in Retinal and Eye*

Research 65 (juillet):28-49. https://doi.org/10.1016/j.preteyeres.2018.03.003.
Burridge, Keith, Magdalena Chrzanowska-Wodnicka, et Cuiling Zhong. 1997. « Focal adhesion assembly ». *Trends in Cell Biology*. Elsevier Ltd. https://doi.org/10.1016/S0962-8924(97)01127-6.
Busskamp, V., J. Duebel, D. Balya, M. Fradot, T. J. Viney, S. Siegert, A. C. Groner, et al. 2010. « Genetic Reactivation of Cone Photoreceptors Restores Visual Responses in Retinitis Pigmentosa ». *Science* 329 (5990): 413-17. https://doi.org/10.1126/science.1190897.
Byrne, Leah C., Deniz Dalkara, Gabriel Luna, Steven K. Fisher, Emmanuelle Clérin, Jose-Alain Sahel, Thierry Léveillard, et John G. Flannery. 2015. « Viral-mediated RdCVF and RdCVFL expression protects cone and rod photoreceptors in retinal degeneration ». *The Journal of Clinical Investigation* 125 (1): 105-16. https://doi.org/10.1172/JCI65654.
Cai, Xue, Shannon M. Conley, Zack Nash, Steven J. Fliesler, Mark J. Cooper, et Muna I. Naash. 2010. « Gene delivery to mitotic and postmitotic photoreceptors Via compacted DNA nanoparticles results in improved phenotype in a mouse model of retinitis pigmentosa ». *The FASEB Journal* 24 (4): 1178-91. https://doi.org/10.1096/fj.09-139147.
Calado, Sofia M., Ana V. Oliveira, Susana Machado, Rudolf Haase, et Gabriela A. Silva. 2014. « Sustained gene expression in the retina by improved episomal vectors ». *Tissue Engineering - Part A* 20 (19-20): 2692-98. https://doi.org/10.1089/ten.tea.2013.0672.
Carss, Keren, Gavin Arno, Marie Erwood, Jonathan Stephens, Alba Sanchis-Juan, Sarah Hull, Karyn Megy, et al. 2017. « Comprehensive Rare Variant Analysis via Whole-Genome Sequencing to Determine the Molecular Pathology of Inherited Retinal Disease ». *American Journal of Human Genetics* 100 (1): 75-90. https://doi.org/10.1016/j.ajhg.2016.12.003.
Cehajic Kapetanovic, Jasmina, Maria I Patrício, et Robert E MacLaren. 2019. « Progress in the development of novel therapies for choroideremia ». *Expert Review of Ophthalmology* 14 (6): 277-85. https://doi.org/10.1080/17469899.2019.1699406.
Chan, Ying Kai, Sean K. Wang, Colin J. Chu, David A. Copland, Alexander J. Letizia, Helena Costa Verdera, Jessica J. Chiang, et al. 2021. « Engineering adeno-associated viral vectors to evade innate immune and inflammatory responses ». *Science Translational Medicine* 13 (580): eabd3438. https://doi.org/10.1126/scitranslmed.abd3438.
Chen, Qian, Junhuang Zou, Zuolian Shen, Weiping Zhang, et Jun Yang. 2014. « Whirlin and PDZ Domain-containing 7 (PDZD7) Proteins Are Both Required to Form the Quaternary Protein Complex Associated with Usher Syndrome Type 2 ». *Journal of Biological Chemistry* 289 (52): 36070-88. https://doi.org/10.1074/jbc.M114.610535.

Cideciyan, Artur V., Samuel G. Jacobson, Arlene V. Drack, Allen C. Ho, Jason Charng, Alexandra V. Garafalo, Alejandro J. Roman, et al. 2019. « Effect of an intravitreal antisense oligonucleotide on vision in Leber congenital amaurosis due to a photoreceptor cilium defect ». *Nature Medicine* 25 (2): 225-28. https://doi.org/10.1038/s41591-018-0295-0.

Corbeel, Lucien, et Kathleen Freson. 2008. « Rab proteins and Rab-associated proteins: Major actors in the mechanism of protein-trafficking disorders ». *European Journal of Pediatrics*. Springer. https://doi.org/10.1007/s00431-008-0740-z.

Coussa, Razek Georges, et Elias I. Traboulsi. 2012. « Choroideremia: A review of general findings and pathogenesis ». *Ophthalmic Genetics* 33 (2): 57-65. https://doi.org/10.3109/13816810.2011.620056.

Cowan, Cameron S., Magdalena Renner, Brigitte Gross-Scherf, David Goldblum, Martin Munz, Jacek Krol, Tamas Szikra, et al. 2019. « Cell types of the human retina and its organoids at single-cell resolution: developmental convergence, transcriptomic identity, and disease map ». *bioRxiv*, juillet, 703348. https://doi.org/10.1101/703348.

Cremers, Frans P.M., Scott A. Armstrong, Miguel C. Seabra, Michael S. Brown, et Joseph L. Goldstein. 1994. « REP-2, a Rab escort protein encoded by the choroideremia-like gene ». *Journal of Biological Chemistry* 269 (3): 2111-17.

Cremers, Frans P.M., Dorien J.R. Van De Pol, Liesbeth P.M. Van Kerkhoff, Berend Wieringa, et Hans Hilger Ropers. 1990. « Cloning of a gene that is rearranged in patients with choroideraemia ». *Nature* 347 (6294): 674-77. https://doi.org/10.1038/347674a0.

Dalkara, D., L. C. Byrne, R. R. Klimczak, M. Visel, L. Yin, W. H. Merigan, J. G. Flannery, et D. V. Schaffer. 2013. « In Vivo-Directed Evolution of a New Adeno-Associated Virus for Therapeutic Outer Retinal Gene Delivery from the Vitreous ». *Science Translational Medicine* 5 (189): 189ra76-189ra76. https://doi.org/10.1126/scitranslmed.3005708.

Deng, Wen-Li, Mei-Ling Gao, Xin-Lan Lei, Ji-Neng Lv, Huan Zhao, Kai-Wen He, Xi-Xi Xia, et al. 2018. « Gene Correction Reverses Ciliopathy and Photoreceptor Loss in iPSC-Derived Retinal Organoids from Retinitis Pigmentosa Patients ». *Stem Cell Reports* 10 (4): 1267-81. https://doi.org/10.1016/J.STEMCR.2018.02.003.

Dimopoulos, Ioannis S, Stephanie Chan, Robert E MacLaren, et Ian M MacDonald. 2015. « Pathogenic mechanisms and the prospect of gene therapy for choroideremia. » *Expert opinion on orphan drugs* 3 (7): 787-98. https://doi.org/10.1517/21678707.2015.1046434.

Dimopoulos, Ioannis S., Stephanie C. Hoang, Alina Radziwon, Natalia M. Binczyk, Miguel C. Seabra, Robert E. MacLaren, Rizwan Somani, Matthew T.S. Tennant, et Ian M. MacDonald. 2018. « Two-Year Results After AAV2-Mediated Gene Therapy for Choroideremia: The

Alberta Experience ». *American Journal of Ophthalmology* 193 (septembre):130-42. https://doi.org/10.1016/j.ajo.2018.06.011.
Dona, Margo, Ralph Slijkerman, Kimberly Lerner, Sanne Broekman, Jeremy Wegner, Taylor Howat, Theo Peters, et al. 2018. « Usherin defects lead to early-onset retinal dysfunction in zebrafish ». *Experimental Eye Research* 173 (août):148-59. https://doi.org/10.1016/J.EXER.2018.05.015.
Dreyer, Bo, Vigdis Brox, Lisbeth Tranebjærg, Thomas Rosenberg, Andrè M. Sadeghi, Claes Möller, et Øivind Nilssen. 2008. « Spectrum of USH2A mutations in Scandinavian patients with Usher syndrome type II ». *Human Mutation* 29 (3): 451-451. https://doi.org/10.1002/humu.9524.
Dreyer, Bo, Lisbeth Tranebjærg, Vigdis Brox, Thomas Rosenberg, Claes Möller, Magdalena Beneyto, Michael D. Weston, et al. 2001. « A Common Ancestral Origin of the Frequent and Widespread 2299delG USH2A Mutation ». *The American Journal of Human Genetics* 69 (1): 228-34. https://doi.org/10.1086/321269.
Duan, Dongsheng. 2018. « Systemic AAV Micro-dystrophin Gene Therapy for Duchenne Muscular Dystrophy. » *Molecular therapy : the journal of the American Society of Gene Therapy* 26 (10): 2337-56. https://doi.org/10.1016/j.ymthe.2018.07.011.
Duan, Yongtao, Abhishek Dhar, Chetan Patel, Mehul Khimani, Swarnali Neogi, Prolay Sharma, Nadavala Siva Kumar, et Rohit L. Vekariya. 2020. « A brief review on solid lipid nanoparticles: Part and parcel of contemporary drug delivery systems ». *RSC Advances*. Royal Society of Chemistry. https://doi.org/10.1039/d0ra03491f.
Ebermann, Inga, Jennifer B. Phillips, Max C. Liebau, Robert K. Koenekoop, Bernhard Schermer, Irma Lopez, Ellen Schäfer, et al. 2010. « PDZD7 is a modifier of retinal disease and a contributor to digenic Usher syndrome ». *Journal of Clinical Investigation* 120 (6): 1812-23. https://doi.org/10.1172/JCI39715.
Eudy, J D, M D Weston, S Yao, D M Hoover, H L Rehm, M Ma-Edmonds, D Yan, et al. 1998. « Mutation of a gene encoding a protein with extracellular matrix motifs in Usher syndrome type IIa. » *Science (New York, N.Y.)* 280 (5370): 1753-57. https://doi.org/10.1126/science.280.5370.1753.
Fink, T L, P J Klepcyk, S M Oette, C R Gedeon, S L Hyatt, T H Kowalczyk, R C Moen, et M J Cooper. 2006. « Plasmid size up to 20 kbp does not limit effective in vivo lung gene transfer using compacted DNA nanoparticles ». *Gene Therapy* 13 (13): 1048-51. https://doi.org/10.1038/sj.gt.3302761.
Furgoch, Mira J.B., Jacqueline Mewes-Arès, Alina Radziwon, et Ian M. MacDonald. 2014. « Molecular genetic diagnostic techniques in choroideremia ». *Molecular Vision* 20:535.
Fuster-García, Carla, Gema García-García, Elisa González-Romero, Teresa Jaijo, María D Sequedo, Carmen Ayuso, Rafael P Vázquez-Manrique, José M Millán, et Elena Aller. 2017. « USH2A Gene Editing Using the CRISPR System. » *Molecular therapy. Nucleic*

acids 8 (septembre):529-41. https://doi.org/10.1016/j.omtn.2017.08.003.
Gagliardi, Giuliana, Karim Ben M'Barek, et Olivier Goureau. 2019. « Photoreceptor cell replacement in macular degeneration and retinitis pigmentosa: A pluripotent stem cell-based approach ». *Progress in Retinal and Eye Research* 71 (juillet):1-25. https://doi.org/10.1016/J.PRETEYERES.2019.03.001.
Gange, William S., Robert A. Sisk, Cagri G. Besirli, Thomas C. Lee, Margaret Havunjian, Hillary Schwartz, Mark Borchert, et al. 2022. « Perifoveal Chorioretinal Atrophy after Subretinal Voretigene Neparvovec-rzyl for RPE65-Mediated Leber Congenital Amaurosis ». *Ophthalmology Retina* 6 (1): 58-64. https://doi.org/10.1016/j.oret.2021.03.016.
Garita-Hernandez, Marcela, Maruša Lampič, Antoine Chaffiol, Laure Guibbal, Fiona Routet, Tiago Santos-Ferreira, Sylvia Gasparini, et al. 2019. « Restoration of visual function by transplantation of optogenetically engineered photoreceptors ». *Nature Communications* 10 (1). https://doi.org/10.1038/s41467-019-12330-2.
Goldberg, Andrew F. X., Orson L. Moritz, et David S. Williams. 2016. « Molecular Basis for Photoreceptor Outer Segment Architecture ». *Progress in Retinal and Eye Research* 55 (novembre):52-81. https://doi.org/10.1016/j.preteyeres.2016.05.003.
Goldmann, T., N. Overlack, U. Wolfrum, et K. Nagel-Wolfrum. 2011. « PTC124-Mediated Translational Readthrough of a Nonsense Mutation Causing Usher Syndrome Type 1C ». *Human Gene Therapy* 22 (5): 537-47. https://doi.org/10.1089/hum.2010.067.
Goldmann, Tobias, Nora Overlack, Fabian Möller, Valery Belakhov, Michiel van Wyk, Timor Baasov, Uwe Wolfrum, et Kerstin Nagel-Wolfrum. 2012. « A comparative evaluation of NB30, NB54 and PTC124 in translational read-through efficacy for treatment of an USH1C nonsense mutation ». *EMBO Molecular Medicine* 4 (11): 1186. https://doi.org/10.1002/EMMM.201201438.
Gonzalez-Cordero, Anai, Kamil Kruczek, Arifa Naeem, Milan Fernando, Magdalena Kloc, Joana Ribeiro, Debbie Goh, et al. 2017. « Stem Cell Reports Ar ticle Recapitulation of Human Retinal Development from Human Pluripotent Stem Cells Generates Transplantable Populations of Cone Photoreceptors ». https://doi.org/10.1016/j.stemcr.2017.07.022.
Goodyear, Richard J., Walter Marcotti, Corn J. Kros, et Guy P. Richardson. 2005. « Development and properties of stereociliary link types in hair cells of the mouse cochlea ». *The Journal of Comparative Neurology* 485 (1): 75-85. https://doi.org/10.1002/cne.20513.
Graefe, Von A. 1858. « Exceptionelles verrhalten des gesichtsfeldes bei pigmentenartung der netzhaut ». *Von Graefe's Arch Ophtlalmol* 4:250-53.

Grati, M'hamed, Jung-Bum Shin, Michael D. Weston, James Green, Manzoor A. Bhat, Peter G. Gillespie, et Bechara Kachar. 2012. « Localization of PDZD7 to the Stereocilia Ankle-Link Associates this Scaffolding Protein with the Usher Syndrome Protein Network ». *Journal of Neuroscience* 32 (41): 14288-93. https://doi.org/10.1523/JNEUROSCI.3071-12.2012.

Grijalvo, Santiago, Gustavo Puras, Jon Zárate, Myriam Sainz-Ramos, Nuseibah A. L. Qtaish, Tania López, Mohamed Mashal, et al. 2019. « Cationic Niosomes as Non-Viral Vehicles for Nucleic Acids: Challenges and Opportunities in Gene Delivery ». *Pharmaceutics* 11 (2): 50. https://doi.org/10.3390/pharmaceutics11020050.

Guiner, Caroline Le, Laurent Servais, Marie Montus, Thibaut Larcher, Bodvaël Fraysse, Sophie Moullec, Marine Allais, et al. 2017. « Long-term microdystrophin gene therapy is effective in a canine model of Duchenne muscular dystrophy ». *Nature Communications* 8 (1): 16105. https://doi.org/10.1038/ncomms16105.

Guo, Yonglong, Peiyuan Wang, Jacey Hongjie Ma, Zekai Cui, Quan Yu, Shiwei Liu, Yunxia Xue, et al. 2019. « Modeling Retinitis Pigmentosa: Retinal Organoids Generated From the iPSCs of a Patient With the USH2A Mutation Show Early Developmental Abnormalities ». *Frontiers in Cellular Neuroscience* 13 (août):361. https://doi.org/10.3389/fncel.2019.00361.

Haase, Rudolf, Orestis Argyros, Suet-Ping Wong, Richard P. Harbottle, Hans J. Lipps, Manfred Ogris, Terese Magnusson, Maria G. Vizoso Pinto, Jürgen Haas, et Armin Baiker. 2010. « pEPito: a significantly improved non-viral episomal expression vector for mammalian cells ». *BMC Biotechnology* 10 (1): 20. https://doi.org/10.1186/1472-6750-10-20.

Hallam, Dean, Gerrit Hilgen, Birthe Dorgau, Lili Zhu, Min Yu, Sanja Bojic, Philip Hewitt, et al. 2018. « Human-Induced Pluripotent Stem Cells Generate Light Responsive Retinal Organoids with Variable and Nutrient-Dependent Efficiency ». *STEM CELLS* 36 (10): 1535-51. https://doi.org/10.1002/stem.2883.

Han, Ian C., Erin Burnight, Mallory J. Ulferts, Kristan S. Worthington, Stephen R. Russell, Elliott H. Sohn, Robert F Mullins, Edwin Stone, Budd A Tucker, et Luke Aaron Wiley. 2019. « Helper-Dependent Adenovirus Transduces the Human and Rat Retina but Elicits an Inflammatory Reaction When Delivered Subretinally in Rats ». *Human Gene Therapy*, août, hum.2019.159. https://doi.org/10.1089/hum.2019.159.

Han, Zongchao, Shannon M. Conley, Rasha Makkia, Junjing Guo, Mark J. Cooper, et Muna I. Naash. 2012. « Comparative Analysis of DNA Nanoparticles and AAVs for Ocular Gene Delivery ». *PLoS ONE* 7 (12). https://doi.org/10.1371/journal.pone.0052189.

Hartel, Bas P., Maria Löfgren, Patrick L.M. Huygen, Iris Guchelaar, Nicole Lo-A-Njoe Kort, Andre M. Sadeghi, Erwin van Wijk, et al. 2016. « A combination of two truncating mutations in USH2A causes more severe and progressive hearing impairment in Usher syndrome type

IIa ». *Hearing Research* 339 (septembre):60-68. https://doi.org/10.1016/J.HEARES.2016.06.008.
Hartong, Dyonne T., Eliot L. Berson, et Thaddeus P. Dryja. 2006. « Retinitis pigmentosa ». *Lancet*. https://doi.org/10.1016/S0140-6736(06)69740-7.
Hasan, Mahadi, Anowara Khatun, Tatsuya Fukuta, et Kentaro Kogure. 2020. « Noninvasive transdermal delivery of liposomes by weak electric current ». *Advanced Drug Delivery Reviews*. Elsevier B.V. https://doi.org/10.1016/j.addr.2020.06.016.
Hoon, Mrinalini, Haruhisa Okawa, Luca Della Santina, et Rachel O. L. Wong. 2014. « Functional Architecture of the Retina: Development and Disease ». *Progress in Retinal and Eye Research* 42 (septembre):44-84. https://doi.org/10.1016/j.preteyeres.2014.06.003.
Howe, Kerstin, Matthew D Clark, Carlos F Torroja, James Torrance, Camille Berthelot, Matthieu Muffato, John E Collins, et al. 2013. « The zebrafish reference genome sequence and its relationship to the human genome. » *Nature* 496 (7446): 498-503. https://doi.org/10.1038/nature12111.
Huang, Dali, James D. Eudy, Eva Uzvolgyi, Jack R. Davis, Catherine B. Talmadge, Dalyir Pretto, Michael D. Weston, et al. 2002. « Identification of the Mouse and Rat Orthologs of the Gene Mutated in Usher Syndrome Type IIA and the Cellular Source of USH2A mRNA in Retina, a Target Tissue of the Disease ». *Genomics* 80 (2): 195-203. https://doi.org/10.1006/GENO.2002.6823.
Hunter, D. G., G. A. Fishman, R. S. Mehta, et F. L. Kretzer. 1986. « Abnormal Sperm and Photoreceptor Axonemes in Usher's Syndrome ». *Archives of Ophthalmology* 104 (3): 385-89. https://doi.org/10.1001/archopht.1986.01050150085033.
Iafisco, Michele, María Esperanza Ruiz, Sebastián Scioli Montoto, et Giuliana Muraca. 2020. « Solid Lipid Nanoparticles for Drug Delivery: Pharmacological and Biopharmaceutical Aspects ». https://doi.org/10.3389/fmolb.2020.587997.
Ita, Kevin. 2016. « Transdermal iontophoretic drug delivery: Advances and challenges ». *Journal of Drug Targeting*. Taylor and Francis Ltd. https://doi.org/10.3109/1061186X.2015.1090442.
Jenke, Bok Hee C, Christian P Fetzer, Isa M Stehle, Franziska Jönsson, Frank O Fackelmayer, Harald Conradt, Jürgen Bode, et Hans J Lipps. 2002. « An episomally replicating vector binds to the nuclear matrix protein SAF-A in vivo. » *EMBO reports* 3 (4): 349-54. https://doi.org/10.1093/embo-reports/kvf070.
Johnson, Christiana J., Lennart Berglin, Micah A. Chrenek, T. M. Redmond, Jeffrey H. Boatright, et John M. Nickerson. 2008. « Technical brief: Subretinal injection and electroporation into adult mouse eyes ». *Molecular Vision* 14 (décembre):2211-26.
Jung, Jae Hwan, Bryce Chiang, Hans E. Grossniklaus, et Mark R. Prausnitz. 2018. « Ocular drug delivery targeted by iontophoresis in

the suprachoroidal space using a microneedle ». *Journal of Controlled Release* 277 (mai):14-22. https://doi.org/10.1016/j.jconrel.2018.03.001.
Kelley, Ryan A, Shannon M Conley, Rasha Makkia, Jamie N Watson, Zongchao Han, Mark J Cooper, et Muna I Naash. 2018. « DNA nanoparticles are safe and nontoxic in non-human primate eyes ». *International Journal of Nanomedicine* Volume 13 (mars):1361-79. https://doi.org/10.2147/IJN.S157000.
Kennedy, Breandán, et Jarema Malicki. 2009. « What drives cell morphogenesis: A look inside the vertebrate photoreceptor ». *Developmental Dynamics* 238 (9): 2115-38. https://doi.org/10.1002/dvdy.22010.
Khabou, Hanen, Chloé Cordeau, Laure Pacot, Sylvain Fisson, et Deniz Dalkara. 2018. « Dosage Thresholds and Influence of Transgene Cassette in Adeno-Associated Virus–Related Toxicity ». *Human Gene Therapy* 29 (11): 1235-41. https://doi.org/10.1089/hum.2018.144.
Koirala, Adarsha, Shannon M. Conley, Rasha Makkia, Zhao Liu, Mark J. Cooper, Janet R. Sparrow, et Muna I. Naash. 2013a. « Persistence of non-viral vector mediated RPE65 expression: Case for viability as a gene transfer therapy for RPE-based diseases ». *Journal of Controlled Release* 172 (3): 745-52. https://doi.org/10.1016/j.jconrel.2013.08.299.
———. 2013b. « Persistence of non-viral vector mediated RPE65 expression: Case for viability as a gene transfer therapy for RPE-based diseases ». *Journal of Controlled Release* 172 (3): 745-52. https://doi.org/10.1016/j.jconrel.2013.08.299.
Koirala, Adarsha, Rasha S Makkia, Shannon M Conley, Mark J Cooper, et Muna I Naash. 2013. « S/MAR-containing DNA nanoparticles promote persistent RPE gene expression and improvement in RPE65-associated LCA. » *Human molecular genetics* 22 (8): 1632-42. https://doi.org/10.1093/hmg/ddt013.
Krock, Bryan L., Joseph Bilotta, et Brian D. Perkins. 2007. « Noncell-autonomous photoreceptor degeneration in a zebrafish model of choroideremia ». *Proceedings of the National Academy of Sciences of the United States of America* 104 (11): 4600-4605. https://doi.org/10.1073/pnas.0605818104.
Kusuluri, Deva K., Baran E. Güler, Barbara Knapp, Nicola Horn, Karsten Boldt, Marius Ueffing, Gabriela Aust, et Uwe Wolfrum. 2021. « Adhesion G protein-coupled receptor VLGR1/ADGRV1 regulates cell spreading and migration by mechanosensing at focal adhesions ». *iScience* 24 (4). https://doi.org/10.1016/j.isci.2021.102283.
Lee, Cody S., Elliot S. Bishop, Ruyi Zhang, Xinyi Yu, Evan M. Farina, Shujuan Yan, Chen Zhao, et al. 2017. « Adenovirus-mediated gene delivery: Potential applications for gene and cell-based therapies in the new era of personalized medicine ». *Genes & Diseases* 4 (2): 43-63. https://doi.org/10.1016/J.GENDIS.2017.04.001.

Leikas, Aleksi J., Seppo Ylä-Herttuala, et Juha E. K. Hartikainen. 2023. « Adenoviral Gene Therapy Vectors in Clinical Use—Basic Aspects with a Special Reference to Replication-Competent Adenovirus Formation and Its Impact on Clinical Safety ». *International Journal of Molecular Sciences* 24 (22): 16519. https://doi.org/10.3390/ijms242216519.

Lenassi, Eva, Anthony G. Robson, Linda M. Luxon, Maria Bitner-Glindzicz, et Andrew R. Webster. 2015. « Clinical Heterogeneity in a Family With Mutations in *USH2A* ». *JAMA Ophthalmology* 133 (3): 352. https://doi.org/10.1001/jamaophthalmol.2014.5163.

Lenassi, Eva, Zubin Saihan, Maria Bitner-Glindzicz, et Andrew R. Webster. 2014. « The effect of the common c.2299delG mutation in USH2A on RNA splicing ». *Experimental Eye Research* 122 (mai):9-12. https://doi.org/10.1016/J.EXER.2014.02.018.

Lenassi, Eva, Ajoy Vincent, Zheng Li, Zubin Saihan, Alison J Coffey, Heather B Steele-Stallard, Anthony T Moore, et al. 2015. « A detailed clinical and molecular survey of subjects with nonsyndromic USH2A retinopathy reveals an allelic hierarchy of disease-causing variants ». *European Journal of Human Genetics* 23 (10): 1318-27. https://doi.org/10.1038/ejhg.2014.283.

Lentz, Jennifer, et Bronya Keats. 1993. *Usher Syndrome Type II*. *GeneReviews®*. University of Washington, Seattle.

Liew, Gerald, Michel Michaelides, et Catey Bunce. 2014. « A comparison of the causes of blindness certifications in England and Wales in working age adults (16-64 years), 1999-2000 with 2009-2010 ». *BMJ Open* 4 (2): 4015. https://doi.org/10.1136/bmjopen-2013-004015.

Linnert, Joshua, Barbara Knapp, Baran E. Güler, Karsten Boldt, Marius Ueffing, et Uwe Wolfrum. 2023. « Usher Syndrome Proteins ADGRV1 (USH2C) and CIB2 (USH1J) Interact and Share a Common Interactome Containing TRiC/CCT-BBS Chaperonins ». *Frontiers in Cell and Developmental Biology* 11:1199069. https://doi.org/10.3389/fcell.2023.1199069.

Liu, X., O. V. Bulgakov, K. N. Darrow, B. Pawlyk, M. Adamian, M. C. Liberman, et T. Li. 2007. « Usherin is required for maintenance of retinal photoreceptors and normal development of cochlear hair cells ». *Proceedings of the National Academy of Sciences* 104 (11): 4413-18. https://doi.org/10.1073/pnas.0610950104.

Liu, Xue-Zhong, Carolyn Hope, Chuan Yu Liang, Jiu Mu Zou, Li Rong Xu, T. Cole, Robert F. Mueller, et al. 1999. « A Mutation (2314delG) in the Usher Syndrome Type IIA Gene: High Prevalence and Phenotypic Variation ». *The American Journal of Human Genetics* 64 (4): 1221-25. https://doi.org/10.1086/302332.

Llonch, Sílvia, Madalena Carido, et Marius Ader. 2018. « Organoid technology for retinal repair ». *Developmental Biology* 433 (2): 132-43. https://doi.org/10.1016/J.YDBIO.2017.09.028.

Lu, Bin, Shaomei Wang, Peter J. Francis, Tiansen Li, David M. Gamm, Elizabeth E. Capowski, et Raymond D. Lund. 2010. « Cell

Transplantation to Arrest Early Changes in an Ush2a Animal Model ». *Investigative Opthalmology & Visual Science* 51 (4): 2269. https://doi.org/10.1167/iovs.09-4526.
MacDonald, Ian M, Stacey CM Hume, Stephanie Chan, et Miguel C Seabra. 2015. *GeneReviews - Choroideremia -*. *GeneReviews*. Lippincott Williams and Wilkins. https://doi.org/10.1097/ICU.0000000000000392.
MacDonald, Ian M, Yves Sauvé, et Paul A Sieving. 2007. « Preventing blindness in retinal disease: ciliary neurotrophic factor intraocular implants. » *Canadian journal of ophthalmology. Journal canadien d'ophtalmologie* 42 (3): 399-402. https://doi.org/10.3129/can j ophthalmol.i07-039.
Macé, Emilie, Romain Caplette, Olivier Marre, Abhishek Sengupta, Antoine Chaffiol, Peggy Barbe, Mélissa Desrosiers, et al. 2015. « Targeting channelrhodopsin-2 to ON-bipolar cells with vitreally administered AAV restores on and off visual responses in blind mice ». *Molecular Therapy* 23 (1): 7-16. https://doi.org/10.1038/mt.2014.154.
Maddalena, Andrea, Patrizia Tornabene, Paola Tiberi, Renato Minopoli, Anna Manfredi, Margherita Mutarelli, Settimio Rossi, et al. 2018. « Triple Vectors Expand AAV Transfer Capacity in the Retina. » *Molecular therapy : the journal of the American Society of Gene Therapy* 26 (2): 524-41. https://doi.org/10.1016/j.ymthe.2017.11.019.
Major, Lauren, Michelle E. McClements, et Robert E. MacLaren. 2023. « A Review of CRISPR Tools for Treating Usher Syndrome: Applicability, Safety, Efficiency, and In Vivo Delivery ». *International Journal of Molecular Sciences* 24 (8): 7603. https://doi.org/10.3390/ijms24087603.
Malamas, Anthony S., Maneesh Gujrati, China M. Kummitha, Rongzuo Xu, et Zheng Rong Lu. 2013. « Design and evaluation of new pH-sensitive amphiphilic cationic lipids for siRNA delivery ». *Journal of controlled release : official journal of the Controlled Release Society* 171 (3): 296-307. https://doi.org/10.1016/J.JCONREL.2013.06.019.
Martens, Joost H. A., Matty Verlaan, Eric Kalkhoven, Josephine C. Dorsman, et Alt Zantema. 2002. « Scaffold/Matrix Attachment Region Elements Interact with a p300-Scaffold Attachment Factor A Complex and Are Bound by Acetylated Nucleosomes ». *Molecular and Cellular Biology* 22 (8): 2598-2606. https://doi.org/10.1128/mcb.22.8.2598-2606.2002.
Matsuda, Takahiko, et Constance L. Cepko. 2004. « Electroporation and RNA interference in the rodent retina in vivo and in vitro ». *Proceedings of the National Academy of Sciences of the United States of America* 101 (1): 16-22. https://doi.org/10.1073/pnas.2235688100.
———. 2007. « Controlled expression of transgenes introduced by in vivo electroporation ». *Proceedings of the National Academy of*

Sciences of the United States of America 104 (3): 1027-32. https://doi.org/10.1073/pnas.0610155104.
MEDAWAR, P B. 1948. « Immunity to homologous grafted skin; the fate of skin homografts transplanted to the brain, to subcutaneous tissue, and to the anterior chamber of the eye. » *British journal of experimental pathology* 29 (1): 58-69.
Mellough, Carla B., Joseph Collin, Rachel Queen, Gerrit Hilgen, Birthe Dorgau, Darin Zerti, Majed Felemban, Kathryn White, Evelyne Sernagor, et Majlinda Lako. 2019. « Systematic Comparison of Retinal Organoid Differentiation from Human Pluripotent Stem Cells Reveals Stage Specific, Cell Line, and Methodological Differences ». *STEM CELLS Translational Medicine* 8 (7): sctm.18-0267. https://doi.org/10.1002/sctm.18-0267.
Melo, Jimmy de, et Seth Blackshaw. 2011. « In vivo electroporation of developing mouse retina ». *Journal of Visualized Experiments*, nº 52. https://doi.org/10.3791/2847.
———. 2018. « In vivo electroporation of developing mouse retina ». In *Methods in Molecular Biology*, 1715:101-11. Humana Press Inc. https://doi.org/10.1007/978-1-4939-7522-8_8.
Meyer, J. S., R. L. Shearer, E. E. Capowski, L. S. Wright, K. A. Wallace, E. L. McMillan, S.-C. Zhang, et D. M. Gamm. 2009. « Modeling early retinal development with human embryonic and induced pluripotent stem cells ». *Proceedings of the National Academy of Sciences* 106 (39): 16698-703. https://doi.org/10.1073/pnas.0905245106.
Michalski, N., V. Michel, A. Bahloul, G. Lefevre, J. Barral, H. Yagi, S. Chardenoux, et al. 2007. « Molecular Characterization of the Ankle-Link Complex in Cochlear Hair Cells and Its Role in the Hair Bundle Functioning ». *Journal of Neuroscience* 27 (24): 6478-88. https://doi.org/10.1523/JNEUROSCI.0342-07.2007.
Mirkovitch, Jovan, Marc Edouard Mirault, et Ulrich K. Laemmli. 1984. « Organization of the higher-order chromatin loop: specific DNA attachment sites on nuclear scaffold ». *Cell* 39 (1): 223-32. https://doi.org/10.1016/0092-8674(84)90208-3.
Mitra, Rajendra N., Zongchao Han, Miles Merwin, Muhammed Al Taai, Shannon M. Conley, et Muna I. Naash. 2014. « Synthesis and characterization of glycol chitosan DNA nanoparticles for retinal gene delivery ». *ChemMedChem* 9 (1): 189-96. https://doi.org/10.1002/cmdc.201300371.
Mitra, Rajendra Narayan, Min Zheng, Ellen R. Weiss, et Zongchao Han. 2018a. « Genomic form of rhodopsin DNA nanoparticles rescued autosomal dominant Retinitis pigmentosa in the P23H knock-in mouse model ». *Biomaterials* 157 (mars):26-39. https://doi.org/10.1016/j.biomaterials.2017.12.004.
———. 2018b. « Genomic form of rhodopsin DNA nanoparticles rescued autosomal dominant Retinitis pigmentosa in the P23H knock-in mouse model ». *Biomaterials* 157 (mars):26-39. https://doi.org/10.1016/j.biomaterials.2017.12.004.

Mitsios, Andreas, Adam M. Dubis, et Mariya Moosajee. 2018. « Choroideremia: from genetic and clinical phenotyping to gene therapy and future treatments ». *Therapeutic Advances in Ophthalmology* 10 (janvier):251584141881749. https://doi.org/10.1177/2515841418817490.

Moosajee, Mariya, Simon C. Ramsden, Graeme Cm Black, Miguel C. Seabra, et Andrew R. Webster. 2014. « Clinical utility gene card for: Choroideremia ». *European Journal of Human Genetics* 22 (4). https://doi.org/10.1038/ejhg.2013.183.

Moosajee, Mariya, Dhani Tracey-White, Matthew Smart, Marla Weetall, Simona Torriano, Vasiliki Kalatzis, Lyndon da Cruz, Peter Coffey, Andrew R. Webster, et Ellen Welch. 2016. « Functional rescue of REP1 following treatment with PTC124 and novel derivative PTC-414 in human choroideremia fibroblasts and the nonsense-mediated zebrafish model ». *Human Molecular Genetics* 25 (16): 3416-31. https://doi.org/10.1093/hmg/ddw184.

Neuhaus, Christine, Tobias Eisenberger, Christian Decker, Sandra Nagl, Cornelia Blank, Markus Pfister, Ingo Kennerknecht, et al. 2017. « Next-generation sequencing reveals the mutational landscape of clinically diagnosed Usher syndrome: copy number variations, phenocopies, a predominant target for translational read-through, and PEX26 mutated in Heimler syndrome. » *Molecular genetics & genomic medicine* 5 (5): 531-52. https://doi.org/10.1002/mgg3.312.

Nickerson, John M., Penny Goodman, Micah A. Chrenek, Christiana J. Bernal, Lennart Berglin, T. Michael Redmond, et Jeffrey H. Boatright. 2012. « Subretinal delivery and electroporation in pigmented and nonpigmented adult mouse eyes ». *Methods in Molecular Biology* 884:53-69. https://doi.org/10.1007/978-1-61779-848-1_4.

Okita, Keisuke, Yasuko Matsumura, Yoshiko Sato, Aki Okada, Asuka Morizane, Satoshi Okamoto, Hyenjong Hong, et al. 2011. « A more efficient method to generate integration-free human iPS cells ». *Nature Methods* 8 (5): 409-12. https://doi.org/10.1038/nmeth.1591.

Oliveira, Ana V., Adriana Marcelo, Ana M. Rosa da Costa, et Gabriela A. Silva. 2016. « Evaluation of cystamine-modified hyaluronic acid/chitosan polyplex as retinal gene vector ». *Materials Science and Engineering C* 58 (janvier):264-72. https://doi.org/10.1016/j.msec.2015.08.047.

Oliveira, Ana Vanessa Vieira, Gabriela Araújo Silva, et Daniel C. Chung. 2015. « Enhancement of chitosan-mediated gene delivery through combination with phiC31 integrase ». *Acta Biomaterialia* 17 (avril):89-97. https://doi.org/10.1016/j.actbio.2015.01.013.

Pagon, Roberta A. 1988. « Retinitis pigmentosa ». *Survey of Ophthalmology* 33 (3): 137-77. https://doi.org/10.1016/0039-6257(88)90085-9.

Pardue, Machelle T, et Rachael S Allen. 2018. « Neuroprotective strategies for retinal disease. » *Progress in retinal and eye research* 65:50-76. https://doi.org/10.1016/j.preteyeres.2018.02.002.

Parfitt, David A., Amelia Lane, Conor M. Ramsden, Amanda-Jayne F. Carr, Peter M. Munro, Katarina Jovanovic, Nele Schwarz, et al. 2016. « Identification and Correction of Mechanisms Underlying Inherited Blindness in Human iPSC-Derived Optic Cups ». *Cell Stem Cell* 18 (6): 769-81. https://doi.org/10.1016/j.stem.2016.03.021.

Pensado, Andrea, Francisco J. Diaz-Corrales, Berta De la Cerda, Lourdes Valdés-Sánchez, Ana Aramburu del Boz, Daniel Rodriguez-Martinez, Ana B. García-Delgado, Begoña Seijo, Shomi S. Bhattacharya, et Alejandro Sanchez. 2016. « Span poly-L-arginine nanoparticles are efficient non-viral vectors for PRPF31 gene delivery: An approach of gene therapy to treat retinitis pigmentosa ». *Nanomedicine: Nanotechnology, Biology, and Medicine* 12 (8): 2251-60. https://doi.org/10.1016/j.nano.2016.06.007.

Pérez-Carro, Raquel, Fiona Blanco-Kelly, Lilián Galbis-Martínez, Gema García-García, Elena Aller, Blanca García-Sandoval, Pablo Mínguez, et al. 2018. « Unravelling the pathogenic role and genotype-phenotype correlation of the USH2A p.(Cys759Phe) variant among Spanish families. » *PloS one* 13 (6): e0199048. https://doi.org/10.1371/journal.pone.0199048.

Piechaczek, C, C Fetzer, A Baiker, J Bode, et H J Lipps. 1999. « A vector based on the SV40 origin of replication and chromosomal S/MARs replicates episomally in CHO cells. » *Nucleic acids research* 27 (2): 426-28.

Pierrache, Laurence H.M., Bas P. Hartel, Erwin van Wijk, Magda A. Meester-Smoor, Frans P.M. Cremers, Elfride de Baere, Julie de Zaeytijd, et al. 2016. « Visual Prognosis in USH2A-Associated Retinitis Pigmentosa Is Worse for Patients with Usher Syndrome Type IIa Than for Those with Nonsyndromic Retinitis Pigmentosa ». *Ophthalmology* 123 (5): 1151-60. https://doi.org/10.1016/J.OPHTHA.2016.01.021.

Planul, Arthur, et Deniz Dalkara. 2017. « Vectors and Gene Delivery to the Retina ». *Annual Review of Vision Science* 3 (1): 121-40. https://doi.org/10.1146/annurev-vision-102016-061413.

Puppo, A, G Cesi, E Marrocco, P Piccolo, S Jacca, D M Shayakhmetov, R J Parks, et al. 2014. « Retinal transduction profiles by high-capacity viral vectors. » *Gene therapy* 21 (10): 855-65. https://doi.org/10.1038/gt.2014.57.

Puras, G., M. Mashal, J. Zárate, M. Agirre, E. Ojeda, S. Grijalvo, R. Eritja, et al. 2014. « A novel cationic niosome formulation for gene delivery to the retina ». *Journal of Controlled Release* 174 (1): 27-36. https://doi.org/10.1016/j.jconrel.2013.11.004.

Puras, G., J. Zarate, M. Aceves, A. Murua, A. R. Díaz, M. Avilés-Triguero, E. Fernández, et J. L. Pedraz. 2013. « Low molecular weight oligochitosans for non-viral retinal gene therapy ». *European Journal of Pharmaceutics and Biopharmaceutics* 83 (2): 131-40. https://doi.org/10.1016/j.ejpb.2012.09.010.

Quesne Stabej, Polona Le, Zubin Saihan, Nell Rangesh, Heather B Steele-Stallard, John Ambrose, Alison Coffey, Jenny Emmerson, et al. 2012. « Comprehensive sequence analysis of nine Usher syndrome genes in the UK National Collaborative Usher Study ». *Journal of Medical Genetics* 49 (1): 27-36. https://doi.org/10.1136/jmedgenet-2011-100468.

Radziwon, Alina, Gavin Arno, Dianna K. Wheaton, Ellen M. McDonagh, Emma L. Baple, Kaylie Webb-Jones, David G. Birch, Andrew R. Webster, et Ian M. MacDonald. 2017. « Single-base substitutions in the CHM promoter as a cause of choroideremia ». *Human Mutation* 38 (6): 704-15. https://doi.org/10.1002/humu.23212.

Rajala, Ammaji, Yuhong Wang, Ye Zhu, Michelle Ranjo-Bishop, Jian Xing Ma, Chuanbin Mao, et Raju V.S. Rajala. 2014. « Nanoparticle-assisted targeted delivery of eye-specific genes to eyes significantly improves the vision of blind mice in vivo ». *Nano Letters* 14 (9): 5257-63. https://doi.org/10.1021/nl502275s.

Rak, Alexey, Olena Pylypenko, Anca Niculae, Konstantin Pyatkov, Roger S Goody, et Kirill Alexandrov. 2004. « Structure of the Rab7:REP-1 complex: insights into the mechanism of Rab prenylation and choroideremia disease. » *Cell* 117 (6): 749-60. https://doi.org/10.1016/j.cell.2004.05.017.

Ramos, João Nuno, João Carlos Ribeiro, Andreia Carvalho Pereira, Sónia Ferreira, Isabel Catarina Duarte, et Miguel Castelo-Branco. 2019. « Evidence for impaired olfactory function and structural brain integrity in a disorder of ciliary function, Usher syndrome ». *NeuroImage: Clinical* 22:101757. https://doi.org/10.1016/j.nicl.2019.101757.

Rebibo-Sabbah, Annie, Igor Nudelman, Zubair M. Ahmed, Timor Baasov, et Tamar Ben-Yosef. 2007. « In vitro and ex vivo suppression by aminoglycosides of PCDH15 nonsense mutations underlying type 1 Usher syndrome ». *Human Genetics* 122 (3-4): 373-81. https://doi.org/10.1007/s00439-007-0410-7.

Regent, Florian, Lise Morizur, Léa Lesueur, Walter Habeler, Alexandra Plancheron, Karim Ben M'Barek, et Christelle Monville. 2019. « Automation of human pluripotent stem cell differentiation toward retinal pigment epithelial cells for large-scale productions ». *Scientific Reports* 9 (1): 1-11. https://doi.org/10.1038/s41598-019-47123-6.

Reichel, Felix F., Daniyar L. Dauletbekov, Reinhild Klein, Tobias Peters, G. Alex Ochakovski, Immanuel P. Seitz, Barbara Wilhelm, et al. 2017. « AAV8 Can Induce Innate and Adaptive Immune Response in the Primate Eye ». *Molecular Therapy* 25 (12): 2648-60. https://doi.org/10.1016/j.ymthe.2017.08.018.

Reichel, Felix Friedrich, Immanuel Seitz, Fabian Wozar, Spyridon Dimopoulos, Ronja Jung, Melanie Kempf, Susanne Kohl, et al. 2022. « Development of retinal atrophy after subretinal gene therapy with voretigene neparvovec ». *British Journal of Ophthalmology*. https://doi.org/10.1136/bjophthalmol-2021-321023.

Reichman, Sacha, Amélie Slembrouck, Giuliana Gagliardi, Antoine Chaffiol, Angélique Terray, Céline Nanteau, Anais Potey, et al. 2017. « Generation of Storable Retinal Organoids and Retinal Pigmented Epithelium from Adherent Human iPS Cells in Xeno-Free and Feeder-Free Conditions ». *STEM CELLS* 35 (5): 1176-88. https://doi.org/10.1002/stem.2586.

Reiners, Jan, Kerstin Nagel-Wolfrum, Karin Jürgens, Tina Märker, et Uwe Wolfrum. 2006. « Molecular basis of human Usher syndrome: Deciphering the meshes of the Usher protein network provides insights into the pathomechanisms of the Usher disease ». *Experimental Eye Research* 83 (1): 97-119. https://doi.org/10.1016/J.EXER.2005.11.010.

Reiners, Jan, Erwin van Wijk, Tina Märker, Ulrike Zimmermann, Karin Jürgens, Heleen te Brinke, Nora Overlack, et al. 2005. « Scaffold protein harmonin (USH1C) provides molecular links between Usher syndrome type 1 and type 2 ». *Human Molecular Genetics* 14 (24): 3933-43. https://doi.org/10.1093/hmg/ddi417.

Ribeiro, João Carlos, Bárbara Oliveiros, Paulo Pereira, Natália António, Thomas Hummel, António Paiva, et Eduardo D. Silva. 2016. « Accelerated age-related olfactory decline among type 1 Usher patients ». *Scientific Reports* 6 (1): 28309. https://doi.org/10.1038/srep28309.

Richardson, R, D Tracey-White, A Webster, et M Moosajee. 2017. « The zebrafish eye—a paradigm for investigating human ocular genetics ». *Eye* 31 (1): 68-86. https://doi.org/10.1038/eye.2016.198.

Richardson, Rose, Matthew Smart, Dhani Tracey-White, Andrew R. Webster, et Mariya Moosajee. 2017. « Mechanism and evidence of nonsense suppression therapy for genetic eye disorders ». *Experimental Eye Research* 155 (février):24-37. https://doi.org/10.1016/J.EXER.2017.01.001.

Rivolta, Carlo, Eliot L. Berson, et Thaddeus P. Dryja. 2002. « Paternal Uniparental Heterodisomy With Partial Isodisomy of Chromosome 1 in a Patient With Retinitis Pigmentosa Without Hearing Loss and a Missense Mutation in the Usher Syndrome Type II Gene USH2A ». *Archives of Ophthalmology* 120 (11): 1566. https://doi.org/10.1001/archopht.120.11.1566.

Roig-Merino, Alicia, Manuela Urban, Matthias Bozza, Julia D. Peterson, Louise Bullen, Marleen Büchler-Schäff, Sina Stäble, et al. 2022. « An episomal DNA vector platform for the persistent genetic modification of pluripotent stem cells and their differentiated progeny ». *Stem Cell Reports* 17 (1): 143-58. https://doi.org/10.1016/j.stemcr.2021.11.011.

Russell, Stephen R., Arlene V. Drack, Artur V. Cideciyan, Samuel G. Jacobson, Bart P. Leroy, Caroline Van Cauwenbergh, Allen C. Ho, et al. 2022. « Intravitreal Antisense Oligonucleotide Sepofarsen in Leber Congenital Amaurosis Type 10: A Phase 1b/2 Trial ». *Nature Medicine* 28 (5): 1014-21. https://doi.org/10.1038/s41591-022-01755-w.

Sahly, Iman, Eric Dufour, Cataldo Schietroma, Vincent Michel, Amel Bahloul, Isabelle Perfettini, Elise Pepermans, et al. 2012. « Localization of Usher 1 proteins to the photoreceptor calyceal processes, which are absent from mice. » *The Journal of cell biology* 199 (2): 381-99. https://doi.org/10.1083/jcb.201202012.

Samanta, Ananya, Katarina Stingl, Susanne Kohl, Jessica Ries, Joshua Linnert, et Kerstin Nagel-Wolfrum. 2019. « Ataluren for the Treatment of Usher Syndrome 2A Caused by Nonsense Mutations ». *International Journal of Molecular Sciences* 20 (24): 6274. https://doi.org/10.3390/ijms20246274.

Sanjurjo-Soriano, Carla, Nejla Erkilic, David Baux, Daria Mamaeva, Christian P. Hamel, Isabelle Meunier, Anne-Françoise Roux, et Vasiliki Kalatzis. 2019. « Genome editing in patient iPSC efficiently corrects the most prevalent USH2A mutations and reveals intriguing mutant mRNA expression profiles ». *Molecular Therapy - Methods & Clinical Development*, novembre. https://doi.org/10.1016/J.OMTM.2019.11.016.

Sarkar, Hajrah, et Mariya Moosajee. 2022. « Choroideremia: molecular mechanisms and therapies ». *Trends in Molecular Medicine*. Elsevier Ltd. https://doi.org/10.1016/j.molmed.2022.02.011.

Schneckenburger, Herbert. 2019. « Laser-assisted optoporation of cells and tissues – a mini-review ». *Biomedical Optics Express* 10 (6): 2883. https://doi.org/10.1364/boe.10.002883.

Schwaller, Fred, Valérie Bégay, Gema García-García, Francisco J. Taberner, Rabih Moshourab, Brennan McDonald, Trevor Docter, et al. 2021. « USH2A is a Meissner's corpuscle protein necessary for normal vibration sensing in mice and humans ». *Nature Neuroscience* 24 (1): 74-81. https://doi.org/10.1038/s41593-020-00751-y.

Schwander, Martin, Bechara Kachar, et Ulrich Müller. 2010. « Review series: The cell biology of hearing. » *The Journal of cell biology* 190 (1): 9-20. https://doi.org/10.1083/jcb.201001138.

Schwarz, Daniel, et Andreas T. Schaefer. 2020. « Targeted In Vivo Electroporation Using Nanoengineered Microelectrodes ». In *Methods in Molecular Biology*, 2050:113-20. Humana Press Inc. https://doi.org/10.1007/978-1-4939-9740-4_12.

Schwarz, Nele, Amanda-Jayne Carr, Amelia Lane, Fabian Moeller, Li Li Chen, Mònica Aguilà, Britta Nommiste, et al. 2015. « Translational read-through of the RP2 Arg120stop mutation in patient iPSC-derived retinal pigment epithelium cells. » *Human molecular genetics* 24 (4): 972-86. https://doi.org/10.1093/hmg/ddu509.

Schwarz, Nele, Amelia Lane, Katarina Jovanovic, David A. Parfitt, Monica Aguila, Clare L. Thompson, Lyndon da Cruz, et al. 2017. « Arl3 and RP2 regulate the trafficking of ciliary tip kinesins ». *Human Molecular Genetics* 26 (13): 2480-92. https://doi.org/10.1093/hmg/ddx143.

Seabra, M. C., Y. K. Ho, et J. S. Anant. 1995. « Deficient geranylgeranylation of Ram/Rab27 in choroideremia ». *Journal of*

Biological Chemistry 270 (41): 24420-27. https://doi.org/10.1074/jbc.270.41.24420.
Seabra, Miguel C., Michael S. Brown, et Joseph L. Goldstein. 1993. « Retinal degeneration in choroideremia: Deficiency of Rab geranylgeranyl transferase ». *Science* 259 (5093): 377-81. https://doi.org/10.1126/science.8380507.
Seabra, Miguel C., Emilie H. Mules, et Alistair N. Hume. 2002. « Rab GTPases, intracellular traffic and disease ». *Trends in Molecular Medicine*. Trends Mol Med. https://doi.org/10.1016/S1471-4914(01)02227-4.
Seabra, Miguel C., et Christina Wasmeier. 2004. « Controlling the location and activation of Rab GTPases ». *Current Opinion in Cell Biology*. Curr Opin Cell Biol. https://doi.org/10.1016/j.ceb.2004.06.014.
Sengillo, Jesse D., Thiago Cabral, Kaspar Schuerch, Jimmy Duong, Winston Lee, Katherine Boudreault, Yu Xu, et al. 2017. « Electroretinography Reveals Difference in Cone Function between Syndromic and Nonsyndromic USH2A Patients ». *Scientific Reports* 7 (1): 11170. https://doi.org/10.1038/s41598-017-11679-y.
Sengupta, Abhishek, Antoine Chaffiol, Emilie Macé, Romain Caplette, Mélissa Desrosiers, Maruša Lampič, Valérie Forster, et al. 2016. « Red-shifted channelrhodopsin stimulation restores light responses in blind mice, macaque retina, and human retina ». *EMBO Molecular Medicine* 8 (11): 1248-64. https://doi.org/10.15252/emmm.201505699.
Seo, Seongjin, et Poppy Datta. 2017. « Photoreceptor outer segment as a sink for membrane proteins: hypothesis and implications in retinal ciliopathies ». *Human Molecular Genetics* 26 (R1): R75-82. https://doi.org/10.1093/hmg/ddx163.
Shirley, Jamie L., Ype P. de Jong, Cox Terhorst, et Roland W. Herzog. 2020. « Immune Responses to Viral Gene Therapy Vectors ». *Molecular Therapy*. Cell Press. https://doi.org/10.1016/j.ymthe.2020.01.001.
Shirley, Jamie L, Ype P De Jong, Cox Terhorst, et Roland W Herzog. 2020. « Immune Responses to Viral Gene Therapy Vectors ». *Molecular Therapy* 28:709-22. https://doi.org/10.1016/j.ymthe.2020.01.001.
Simunovic, Matthew P., Jasleen K. Jolly, Kanmin Xue, Thomas L. Edwards, Markus Groppe, Susan M. Downes, et Robert E. Maclaren. 2016. « The spectrum of CHM gene mutations in choroideremia and their relationship to clinical phenotype ». *Investigative Ophthalmology and Visual Science* 57 (14): 6033-39. https://doi.org/10.1167/iovs.16-20230.
Slijkerman, Radulfus WN, Christel Vaché, Margo Dona, Gema García-García, Mireille Claustres, Lisette Hetterschijt, Theo A Peters, et al. 2016a. « Antisense Oligonucleotide-based Splice Correction for USH2A-associated Retinal Degeneration Caused by a Frequent Deep-intronic Mutation ». *Molecular Therapy - Nucleic Acids* 5 (janvier). https://doi.org/10.1038/MTNA.2016.89.

———. 2016b. « Antisense Oligonucleotide-based Splice Correction for USH2A-associated Retinal Degeneration Caused by a Frequent Deep-intronic Mutation ». *Molecular Therapy - Nucleic Acids* 5 (janvier). https://doi.org/10.1038/MTNA.2016.89.

Slijkerman, Ralph, Alexander Goloborodko, Sanne Broekman, Erik de Vrieze, Lisette Hetterschijt, Theo Peters, Milou Gerits, Hannie Kremer, et Erwin van Wijk. 2018. « Poor Splice-Site Recognition in a Humanized Zebrafish Knockin Model for the Recurrent Deep-Intronic c.7595-2144A>G Mutation in *USH2A* ». *Zebrafish* 15 (6): 597-609. https://doi.org/10.1089/zeb.2018.1613.

Slijkerman, Ralph WN, Hannie Kremer, et Erwin van Wijk. 2017. « Molecular Genetics of Usher Syndrome: Current State of Understanding ». In *eLS*, 1-12. Chichester, UK: John Wiley & Sons, Ltd. https://doi.org/10.1002/9780470015902.a0021456.pub2.

Smith, R. J. H., C. I. Berlin, J. F. Hejtmancik, B. J. B. Keats, W. J. Kimberling, R. A. Lewis, C. G. Möller, M. Z. Pelias, et L. Tranebjærǵ. 1994. « Clinical diagnosis of the Usher syndromes ». *American Journal of Medical Genetics* 50 (1): 32-38. https://doi.org/10.1002/ajmg.1320500107.

Song, Hongman, Ronald A. Bush, Yong Zeng, Haohua Qian, Zhijian Wu, et Paul A. Sieving. 2019. « Trans-ocular Electric Current In Vivo Enhances AAV-Mediated Retinal Gene Transduction after Intravitreal Vector Administration ». *Molecular Therapy - Methods and Clinical Development* 13 (juin):77-85. https://doi.org/10.1016/j.omtm.2018.12.006.

Song, Hongman, Yong Zeng, Sheik Pran Babu Sardar Pasha, Ronald A. Bush, Camasamudram Vijayasarathy, Haohua Qian, Lisa Wei, Henry E. Wiley, Zhijian Wu, et Paul A. Sieving. 2020. « Trans-ocular electric current in vivo enhances aav-mediated retinal transduction in large animal eye after intravitreal vector administration ». *Translational Vision Science and Technology* 9 (7): 1-13. https://doi.org/10.1167/tvst.9.7.28.

Sonoda, Shozo, Katsuro Tachibana, Toshifumi Yamashita, Makoto Shirasawa, Hiroto Terasaki, Eisuke Uchino, Ryo Suzuki, Kazuo Maruyama, et Taiji Sakamoto. 2012. « Selective gene transfer to the retina using intravitreal ultrasound irradiation ». *Journal of Ophthalmology* 2012. https://doi.org/10.1155/2012/412752.

Sorsby, Arnold, A. Franceschetti, B. Ruby Joseph, et J. B. Davey. 1952. « Choroideremia: Clinical and genetic aspects ». *British Journal of Ophthalmology* 36 (10): 547-81. https://doi.org/10.1136/bjo.36.10.547.

Sorusch, Nasrin, Katharina Bauß, Janet Plutniok, Ananya Samanta, Barbara Knapp, Kerstin Nagel-Wolfrum, et Uwe Wolfrum. 2017. « Characterization of the ternary Usher syndrome SANS/ush2a/whirlin protein complex ». *Human Molecular Genetics* 26 (6): ddx027. https://doi.org/10.1093/hmg/ddx027.

Souied, Eric H., Silvia N.M. Reid, Natik I. Piri, Leonid E. Lerner, Steven Nusinowitz, et Debora B. Farber. 2008. « Non-invasive gene

transfer by iontophoresis for therapy of an inherited retinal degeneration ». *Experimental Eye Research* 87 (3): 168-75. https://doi.org/10.1016/j.exer.2008.04.009.
Sun, Da, Bhubanananda Sahu, Songqi Gao, Rebecca M. Schur, Amita M. Vaidya, Akiko Maeda, Krzysztof Palczewski, et Zheng Rong Lu. 2017. « Targeted Multifunctional Lipid ECO Plasmid DNA Nanoparticles as Efficient Non-viral Gene Therapy for Leber's Congenital Amaurosis ». *Molecular Therapy - Nucleic Acids* 7 (juin):42-52. https://doi.org/10.1016/j.omtn.2017.02.005.
Sun, Da, Rebecca M. Schur, Avery E. Sears, Song Qi Gao, Wenyu Sun, Amirreza Naderi, Timothy Kern, Krzysztof Palczewski, et Zheng Rong Lu. 2020. « Stable Retinoid Analogue Targeted Dual pH-Sensitive Smart Lipid ECO/ pDNA Nanoparticles for Specific Gene Delivery in the Retinal Pigment Epithelium ». *ACS Applied Bio Materials* 3 (5): 3078-86. https://doi.org/10.1021/acsabm.0c00130.
Sun, Da, Rebecca M. Schur, Avery E. Sears, Song Qi Gao, Amita Vaidya, Wenyu Sun, Akiko Maeda, Timothy Kern, Krzysztof Palczewski, et Zheng Rong Lu. 2019. « Non-viral Gene Therapy for Stargardt Disease with ECO/pRHO-ABCA4 Self-Assembled Nanoparticles ». *Molecular Therapy*. https://doi.org/10.1016/j.ymthe.2019.09.010.
Sun, Da, Wenyu Sun, Song Qi Gao, Jonathan Lehrer, Amirreza Naderi, Cheng Wei, Sangjoon Lee, et al. 2022. « Effective gene therapy of Stargardt disease with PEG-ECO/pGRK1-ABCA4-S/MAR nanoparticles ». *Molecular Therapy - Nucleic Acids* 29 (septembre):823-35. https://doi.org/10.1016/j.omtn.2022.08.026.
Takahashi, Kazutoshi, et Shinya Yamanaka. 2006. « Induction of Pluripotent Stem Cells from Mouse Embryonic and Adult Fibroblast Cultures by Defined Factors ». *Cell* 126 (4): 663-76. https://doi.org/10.1016/j.cell.2006.07.024.
Talcott, Katherine E, Kavitha Ratnam, Sanna M Sundquist, Anna S Lucero, Brandon J Lujan, Weng Tao, Travis C Porco, Austin Roorda, et Jacque L Duncan. 2011. « Longitudinal study of cone photoreceptors during retinal degeneration and in response to ciliary neurotrophic factor treatment. » *Investigative ophthalmology & visual science* 52 (5): 2219-26. https://doi.org/10.1167/iovs.10-6479.
Tebbe, Lars, Maggie L. Mwoyosvi, Ryan Crane, Mustafa S. Makia, Mashal Kakakhel, Dominic Cosgrove, Muayyad R. Al-Ubaidi, et Muna I. Naash. 2023. « The Usherin Mutation c.2299delG Leads to Its Mislocalization and Disrupts Interactions with Whirlin and VLGR1 ». *Nature Communications* 14 (1): 972. https://doi.org/10.1038/s41467-023-36431-1.
Toms, Maria, Maria Bitner-Glindzicz, Andrew Webster, et Mariya Moosajee. 2015. « Usher syndrome: a review of the clinical phenotype, genes and therapeutic strategies ». *Expert Review of Ophthalmology* 10 (3): 241-56. https://doi.org/10.1586/17469899.2015.1033403.

Toms, Maria, Adam M Dubis, Erik de Vrieze, Dhani Tracey-White, Andreas Mitsios, Matthew Hayes, Sanne Broekman, et al. 2020. « Clinical and preclinical therapeutic outcome metrics for USH2A-related disease. » *Human molecular genetics*, janvier. https://doi.org/10.1093/hmg/ddaa004.

Touchard, Elodie, Marianne Berdugo, Pascal Bigey, Mohamed El Sanharawi, Michèle Savoldelli, Marie Christine Naud, Jean Claude Jeanny, et Francine Behar-Cohen. 2012. « Suprachoroidal electrotransfer: A nonviral gene delivery method to transfect the choroid and the retina without detaching the retina ». *Molecular Therapy* 20 (8): 1559-70. https://doi.org/10.1038/mt.2011.304.

Trapani, Ivana, et Alberto Auricchio. 2019. « Has retinal gene therapy come of age? From bench to bedside and back to bench ». *Human Molecular Genetics* 28 (R1): R108-18. https://doi.org/10.1093/hmg/ddz130.

Trapani, Ivana, Pasqualina Colella, Andrea Sommella, Carolina Iodice, Giulia Cesi, Sonia Simone, Elena Marrocco, et al. 2014. « Effective delivery of large genes to the retina by dual AAV vectors ». *EMBO Molecular Medicine* 6 (2): 194-211. https://doi.org/10.1002/emmm.201302948.

Tucker, Budd A, Robert F Mullins, Luan M Streb, Kristin Anfinson, Mari E Eyestone, Emily Kaalberg, Megan J Riker, Arlene V Drack, Terry A Braun, et Edwin M Stone. 2013. « Patient-specific iPSC-derived photoreceptor precursor cells as a means to investigate retinitis pigmentosa ». *eLife* 2 (août):e00824. https://doi.org/10.7554/eLife.00824.

Usher, C. 1914. « On the inheritance of retinitis pigmentosa;with note of cases ». *Royal London Opthalmol Hosp Rep* 19:130-236.

Vaché, Christel, Thomas Besnard, Pauline le Berre, Gema García-García, David Baux, Lise Larrieu, Caroline Abadie, et al. 2012. « Usher syndrome type 2 caused by activation of an USH2A pseudoexon: Implications for diagnosis and therapy ». *Human Mutation* 33 (1): 104-8. https://doi.org/10.1002/humu.21634.

Veleri, Shobi, Csilla H Lazar, Bo Chang, Paul A Sieving, Eyal Banin, et Anand Swaroop. 2015. « Biology and therapy of inherited retinal degenerative disease: insights from mouse models. » *Disease models & mechanisms* 8 (2): 109-29. https://doi.org/10.1242/dmm.017913.

Verbakel, Sanne K., Ramon A.C. van Huet, Camiel J.F. Boon, Anneke I. den Hollander, Rob W.J. Collin, Caroline C.W. Klaver, Carel B. Hoyng, Ronald Roepman, et B. Jeroen Klevering. 2018a. « Non-syndromic retinitis pigmentosa ». *Progress in Retinal and Eye Research*. Elsevier Ltd. https://doi.org/10.1016/j.preteyeres.2018.03.005.

———. 2018b. « Non-syndromic retinitis pigmentosa ». *Progress in Retinal and Eye Research* 66 (septembre):157-86. https://doi.org/10.1016/j.preteyeres.2018.03.005.

Verschueren, Anna, Leyna Boucherit, Ulisse Ferrari, Stéphane Fouquet, Céline Nouvel-Jaillard, Michel Paques, Serge Picaud, et José-Alain Sahel. 2022. « Planar Polarity in Primate Cone Photoreceptors: A Potential Role in Stiles Crawford Effect Phototropism ». *Communications Biology* 5 (1): 89. https://doi.org/10.1038/s42003-021-02998-y.

Wan, Caifeng, Fenghua Li, et Hongli Li. 2015. « Gene therapy for ocular diseases meditated by ultrasound and microbubbles (Review) ». *Molecular Medicine Reports*. Spandidos Publications. https://doi.org/10.3892/mmr.2015.4054.

Wavre-Shapton, Silène T., Tanya Tolmachova, Mafalda Lopes da Silva, Clare E. Futter, et Miguel C. Seabra. 2013. « Conditional Ablation of the Choroideremia Gene Causes Age-Related Changes in Mouse Retinal Pigment Epithelium ». Édité par Alfred Lewin. *PLoS ONE* 8 (2): e57769. https://doi.org/10.1371/journal.pone.0057769.

Welby, Emily, Jorn Lakowski, Valentina Di Foggia, Dimitri Budinger, Anai Gonzalez-Cordero, Aaron T.L. Lun, Michael Epstein, et al. 2017. « Isolation and Comparative Transcriptome Analysis of Human Fetal and iPSC-Derived Cone Photoreceptor Cells ». *Stem Cell Reports* 9 (6): 1898-1915. https://doi.org/10.1016/j.stemcr.2017.10.018.

Welch, Ellen M., Elisabeth R. Barton, Jin Zhuo, Yuki Tomizawa, Westley J. Friesen, Panayiota Trifillis, Sergey Paushkin, et al. 2007. « PTC124 targets genetic disorders caused by nonsense mutations ». *Nature* 447 (7140): 87-91. https://doi.org/10.1038/nature05756.

Weston, M.D., J.D. Eudy, S. Fujita, S.-F. Yao, S. Usami, C. Cremers, J. Greenburg, et al. 2000. « Genomic Structure and Identification of Novel Mutations in Usherin, the Gene Responsible for Usher Syndrome Type IIa ». *The American Journal of Human Genetics* 66 (4): 1199-1210. https://doi.org/10.1086/302855.

Wijk, Erwin van, Ronald J E Pennings, Heleen te Brinke, Annemarie Claassen, Helger G Yntema, Lies H Hoefsloot, Frans P M Cremers, Cor W R J Cremers, et Hannie Kremer. 2004. « Identification of 51 novel exons of the Usher syndrome type 2A (USH2A) gene that encode multiple conserved functional domains and that are mutated in patients with Usher syndrome type II. » *American journal of human genetics* 74 (4): 738-44. https://doi.org/10.1086/383096.

Wijk, Erwin van, Bert van der Zwaag, Theo Peters, Ulrike Zimmermann, Heleen te Brinke, Ferry F.J. Kersten, Tina Märker, et al. 2006. « The DFNB31 gene product whirlin connects to the Usher protein network in the cochlea and retina by direct association with USH2A and VLGR1 ». *Human Molecular Genetics* 15 (5): 751-65. https://doi.org/10.1093/hmg/ddi490.

Wong, Josephine H.C., Jessica Y.W. Ma, Andrew I. Jobling, Alice Brandli, Ursula Greferath, Erica L. Fletcher, et Kirstan A. Vessey. 2022. « Exploring the pathogenesis of age-related macular degeneration: A review of the interplay between retinal pigment epithelium dysfunction and the innate immune system ». *Frontiers in*

Neuroscience. Frontiers Media S.A. https://doi.org/10.3389/fnins.2022.1009599.
Wu, Mengliang, Erica L. Fletcher, Holly R. Chinnery, Laura E. Downie, et Scott N. Mueller. 2024. « Redefining Our Vision: An Updated Guide to the Ocular Immune System ». *Nature Reviews Immunology*, août, 1-16. https://doi.org/10.1038/s41577-024-01064-y.
Xie, Wenyue, Su Liu, Hong Su, Zhigang Wang, Yuanyi Zheng, et Yi Fu. 2010. « Ultrasound microbubbles enhance recombinant adeno-associated virus vector delivery to retinal ganglion cells in vivo ». *Academic Radiology* 17 (10): 1242-48. https://doi.org/10.1016/j.acra.2010.05.008.
Xue, Kanmin, et Robert E. MacLaren. 2018. « Ocular gene therapy for choroideremia: clinical trials and future perspectives ». *Expert Review of Ophthalmology*. Taylor and Francis Ltd. https://doi.org/10.1080/17469899.2018.1475232.
Yan, Weiming, Pan Long, Tao Chen, Wei Liu, Lu Yao, Ze Ren, Xiangqian Li, et al. 2018. « A Natural Occurring Mouse Model with Adgrv1 Mutation of Usher Syndrome 2C and Characterization of its Recombinant Inbred Strains. » *Cellular physiology and biochemistry : international journal of experimental cellular physiology, biochemistry, and pharmacology* 47 (5): 1883-97. https://doi.org/10.1159/000491068.
Yang, Jun, Xiaoqing Liu, Yun Zhao, Michael Adamian, Basil Pawlyk, Xun Sun, D. Randy McMillan, M. Charles Liberman, et Tiansen Li. 2010. « Ablation of Whirlin Long Isoform Disrupts the USH2 Protein Complex and Causes Vision and Hearing Loss ». Édité par Gregory J. Pazour. *PLoS Genetics* 6 (5): e1000955. https://doi.org/10.1371/journal.pgen.1000955.
Yao, Lu, Lei Zhang, Lin-Song Qi, Wei Liu, Jing An, Bin Wang, Jun-Hui Xue, et Zuo-Ming Zhang. 2016. « The Time Course of Deafness and Retinal Degeneration in a Kunming Mouse Model for Usher Syndrome ». Édité par Tiansen Li. *PLOS ONE* 11 (5): e0155619. https://doi.org/10.1371/journal.pone.0155619.
Ye, Guo Jie, Ewa Budzynski, Peter Sonnentag, T. Michael Nork, Nader Sheibani, Zafer Gurel, Sanford L. Boye, et al. 2016. « Cone-Specific Promoters for Gene Therapy of Achromatopsia and Other Retinal Diseases ». *Human Gene Therapy* 27 (1): 72-82. https://doi.org/10.1089/hum.2015.130.
Zhai, Yi, Manlong Xu, Alina Radziwon, Ioannis S. Dimopoulos, Paul Crichton, Rachel Mah, Robert E. MacLaren, Rizwan Somani, Matthew T. Tennant, et Ian M. MacDonald. 2023. « AAV2-Mediated Gene Therapy for Choroideremia: 5-Year Results and Alternate Anti-sense Oligonucleotide Therapy ». *American Journal of Ophthalmology* 248 (avril):145-56. https://doi.org/10.1016/j.ajo.2022.12.022.
Zhong, Xiufeng, Christian Gutierrez, Tian Xue, Christopher Hampton, M. Natalia Vergara, Li-Hui Cao, Ann Peters, et al. 2014. « Generation of three-dimensional retinal tissue with functional photoreceptors

from human iPSCs ». *Nature Communications* 5 (1): 4047. https://doi.org/10.1038/ncomms5047.
Zhou, Xi Yuan, Qing Liao, Yi Min Pu, Yong Qiang Tang, Xiao Gong, Jia Li, Yan Xu, et Zhi Gang Wang. 2009. « Ultrasound-mediated microbubble delivery of pigment epithelium-derived factor gene into retina inhibits choroidal neovascularization ». *Chinese Medical Journal* 122 (22): 2711-17. https://doi.org/10.3760/cma.j.issn.0366-6999.2009.22.007.
Zou, Junhuang, Rong Li, Zhongde Wang, et Jun Yang. 2019. « Studies of the Periciliary Membrane Complex in the Syrian Hamster Photoreceptor ». In , 543-47. https://doi.org/10.1007/978-3-030-27378-1_89.
Zou, Junhuang, Ling Luo, Zuolian Shen, Vince A. Chiodo, Balamurali K. Ambati, William W. Hauswirth, et Jun Yang. 2011. « Whirlin Replacement Restores the Formation of the USH2 Protein Complex in Whirlin Knockout Photoreceptors ». *Investigative Opthalmology & Visual Science* 52 (5): 2343. https://doi.org/10.1167/iovs.10-6141.
Zou, Junhuang, Pranav D. Mathur, Tihua Zheng, Yong Wang, Ali Almishaal, Albert H. Park, et Jun Yang. 2015. « Individual USH2 proteins make distinct contributions to the ankle link complex during development of the mouse cochlear stereociliary bundle ». *Human Molecular Genetics* 24 (24): 6944-57. https://doi.org/10.1093/hmg/ddv398.